Author:
Mulvee, Matt

Title:
Design and Construction of Hybrid Supramolecular Hydrogels

Design and Construction of Hybrid Supramolecular Hydrogels

Matthew Thomas Mulvee

A dissertation submitted to the University of Bristol in accordance with the requirements for the award of the degree of Doctor of Philosophy in the Faculty of Sciences, School of Chemistry, March 2018.

Word Count: 55,020

Abstract

The process of forming supramolecular hydrogels through the assembly of gelators into high-aspect ratio nanofilaments is heavily kinetically dependent. Furthermore, the assembly process is highly sensitive to conditions such as ionic strength and temperature. Therefore, the process and environment in which self-assembly occurs can considerably alter the structures formed and the subsequent macroscopic properties of the hydrogel.

Since the type of trigger used and experimental conditions can affect the gel properties, investigations into novel stimuli and the effect on hydrogel properties are warranted. The first experimental chapter of the thesis demonstrates the use of nitric oxide radicals for the dephosphorylation of the N-fluorenylmethyloxycarbonyl tyrosine phosphate (FYP) to form *N*-fluorenylmethyloxycarbonyl tyrosine (FY) gelator molecules. This novel stimulus resulted in much narrower filaments with a reversed supramolecular chirality, compared to filaments form through enzymatic cleavage of FYP.

The second chapter of the work highlights the design and construction of a nucleotide-amino acid multicomponent hydrogel. This is achieved through the addition of an inorganic stimulus, silver ions, to guanosine monophosphate (GMP) *N*-fluorenylmethyloxycarbonyl tyrosine (FY) solution. This exploits the association between silver and the guanine residue of GMP to form Ag-GMP dimers *via* an enolate tautomer and subsequent abstraction of a proton. The subsequent drop in pH can then triggers the gelation of the second gelator, FY. The ratio of Ag:GMP affects the assembly kinetics, the supramolecular organisation and the mechanical properties of the hydrogel. Higher stoichiometries result in rapid gelation and non-orthogonal assembly. However, at lower stoichiometries, this disruptive assembly is avoided, and FY filaments can be selectively disassembled through the raising of pH. This demonstrates the possibility of creating a hydrogel with adaptable network density and mechanical properties.

The final chapter investigates the potential of a nucleotide-based hydrogel (Ag-GMP hydrogel) as an antimicrobial agent. The antibacterial properties of this gel were characterised using a series of microbiological techniques. Significantly, the gel demonstrated substantial killing of gram-negative bacteria (*E. coli*) and gram-positive bacteria (*E. faecalis*). Gel electrophoresis experiments indicated that this activity seems to be, in part, due to damage caused to the chromosomal DNA.

Acknowledgements

I am very fortunate to be grateful to many people for their help and support throughout my PhD.

Firstly, I would like to thank my primary supervisor Dr Avinash Patil for providing me with projects detailed in this thesis and willingness to change the direction of my PhD. Avi's supervision has been particularly important in my development as an independent scientist, which I am appreciative of. I would also like to thank my other supervisors, Dr Natasa Vasiljevic and Professor Stephen Mann. Natasa provided guidance throughout my PhD and helpful recommendations. She was also extremely helpful at introducing concepts at the start of my PhD. Steve also provide me with valuable guidance throughout my PhD, helping me to focus on the most interesting questions. I would also like to thank Professor Howard Jenkinson, Dr Angela Nobbs, and Dr Lindsay Dutton for welcoming me to their group and introducing me to microbiology. The experience was very fulfilling and was an important process in becoming an independent scientist. I'm also very grateful for the support provided by members of the management and administrative team for the Bristol Centre for Functional. In particular, Dr Annela Seddon and Dr Terry McMaster. Their supervision throughout my PhD allowed me to get as much from my PhD experience as possible.

I'd also like to thank all the members of the Mann group for making the last 4 years so enjoyable. I learnt a lot from the Mann group, for which I'll always be grateful! Further thanks go to the INASCON 2018 committee members for a great year and their hard work. I also have many collaborators and colleagues to thank for their invaluable assistance throughout the projects: Dr Paul Lawrence for his help with NMR, Dr Sean Davis, Dr Jean-Charles Eloi, and Jonathan Jones for their help with TEM and EDX, Jen Coombs, Judith Mantel and Professor Paul Verkade for assistance with cryogenic TEM, Dr Jordan Fletcher for assistance with CD, Dr Gavin Hazell for his help with the SANS work, Sam Briggs and Maddy Nichols for their assistance with DSC, Ed Alred, Dr Kamendra Sharma and Dr Cheryl Flynn for their help with rheology.

For their help proofreading, Dr Avinash Patil, Dr Natasa Vasiljevic, Jen Coombs, Sam Briggs, Jonny Furze, Maddy Nichols, Dr Nicholas Martin, Dr Pavan K. Bosukonda, and my family your help is greatly valued.

Lastly, I'd like to thank Jen Coombs for her completely invaluable support throughout my PhD and her patience whilst I was 'almost finished' for several months!

Author’s declaration

I declare that the work in this dissertation was carried out in accordance with the requirements of the University's Regulations and Code of Practice for Research Degree Programmes and that it has not been submitted for any other academic award. Except where indicated by specific reference in the text, the work is the candidate's own work. Work done in collaboration with, or with the assistance of, others, is indicated as such. Any views expressed in the dissertation are those of the author.

SIGNED: ..... DATE: .....

Table of Contents

List of Abbreviations

AFM atomic force microscopy

Ag silver

$AgNO_3$ silver nitrate

ALP alkaline phosphatase

Aq aqueous

ATR-FTIR Attenuated total reflectance Fourier transform infrared spectroscopy

B_0 external magnetic field

CD circular dichroism spectroscopy

CFU colony forming units

D_2O deuterated water

DMSO dimethylsulfoxide

DMSO-d_6 deuterated dimethylsulfoxide

DNA deoxyribonucleic acid

DSC differential scanning calorimetry

E. coli Escherichia coli

EDX Energy-dispersive X-ray (spectroscopy)

E. faecalis enterococcus faecalis

EM electron microscopy

Fmoc	Fluorenylmethyloxycarbonyl
FY	Fmoc-tyrosine
FYP	Fmoc-tyrosine-phosphate
FT-IR	Fourier transform infrared (spectroscopy)
G*	complex modulus
G’	storage modulus
G’’	loss modulus
GdL	glucono-δ-lactone
GMP	guanosine monophosphate
H	enthalpy
H-bonding	hydrogen bonding
HCl	hydrochloric acid
HT	high tension voltage
Hz	hertz
LMWG	low-molecular-weight-gelator
LVR	linear viscoelastic region
M	moles per dm^3
mL	millimetres
mM	millimoles per dm^3
MW	molecular weight

NaOH	sodium hydroxide
NaOD	sodium hydroxide deuterated
nm	nanometre
NMR	nuclear magnetic resonance (spectroscopy)
OH	hydroxyl group
Pa	pascal
Pa.S	pascal second
pH	negative logarithm of the concentration of hydrogen ions
pK_a	negative logarithm of the acid disassociation constant
PO_3^{2-}	phosphate group
ppm	parts per million
Q	momentum transfer or scattering vector (SANS)
qGMP	G-quartet of guanosine monophosphate
S	entropy
SANS	small-angle neutron scattering
SDS	sodium dodecyl sulfate
SEM	scanning electron microscopy
SNP	sodium nitroprusside
sol	solution
STEM	scanning transmission electron microscopy

T	temperature
TEM	transmission electron microscopy
T_{gel}	gel-sol transition temperature
UV	ultraviolet
UV-Vis	ultraviolet-visible spectroscopy
Å	angstrom
δ	chemical shift (NMR)
δ	phase difference (rheology)
h	Planck's constant
γ	shear strain
η	viscosity
µL	microlitre
λ	wavelength

Chapter 1
Introduction

Chapter Outline:

In this chapter, the basics of self-assembly are summarised with examples of natural and synthetic systems. Then fundamentals of supramolecular hydrogelation and the state of the field are introduced with references to the experimental chapters to follow. Thus, the reader may become to be familiar with the key concepts necessary to understand the experimental results reported later.

Self-assembly:

Self-assembly is ubiquitous in natural systems, being responsible for the emergence and maintenance of life (*e.g.* protein folding, virus assemblies and the formation of cell membranes).[1–3] Grzybowski *et al.* define self-assembly as the "spontaneous formation of organized structures from many discrete components that interact with one another either directly and/or through the environment." [4] This definition rules out less ordered aggregation processes such as precipitation and the requirement for discrete building blocks rules out the pattern formation in continuous media.

The transformation from a less ordered state to a more ordered state results from a reduction in the Gibbs free energy. At a constant temperature (T), pressure and number of molecules the changes in enthalpy (H) and entropy (S) determine the spontaneity of self-assembly processes:

$$\Delta G = \Delta H - T\Delta S \qquad \text{equation 1.1}$$

These processes occur through a balance of attractive and repulsive non-covalent forces (van der Waals, electrostatic, hydrophobic *etc.*) between neighbouring molecules (intermolecular forces) and within molecules (intramolecular interactions). These forces are individually weak (2-250 kJ mol^{-1}) in comparison to covalent bonds (100-400 kJ mol^{-1}),[5–10] yet collectively they can yield stable structures with extraordinarily different structures and function. A summary of these interactions is included below.

Van der Waals (VdW) Forces

VdW forces are non-directional and arise from the fluctuations of electron distribution of two neighbouring molecules to induce temporary electric dipoles.[6,11,12] These interactions are generally fairly weak ~5 kJ mol^{-1}.[6,12] As they arise from neighbouring bodies, these interactions are ubiquitous and therefore it is hard to design supramolecular structures using predominantly VdW forces, though

such forces are used to drive the assembly of nanoparticles. [13,14] Furthermore, several groups have utilised vdW forces to direct 2D self-assembly on surfaces. [15–17]

Molecular-dipole

Dipole-dipole forces allow molecules with a permanent electric dipole moment to interact in low-dielectric solvents *e.g.* n-hexane. However, charges are needed to induce significant electrostatic interactions in water as the dipole forces are screened by water. [6]

Ion-Ion Electrostatic Interactions

Almost as ubiquitous as vdW forces, electrostatic interactions are long-range Coulombic forces, which can be either attractive (between opposite charges) or repulsive (between like-charges).[6,10–12,18] Through the alignment of opposite charges, electrostatic interactions can be used to direction assembly in one dimension.[19–21] Such interactions can be very strong (~500 kJ mol^{-1}) and are determined by the dielectric constant of the solvent, the concentration, and the chemical nature (*e.g.*, size and valence) of the surrounding counterions, which can screen the charges.[6,12,20,22–28]

Most commonly, attractive electrostatic forces are exploited to trigger self-assembly *e.g.* oppositely charged peptide amphiphiles[29] or binary nanoparticle crystals.[30] However, Aida's group have demonstrated the use of electrostatic repulsion to impart unusual behaviour into two different polymeric gels. Firstly, Liu *et al.* demonstrated that the inclusion of unilamellar titanate(IV) nanosheets into the hydrogel resulted in anisotropic mechanical properties.[31] Such a hydrogel easily deforms due to a shear force applied parallel to the nanosheets (Figure 1.1a) but it resists compression orthogonal to the sheets due to electrostatic repulsion between the sheets (Figure 1.1b). Kim *et al.* also used a similar approach to produce a thermoresponsive hydrogel actuator.[30] Electrostatic repulsion is triggered by a thermoresponsive phase transition in the gel, with heating expanding the gel and cooling causing contraction. Thus, an L-shaped hydrogel demonstrated unidirectional procession (in effect, walking) in response to heating cycles (Figure 1.1c)!

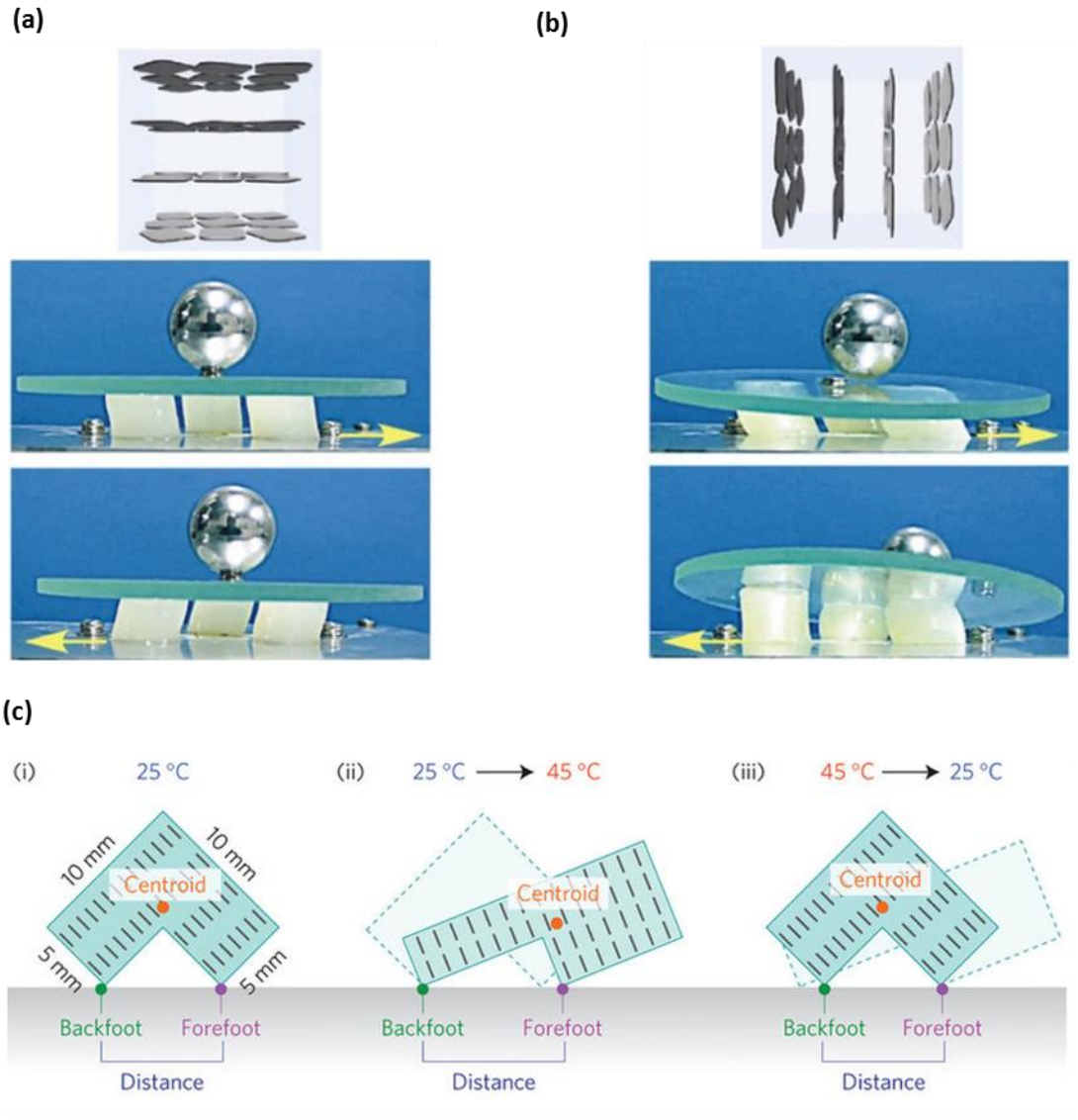

Figure 1.1 Demonstrations of vibration isolation. On a mechanical oscillator, a glass stage featuring a metal sphere was supported by three cylindrical pillars of magnetically structured hydrogel containing cofacially oriented titanate(IV) nanosheets in parallel (a) or orthogonal (b) direction to the cylinder cross-section. Adapted from ref. 31 (c) Internal design of the actuator (5 mm thick) and its ideal processing mechanism in response to heat cycles. Adapted from ref. 30.

Hydrogen bonding

Hydrogen bonding occurs between an electronegative atom (*e.g.* N, O, or F) and a hydrogen atom covalently bonded to a second electronegative atom, inducing a slight positive charge on the hydrogen atom. These two species are the hydrogen bond acceptor and donor, respectively. Thus, it can be considered a dipolar interaction and is largely electrostatic in nature. [6,32] Though stronger than vdW

forces, the hydrogen bond is considerably weaker than ionic interactions with typical strengths of 10-40 kJ mol^{-1} and depends strongly on the solvent conditions. [6,12,33] Hydrogen bonds are however highly directional and can be combined to increase specificity, either intermolecularly or intramolecularly. [17,34–39] Thus, hydrogen bonding is one of the key forces determining supramolecular structure in self-assembly. For instance, the secondary structure of protein folding is heavily determined by hydrogen bonding, with intramolecular bonding favouring α-helices and intermolecular bonding favouring β-sheets. [18] This process is key to proper function as misfolded polypeptides have a propensity to form aggregates which are associated with Alzheimer's, Parkinson's and Huntington's diseases, and atherosclerosis. [40–47]

Hydrophobic effect

Unlike the previous enthalpic interactions, the hydrophobic effect is an entropic organising force of non-polar molecules to avoid contact with an aqueous solvent. [2,9,12,22,48,49] Water molecules are not able to form favourable interactions with the apolar molecules and instead preferentially form hydrogen bonds with each other. When these species are mixed they, in a sense, act 'frozen' to maintain interaction with like molecules. Thus, apolar moieties are repelled by the aqueous solvent and aggregate to minimise their contact with water. Both expelled species then have an increased entropy resulting from the increased degrees of freedom. This process is less specific and as such, the effect is less geometrically constrained and can result in amorphous assembly. This effect is a key driving force for self-assembly in aqueous solvents.[33,50] For instance, it is the primary driving force for monomeric surfactants to assemble in aqueous solvents and is responsible for the assembly of cell membranes and intracellular compartments.[4,49]

Aromatic Stacking (π-π stacking)

These are attractive electrostatic interactions (5-40 kJ mol^{-1}) that occur through the stacking of aromatic moieties. The π electrons form a quadrupole moment due to the stronger electronegativity of sp^2 carbons compared to hydrogen atoms. This polarity creates a partial negative charge on both

faces of the aromatic ring and a slight positive charge around the σ-framework of the aromatic ring (Figure 1.2a).[32,51–54] This polarity determines the geometry of the interactions as face-centred stacking would be unfavourable and instead aromatic rings interact *via* T-shaped (edge to face) and parallel displaced stacking (Figure 12b and c).[32] Such arrangements induce directional growth, tending to be more ordered than assembly through the hydrophobic effect alone, thus they are often introduced to encourage self-assembly in water.[12] Unsurprisingly, therefore aromatic-aromatic interactions are key to stabilising protein structures across multiple length scales by stabilising the secondary, tertiary and quaternary structure. The prevalence of these interactions is thought to be key to the evolution of proteins. [55]

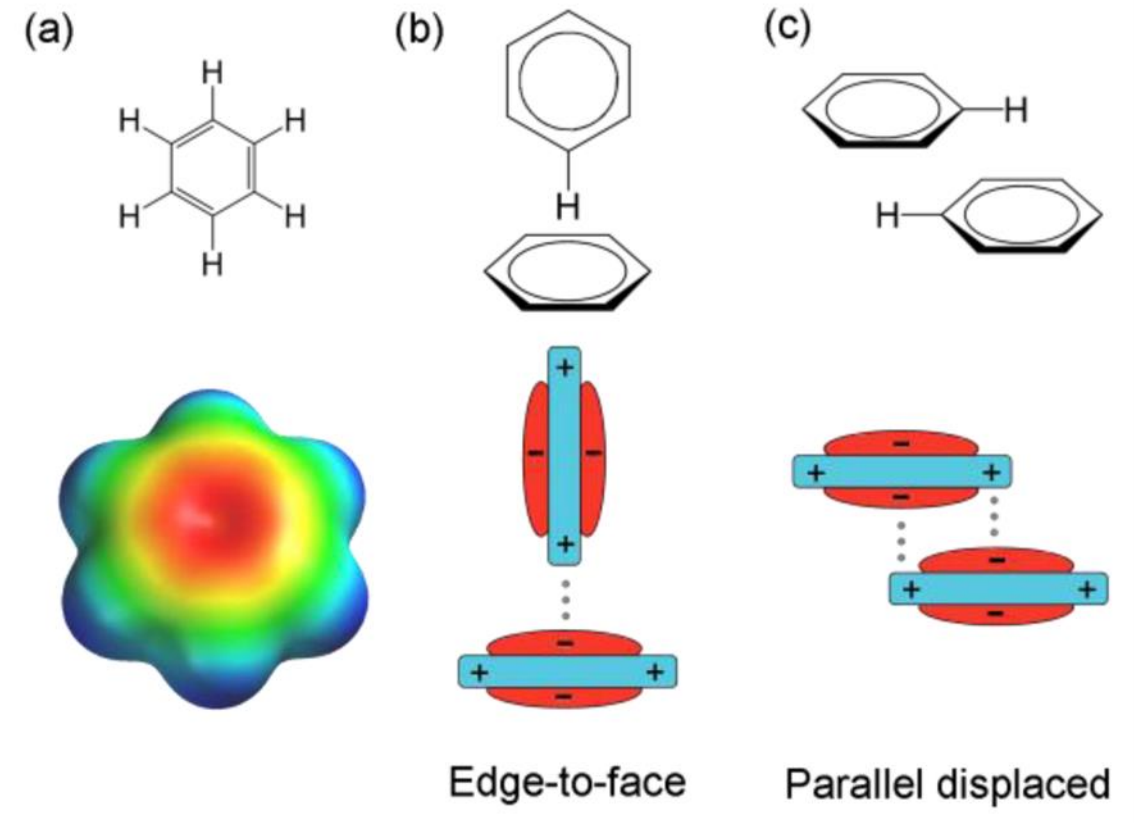

Figure 1.2 (a) Electrostatic potential surface of a benzene molecule. (b) and (c) schematic representations of interaction geometries of a benzene dimer. Adapted from ref. 55.

Rather than due to any one force, self-assembly occurs by the delicate balance of different non-covalent interactions. For instance, Tsonchev *et al.* demonstrated that the assembly of peptide

amphiphiles (peptide residues covalently linked to a hydrophobic segment) is dependent on hydrogen bonding, electrostatic and hydrophobic interactions.[56] Through the combination of molecular dynamics simulations and experimental observations, a phase diagram was constructed to relate changes in environmental conditions to self-assembly and phase transitions between different supramolecular structures.

Type of Interaction	Typical Strengths (kJ mol^{-1})
Van der Waals	~5
Electrostatic	~500
Hydrogen bonding	10-40
Hydrophobic effect	N/A
Aromatic/π-π stacking	5-40

Table 1.1 Strength of non-covalent forces

Self-assembly in nature and biomimicry

The interactions summarised above are responsible for a diverse variety of structures found in nature. These functional structures are formed of biocompatible building units and assemble in aqueous solutions, thus they provide inspiration for the formation of many structures over different length scales. [12,57–62] In this section, natural assemblies and synthetic structures are summarised below.

The nucleic acid molecules of DNA and RNA are fundamental to life, being critical to gene heredity, regulation and expression. Double-stranded DNA assembly occurs through complementary hydrogen bonding between the two strands and this assembly then is reinforced by π-π stacking between the nucleobases (Figure 1.3a). These biological polymers can be synthesised with an almost infinite number of sequences. [63] Thus, their propensity to self-associate and their biological nature has made them a useful building unit for bottom-up designed assembly. Such structures have relevance as

vehicles for drug delivery and biosensing. [63–66] For instance, Andersen *et al.* generated a nanoscale box through a bottom-up approach that would open under certain conditions (in this report, complementary DNA, though other stimuli are possible triggers) and allowing for controlled release of cargo.[67]

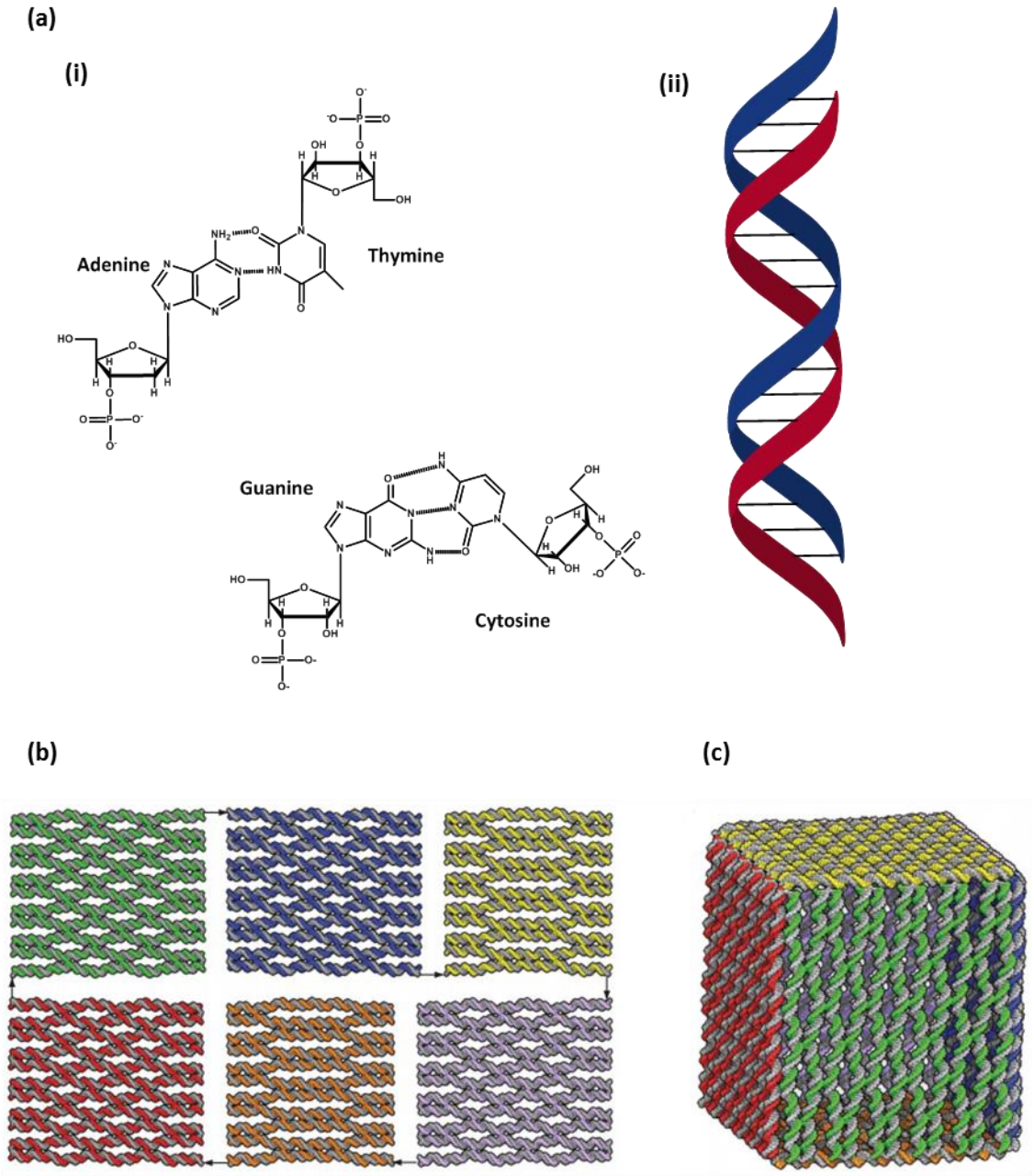

Figure 1.3 (a) (i) Hydrogen bonding between nucleosides directs assembly into (ii) a double helix with π-π stacking between nucleobases. Molecular models of the six DNA sheets in a flat (b) and cubic higher-order structure (c). Adapted from ref. 67.

DNA and organelles are confined to the cell and isolated from the external environment through the assembly of phospholipids into the cytoplasmic membrane. These amphiphilic molecules form a bilayer to expose their polar head groups (the phosphate and glycerol), whilst the nonpolar chains cluster in the membrane. This leads to the stabilisation of transmembrane proteins.[68] These stable membranes act as a barrier to water-soluble ions whilst its non-covalent and dynamic assembly imparts fluidity allowing for the uptake of particles *via* mechanisms such as endocytosis.[69]

Aggregated species are also fundamental for the light-harvesting antennae of photosynthetic plants and bacteria. Many structurally diverse photosynthetic antennae exist in nature, including the green sulphur bacterial chlorosome (a complex of aggregated pigment molecules), higher plant light-harvesting complexes and the purple bacterial light-harvesting complexes (both of these are membrane pigment-protein complexes).[61] Despite the structural variances, they all feature highly ordered arrays of pigments. For instance, crystal structures of the light-harvesting antenna complexes of photosynthetic bacteria show the presence of highly symmetric supramolecular architectures. [70–72]

In these light-harvesting complexes, sophisticated self-organised chromophore arrays are essential for efficient light capture and funnelling exciton flux to the reaction centre, where the electron transfer drives photosynthesis (Figure 1.4a).[61,70–74] The coupling of many hundreds of these chromophores enables a strong transition dipole moment along the head-to-tail arrangement of the chromophores. This allows for the transfer of exciton energy to peripheral chromophores in a few picoseconds and allowing for remarkable transfer efficiencies of more than 95%. [74–76]

(a)

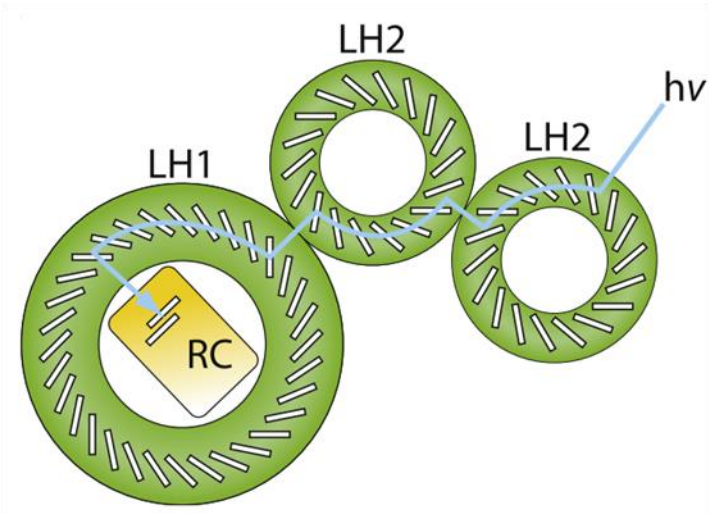

(b)

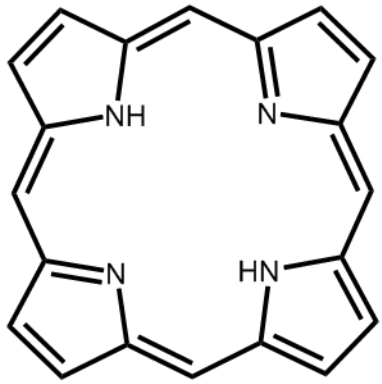

Figure 1.4 (a) A schematic demonstrating energy transfer through the bacterial light harvesting system (blue arrow), entering as a photon at light-harvesting complex 2 (LH2), traveling though another LH2, then the LH1 before arriving at the reaction centre (RC) Adapted from ref. 61. (b) Chemical structure of the simplest porphyrin, composed of four pyrrole subunits.

Accordingly, much research has been done into creating synthetic light-harvesting antenna consisting of multiple porphyrin units, analogous to the pigment units bacteriochlorophyll and chlorophyll; the chromophores for bacteria and plants, respectively.[72,75,77,78] Porphyrins (Figure 1.4b) are large, flat, conjugated tetrapyrrole macrocycles, which can be functionalised to allow further interactions between the molecules.[79–82] With the appropriate choice of substituents, the assembly of porphyrins can be promoted by intermolecular π–π interactions, electrostatic interactions, hydrogen bonding, and metal coordination. As a result, many self-assembled photo-responsive structures have been formed using porphyrins including nanoporous solid materials, rigid and ordered monolayers, rings,

columnar stacks, linear tapes, rigid rods and nanoparticles. [23,48,70,78,79,83–85] The assembly of an iconic porphyrin, meso-(4-sulfonatophenyl) porphyrin (H_2TPPS_4), depends heavily on the experimental conditions (pH, ionic strength, ageing of stock solutions). For instance, Arteaga *et al.,* demonstrated that flows directed the chirality of assembled porphyrin structures that chaotic flows were responsible for producing a racemic mixture of chiral shaped supramolecular species.[86] Even the order of addition of protons and NaCl determined whether self-assembly occurred. [87]

Supramolecular hydrogels

Supramolecular hydrogels are an excellent example of self-assembly structures, which can be composed of all the previously mentioned biomolecules and, through their hierarchical assembly, produce viscoelastic gels. (This class of gels has several names, supramolecular gels, molecular gels, low molecular weight gels and self-assembled gels which all cover the same types of gels. This differentiates them from polymeric gels whereby polymers are chemically or physically crosslinked to form a three-dimensional network.)

Lloyd famously claimed that "colloidal gels are easier to recognise than define" and proposed that gels must be composed of a liquid and solid component which together have the mechanical properties of a solid.[88] Hermans expanded the definition stating that both the dispersed component and dispersing medium extend themselves continuously throughout the whole system.[89] These are useful but imprecise definitions as not all colloidal suspensions form molecular gels and not all molecular gels are colloidal.[90] Ferry proposed a less rigorous definition that a gel is a substantially diluted system which exhibits no steady state flow.[91]

It is possible to link the microscopic and macroscopic definitions of a gel, importantly defining structural and mechanical properties to create a definition that encompasses both. Such that "gels are viscoelastic solid-like materials comprised of an elastic network that extends through the solvent and is permanent for the time-scale of the experiment." [33,90,92,93] It is the entrapment and adhesion of the

solvent in a large surface area, three-dimensional matrix that produces the solid-like behaviour and thus prevents steady-state flow (Figure 1.5b).[39,92–95]

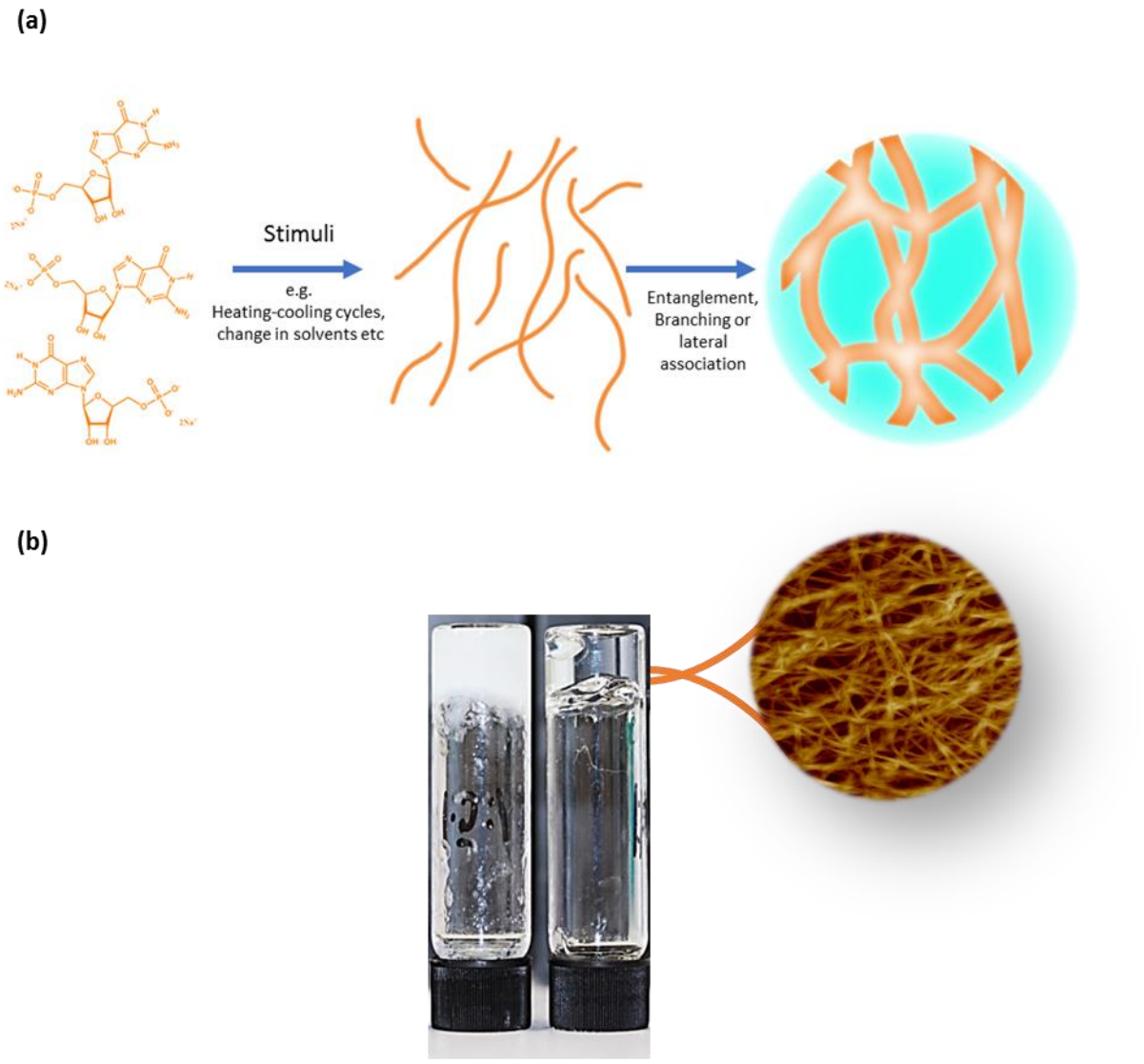

Figure 1.5 (a) Scheme of gelation (b) Self- supported supramolecular hydrogels resisting flow due to entrapment of solvent by network

In the case of molecular hydrogels, the solvent is aqueous, and, unlike polymeric gels, they are formed through the assembly of low weight molecular gelators (LWMG) into one-dimensional filaments which then comprise the three-dimensional network. LWMG are arbitrarily defined as <3000 Da, [93] which corresponds to *ca.* 25 amino acids or 16 glucose units, though many gelators are much smaller. These

gelators are essentially zero-dimensional objects which assemble *via* non-covalent interactions into one-dimensional filaments. These then entangle, branch and laterally associate to form a three-dimensional hydrogel network (Figure 1.5a).[96–98] The morphology of these filaments may be strands, ribbons, tapes or any aggregate with a large aspect ratio that can entangle or branch.[21,95,99,100] Herein, the term 'hydrogel' will refer to molecular hydrogels rather than polymeric hydrogels, unless stated otherwise.

The applicability of all gelators first existing as zero-dimensional dissolved molecules, as in the common schematic of gelation (Figure 1.5a), has recently been challenged by Adams *et al.*[99,101] It is clear that certain amphiphilic gelators act as surfactants with very low critical micelle concentrations (<0.2 mM), thus, depending on the concentration, spherical or wormlike micelles may first exist prior to gelation.[101–107] It is not currently clear however whether these structures are retained in the gelation process or whether a structural reorganisation occurs. However, it is likely the presence of different micellar assemblies, rather than molecularly dissolved gelators, will impact gelation and result in different gel properties due to different assembly processes. For instance, Draper *et al.* demonstrated that a common gelator, known as 2NapFF (2-(naphthalen- 2-yl)-acetamido)-3- phenylpropanamido)-3- phenylpropanoicacid), formed micelles and through heating cycles (perhaps the most common process solubilise gelators) would irreversibly dehydrate the micelle fibres.[102] This resulted in the fusion of the fibres and different rheological properties to those that had not undergone the same cycles.

Still, gelation is always initiated by a trigger (*e.g.* lowering of temperature, [92,108,109] charge screening to lower repulsion and hydrophilicity, [20,110] cleavages of hydrophilic residues, [111–113] *etc.*) to lower the solubility of a well-dissolved gelator to form an isotropic supersaturated solution. [33,92,93] (The author is not aware of any examples whereby gelation occurs instantly for a single gelator after dissolution, though this can be achieved through the mixing of two gelators.)[114,115] This supersaturation drives aggregation *via* stochastic nucleation rather than spinodal decomposition (rapid unmixing with no

barrier to nucleation).[90,95] Also, unlike crystallisation whereby macrophase separation occurs and the separation solid and liquid components are often visible, gelation occurs *via* microphase separation to form a continuous phase.[93,108,116]

As this supersaturation is not at equilibrium, error correction in the assembly process is often not possible and such processes are often kinetically dependent. [99] In fact, the rate of the assembly can be comparable to the rate of the mixing of components and ultimately affects how gelation occurs. [117–119] It is now well observed that the pathway to gelation can affect the supramolecular structure and the properties of the hydrogel.[20,38,120–125] This will be explored in Chapter 3 by demonstrating a novel stimulus and the consequences of this process. Further to this, kinetically trapped gel structures could be altered by using elevated temperatures to overcome kinetic barriers to evolve into the same gel prepared through other routes. [4,126–128] This implies that there is a thermodynamic minimum which can be reversibly accessed.[129] Several reports demonstrate that small modifications to gelator structures can affect the supramolecular structure through subtly different intermolecular interactions. [130–134] These observations indicate that there are both thermodynamic and kinetic aspects to the formation and subsequent structure of hydrogels.

As most LWMGs that gel water are amphiphilic, the assembly into fibres requires a delicate balance of gelator-gelator and gelator-solvent interactions.[33,99,129,135] This balance may result in molecularly dissolved gelators, ordered or amorphous aggregation (*e.g.* crystallisation or precipitation, respectively), or filament growth. [33,92,123,136]

Since these interactions are enthalpically weak, aggregation in aqueous solvents, at the molecular level, is normally entropy driven, owing to the dominance of the hydrophobic effect confirmed by studies into the thermodynamics of gel solubilization. [50,137,138] However, the thermodynamics of the one-dimensional assembly is not well understood. As this process is often considered an intermediate structure, between being fully solubilised and forming a solid aggregate, the gel state is considered a kinetically trapped metastable state, avoiding transformation to the crystal state. [12,34,108,136] Indeed,

the crystal state should allow for more interactions between gelators in three dimensions rather than just one. [12,129,139] Metastable gels have exhibited gel-crystal transitions, which limits long-term stability of the gel state through gradual disassembly of the gel network. [108,139–145]

However, as the gelators are amphiphilic, maintaining solvent interactions in one-dimensional assemblies is expected to be favourable, as with the formation of wormlike micelles. [146,147] Also, self-healing gels rely on the gel state being, at the very least, a local thermodynamic minimum that can be reversibly accessed.[129,148] Molecular dynamics simulations have been used by Tuttle *et al.* and Ulijn *et al.* to understand gelation under thermodynamic control. [50,107] Thermodynamically stable gels may exist in a deep energy minimum surrounded by a high activation barrier which makes access to the crystal state impossible.[34]

Indeed, Ulijn *et al.* demonstrated that the solvophilic interactions (favourable interactions with the solvent, either organic or aqueous) are key to forming thermodynamically favourable one-dimensional fibres over three-dimensional crystals. [129] Their model considers the thermodynamics of the initial fibre formation, as this stage was deemed critical for determining whether one-dimensional or three-dimensional structures formed. Prisms were used as analogues for gelators, with the number of solvophilic and solvophobic faces and the interaction strength between prisms and the solvent determined by the user. Without any solvophilic faces, the Gibbs free energy for fibre formation is always positive and crystallisation is preferred. However, by introducing amphiphilicity to the assembling units, fibre formation was thermodynamically favoured for certain parameters of interactions, *i.e.* gelator- gelator and gelator-solvent interactions. These parameters also determined fibre thickness and the model could be verified by experimental conditions for a well-known gelator, *N*-(fluorenyl- 9-methyloxycarbonyl)-diphenylalanine (Fmoc-diphenylalanine of Fmoc-FF). However, if the network formation involves significant overlap of the fibre surfaces, then the approximations of the model are no longer valid. In this case, the network would be a metastable state and will tend towards the crystal state.

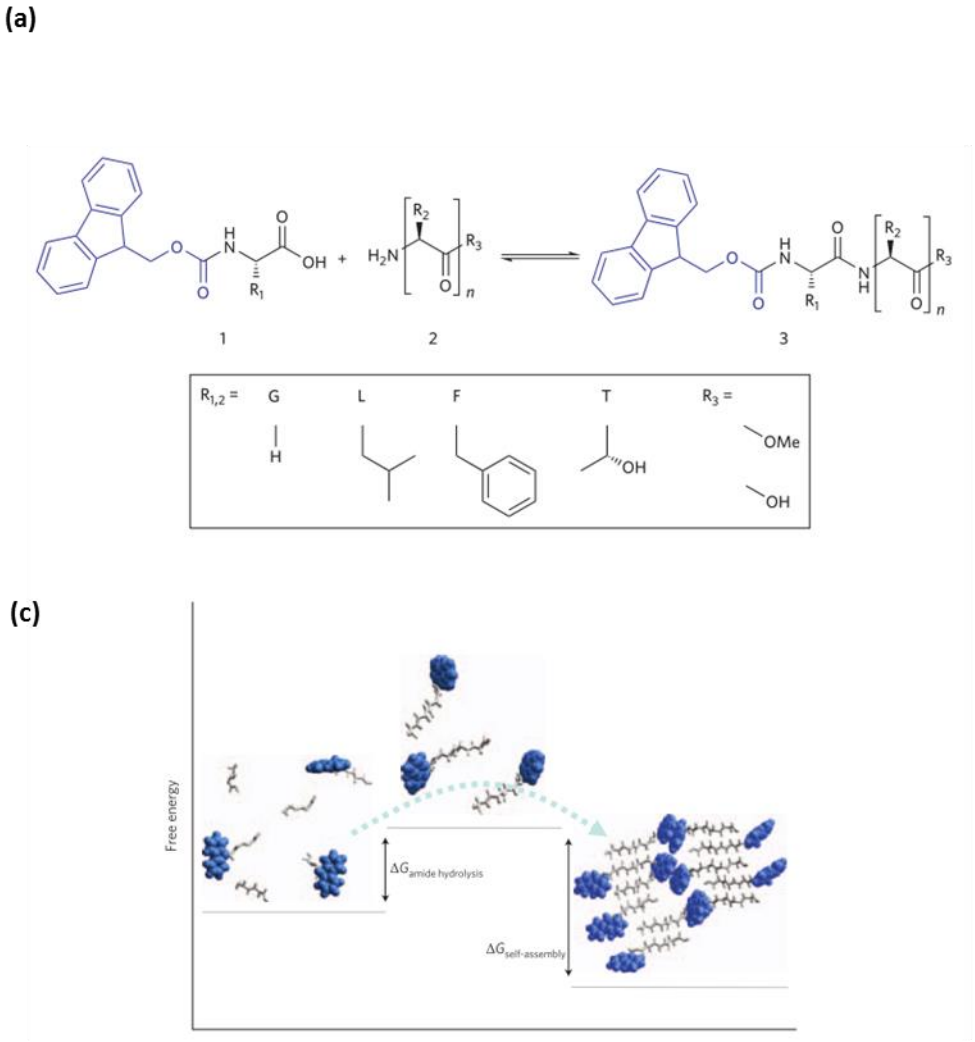

Figure 1.6 Self-assembly under thermodynamic control. (a) Reversible, enzyme-assisted hydrolysis reaction (b) formed using different nucleophiles. (c) Representation of free energy profile of enzyme-assisted self-assembly of peptide derivatives. Amide hydrolysis, the first stage, is thermodynamically unfavourable but is promoted if the self-assembly results in a thermodynamically stable structure. The reversibility of these steps allows for the most thermodynamically stable structure to be formed. Adapted from ref. 105

Williams *et al.* demonstrated that by working close to equilibrium (*i.e.* with small changes of Gibbs free energy), it is possible to form gels under thermodynamic control. [107] This is more akin to self-assembly in natural systems where conditions are overall constant, and assembly occurs through spatially confined molecular mechanisms.[18,149,150] Through reversible enzyme-catalysed condensation reactions, self-correction in the assembly process could occur. Thus, the most stable molecular self-assembly structures would be formed through thermodynamic control. Reactions were carried out

with a series of different nucleophilic dipeptides that could reversibly condense with *N*-protected amino acids, the final products having different stabilities. It was demonstrated, through HPLC analysis of the peptide chain formed, that the most stable structure would be produced in two methodologies. Firstly, with multiple nucleophiles present in the reaction media, the most stable product would form due to the reversibility of the reaction. In the second approach, this reversibility was exploited, as the nucleophile which produced the most stable structure could be added after structures were already formed. These would disassemble and reassemble after reaction with the preferred nucleophilic amino acids. This demonstrated that by working close to equilibrium, the most thermodynamically stable structures could be formed.

Overcoming serendipity

The thermodynamic and kinetic components of gelation make the *de novo* design of new gelators challenging. As previously mentioned, the assembly must favour one-dimensional growth into aggregates that can entangle to form a hydrogel network. Predicting which molecules will do this is difficult and gelation is often described as an empirical science with many gelators being discovered serendipitously.[39,92,136,151] Currently, *a priori* design rules are lacking for synthesising new gelators. Many analogues of gelators do not gel. Altering the gelator structure can affect its sterics, ability to form directional interactions and its conformations. For instance, Fmoc-TF-OMe (*N*-(fluorenyl-9-methyloxycarbonyl)-threonine-phenylalanine-propanoate) forms gels but replacing the threonine with serine produces a non-gelator.[152] The threonine analogue shields the methyl residue from water contact by inducing a twisted conformation and the additional chiral centre constrains the structure encouraging directional hydrogen-bonding. These features induce a twist as the self-assembled structures form to favour epitaxial growth and thus preventing indefinite growth in two dimensions. This causes, filaments, capable of gelling water, rather than two-dimensional sheets to form.

One approach to designing new gelators has been to link gelation to crystal structures, though it is not clear that there is a link between the interactions favouring crystallisation and gelation. [99] In fact, the

work previously mentioned by Uljn *et al.* demonstrates different interactions are key to fibre formation. [129] Further to this, multiple reports demonstrate different packing between the crystal and gel state. [139,153,154]

Library and computational approaches have also been employed to determine which similar candidates are likely to gel. For instance, Frederix *et al.* used coarse grain molecular dynamics to probe the aggregation propensity in water of all 8000 possible combinations of amino acids to form tripeptides. [50] Unsurprisingly, the most hydrophobic combinations exhibited the strongest propensity for aggregation (AP). However, amphiphilic peptides also demonstrate a tendency to aggregate and, as these are easier to dissolve, a positive bias was included in the model to favour hydrophilic amino acids. From this modified model, several design rules were generated, *e.g.* inclusion of proline on the N-terminus induces a kink and more ordered self-assembly or that zwitterionic peptides have an increased AP, presumably through the alignment of appositive charges. However, the rationale is not always straightforward. Though the structures generated are validated by reports in the literature and experimental observations. For instance, aggregation was confirmed with diffusion-ordered NMR and dynamic light scattering experiments and the conformation and structure were determined by Fourier-transform infrared spectroscopy and transmission electron microscopy.

Also, Gupta *et al.* used a computational approach to predict the gelation likelihood for different molecules. [155] Quantitative structure-property relationships were used, a technology that links measured properties to chemical structure, and have proven successful in drug discovery. However, a simple association between the physical descriptors and the capability to gel was not discovered. Thus, more complex models were developed and added to the approach. By using several techniques, it was possible to overcome the individual failings from each model in the hope to avoid false positives. Predictions by this approach were validated by literature reports and were expected to be more reliable if similar structures to the test molecules were submitted.

As gels are dynamic assemblies, another approach has been to create dynamic combinatorial libraries. These are formed by the combining components that react through reversible covalent bonds or non-covalent interactions. The structures can be adjusted through external stimuli and over time the distribution of products tends towards the thermodynamic minimum.[108] Such approaches can bias processes that form a gel phase and select components to form stable materials. Indeed, this approach was used to study derivatives of the versatile hydrazine functionalised guanosine gelator. Through this approach, Lehn and Sreenivasachary could determine the most stable derivative and present a strategy for others to determine the best selection of constituents form stable hydrogels. [144]

These approaches were powerful at determining similar candidates likely to gel but often lack an explanation as to why gelation occurs. However, the number of gelators discovered serendipitously indicates that their formation is a general phenomenon and a common process. Thus, it makes sense to seek the inspiration of self-assembly in water from nature for different classes of gelators are described below.

Gelators

Self-assembly is integral to the formation of many different intricate systems in nature and provides inspiration to design novel supramolecular structures. [70,71,85,151,156] For instance, biological systems have three key classes of biomolecules (nucleic acids, proteins and polysaccharides) which are excellent examples of molecules that self-assemble in water to carry out biological functions. Therefore, it is not surprising that these molecules provide inspiration for the discovery of new hydrogelators.

Sugars are good candidates as gelators as they are biocompatible and can be modified to tune their solubility. A common strategy is the introduction of an aromatic group to promote π-π stacking.[157,158] Bhattacharya and Acharya demonstrated that the acyclic derivates lacked the conformational rigidity to gel. [159] Whereas the cyclic derivatives were conformationally restricted imposing directional hydrogen bonding to encourage filament formation and subsequent hydrogelation.

Amino acids are another excellent candidate as hydrogelators as they are readily available, and there is extensive research into peptide synthesis and the structures that they form. Also, they have a vast sequence space available such that the balance of different physical properties can be encoded into the gelator structure.[159]

Oligopeptides often possess sufficient conformational flexibility to favour non-covalent interactions.[151] As a result, oligopeptide-based hydrogels are prevalent.[110,160–165] For example, Schneider and Pochan designed de novo β-hairpin peptides for the formation of supramolecular hydrogels.[161,165] These peptides exist in an unfolded, random coil structure and are very soluble in water. However, upon stimuli triggering their folding, the peptides undergo a conformational change to form amphiphilic β-hairpins and self-assemble into a highly crosslinked network of filaments yielding rigid hydrogels.

However, perhaps one of the most researched class of hydrogels are peptide amphiphiles. Protected amino acids, *i.e.* with an attached aromatic group, are of particular interest as these groups introduce a significant increase in possible intermolecular interactions through π-π stacking and the hydrophobic effect. For instance, Shi *et al.* demonstrated that by derivatizing phenylalanine with a cinnamoyl group they were able to form the smallest peptide-based hydrogelator to date, thus indicating that aromatic groups can provide sufficient aromatic-aromatic interactions to stabilise hydrogelation (Figure 1.#a).[166]

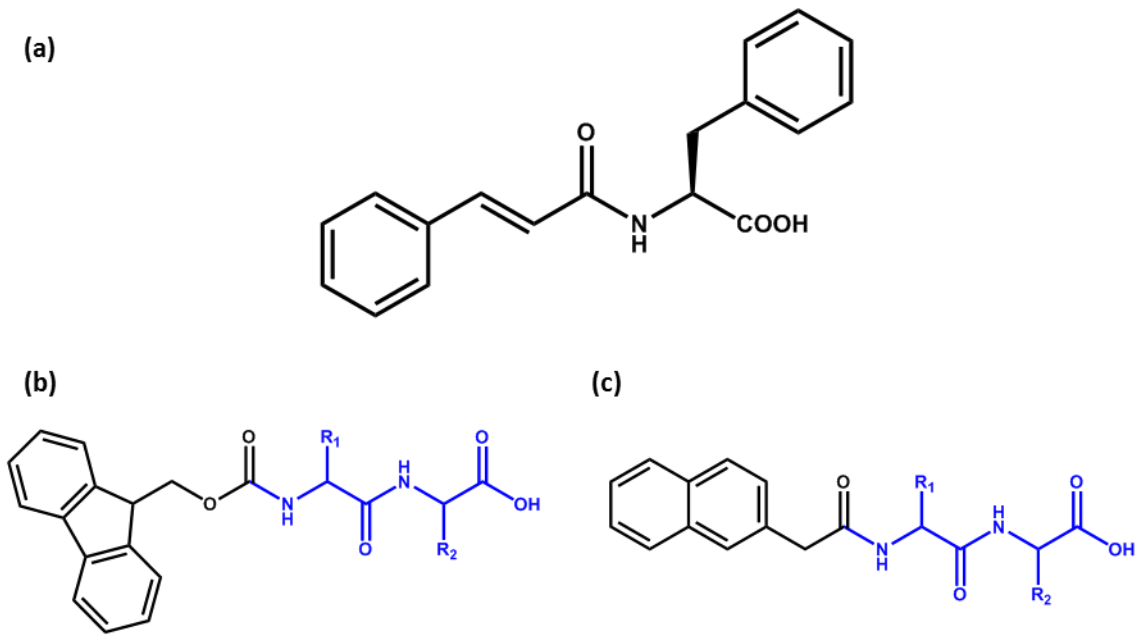

Figure 1.7 (a) Smallest peptide-based hydrogelator to date. Generic structure of (b) Fmoc- and (c) Naphthalene-based gelators, the aromatic substituent is in black and example of dipeptide chain is blue.

Therefore, it is not surprising that other aromatic motifs have been found to be capable of stabilising self-assembly. Zhang *et al.* unexpectedly discovered the first fluorenylmethyloxycarbonyl (Fmoc) dipeptide hydrogel during the synthesis of pyrene butyryl dialanine. [167] As a commercially available biomolecule, Fmoc-protected amino acids and peptides have been used a hydrogelator by multiple groups and have been extensively researched.

With biocompatibility in mind, alternative aromatic moieties were investigated, which lead to the use of naphthalene group as the protecting group in peptide-based hydrogels. As a common fragment found in clinically-approved drug molecules, *e.g.* propranolol, naphazoline and nafronyl, it has been found to be more biocompatible than the Fmoc group.[151] It has since been established that Naphthalene-di-phenylalanine is an exceptionally effective hydrogelator, leading it to become a motif to which other biofunctional molecules can be attached to.[168–170] For instance, Yang *et al*. reported d-Glucosamine-based supramolecular hydrogels capable of wound healing. [171] Also, the same group designed a hydrogelator which gelated *via* cleavage of phosphate group with the enzyme phosphatase and could be returned to sol state *via* phosphorylation in the presence of kinase and adenosine

triphosphate. [113] Significantly, subcutaneous injection of the phosphorylated hydrogelator in mice caused in vivo gelation and no long-term in vivo toxicity of the hydrogelator was observed.

Many hydrogels are also derived from nucleobases and their derivatives due to their existing propensity to self-assemble into higher order structures. The nucleobases, particularly the purines (adenine and guanine), have multiple faces for hydrogen bonding and these residues are readily able to π-stack with one another.[108] Furthermore, addition of either just a ribose sugar or also a phosphate group, forming either nucleosides or nucleotides, respectively, increases solubility and provides more motifs for intermolecular interactions.[108]

These water-soluble molecules often require derivatization to attach hydrophobic group to introduce the necessary degree of hydrophobicity for hydrogelation.[108] For instance, Park *et al.* demonstrated that introducing hydrophobic moieties to 2'-Deoxyuridine yielded a series of hydrogelators. [172] Prior to functionalisation, 2'-deoxyuridine itself is very hydrophilic due to the multiple functional groups capable of hydrogen bonding but derivatization allowed for a suitable balance between hydrophilicity and hydrophobicity to yield a series of hydrogels. Shimizu *et al.* demonstrated the gelation of 3'-phosphorylated thymidine bolaamphiphile. [173] Despite a variety of linker lengths being used, only the longer chains imparted sufficient hydrophobicity for gelation. Also, Shimizu *et al.* reported that it was necessary for the phosphate group to be ionised (*via* neutral or high pHs) to introduce sufficient solubility. Taken together, these two requirements further demonstrate the necessary balance between hydrophilicity and hydrophobicity for gelation *via* derivatization with functional groups.

Conversely, guanosine-based hydrogels can be formed without functionalization. For instance, guanosine monophosphate (GMP) hydrogels have been reported for more than 40 years, with most hydrogels being formed using acidic pH or by adding excess alkali metals. [174–176] This is possible due to the self-complementary hydrogen bonding present in the guanosine nucleobase.

A major limitation of such gels is their poor lifetime stability; arising from crystallisation of the nucleoside within a few hours causing a collapse of the hydrogel. [140–145] This occurs because of

hydrogelators in solution aggregate and forms a nucleation point thereby lowering the gelator concentration in solution allowing more hydrogelator molecules to be released from the gel and incorporated into the crystal. Davis *et al.* have overcome this by forming a guanosine-borate ester, and doing so elevates the solubility of guanosine to form a hydrogel with enhanced stability. [176]

Conversely, Dash *et al.* exploited the known ability for GMP to chelate silver ions, [177–179] to generate stable hydrogels without the need for functionalization. [156] Doing so yielded a gel matrix comprised of silver ions and nanofilaments adorned with discrete silver nanoparticles.

There are of course other classes of hydrogelators, with many being derivatives of small organic molecules. For instance, urea-based and pyridine-based moieties are common motifs used in hydrogelators.[138,180–184] Also, functionalisation of hydrophilic groups, *e.g.* dye molecules, acidic residues *etc.*, with alkyl groups introduces sufficient hydrophobicity to promote self-assembly and subsequent gelation. [119,138,185–188] Chromophores are another common motif as they often contain aromatic residues to allow for π- π stacking and hydrophobic interactions to encourage directional interactions promoting epitaxial growth, and can be functionalised to modulate water solubility allowing for filament formation. [25,27,189–192]

Multicomponent system

Owing to the diversity of gelators, a growing area of research is the formation of multicomponent supramolecular hydrogels through the gelation of two (or more) gelators. These gelators often have different functionality or responsiveness to a stimulus, *e.g.* light, pH, temperature *etc.* Also, the gelators can be combined with other components to affect their mechanical properties or long-term stability.

For instance, Ryan *et al.* stabilised Fmoc-F_5-Phenylalanine hydrogels through co-assembly with polyethyleneglycol (PEG) functionalised monomers. [193] Assembly of Fmoc-F_5-Phenylalanine alone produces unstable hydrogels, lasting only one to two weeks, due to the hydrophobic nature of the

gelator. Also, these gels wouldn't reform after being sheared, which is particularly relevant to biomedical applications,[161,194,195] as the hydrophobic fibrils were desolvated and couldn't reform. Thus, a proportion of the monomers were functionalised with PEG to increase solution phase stability. This produced a more stable hydrogel that also fully recovered after the cessation of strain.

Multicomponent supramolecular hydrogels are also appealing to optoelectronic applications as it should be possible to form bulk p-n heterojunctions from gelators with sufficiently different electronic properties.[25,136,190,196–198] For instance, Ardoña *et al.* demonstrated the kinetics of the co-assembly of different peptide-based chromophores determined the mixing of these gelators and hence the energy transport properties. [25] This is another example of the stimuli affecting the supramolecular ordering and consequently the properties of the material.

Also, the gelators in the multicomponent supramolecular hydrogels can have different stability to different stimuli *e.g.* light, heat, pH changes *etc.* For instance, Draper *et al.* could selectively remove the fibres of one gelator by a light-triggered gel-to-sol transition. [199] The ability to tune the network density and mechanical properties is appealing to drug release and tissue scaffold applications. [200,201]

The design of a new multicomponent supramolecular hydrogel is the focus of the work detailed in Chapter 4, along with an expanded introduction to multicomponent hydrogels. Presented is the gelation of one gelator used to trigger the gelation of the second gelator. The second gelator is more susceptible to pH and thus it is possible to selectively remove one gelator. It is also demonstrated that the kinetics of assembly dramatically affects the properties of the resulting hydrogel.

Applications

As a wide class of gelators exists, molecular hydrogels are excellent candidates for a diverse range of applications. The type of gelator can be chosen for different concerns (*i.e.* biocompatibility, processing, cost *etc.*) and can be functionalised. They also differ from crosslinked polymeric gels which often can't be altered once gelled. [99] Conversely, the network of molecular hydrogels is dynamic and

can be reversibly destroyed by a change environmental conditions (*e.g.* pH, ionic strength) or through the input of energy (*e.g.* heat, light, shear strain.)

The high water content and amphiphilic nature of molecular gels allows for high drug loading and makes them an ideal candidate to deliver therapeutic drugs. [202–206] These can be designed to break down and release their cargo under specific conditions such as pH or through enzyme hydrolysis to allow for very localised drug release. Molecular hydrogels can even be used to encapsulate live cells. [207,208]

The aforementioned properties *i.e.* high-water content, porosity, biocompatible materials also make hydrogels excellent candidate materials for tissue engineering. These are being researched to replace polymers which are often not adhesive to cells.[209] However, the structures formed are often susceptible to the experimental conditions used. For instance, Stupp *et al.* demonstrated that the thermodynamically favoured form of the peptide amphiphiles were long bundled fibres. Whereas, the metastable form of the peptide amphiphiles were short monodisperse fibres. The former promoted cell adhesion and survival.[24] Kasai *et al.* demonstrated that fibril structure was crucial for obtaining hydrogels with biological activity.[210]

As applied shear-strain can overcome the weak interactions responsible for filament assembly, [194,211–213] so-called 'shear-thinning' gels can be injected as a liquid and regel almost instantly. Gaharwar *et al.* produced a hydrogel containing silicate nanoplatelets which instantly re-gels after the high strain is removed.[195] The silicate nanoplatelets could induce blood clotting and therefore can be used as a physical barrier to prevent haemorrhage.

Alongside the network structure, the assembly into one-dimensional filaments is particularly relevant to photoresponsive applications. [116] The self-assembly of one-dimensional nanostructures may be the best candidate for use in electronic devices (such as field effect transistors or photovoltaic devices) due to their intriguing optoelectronic properties, which include sharp exciton transitions, high exciton mobilities and photoconductivity. [25,73,79,190,196–198,214,215] For instance, Weingarten *et al.* functionalised

a perylene monoimide chromophore that would gel through appropriate charge screening by introducing different salts or a cationic nickel catalyst.[27] The salt used affected H_2 production, with multivalent cations performing better than monovalent cations. This increases the electronic coupling of the chromophores and the nickel catalyst can be used for light-driven hydrogen production. Recent research by Dave Adams group has demonstrated several chromophores can be functionalised to form gels, with their conductivity improved and combined in multicomponent systems to form photonic donor–acceptor pairs. [25,191,196]

Summary

Summarised above are many opportunities to use the fundamental of self-assembly in water to form a myriad of structures and materials. Of these, hydrogels are perhaps one of the most interesting owing to their versatility and hierarchical assembly. As mentioned so far, the experimental conditions used for the formation of hydrogels can dramatically affect the supramolecular ordering of the gelators. As a result, these changes are then amplified in the hierarchical assembly to produce gels with very different properties, *e.g.* cell adhesion, energy transport, mechanical strengths *etc.*

Hence, the work carried out in this thesis will explore the effects of different stimuli on the assembly and properties of different hydrogels. Firstly, a novel stimulus, *i.e.* radicals, will be employed as a trigger for supramolecular gelation. Then the gelation of one gelator will be used to trigger the gelator of a second, pH-responsive, gelator to generate a novel multicomponent hydrogel. In both chapters, the consequence of these new stimuli on the supramolecular organisation and macroscopic properties of the gel will be investigated. For the third and final experimental chapter, silver will be used to trigger the gelation of guanosine monophosphate. The ratio of silver to gelator has already been demonstrated to affect the mechanical properties of this gel. Instead, the antibacterial properties of this material will be studied, and the stimulus chosen, *i.e.* molar ratio of silver, will be contrasted between samples and against gels formed without silver present.

References

(1) Mann, S. The Origins of Life: Old Problems, New Chemistries. *Angew. Chemie Int. Ed.* 2013, *52*, 155–162.

(2) Dzieciol, A. J.; Mann, S. Designs for Life: Protocell Models in the Laboratory. *Chem. Soc. Rev.* 2012, *41*, 79.

(3) Luisi, P. L. Chemistry Constraints on the Origin of Life. *Isr. J. Chem.* 2015, *55* (8), 906–918.

(4) Grzybowski, B. a.; Wilmer, C. E.; Kim, J.; Browne, K. P.; Bishop, K. J. M. Self-Assembly: From Crystals to Cells. *Soft Matter* 2009, *5* (6), 1110.

(5) Fleming, S.; Ulijn, R. V. Design of Nanostructures Based on Aromatic Peptide Amphiphiles. *Chem. Soc. Rev.* 2014, *43* (23), 8150–8177.

(6) Bishop, K. J. M.; Wilmer, C. E.; Soh, S.; Grzybowski, B. A. Nanoscale Forces and Their Uses in Self-Assembly. *Small* 2009, *5* (14), 1600–1630.

(7) Claessens, C. G.; Stoddart, J. F. Review Commentary: π-π Interactions in Self-Assembly. *J. Phys. Org. Chem.* 1997, *10* (5), 254–272.

(8) Prins, L. J.; Reinhoudt, D. N.; Timmerman, P. Noncovalent Synthesis Using Hydrogen Bonding. *Angew. Chemie Int. Ed.* 2001, *40* (13), 2382–2426.

(9) Meyer, E. E.; Rosenberg, K. J.; Israelachvili, J. Recent Progress in Understanding Hydrophobic Interactions. *Proc. Natl. Acad. Sci.* 2006, *103* (43), 15739–15746.

(10) Faul, C. F. J.; Antonietti, M. Ionic Self-Assembly: Facile Synthesis of Supramolecular Materials. *Adv. Mater.* 2003, *15* (9), 673–683.

(11) Boyle, J. Lehninger Principles of Biochemistry (4th Ed.): Nelson, D., and Cox, M. *Biochem. Mol. Biol. Educ.* 2005, *33* (1), 74–75.

(12) Wang, J.; Liu, K.; Xing, R.; Yan, X. Peptide Self-Assembly: Thermodynamics and Kinetics. *Chem. Soc. Rev.* 2016, *45* (20), 5589–5604.

(13) Park, J.; Joo, J.; Kwon, S. G.; Jang, Y.; Hyeon, T. Synthesis of Monodisperse Spherical Nanocrystals. *Angew. Chemie Int. Ed.* 2007, *46* (25), 4630–4660.

(14) Motte, L.; Billoudet, F.; Pileni, M. P. Self-Assembled Monolayer of Nanosized Particles Differing by Their Sizes. *J. Phys. Chem.* 1995, *99* (44), 16425–16429.

(15) Ascolani, H.; van der Meijden, M. W.; Cristina, L. J.; Gayone, J. E.; Kellogg, R. M.; Fuhr, J. D.; Lingenfelder, M. Van Der Waals Interactions in the Self-Assembly of 5-Amino[6]Helicene on Cu(100) and Au(111). *Chem. Commun.* 2014.

(16) Gao, H.-Y.; Wagner, H.; Held, P. A.; Du, S.; Gao, H.-J.; Studer, A.; Fuchs, H. In-Plane Van Der Waals Interactions of Molecular Self-Assembly Monolayer. *Appl. Phys. Lett.* 2015, *106* (8), 081606.

(17) Tahara, K.; Lei, S.; Adisoejoso, J.; De Feyter, S.; Tobe, Y. Supramolecular Surface-Confined Architectures Created by Self-Assembly of Triangular Phenylene–ethynylene Macrocycles via van Der Waals Interaction. *Chem. Commun* 2010, *46*, 8507–8525.

(18) Mendes, A. C.; Baran, E. T.; Reis, R. L.; Azevedo, H. S. Self-Assembly in Nature: Using the Principles of Nature to Create Complex Nanobiomaterials. *Wiley Interdiscip. Rev. Nanomedicine Nanobiotechnology* 2013, *5* (6), 582–612.

(19) Xu, X.-D.; Chen, C.-S.; Lu, B.; Cheng, S.-X.; Zhang, X.-Z.; Zhuo, R.-X. Coassembly of Oppositely Charged Short Peptides into Well-Defined Supramolecular Hydrogels. *J. Phys. Chem. B* 2010, *114* (7), 2365–2372.

(20) Carrick, L. M.; Aggeli, A.; Boden, N.; Fisher, J.; Ingham, E.; Waigh, T. A. Effect of Ionic Strength on the Self-Assembly, Morphology and Gelation of PH Responsive β-Sheet Tape-Forming Peptides. *Tetrahedron* 2007, *63* (31), 7457–7467.

(21) Hu, Y.; Lin, R.; Zhang, P.; Fern, J.; Cheetham, A. G.; Patel, K.; Schulman, R.; Kan, C.; Cui, H. Electrostatic-Driven Lamination and Untwisting of β-Sheet Assemblies. *ACS Nano* 2016, *10* (1), 880–888.

(22) Caplan, M. R.; Moore, P. N.; Zhang, S.; Kamm, R. D.; Lauffenburger, D. A. Self-Assembly of a β-Sheet Protein Governed by Relief of Electrostatic Repulsion Relative to van Der Waals Attraction. *Biomacromolecules* 2000, *1* (4), 627–631.

(23) Zou, Q.; Zhang, L.; Yan, X.; Wang, A.; Ma, G.; Li, J.; Möhwald, H.; Mann, S. Multifunctional Porous Microspheres Based on Peptide-Porphyrin Hierarchical Co-Assembly. *Angew. Chem. Int. Ed. Engl.* 2014, *53* (9), 2366–2370.

(24) Tantakitti, F.; Boekhoven, J.; Wang, X.; Kazantsev, R. V.; Yu, T.; Li, J.; Zhuang, E.; Zandi, R.; Ortony, J. H.; Newcomb, C. J.; Palmer, L. C.; Shekhawat, G. S.; De La Cruz, M. O.; Schatz, G. C.; Stupp, S. I. Energy Landscapes and Functions of Supramolecular Systems. *Nat. Mater.* 2016, *15* (4), 469–476.

(25) Ardoña, H. A. M.; Draper, E. R.; Citossi, F.; Wallace, M.; Serpell, L. C.; Adams, D. J.; Tovar, J. D. Kinetically Controlled Coassembly of Multichromophoric Peptide Hydrogelators and the Impacts on Energy Transport. *J. Am. Chem. Soc.* 2017, *139* (25), 8685–8692.

(26) Aumiller, W. M.; Keating, C. D. Phosphorylation-Mediated RNA/Peptide Complex Coacervation as a Model for Intracellular Liquid Organelles. *Nat. Chem.* 2015, *8* (2), 129–137.

(27) Weingarten, A. S.; Kazantsev, R. V.; Palmer, L. C.; McClendon, M.; Koltonow, A. R.; Samuel, A. P. S.; Kiebala, D. J.; Wasielewski, M. R.; Stupp, S. I. Self-Assembling Hydrogel Scaffolds for Photocatalytic Hydrogen Production. *Nat. Chem.* 2014, *6* (11), 964–970.

(28) Koga, S.; Williams, D. S.; Perriman, A. W.; Mann, S. [SI] Peptide–nucleotide Microdroplets as a Step towards a Membrane-Free Protocell Model. *Nat. Chem.* 2011, *3* (9), 720–724.

(29) Niece, K. L.; Hartgerink, J. D.; Donners, J. J. J. M.; Stupp, S. I. Self-Assembly Combining Two Bioactive Peptide-Amphiphile Molecules into Nanofibers by Electrostatic Attraction. *J. Am. Chem. Soc.* 2003, *125* (24), 7146–7147.

(30) Kalsin, A. M.; Fialkowski, M.; Paszewski, M.; Smoukov, S. K.; Bishop, K. J. M.; Grzybowski, B. A. Electrostatic Self-Assembly of Binary Nanoparticle Crystals with a Diamond-Like Lattice. *Science (80-.).* 2006, *312* (5772), 420–424.

(31) Liu, M.; Ishida, Y.; Ebina, Y.; Sasaki, T.; Hikima, T.; Takata, M.; Aida, T. An Anisotropic Hydrogel with Electrostatic Repulsion between Cofacially Aligned Nanosheets. *Nature* 2015, *517* (7532), 68–72.

(32) Dhotel, A.; Chen, Z.; Delbreilh, L.; Youssef, B.; Saiter, J.-M.; Tan, L. Molecular Motions in Functional Self-Assembled Nanostructures. *Int. J. Mol. Sci.* 2013, *14* (2), 2303–2333.

(33) Estroff, L. a; Hamilton, A. D. Water Gelation by Small Organic Molecules. *Chem. Rev.* 2004, *104* (3), 1201–1217.

(34) Adams, D. J.; Morris, K.; Chen, L.; Serpell, L. C.; Bacsa, J.; Day, G. M. The Delicate Balance

between Gelation and Crystallisation: Structural and Computational Investigations. *Soft Matter* 2010, *6* (17), 4144.

(35) Xing, P.; Li, P.; Chen, H.; Hao, A.; Zhao, Y. Understanding Pathway Complexity of Organic Micro/Nanofiber Growth in Hydrogen-Bonded Coassembly of Aromatic Amino Acids. *ACS Nano* 2017, *11* (4), 4206–4216.

(36) Yashima, E.; Ousaka, N.; Taura, D.; Shimomura, K.; Ikai, T.; Maeda, K. Supramolecular Helical Systems: Helical Assemblies of Small Molecules, Foldamers, and Polymers with Chiral Amplification and Their Functions. *Chem. Rev.* 2016, *116* (22), 13752–13990.

(37) Ooi, H. W.; Hafeez, S.; van Blitterswijk, C. A.; Moroni, L.; Baker, M. B. Hydrogels That Listen to Cells: A Review of Cell-Responsive Strategies in Biomaterial Design for Tissue Regeneration. *Mater. Horizons* 2017, *4* (6), 1020–1040.

(38) Poolman, J. M.; Boekhoven, J.; Besselink, A.; Olive, A. G. L.; Esch, J. H. Van; Eelkema, R.; van Esch, J. H.; Eelkema, R. Variable Gelation Time and Stiffness of Low-Molecular-Weight Hydrogels through Catalytic Control over Self-Assembly. *Nat. Protoc.* 2014, *9* (4), 977–988.

(39) Dong, R.; Pang, Y.; Su, Y.; Zhu, X. Supramolecular Hydrogels: Synthesis, Properties and Their Biomedical Applications. *Biomater. Sci.* 2015, *3* (7), 937–954.

(40) Souza, J. M.; Giasson, B. I.; Chen, Q.; Lee, V. M.-Y.; Ischiropoulos, H. Dityrosine Cross-Linking Promotes Formation of Stable α-Synuclein Polymers. *J. Biol. Chem.* 2000, *275* (24), 18344–18349.

(41) Amadò, R.; Aeschbach, R.; Neukom, H. Dityrosine: In Vitro Production and Characterization. *Methods Enzymol.* 1984, *107* (C), 377–388.

(42) Capeillere-Blandin, C.; Delaveau, T.; Descamps-Latscha, B. Structural Modifications of Human Beta 2 Microglobulin Treated with Oxygen-Derived Radicals. *Biochem. J.* 1991, *277 (Pt 1*, 175–182.

(43) Zhang, S.; Fox, D. M.; Urbanc, B. Insights into Formation and Structure of Aβ Oligomers Cross-Linked via Tyrosines. *J. Phys. Chem. B* 2017, *121* (22), 5523–5535.

(44) Gracanin, M.; Hawkins, C. L.; Pattison, D. I.; Davies, M. J. Singlet-Oxygen-Mediated Amino Acid and Protein Oxidation: Formation of Tryptophan Peroxides and Decomposition Products. *Free Radic. Biol. Med.* 2009, *47* (1), 92–102.

(45) Wright, A.; Bubb, W. A.; Hawkins, C. L.; Davies, M. J. Singlet Oxygen-Mediated Protein Oxidation: Evidence for the Formation of Reactive Side Chain Peroxides on Tyrosine Residues. *Photochem Photobiol* 2002, *76* (1), 35–46.

(46) Lee, D.-I.; Hwang, S.; Choi, J. Y.; Ahn, I.-S.; Lee, C.-H. A Convenient Preparation of Dityrosine via Mn(III)-Mediated Oxidation of Tyrosine. *Process Biochem.* 2008, *43* (9), 999–1003.

(47) Shamovsky, I. L.; Riopelle, R. J.; Ross, G. M. Ab Initio Studies on the Mechanism of Tyrosine Coupling. *J. Phys. Chem. A* 2001, *105* (6), 1061–1070.

(48) Kano, K.; Fukuda, K.; Wakami, H.; Nishiyabu, R.; Pasternack, R. F. Factors Influencing Self-Aggregation Tendencies of Cationic Porphyrins in Aqueous Solution. *J. Am. Chem. Soc.* 2000, *122* (31), 7494–7502.

(49) Tanford, C. The Hydrophobic Effect and the Organization of Living Matter. *Science (80-.).* 1978, *200* (4345), 1012–1018.

(50) Frederix, P. W. J. M.; Scott, G. G.; Abul-Haija, Y. M.; Kalafatovic, D.; Pappas, C. G.; Javid, N.;

Hunt, N. T.; Ulijn, R. V.; Tuttle, T. Exploring the Sequence Space for (Tri-)Peptide Self-Assembly to Design and Discover New Hydrogels. *Nat. Chem.* 2015, *7* (1), 30–37.

(51) Cockroft, S. L.; Perkins, J.; Zonta, C.; Adams, H.; Spey, S. E.; Low, C. M. R.; Vinter, J. G.; Lawson, K. R.; Urch, C. J.; Hunter, C. A. Substituent Effects on Aromatic Stacking Interactions. *Org. Biomol. Chem.* 2007, *5* (7), 1062.

(52) Liyanage, W.; Nilsson, B. L. Substituent Effects on the Self-Assembly/Coassembly and Hydrogelation of Phenylalanine Derivatives. *Langmuir* 2016, *32* (3), 787–799.

(53) Carver, F. J.; Hunter, C. A.; Carver, F. J.; Seward, E. M. Structure–activity Relationship for Quantifying Aromatic Interactions†. *Chem. Commun.* 1998, No. 7, 775–776.

(54) Cozzi, F.; Ponzini, F.; Annunziata, R.; Cinquini, M.; Siegel, J. S. Polar Interactions between Stackedπ Systems in Fluorinated 1,8-Diarylnaphthalenes: Importance of Quadrupole Moments in Molecular Recognition. *Angew. Chemie Int. Ed. English* 1995, *34* (9), 1019–1020.

(55) Burley, S.; Petsko, G. Aromatic-Aromatic Interaction: A Mechanism of Protein Structure Stabilization. *Science (80-.).* 1985, *229* (4708), 23–28.

(56) Tsonchev, S.; Niece, K. L.; Schatz, G. C.; Ratner, M. A.; Stupp, S. I. Phase Diagram for Assembly of Biologically-Active Peptide Amphiphiles †. *J. Phys. Chem. B* 2008, *112* (2), 441–447.

(57) Webber, M. J.; Langer, R. Drug Delivery by Supramolecular Design. *Chem. Soc. Rev.* 2017, *46* (21), 6600–6620.

(58) Sanchez, C.; Arribart, H.; Guille, M. M. G. Biomimetism and Bioinspiration as Tools for the Design of Innovative Materials and Systems. *Nat. Mater.* 2005, *4* (4), 277–288.

(59) Sanchez, C.; Belleville, P.; Popall, M.; Nicole, L. Applications of Advanced Hybrid Organic-Inorganic Nanomaterials: From Laboratory to Market. *Chem. Soc. Rev.* 2011, *40* (2), 696–753.

(60) Cornelissen, J. J. L. M.; Rowan, A. E.; Nolte, R. J. M.; Sommerdijk, N. A. J. M. Chiral Architectures from Macromolecular Building Blocks. *Chem. Rev.* 2001, *101* (12), 4039–4070.

(61) McConnell, I.; Li, G.; Brudvig, G. W. Energy Conversion in Natural and Artificial Photosynthesis. *Chem. Biol.* 2010, *17* (5), 434–447.

(62) Li, L.; Kang, S.; Harden, J.; Sun, Q.; Zhou, X.; Dai, L.; Jakli, A.; Kumar, S.; Li, Q. Nature-inspired Light-harvesting Liquid Crystalline Porphyrins for Organic Photovoltaics. *Liq. Cryst.* 2008, *35* (3), 233–239.

(63) Li, H.; LaBean, T. H.; Leong, K. W. Nucleic Acid-Based Nanoengineering: Novel Structures for Biomedical Applications. *Interface Focus* 2011, *1* (5), 702–724.

(64) Pinheiro, A. V.; Han, D.; Shih, W. M.; Yan, H. Challenges and Opportunities for Structural DNA Nanotechnology. *Nature Nanotechnology*. 2011, 763–772.

(65) Krishnan, Y.; Simmel, F. C. Nucleic Acid Based Molecular Devices. *Angew. Chem. Int. Ed. Engl.* 2011, *50* (14), 3124–3156.

(66) Dietz, H.; Douglas, S. M.; Shih, W. M. Folding DNA into Twisted and Curved Nanoscale Shapes. *Science (80-.).* 2009, *325* (5941), 725–730.

(67) Andersen, E. S.; Dong, M.; Nielsen, M. M.; Jahn, K.; Subramani, R.; Mamdouh, W.; Golas, M. M.; Sander, B.; Stark, H.; Oliveira, C. L. P.; Pedersen, J. S.; Birkedal, V.; Besenbacher, F.; Gothelf, K. V; Kjems, J. Self-Assembly of a Nanoscale DNA Box with a Controllable Lid. *Nature* 2009, *459* (7243), 73–76.

(68) Dan, N.; Safran, S. A. Effect of Lipid Characteristics on the Structure of Transmembrane Proteins. *Biophys. J.* 1998, *75* (3), 1410–1414.

(69) Lingwood, D.; Simons, K. Lipid Rafts As a Membrane-Organizing Principle. *Science (80-.).* 2010, *327* (5961), 46–50.

(70) Choi, M. S.; Yamazaki, T.; Yamazaki, I.; Aida, T. Bioinspired Molecular Design of Light-Harvesting Multiporphyrin Arrays. *Angew. Chemie - Int. Ed.* 2003, *43* (2), 150–158.

(71) McDermott, G.; Prince, S. M.; Freer, A. A.; Hawthornthwaite-Lawless, A. M.; Papiz, M. Z.; Cogdell, R. J.; Isaacs, N. W. Crystal Structure of an Integral Membrane Light-Harvesting Complex from Photosynthetic Bacteria. *Nature* 1995, *374* (6522), 517–521.

(72) Hoeben, F. J. M.; Jonkheijm, P.; Meijer, E. W.; Schenning, A. P. H. J. About Supramolecular Assemblies of Pi-Conjugated Systems. *Chem. Rev.* 2005, *105* (4), 1491–1546.

(73) Nam, Y. S.; Shin, T.; Park, H.; Magyar, A. P.; Choi, K.; Fantner, G.; Nelson, K. A.; Belcher, A. M. Virus-Templated Assembly of Porphyrins into Light-Harvesting Nanoantennae. *J. Am. Chem. Soc.* 2010, *132* (5), 1462–1463.

(74) Gust, D.; Moore, T. A.; Moore, A. L. Mimicking Photosynthetic Solar Energy Transduction. *Acc. Chem. Res.* 2001, *34* (1), 40–48.

(75) Kim, J. H.; Lee, M.; Lee, J. S.; Park, C. B. Self-Assembled Light-Harvesting Peptide Nanotubes for Mimicking Natural Photosynthesis. *Angew. Chemie - Int. Ed.* 2012, *51* (2), 517–520.

(76) Sundström, V.; Pullerits, T.; van Grondelle, R. Photosynthetic Light-Harvesting: Reconciling Dynamics and Structure of Purple Bacterial LH2 Reveals Function of Photosynthetic Unit. *J. Phys. Chem. B* 1999, *103* (13), 2327–2346.

(77) Fagadar-Cosma, E.; Mirica, M. C.; Balcu, I.; Bucovicean, C.; Cretu, C.; Armeanu, I.; Fagadar-Cosma, G. Syntheses, Spectroscopic and AFM Characterization of Some Manganese Porphyrins and Their Hybrid Silica Nanomaterials. *Molecules* 2009, *14* (4), 1370–1388.

(78) Schwab, A. D.; Smith, D. E.; Rich, C. S.; Young, E. R.; Smith, W. F.; de Paula, J. C.; Paula, J. C. De; de Paula, J. C. Porphyrin Nanorods. *J. Phys. Chem. B* 2003, *107* (41), 11339–11345.

(79) Schwab, A. D.; Smith, D. E.; Bond-Watts, B.; Johnston, D. E.; Hone, J.; Johnson, A. T.; de Paula, J. C.; Smith, W. F. Photoconductivity of Self-Assembled Porphyrin Nanorods. *Nano Lett.* 2004, *4* (7), 1261–1265.

(80) Ma, D.; Lin, Q.-M.; Zhang, L.-M.; Liang, Y.-Y.; Xue, W. A Star-Shaped Porphyrin-Arginine Functionalized Poly(L-Lysine) Copolymer for Photo-Enhanced Drug and Gene Co-Delivery. *Biomaterials* 2014, *35* (14), 4357–4367.

(81) Pisarek, S.; Maximova, K.; Gryko, D. Strategies toward the Synthesis of Amphiphilic Porphyrins. *Tetrahedron* 2014, *70* (38), 6685–6715.

(82) Dong, R.; Bo, Y.; Tong, G.; Zhou, Y.; Zhu, X.; Lu, Y. Self-Assembly and Optical Properties of a Porphyrin-Based Amphiphile. *Nanoscale* 2014, *6* (9), 4544.

(83) Brown, E.; Verkade, P. The Use of Markers for Correlative Light Electron Microscopy. *Protoplasma* 2010, *244* (1–4), 91–97.

(84) De Luca, G.; Romeo, A.; Scolaro, L. M. Counteranion Dependent Protonation and Aggregation of Tetrakis(4-Sulfonatophenyl)Porphyrin in Organic Solvents. *J. Phys. Chem. B* 2006, *110* (14), 7309–7315.

(85) Patil, A. J.; Lee, Y. C.; Yang, J. W.; Mann, S. Mesoscale Integration in Titania/J-Aggregate Hybrid Nanofibers. *Angew. Chemie - Int. Ed.* 2012, *51* (3), 733–737.

(86) Arteaga, O.; Canillas, A.; Crusats, J.; El-Hachemi, Z.; Llorens, J.; Sacristan, E.; Ribo, J. M. Emergence of Supramolecular Chirality by Flows. *ChemPhysChem* 2010, *11* (16), 3511–3516.

(87) Escudero, C.; D'Urso, A.; Lauceri, R.; Bonaccorso, C.; Sciotto, D.; Di Bella, S.; El-Hachemi, Z.; Crusats, J.; Ribó, J. M.; Purrello, R. Hierarchical Dependence of Porphyrin Self-Aggregation: Controlling and Exploiting the Complexity. *J. Porphyr. Phthalocyanines* 2010, *14* (08), 708–712.

(88) Lloyd, J. D. *Colloid Chemistry I*; Antonietti, M., Ed.; Topics in Current Chemistry; Springer Berlin Heidelberg: Berlin, Heidelberg, 2003; Vol. 226.

(89) Helman, P. H. Physics and Chemistry of Cellulose Fibres. In *Colloid Science*; Elsevier, 1949; 483–650.

(90) Weiss, R. G. The Past, Present, and Future of Molecular Gels. What Is the Status of the Field, and Where Is It Going? *J. Am. Chem. Soc.* 2014, *136* (21), 7519–7530.

(91) Ferry, J. D. *Viscoelastic Properties of Polymers*; 1980.

(92) Sangeetha, N. M.; Maitra, U. Supramolecular Gels: Functions and Uses. *Chem. Soc. Rev.* 2005, *34* (10), 821.

(93) Lan, Y.; Corradini, M. G.; Weiss, R. G.; Raghavan, S. R.; Rogers, M. A. To Gel or Not to Gel: Correlating Molecular Gelation with Solvent Parameters. *Chem. Soc. Rev.* 2015, *44* (17), 6035–6058.

(94) Ryan, D. M.; Anderson, S. B.; Senguen, F. T.; Youngman, R. E.; Nilsson, B. L. Self-Assembly and Hydrogelation Promoted by F 5 -Phenylalanine. *Soft Matter* 2010, *6* (3), 475–479.

(95) Weiss, R. G.; Terech, P. *Molecular Gels*; Weiss, R. G., Terech, P., Eds.; Springer Netherlands: Dordrecht, 2006.

(96) Li, J.-L.; Liu, X.-Y.; Wang, R.-Y.; Xiong, J.-Y. Architecture of a Biocompatible Supramolecular Material by Supersaturation-Driven Fabrication of Its Fiber Network. *J. Phys. Chem. B* 2005, *109* (51), 24231–24235.

(97) Wang, R.-Y.; Liu, X.-Y.; Narayanan, J.; Xiong, J.-Y.; Li, J.-L. Architecture of Fiber Network: From Understanding to Engineering of Molecular Gels. *J. Phys. Chem. B* 2006, *110* (51), 25797–25802.

(98) Liu, X. Y. Gelation with Small Molecules: From Formation Mechanism to Nanostructure Architecture; Springer, Berlin, Heidelberg, 2005; 1–37.

(99) Draper, E. R.; Adams, D. J. Low-Molecular-Weight Gels: The State of the Art. *Chem* 2017, *3* (3), 390–410.

(100) Hule, R. A.; Nagarkar, R. P.; Hammouda, B.; Schneider, J. P.; Pochan, D. J. Dependence of Self-Assembled Peptide Hydrogel Network Structure on Local Fibril Nanostructure. *Macromolecules* 2009, *42* (18), 7137–7145.

(101) Cardoso, A. Z.; Mears, L. L. E.; Cattoz, B. N.; Griffiths, P. C.; Schweins, R.; Adams, D. J. Linking Micellar Structures to Hydrogelation for Salt-Triggered Dipeptide Gelators. *Soft Matter* 2016, *12* (15), 3612–3621.

(102) Adams, D. J.; Draper, E.; Su, H.; Brasnett, C.; Poole, R.; Rogers, S.; Cui, H.; Seddon, A. Opening a Can of Worm(-like Micelle)s: The Effect of Temperature of Solutions of Functionalised

Dipeptides. *Angew. Chemie Int. Ed.* 2017.

(103) Sadownik, J. W.; Leckie, J.; Ulijn, R. V. Micelle to Fibre Biocatalytic Supramolecular Transformation of an Aromatic Peptide Amphiphile. *Chem. Commun.* 2011, *47* (2), 728–730.

(104) Thornton, K.; Abul-Haija, Y. M.; Hodson, N.; Ulijn, R. V. Mechanistic Insights into Phosphatase Triggered Self-Assembly Including Enhancement of Biocatalytic Conversion Rate. *Soft Matter* 2013, *9* (39), 9430.

(105) Lee, O.-S.; Cho, V.; Schatz, G. C. Modeling the Self-Assembly of Peptide Amphiphiles into Fibers Using Coarse-Grained Molecular Dynamics. *Nano Lett.* 2012, *12* (9), 4907–4913.

(106) Abul-Haija, Y. M.; Roy, S.; Frederix, P. W. J. M.; Javid, N.; Jayawarna, V.; Ulijn, R. V. Biocatalytically Triggered Co-Assembly of Two-Component Core/Shell Nanofibers. *Small* 2014, *10* (5), 973–979.

(107) Williams, R. J.; Smith, A. M.; Collins, R.; Hodson, N.; Das, A. K.; Ulijn, R. V. Enzyme-Assisted Self-Assembly under Thermodynamic Control. *Nat. Nanotechnol.* 2009, *4* (1), 19–24.

(108) Peters, G. M.; Davis, J. T. Supramolecular Gels Made from Nucleobase, Nucleoside and Nucleotide Analogs. *Chem. Soc. Rev.* 2016, *45* (11), 3188–3206.

(109) George, M.; Weiss, R. G. Molecular Organogels. Soft Matter Comprised of Low-Molecular-Mass Organic Gelators and Organic Liquids. *Acc. Chem. Res.* 2006, *39* (8), 489–497.

(110) Salick, D. A.; Kretsinger, J. K.; Pochan, D. J.; Schneider, J. P. Inherent Antibacterial Activity of a Peptide-Based β-Hairpin Hydrogel. *J. Am. Chem. Soc.* 2007, *129* (47), 14793–14799.

(111) Patil, A. J.; Kumar, R. K.; Barron, N. J.; Mann, S. Cerium Oxide Nanoparticle-Mediated Self-Assembly of Hybrid Supramolecular Hydrogels. *Chem. Commun.* 2012, *48* (64), 7934.

(112) Yang, Z.; Gu, H.; Fu, D.; Gao, P.; Lam, J. K.; Xu, B. Enzymatic Formation of Supramolecular Hydrogels. *Adv. Mater.* 2004, *16* (16), 1440–1444.

(113) Yang, Z.; Liang, G.; Wang, L.; Xu, B. Using a Kinase/Phosphatase Switch to Regulate a Supramolecular Hydrogel and Forming the Supramolecular Hydrogel in Vivo. *J. Am. Chem. Soc.* 2006, *128* (9), 3038–3043.

(114) Edwards, W.; Smith, D. K. Enantioselective Component Selection in Multicomponent Supramolecular Gels. *J. Am. Chem. Soc.* 2014, *136* (3), 1116–1124.

(115) Edwards, W.; Smith, D. K. Dynamic Evolving Two-Component Supramolecular Gels—Hierarchical Control over Component Selection in Complex Mixtures. *J. Am. Chem. Soc.* 2013, *135* (15), 5911–5920.

(116) Babu, S. S.; Praveen, V. K.; Ajayaghosh, A. Functional π-Gelators and Their Applications. *Chem. Rev.* 2014, *114* (4), 1973–2129.

(117) Aufderhorst-Roberts, A.; Frith, W. J.; Donald, A. M. Micro-Scale Kinetics and Heterogeneity of a PH Triggered Hydrogel. *Soft Matter* 2012, *8* (21), 5940–5946.

(118) Adams, D. J.; Butler, M. F.; Frith, W. J.; Kirkland, M.; Mullen, L.; Sanderson, P. A New Method for Maintaining Homogeneity during Liquid–hydrogel Transitions Using Low Molecular Weight Hydrogelators. *Soft Matter* 2009, *5* (9), 1856.

(119) Wang, H.; Yang, Z.; Adams, D. J. Controlling Peptide Based Hydrogelation. *Mater. Today* 2012, *15* (11), 500–507.

(120) Greenfield, M. A.; Hoffman, J. R.; Olvera de la Cruz, M.; Stupp, S. I. Tunable Mechanics of

Peptide Nanofiber Gels. *Langmuir* 2010, *26* (5), 3641–3647.

(121) Roy, S.; Javid, N.; Sefcik, J.; Halling, P. J.; Ulijn, R. V. Salt-Induced Control of Supramolecular Order in Biocatalytic Hydrogelation. *Langmuir* 2012, *28* (48), 16664–16670.

(122) Helen, W.; de Leonardis, P.; Ulijn, R. V.; Gough, J.; Tirelli, N. Mechanosensitive Peptide Gelation: Mode of Agitation Controls Mechanical Properties and Nano-Scale Morphology. *Soft Matter* 2011, *7* (5), 1732–1740.

(123) Raeburn, J.; Zamith Cardoso, A.; Adams, D. J. The Importance of the Self-Assembly Process to Control Mechanical Properties of Low Molecular Weight Hydrogels. *Chem. Soc. Rev.* 2013, *42* (12), 5143.

(124) Ding, B.; Li, Y.; Qin, M.; Ding, Y.; Cao, Y.; Wang, W. Two Approaches for the Engineering of Homogeneous Small-Molecule Hydrogels. *Soft Matter* 2013, *9* (18), 4672.

(125) Chen, L.; Raeburn, J.; Sutton, S.; Spiller, D. G.; Williams, J.; Sharp, J. S.; Griffiths, P. C.; Heenan, R. K.; King, S. M.; Paul, A.; Furzeland, S.; Atkins, D.; Adams, D. J. Tuneable Mechanical Properties in Low Molecular Weight Gels. *Soft Matter* 2011, *7* (20), 9721.

(126) Korevaar, P. A.; Newcomb, C. J.; Meijer, E. W.; Stupp, S. I. Pathway Selection in Peptide Amphiphile Assembly. *J. Am. Chem. Soc.* 2014, *136* (24), 8540–8543.

(127) Barker, E. C.; Martin, A. D.; Garvey, C. J.; Goh, C. Y.; Jones, F.; Mocerino, M.; Skelton, B. W.; Ogden, M. I.; Becker, T. Thermal Annealing Behaviour and Gel to Crystal Transition of a Low Molecular Weight Hydrogelator. *Soft Matter* 1006, *13* (13), 1006–1011.

(128) Otero, R.; Schöck, M.; Molina, L. M.; Laegsgaard, E.; Stensgaard, I.; Hammer, B.; Besenbacher, F. Guanine Quartet Networks Stabilized by Cooperative Hydrogen Bonds. *Angew. Chemie Int. Ed.* 2005, *44* (15), 2270–2275.

(129) Ramos Sasselli, I.; Halling, P. J.; Ulijn, R. V.; Tuttle, T. Supramolecular Fibers in Gels Can Be at Thermodynamic Equilibrium: A Simple Packing Model Reveals Preferential Fibril Formation versus Crystallization. *ACS Nano* 2016, *10* (2), 2661–2668.

(130) Deng, M.; Zhang, L.; Jiang, Y.; Liu, M. Role of Achiral Nucleobases in Multicomponent Chiral Self-Assembly: Purine-Triggered Helix and Chirality Transfer. *Angew. Chemie Int. Ed.* 2016, *55* (48), 15062–15066.

(131) Tang, C.; Ulijn, R. V.; Saiani, A. Effect of Glycine Substitution on Fmoc-Diphenylalanine Self-Assembly and Gelation Properties. *Langmuir* 2011, *27* (23), 14438–14449.

(132) Fleming, S.; Frederix, P. W. J. M.; Ramos Sasselli, I.; Hunt, N. T.; Ulijn, R. V.; Tuttle, T. Assessing the Utility of Infrared Spectroscopy as a Structural Diagnostic Tool for β-Sheets in Self-Assembling Aromatic Peptide Amphiphiles. *Langmuir* 2013, *29* (30), 9510–9515.

(133) Cheng, G.; Castelletto, V.; Moulton, C. M.; Newby, G. E.; Hamley, I. W. Hydrogelation and Self-Assembly of Fmoc-Tripeptides: Unexpected Influence of Sequence on Self-Assembled Fibril Structure, and Hydrogel Modulus and Anisotropy. *Langmuir* 2010, *26* (7), 4990–4998.

(134) Fleming, S.; Debnath, S.; Frederix, P. W. J. M.; Tuttle, T.; Ulijn, R. V. Aromatic Peptide Amphiphiles: Significance of the Fmoc Moiety. *Chem. Commun. (Camb).* 2013, *49*, 10587–10589.

(135) Wu, S.; Gao, J.; Emge, T. J.; Rogers, M. A. Influence of Solvent on the Supramolecular Architectures in Molecular Gels. *Soft Matter* 2013, *9* (25), 5942.

(136) Raeburn, J.; Adams, D. J. Multicomponent Low Molecular Weight Gelators. *Chem. Commun.*

2015, *51* (25), 5170–5180.

(137) Nebot, V. J.; Armengol, J.; Smets, J.; Prieto, S. F.; Escuder, B.; Miravet, J. F. Molecular Hydrogels from Bolaform Amino Acid Derivatives: A Structure-Properties Study Based on the Thermodynamics of Gel Solubilization. *Chem. - A Eur. J.* 2012, *18* (13), 4063–4072.

(138) Du, X.; Zhou, J.; Shi, J.; Xu, B. Supramolecular Hydrogelators and Hydrogels: From Soft Matter to Molecular Biomaterials. *Chem. Rev.* 2015, *115* (24), 13165–13307.

(139) Draper, E. R.; Morris, K. L.; Little, M. A.; Raeburn, J.; Colquhoun, C.; Cross, E. R.; McDonald, T. O.; Serpell, L. C.; Adams, D. J. Hydrogels Formed from Fmoc Amino Acids. *CrystEngComm* 2015, *17* (42), 8047–8057.

(140) Buerkle, L. E.; Li, Z.; Jamieson, A. M.; Rowan, S. J. Tailoring the Properties of Guanosine-Based Supramolecular Hydrogels. *Langmuir* 2009, *25* (15), 8833–8840.

(141) Way, A. E.; Korpusik, A. B.; Dorsey, T. B.; Buerkle, L. E.; von Recum, H. A.; Rowan, S. J. Enhancing the Mechanical Properties of Guanosine-Based Supramolecular Hydrogels with Guanosine-Containing Polymers. *Macromolecules* 2014, *47* (5), 1810–1818.

(142) Peters, G. M.; Skala, L. P.; Plank, T. N.; Hyman, B. J.; Manjunatha Reddy, G. N.; Marsh, A.; Brown, S. P.; Davis, J. T. A G 4 ·K + Hydrogel Stabilized by an Anion. *J. Am. Chem. Soc.* 2014, *136* (36), 12596–12599.

(143) Bimalendu Adhikari, P.; Kraatz, H.-B.; Adhikari, B.; Afzal Shah ac, ab; Shah, A.; Kraatz, H.-B. Self-Assembly of Guanosine and Deoxy-Guanosine into Hydrogels: Monovalent Cation Guided Modulation of Gelation, Morphology and Self-Healing Properties. *J. Mater. Chem. B* 2014, *2* (30), 4802.

(144) Sreenivasachary, N.; Lehn, J.-M. Gelation-Driven Component Selection in the Generation of Constitutional Dynamic Hydrogels Based on Guanine-Quartet Formation. *Proc. Natl. Acad. Sci.* 2005, *102*, 5938–5943.

(145) Li, Z.; Buerkle, L. E.; Orseno, M. R.; Streletzky, K. A.; Seifert, S.; Jamieson, A. M.; Rowan, S. J. Structure and Gelation Mechanism of Tunable Guanosine-Based Supramolecular Hydrogels. *Langmuir* 2010, *26* (12), 10093–10101.

(146) Dreiss, C. A. Wormlike Micelles: Where Do We Stand? Recent Developments, Linear Rheology and Scattering Techniques. *Soft Matter* 2007, *3* (8), 956–970.

(147) Berret, J.-F. Rheology of Wormlike Micelles: Equilibrium Properties and Shear Banding Transitions. In *Molecular Gels*; Springer-Verlag: Berlin/Heidelberg, 2005; 667–720.

(148) Yan, C.; Pochan, D. J. Rheological Properties of Peptide-Based Hydrogels for Biomedical and Other Applications. *Chem. Soc. Rev.* 2010, *39* (9), 3528.

(149) Kumar, D. K.; Steed, J. W. Supramolecular Gel Phase Crystallization: Orthogonal Self-Assembly under Non-Equilibrium Conditions. *Chem. Soc. Rev.* 2014, *43* (7), 2080–2088.

(150) Ogi, S.; Sugiyasu, K.; Manna, S.; Samitsu, S.; Takeuchi, M. Living Supramolecular Polymerization Realized through a Biomimetic Approach. *Nat. Chem.* 2014, *6* (3), 188–195.

(151) Du, X.; Zhou, J.; Xu, B. Supramolecular Hydrogels Made of Basic Biological Building Blocks. *Chem. - An Asian J.* 2014, *9* (6), 1446–1472.

(152) Hughes, M.; Xu, H.; Frederix, P. W. J. M.; Smith, A. M.; Hunt, N. T.; Tuttle, T.; Kinloch, I. A.; Ulijn, R. V.; Kale, L.; Schulten, K.; Popelier, P. L. A.; Turner, M. L.; Xiao, P.; Kinloch, I. A.; Ulijn, R. V. Biocatalytic Self-Assembly of 2D Peptide-Based Nanostructures. *Soft Matter* 2011, *7* (21),

10032.

(153) Houton, K. A.; Morris, K. L.; Chen, L.; Schmidtmann, M.; Jones, J. T. A.; Serpell, L. C.; Lloyd, G. O.; Adams, D. J. On Crystal versus Fiber Formation in Dipeptide Hydrogelator Systems. *Langmuir* 2012, *28* (25), 9797–9806.

(154) Barker, E. C.; Martin, A. D.; Garvey, C. J.; Goh, C. Y.; Jones, F.; Mocerino, M.; Skelton, B. W.; Ogden, M. I.; Becker, T. Thermal Annealing Behaviour and Gel to Crystal Transition of a Low Molecular Weight Hydrogelator. *Soft Matter* 2017, *13* (5), 1006–1011.

(155) Gupta, J. K.; Adams, D. J.; Berry, N. G. Will It Gel? Successful Computational Prediction of Peptide Gelators Using Physicochemical Properties and Molecular Fingerprints. *Chem. Sci.* 2016, *7* (7), 4713–4719.

(156) Dash, J.; Patil, A. J.; Das, R. N.; Dowdall, F. L.; Mann, S. Supramolecular Hydrogels Derived from Silver Ion-Mediated Self-Assembly of 5′-Guanosine Monophosphate. *Soft Matter* 2011, *7* (18), 8120.

(157) Kobayashi, H.; Koumoto, K.; Hwa Jung, J.; Shinkai, S. Sol–gel Phase Transition Induced by Fiber–vesicle Structural Changes in Sugar-Based Bolaamphiphiles. *J. Chem. Soc., Perkin Trans. 2* 2002, No. 11, 1930–1936.

(158) Yoza, K.; Amanokura, N.; Ono, Y.; Akao, T.; Shinmori, H.; Takeuchi, M.; Shinkai, S.; Reinhoudt, D. N. Sugar-Integrated Gelators of Organic Solvents—Their Remarkable Diversity in Gelation Ability and Aggregate Structure. *Chem. - A Eur. J.* 1999, *5* (9), 2722–2729.

(159) Bhattacharya, S.; Acharya, S. N. G. Pronounced Hydrogel Formation by the Self-Assembled Aggregates of N -Alkyl Disaccharide Amphiphiles. *Chem. Mater.* 1999, *11* (12), 3504–3511.

(160) Rajagopal, K.; Lamm, M. S.; Haines-Butterick, L. A.; Pochan, D. J.; Schneider, J. P. Tuning the PH Responsiveness of β-Hairpin Peptide Folding, Self-Assembly, and Hydrogel Material Formation. *Biomacromolecules* 2009, *10* (9), 2619–2625.

(161) Schneider, J. P.; Pochan, D. J.; Ozbas, B.; Rajagopal, K.; Pakstis, L.; Kretsinger, J. Responsive Hydrogels from the Intramolecular Folding and Self-Assembly of a Designed Peptide. *J. Am. Chem. Soc.* 2002, *124* (50), 15030–15037.

(162) Bokhari, M. A.; Akay, G.; Zhang, S.; Birch, M. A. The Enhancement of Osteoblast Growth and Differentiation in Vitro on a Peptide Hydrogel—polyHIPE Polymer Hybrid Material. *Biomaterials* 2005, *26* (25), 5198–5208.

(163) Luo, Y.; Shoichet, M. S. A Photolabile Hydrogel for Guided Three-Dimensional Cell Growth and Migration. *Nat. Mater.* 2004, *3* (4), 249–253.

(164) Nagai, Y.; Unsworth, L. D.; Koutsopoulos, S.; Zhang, S. Slow Release of Molecules in Self-Assembling Peptide Nanofiber Scaffold. *J. Control. Release* 2006, *115* (1), 18–25.

(165) Ozbas, B.; Kretsinger, J.; Rajagopal, K.; Schneider, J. P.; Pochan, D. J.; Bulent Ozbas, †; Juliana Kretsinger, ‡; Karthikan Rajagopal, ‡; Joel P. Schneider, *,‡ and; Darrin J. Pochan*, †. Salt-Triggered Peptide Folding and Consequent Self-Assembly into Hydrogels with Tunable Modulus. *Macromolecules* 2004, *37* (19), 7331–7337.

(166) Shi, J.; Gao, Y.; Yang, Z.; Xu, B. Exceptionally Small Supramolecular Hydrogelators Based on Aromatic–aromatic Interactions. *Beilstein J. Org. Chem.* 2011, *7* (1), 167–172.

(167) Zhang, Y.; Gu, H.; Yang, Z.; Xu, B. Supramolecular Hydrogels Respond to Ligand-Receptor Interaction. *J. Am. Chem. Soc.* 2003, *125* (45), 13680–13681.

(168) Li, J.; Gao, Y.; Kuang, Y.; Shi, J.; Du, X.; Zhou, J.; Wang, H.; Yang, Z.; Xu, B. Dephosphorylation of d -Peptide Derivatives to Form Biofunctional, Supramolecular Nanofibers/Hydrogels and Their Potential Applications for Intracellular Imaging and Intratumoral Chemotherapy. *J. Am. Chem. Soc.* 2013, *135* (26), 9907–9914.

(169) McCloskey, A.; Gilmore, B.; Laverty, G. Evolution of Antimicrobial Peptides to Self-Assembled Peptides for Biomaterial Applications. *Pathogens* 2014, *3* (4), 791–821.

(170) Laverty, G.; McCloskey, A. P.; Gilmore, B. F.; Jones, D. S.; Zhou, J.; Xu, B. Ultrashort Cationic Naphthalene-Derived Self-Assembled Peptides as Antimicrobial Nanomaterials. *Biomacromolecules* 2014, *15* (9), 3429–3439.

(171) Yang, Z.; Liang, G.; Ma, M.; Abbah, A. S.; Lu, W. W.; Xu, B. D-Glucosamine-Based Supramolecular Hydrogels to Improve Wound Healing. *Chem. Commun.* 2007, *0* (8), 843–845.

(172) Park, S. M.; Lee, Y. S.; Kim, B. H. Novel Low-Molecular-Weight Hydrogelators Based on 2'-Deoxyuridine. *Chem. Commun.* 2003, *0* (23), 2912–2913.

(173) Iwaura, R.; Yoshida, K.; Masuda, M.; Yase, K.; Shimizu, T. Spontaneous Fiber Formation and Hydrogelation of Nucleotide Bolaamphiphiles. *Chem. Mater.* 2002, *14* (7), 3047–3053.

(174) Gellert, M.; Lipsett, M. N.; Davies, D. R. Helix Formation by Guanylic Acid. *Proc. Natl. Acad. Sci. U. S. A.* 1962, *48* (12), 2013–2018.

(175) Davis, J. T. G-Quartets 40 Years Later: From 5???-GMP to Molecular Biology and Supramolecular Chemistry. *Angew. Chemie Int. Ed.* 2004, *43* (6), 668–698.

(176) Peters, G. M.; Skala, L. P.; Plank, T. N.; Oh, H.; Manjunatha Reddy, G. N.; Marsh, A.; Brown, S. P.; Raghavan, S. R.; Davis, J. T. G4-Quartet·M(+) Borate Hydrogels. *J. Am. Chem. Soc.* 2015.

(177) Loo, K.; Degtyareva, N.; Park, J.; Sengupta, B.; Reddish, M.; Rogers, C. C.; Bryant, A.; Petty, J. T. Ag + -Mediated Assembly of 5'-Guanosine Monophosphate. *J. Phys. Chem. B* 2010, *114* (12), 4320–4326.

(178) Tu, A. T.; Reinosa, J. A. The Interaction of Silver Ion with Guanosine, Guanosine Monophosphate, and Related Compounds. Determination of Possible Sites of Complexing. *Biochemistry* 1966, *5* (10), 3375–3383.

(179) Li, M.; Oakley, R. J.; Bevan, H.; Smarsly, B. M.; Mann, S.; Faul, C. F. J. Nucleotide-Based Templates for Nanoparticle Production-Exploiting Multiple Noncovalent Interactions. *Chem. Mater* 2009, *21*, 3270–3274.

(180) Coubrough, H. M.; Jones, C. D.; Yufit, D. S.; Steed, J. W. Gelation by Histidine-Derived Ureas. *Supramol. Chem.* 2018, *30* (5–6), 384–394.

(181) Steed, J. W. Anion-Tuned Supramolecular Gels: A Natural Evolution from Urea Supramolecular Chemistry. *Chem. Soc. Rev.* 2010, *39* (10), 3686.

(182) Dawn, A.; Andrew, K. S.; Yufit, D. S.; Hong, Y.; Reddy, J. P.; Jones, C. D.; Aguilar, J. A.; Steed, J. W. Supramolecular Gel Control of Cisplatin Crystallization: Identification of a New Solvate Form Using a Cisplatin-Mimetic Gelator. *Cryst. Growth Des.* 2015, *15* (9), 4591–4599.

(183) Foster, J. A.; Piepenbrock, M.-O. M.; Lloyd, G. O.; Clarke, N.; Howard, J. A. K.; Steed, J. W. Anion-Switchable Supramolecular Gels for Controlling Pharmaceutical Crystal Growth. *Nat. Chem.* 2010, *2* (12), 1037–1043.

(184) Seo, J.; Chung, J. W.; Cho, I.; Park, S. Y. Concurrent Supramolecular Gelation and Fluorescence Turn-on Triggered by Coordination of Silver Ion. *Soft Matter* 2012, *8* (29), 7617.

(185) Hanabusa, K.; Miki, T.; Taguchi, Y.; Koyama, T.; Shirai, H. Two-Component, Small Molecule Gelling Agents. *J. Chem. Soc. Chem. Commun.* 1993, No. 18, 1382.

(186) Gillissen, M. A. J.; Koenigs, M. M. E.; Spiering, J. J. H.; Vekemans, J. A. J. M.; Palmans, A. R. A.; Voets, I. K.; Meijer, E. W. Triple Helix Formation in Amphiphilic Discotics: Demystifying Solvent Effects in Supramolecular Self-Assembly. *J. Am. Chem. Soc.* 2014, *136* (1), 336–343.

(187) Dasgupta, A.; Mondal, J. H.; Das, D. Peptide Hydrogels. *RSC Adv.* 2013, *3* (24), 9117.

(188) Baral, A.; Basak, S.; Basu, K.; Dehsorkhi, A.; Hamley, I. W.; Banerjee, A. Time-Dependent Gel to Gel Transformation of a Peptide Based Supramolecular Gelator. *Soft Matter* 2015, *11* (24), 4944–4951.

(189) Rao, K. V.; Jayaramulu, K.; Maji, T. K.; George, S. J. Supramolecular Hydrogels and High-Aspect-Ratio Nanofibers through Charge-Transfer-Induced Alternate Coassembly. *Angew. Chemie* 2010, *122* (25), 4314–4318.

(190) Castilla, A. M.; Draper, E. R.; Nolan, M. C.; Brasnett, C.; Seddon, A.; Mears, L. L. E.; Cowieson, N.; Adams, D. J. Self-Sorted Oligophenylvinylene and Perylene Bisimide Hydrogels. *Sci. Rep.* 2017, *7* (1), 8380.

(191) Draper, E. R.; Schweins, R.; Akhtar, R.; Groves, P.; Chechik, V.; Zwijnenburg, M. A.; Adams, D. J. Reversible Photoreduction as a Trigger for Photoresponsive Gels. *Chem. Mater.* 2016, *28* (17), 6336–6341.

(192) Shao, H.; Parquette, J. R. A π-Conjugated Hydrogel Based on an Fmoc-Dipeptide Naphthalene Diimide Semiconductor. *Chem. Commun.* 2010, *46* (24), 4285.

(193) Ryan, D. M.; Doran, T. M.; Nilsson, B. L. Stabilizing Self-Assembled Fmoc–F 5 –Phe Hydrogels by Co-Assembly with PEG-Functionalized Monomers. *Chem. Commun.* 2011, *47* (1), 475–477.

(194) Guvendiren, M.; Lu, H. D.; Burdick, J. a. Shear-Thinning Hydrogels for Biomedical Applications. *Soft Matter* 2012, *8* (2), 260.

(195) Gaharwar, A. K.; Avery, R. K.; Assmann, A.; Paul, A.; McKinley, G. H.; Khademhosseini, A.; Olsen, B. D. Shear-Thinning Nanocomposite Hydrogels for the Treatment of Hemorrhage. *ACS Nano* 2014, *8* (10), 9833–9842.

(196) Draper, E. R.; Dietrich, B.; Adams, D. J. Self-Assembly, Self-Sorting, and Electronic Properties of a Diketopyrrolopyrrole Hydrogelator. *Chem. Commun.* 2017, *53* (11), 1864–1867.

(197) Nozik, A. J. Nanoscience and Nanostructures for Photovoltaics and Solar Fuels. *Nano Lett.* 2010, *10* (8), 2735–2741.

(198) Draper, E. R.; Lee, J. R.; Wallace, M.; Jäckel, F.; Cowan, A. J.; Adams, D. J. Self-Sorted Photoconductive Xerogels. *Chem. Sci.* 2016, *7* (10), 6499–6505.

(199) Draper, E. R.; Eden, E. G. B.; McDonald, T. O.; Adams, D. J. Spatially Resolved Multicomponent Gels. *Nat. Chem.* 2015, *7* (10), 848–852.

(200) Sutton, S.; Campbell, N. L.; Cooper, A. I.; Kirkland, M.; Frith, W. J.; Adams, D. J. Controlled Release from Modified Amino Acid Hydrogels Governed by Molecular Size or Network Dynamics. *Langmuir* 2009, *25* (17), 10285–10291.

(201) Drury, J. L.; Mooney, D. J. Hydrogels for Tissue Engineering: Scaffold Design Variables and Applications. *Biomaterials* 2003, *24* (24), 4337–4351.

(202) Aaron Lau, K. H. Peptoids for Biomaterials Science. *Biomater. Sci.* 2014, *2* (5), 627–633.

(203) Sharpe, L. A.; Daily, A. M.; Horava, S. D.; Peppas, N. A. Therapeutic Applications of Hydrogels in Oral Drug Delivery. *Expert Opin. Drug Deliv.* 2014, *11* (6), 901–915.

(204) Qiu, Y.; Park, K. Environment-Sensitive Hydrogels for Drug Delivery. *Adv. Drug Deliv. Rev.* 2001, *53* (3), 321–339.

(205) Yu, Z.; Xu, Q.; Dong, C.; Lee, S.; Gao, L.; Li, Y.; D'Ortenzio, M.; Wu, J. Self-Assembling Peptide Nanofibrous Hydrogel as a Versatile Drug Delivery Platform. *Curr. Pharm. Des.* 2015, *21* (29), 4342–4354.

(206) Xuan, S.; Lee, C. U.; Chen, C.; Doyle, A. B.; Zhang, Y.; Guo, L.; John, V. T.; Hayes, D.; Zhang, D. Thermoreversible and Injectable ABC Polypeptoid Hydrogels: Controlling the Hydrogel Properties through Molecular Design. *Chem. Mater.* 2016, *28* (3), 727–737.

(207) Włodarczyk-Biegun, M. K.; Farbod, K.; Werten, M. W. T.; Slingerland, C. J.; de Wolf, F. A.; van den Beucken, J. J. J. P.; Leeuwenburgh, S. C. G.; Cohen Stuart, M. A.; Kamperman, M. Fibrous Hydrogels for Cell Encapsulation: A Modular and Supramolecular Approach. *PLoS One* 2016, *11* (5), e0155625.

(208) Ikeda, M.; Ueno, S.; Matsumoto, S.; Shimizu, Y.; Komatsu, H.; Kusumoto, K.; Hamachi, I. Three-Dimensional Encapsulation of Live Cells by Using a Hybrid Matrix of Nanoparticles in a Supramolecular Hydrogel. *Chem. - A Eur. J.* 2008, *14* (34), 10808–10815.

(209) Yan, H.; Saiani, A.; Gough, J. E.; Miller, A. F. Thermoreversible Protein Hydrogel as Cell Scaffold. *Biomacromolecules* 2006, *7* (10), 2776–2782.

(210) Kasai, S.; Ohga, Y.; Mochizuki, M.; Nishi, N.; Kadoya, Y.; Nomizu, M. Multifunctional Peptide Fibrils for Biomedical Materials. *Biopolymers* 2004, *76* (1), 27–33.

(211) Chen, G.; Hoffman, A. S. Graft Copolymers That Exhibit Temperature-Induced Phase Transitions over a Wide Range of PH. *Nature* 1995, *373* (6509), 49–52.

(212) Mahler, A.; Reches, M.; Rechter, M.; Cohen, S.; Gazit, E. Rigid, Self-Assembled Hydrogel Composed of a Modified Aromatic Dipeptide. *Adv. Mater.* 2006, *18* (11), 1365–1370.

(213) Huang, R.; Qi, W.; Feng, L.; Su, R.; He, Z. Self-Assembling Peptide–polysaccharide Hybrid Hydrogel as a Potential Carrier for Drug Delivery. *Soft Matter* 2011, *7*, 6222.

(214) Eisele, D. M.; Knoester, J.; Kirstein, S.; Rabe, J. P.; Vanden Bout, D. a. Uniform Exciton Fluorescence from Individual Molecular Nanotubes Immobilized on Solid Substrates. *Nat. Nanotechnol.* 2009, *4* (10), 658–663.

(215) Ikeda, A.; Tsuchiya, Y.; Konishi, T.; Ogasawara, S.; Kikuchi, J. Photocurrent-Boosting by Intramembrane Electron Mediation between Titania Nanoparticles Dispersed into Nafion−Porphyrin Composites. *Chem. Mater.* 2005, *17* (15), 4018–4022.

Chapter 2

Experimental Methods

Chapter Outline:

This chapter summarises the methods and equipment used for the experiments contained within this thesis, as well as an overview of the relevant theory of the methods used.

2.1 Laboratory Procedures and Data Processing

Optical microscopy and transmission electron microscopy were analysed using ImageJ (http://rsb.info.nih.gov/ij) or FIJI (http://fiji.sc/). Atomic force microscopy images were analysed and exported using NanoScope Analysis 1.5. Numerical data processing, mathematical operations and graph production were performed on Microsoft Excel 2016 and Origin 2016 64 bit. Nuclear magnetic resonance spectra were analysed using MestReNova. Rheology experiments were undertaken and analysed using rSpace for Kinexsus and processed with Origin 2016 64 bit. Skeletal chemical structures were drawn using ChemBioDraw Professional 15.1 (Cambridgesoft)

Technical details specific to each project are detailed in the relevant chapter.

2.2 Atomic Force Microscopy

Atomic force microscopy (AFM) is a form of scanning probe microscopy to measure local properties such as height, friction, conductivity *etc.* An image is created from raster scans over an image with a cantilever and tip which oscillates close to the sample surface. Deflection of the tip due repulsive forces is measured by a laser pointed at cantilever, which is reflected to the photodiodes to record changes in position in three dimensions. Conventionally, when a free AFM cantilever oscillates at its resonant frequency, there is a phase lag between the excitation of the cantilever and its response of a 90° ($\pi/2$). The interaction of an oscillating AFM tip adds an additional phase shift and is used to produce phase images and can be useful to observe samples during the imaging process.[1]

Samples were prepared by diluting the sample either 10 or 100-fold in deionised water and drop cast on either freshly cleaved mica. These were left to dry before imaging. PeakForce atomic force microscopy was conducted by Dr R Harniman in the Chemical Imaging Facility, University of Bristol, with equipment funded by EPSRC under Grant "Atoms to Applications" Grant ref. (EP/K035746/1).

2.3 Attenuated total reflectance Fourier transform infrared spectroscopy (ATR-FTIR)

FTIR probes the absorption of infrared electromagnetic radiation due to transitions between different vibration modes. This energy gap between vibrational modes is much smaller than electronic transitions but infrared electromagnetic radiation can match the energy gap between vibrational modes, creating absorption induced vibrational transitions. The energy of these transitions is characteristic of bonds in different functional groups in molecules with particular interactions and therefore can be used to identify inter and intramolecular interactions to investigate supramolecular structure.

Attenuated total reflectance Fourier transform infrared spectroscopy (ATR-FTIR) was performed using a PerkinElmer Spectrum 100 FTIR spectrometer fitted with a universal attenuated total reflection accessory. The hydrogels were lyophilized by freezing in liquid nitrogen followed by freeze-drying for at least 24 hours.

2.4 Circular Dichroism Spectroscopy

Circular dichroism (CD) is a very sensitive, non-destructive and rapid method to study stereostructures and the intra- and intermolecular interactions of various classes of chiral supramolecules.[2] CD measures the difference in the absorbance (dichroism) of right and left-handed circularly polarized light. If vertically and horizontally polarized light is in phase you get 45° polarized light. If the polarized light is out of phase by half the wavelength then it ceases to be linearly polarized and is instead circularly polarized light. Also, a quarter waveplate can be used to slow one linearly polarized component to generate circularly polarized light. This polarized light will be absorbed at a particular wavelength by asymmetric chromophores or symmetric chromophores in an asymmetric environment (i.e. a chiral assembly) due to the difference in extinction coefficients. In CD spectroscopy it is not the configuration of the molecule in space, rather the corresponding asymmetric electron distribution that is responsible for absorptions and therefore probed.

CD will be used to understand the chiral supramolecular packing of a series of gelators throughout all three experimental chapters.

CD spectra were recorded at room temperature using a JASCO J-810 spectrometer through the two quartz plates. Samples were prepared by spreading hydrogels (*ca.* 25 µL) between two quartz plates to produce a homogeneous film and to reduce scattering of light by the hydrogel sample. The units used for CD spectra is degrees of ellipticity, a historical convention. It defines the difference between the magnitudes of the electric field vectors or right-circularly and left-circularly polarized light. Such that for 0° there is no difference in the absorbance or right-circularly and left-circularly polarized light.

2.5 Differential Scanning Calorimetry

Differential scanning calorimetry (DSC) is a thermoanalytical technique in which the difference in the amount of heat required to increase the temperature of a sample and reference sample, often an empty pan, is measured as a function of heat flow. As the pressure is kept constant, heat flow is equivalent to enthalpy changes. Thus, DSC can be used to probe phase transitions such as crystallisation, glass transition or as a solid sample melts to a liquid. DSC is used to monitor gel-sol melting transitions for hydrogels and can be used understand differences in the different gel structures.

Differential scanning calorimetry (DSC) was carried out using a Mettler Toledo TGA/DSC1 Star System at a scan rate of 1 °C min^{-1} with a nitrogen flow of 25 mL min^{-1}.

2.6 Optical Microscopy

Alongside conventional optical microscopy, polarized and phase contrast microscopy was used to image hydrogel samples. Phase contrast generates contrast due to different structures having different refractive indices such that light waves become ‘out of phase’ with others. Polarized light uses a polarizing filter to polarise light and second filter below the focal point is perpendicular to the first and therefore no light reaches the detector. However, if the sample is anisotropic double

refraction occurs, polarizing the light perpendicular to one another allowing for light to pass through the second filter and produce contrast against the isotropic background.

Confocal microscopy was also used and differs from conventional fluorescence microscopy in numerous ways. Firstly, excitation of the sample is not from excitation filters but by the beam source and rasters for point-by-point illumination and rejects out of focus light. This allows for illumination at a desired depth to penetrate the structure and in some cases create a three-dimensional image.

2.7 Nuclear Magnetic Resonance Spectroscopy

Nuclear Magnetic Resonance (NMR) spectroscopy probes the chemical environment of certain nuclei which can be used to understand structural information about the molecules studied. NMR spectroscopy relies on nuclear spin (S) of certain nuclei. ^{1}H, ^{13}C and ^{31}P nuclei have a nuclear spin of ½. This spinning charge generates a magnetic field, with a magnetic moment (μ) proportion to the spin. These spins exist in two degenerate states, but in the presence of an external magnetic field (B_0) these states are no longer degenerate, and the spin state aligned with the external field is at a lower energy than the spin state opposed to this field. The energy difference is very small (*ca.* 5J for nuclei experiencing the Earth's magnetic field):

$$\Delta E = \frac{\mu B_0}{S} \qquad (Equation\ 2.1)$$

This energy difference is therefore increased using powerful magnetic fields several orders of magnitude stronger than Earth's. Absorption by the nuclei of the appropriate electromagnetic energy (radio frequencies of 20- 900 MHz), results in excitation of nuclei in the lower energy state to the higher spin state. The charged electrons around the nuclei create a secondary, induced magnetic field that opposes the external applied magnetic field. Thus, different electron density (due to covalent bonding, and through space and bond interactions) shields the nuclei resulting in different resonant frequencies. Thus, it is possible to differentiate nuclei in a molecule and infer information about the chemical environment of each nucleus. However, as the induced field is very small compared to the

applied field these increments are reported in parts per million (ppm). As the resonance peaks depend on the external magnetic field and the radio frequency, the NMR signals are reported as a difference from a reference known as the chemical shift (δ).

$$\delta = \left(\frac{\nu_{sample} - \nu_{ref}}{\nu_{ref}}\right) \times 10^6 \qquad (Equation\ 2.2)$$

Hydrogel samples were either diluted to lower viscosity or freeze-dried and resuspended in the deuterated DMSO to aid NMR measurements as gel samples produce excessively broad peaks. Further experimental details are explained in later chapters. Chemical shifts were recorded in parts per million (ppm).

2.8 Rheology

Rheology is the study of sample behaviour prior to bulk flow, i.e. deformation, in response to the application of force. [3] From this, the mechanical properties of the material can be quantified, which is particularly useful when compared to other samples. Rheological characterisation of supramolecular gels are often necessary as qualitative observations, such as resistance to flow induced by gravity, are not sufficient to differentiate a viscous solution from a self-supporting gel. Also, the behaviour of gels in response to different conditions such as temperature or shear can be investigating with direct relevance to the eventual application of the hydrogel. Materials are classified based on ideal situations for solids and liquids in their response to shear stress (force per area) (σ), however, viscoelastic materials commonly have properties between the two.

A Hookean solid exhibits 'perfectly' elastic behaviour, with the shear stress being proportional to the shear strain (γ) and the shear modulus (G) [3,4]:

$$\sigma = G\gamma \qquad (\boldsymbol{Equation\ 2.3})$$

Whereas for a Newtonian liquid, a shear stress produces a flow of the material with a constant strain rate ($\dot{\gamma}$) which is proportional to the viscosity (η) of the material:

$$\sigma = \eta\dot{\gamma} \qquad (Equation\ 2.4)$$

However, self-assembled hydrogels are classified as viscoelastic materials with the behaviour of both ideal materials which can be characterised using rheology. Rheology is a well-established field with a myriad of measurements that can be taken. For instance, viscosity measures the resistance by the sample to flow by determining the force (stress) required to move a sample a certain speed (shear rate):

$$\eta = \frac{\tau}{\dot{\gamma}} \qquad (Equation\ 2.5)$$

Whereby, η refers to the viscosity, τ to the shear stress, and γ̇ to the shear strain rate. If the viscosity of a sample remains constant with shear rates it classed as a Newtonian material. [3,4] However, many fluids are non-Newtonian and show a shear rate dependence with either shear thinning (bingham, pseudoplastic) or shear thickening (dilatant fluid) viscosities.

Oscillatory experiments are also commonplace for the characterisation of supramolecular gels, whereby the response to deformation without bulk flow is measured. Unlike viscosity measurements, as the name implies, the force applied oscillates with either a constant frequency or amplitude. Depending on the rheometer used there is either an applied stress or strain and the shear strain or shear stress response is recorded.

Shear stress (Pa):

$$\sigma = \frac{Force}{Area} \qquad (Equation\ 2.6)$$

Whereby, F is the force and A the area.

Shear strain:

$$\gamma = \frac{u}{d} \qquad (Equation\ 2.7)$$

Whereby, u is the deflection or displacement and d is the height to measure a deformation of the material.

These forces are applied as a sinusoidal signal and there is a lag between the input and measured shear response measured, measured as the phase difference (δ) in radians. For an elastic material these signals are in phase, for a viscous material, this is out of phase by 90° and viscoelastic materials fall between the two extremes.

The ratio of the maximum stress to the maximum strain at a given frequency (f), measured in Hertz, defines the complex modulus (G*) relative to the radial frequency ($\omega = 2\pi f$) [3] :

$$G^*(\omega) = \frac{\sigma_o}{\gamma_o} \qquad (Equation\ 2.8)$$

At a given frequency, the phase difference is constant with time. The complex modulus and phase difference (or phase angle) is characteristic of a material and describes its ability to store energy (elastic component) and dissipate energy (viscous component). Further to this, G* can be represented as separate moduli describing the elastic and viscous response of a material by the storage, solid-like, moduli (G') and the loss, liquid-like, moduli (G''):

$$G'(\omega) = G^*(\omega)cos\delta \qquad (Equation\ 2.9)$$

$$G''(\omega) = G^*(\omega)sin\delta \qquad (Equation\ 2.10)$$

These are then related by the following relationship to the complex modulus G*:

$$G^*(\omega) = \frac{\sigma_o}{\gamma_o} = G'(\omega) + iG''(\omega) \qquad (Equation\ 2.11)$$

Rheometry was performed using a Malvern Kinexus fitted with a parallel plate geometry (gap width of 200 μm) at room temperature. Prior to rheology experiments, all hydrogel samples were aged for

one day and were added to the rheometer using a spatula to minimise shear. The top plate is lowered, and the normal force is measured and allowed to reach equilibrium. Further experimental are detailed in later chapters.

2.10 Transmission Electron Microscopy

Transmission Electron Microscopy (TEM) uses electrons to image structures at much higher magnification than optical microscopy with an atomic resolution possible. For TEM high energy electrons are generated by thermionic emission from a metallic filament (often tungsten) and focussed onto the sample. These electrons can have no interaction (and are transmitted) or are scattered either elastically (no energy loss) or inelastically (energy loss *via* interactions). Electrons that are transmitted are detected and thus the contrast arises from interactions by the electrons with the sample which lowers their transmission, relative to where the sample is absent.

The electron beam can also be used for energy dispersive X-ray spectroscopy (EDX, EDS), to ionise and remove core-shell electrons. This generates a vacancy which is filled by an electron with a higher quantum number. This process is accompanied by a simultaneous emission of an x-ray of a defined wavelength that is characteristic of different elements and therefore can be used to undertake an elemental analysis of the sample.

Transmission electron microscopy (TEM) was performed in bright-field mode using a JEOL TEM 1400 electron microscope and JEOL TEM 2010 electron microscope operating at 120 keV. TEM samples were prepared by drop casting a dilute suspension of hydrogel (5 µL) onto carbon-coated copper TEM grids for three minutes and wicking excess fluid away using filter paper. All samples were left to dry overnight at room temperature.

Cryogenic-transmission electron microscopy (cryo-TEM) was also undertaken as it allows for the imaging of materials in a hydrated state, with the aim to decrease artefacts that occur from drying.[5,6] This is achieved through rapid freezing of aqueous samples ($\geq 10^4 Ks^{-1}$),[7] which immobilises ice before nucleation can occur to form amorphous ice with the sample density as water to preserve the

structure.[5] Carbon-coated grids are cooled using liquid nitrogen cooled ethane, capable of more rapid cooling than nitrogen alone and therefore result in better quality ice for cryo-TEM imaging.

Cryo-TEM samples were prepared by dilution with deionised and were imaged using an FEI Tecnai Twin Lens electron microscope fitted with an FEI Eagle 4k x4k CCD camera and is operated at 200 keV. Imaging was undertaken with Judith Mantell and sample preparation was aided by Jen Coombs and Judith Mantell.

2.11 Ultraviolet-Visible and Fluorescence (fluorimetry) spectroscopy:

Ultraviolet-Visible (UV-Vis) spectroscopy measured the absorbance of light (A) by chemical systems at a fixed wavelength (λ). This absorbance is determined by the Beer-Lambert law:

$$A = log_{10}\left(\frac{I_0}{I}\right) = \varepsilon Cl \qquad (Equation\ 2.12)$$

Whereby, I_0 and I are the intensity of the incident and transmitted light, respectively, and C refers to the concentration of the chemical species (M), l to the path length (cm) and ε the extinction coefficient ($M^{-1}\ cm^{-1}$). The extinction coefficient is effectively the likelihood of an electronic transition at a fixed wavelength and is an inherent property of the chemical species. Absorption of light occurs dues to the excitation of an electron from the highest occupied electronic orbital (HOMO) to the lowest unoccupied molecular orbital (LUMO). This energy gap is comparable to the wavelength of light (as described by $\Delta E = h\frac{c}{\lambda}$ .Whereby, E is the energy of electromagnetic radiation, h is the Planck's constant, and c is the speed of light). Many inorganic species show charge-transfer absorption and are called charge-transfer complexes. For a complex to demonstrate charge-transfer behaviour, one of its components must have electron donating properties and another component must be able to accept electrons. Absorption of radiation then involves the transfer of an electron from the donor to an orbital associated with the acceptor. For organic species, the energy of UV-vis is sufficient to excite π electrons and valence electrons of heteroatoms.

Conversely, fluorescence spectroscopy (fluorimetry) is the measurement of the LUMO to HOMO transition. This radiative decay occurs when a photon of light is emitted upon transition from an excited electron state to a lower state. Within these electronic states, there are vibrational modes resulting from the dynamic behaviour of bonds (which are probed using FTIR). Each electronic configuration will have the lowest energy state or nuclear configuration which is adopted after the electronic transition. If energy was totally conserved by the molecule it would not be possible to distinguish the incident irradiation and the emitted photons, however, energy is lost through non-radiative mechanisms such as vibrational relaxation such that there is a difference in energy. This often lower such that the emitted photon is stoke-shifted though anti-stoke shifts can occur through charge transfer and aggregation effects.

UV-Vis spectra were recorded at room temperature using a Perkin Elmer LAMBDA 750 UV/Vis/NIR Spectrophotometer through the two quartz plates. Samples were prepared by spreading hydrogels (*ca.* 25 µL) between two quartz plates to produce a homogeneous film and to reduce scattering of light.

2.12 Small-angle neutron scattering (SANS):

Scattering techniques are complementary to microscopic techniques, allowing for analysis on solvated samples, often without the need for modification (*i.e.* negative staining) to the sample. SANS is particularly appropriate as neutrons interact weakly with the nuclei of the sample avoiding radiation damage common with synchrotron x-rays. Scattering techniques provide quantitative information on the size, shape and structure of colloidal particles based on interactions between incident radiations (e.g., light, X-ray or neutrons) and particles. Spectra can be matched to models to extract such information. LMWGs, fit best to cylinder models (and variants *e.g.* a flexible cylinder, a hollow cylinder, or some other long, anisotropic structure) or fractal models. [6,8–10] These fits provide information as to the radius of the structure, the length, network structure *etc.*

Solutions and gels were prepared as described in Chapters 3 and 4, with H_2O and NaOH replaced with D_2O and NaOD. Quartz plates were used and stored in a temperature-controlled sample rack for the duration of the measurements. SANS measurements were performed using the D33 instrument (Institut Laue Langevin, Grenoble, France). A neutron beam, with a fixed wavelength of 10 Å and divergence of $\Delta\lambda/\lambda$ = 9%, allowed measurements over a large range in Q range of 0.005 to 0.3 $Å^{-1}$, by using three sample-detector distances.

The data were reduced to 1D scattering curves of intensity vs. Q using the facility provided software by Isabelle Grillo. This involves the following key steps: the electronic background is subtracted; the full detector images for all data are normalised; scattering from the empty cell is subtracted, and finally the data are radially averaged to produce the 1D curves for each detector position. The absolute scaling of the middle detector position data, taken under optimum conditions, is then used as the reference point for the other two data sets as they are scaled to form a single curve. The instrument-independent data were then fitted to customized models in the SasView software package.[11] All experiments were conducted with the assistance of Dr Gavin Hazell, who also provided assistance with data analysis.

References

(1) Proksch, R.; Yablon, D. G. Loss Tangent Imaging: Theory and Simulations of Repulsive-Mode Tapping Atomic Force Microscopy. *Appl. Phys. Lett.* 2012, *100* (7), 073106.

(2) Yu, G.; Yan, X.; Han, C.; Huang, F. Characterization of Supramolecular Gels. *Chem. Soc. Rev.* 2013, *42* (16), 6697.

(3) Goodwin, J. W.; Hughes, R. W. *Rheology for Chemists an Introduction*; Royal Society of Chemistry: Cambridge, 2000.

(4) Macosko, C. W. *Rheology: Principles, Measurement and Applications*; 1994; Vol. 86.

(5) Dubochet, J.; Adrian, M.; Chang, J. J.; Homo, J. C.; Lepault, J.; McDowall, A. W.; Schultz, P. Cryo-Electron Microscopy of Vitrified Specimens. *Q. Rev. Biophys.* 1988, *21* (2), 129–228.

(6) Mears, L. L. E.; Draper, E. R.; Castilla, A. M.; Su, H.; Zhuola; Dietrich, B.; Nolan, M. C.; Smith, G. N.; Doutch, J.; Rogers, S.; Akhtar, R.; Cui, H.; Adams, D. J. Drying Affects the Fiber Network in Low Molecular Weight Hydrogels. *Biomacromolecules* 2017, acs.biomac.7b00823.

(7) Tivol, W. F.; Briegel, A.; Jensen, G. J. An Improved Cryogen for Plunge Freezing. *Microsc. Microanal.* 2008, *14* (5), 375–379.

(8) Draper, E. R.; Adams, D. J. How Should Multicomponent Supramolecular Gels Be Characterised? *Chem. Soc. Rev.* 2018.

(9) Jamieson, S. A.; Tong, K. W. K.; Hamilton, W. A.; He, L.; James, M.; Thordarson, P. Small Angle Neutron Scattering (SANS) Studies on the Structural Evolution of Pyromellitamide Self-Assembled Gels. *Langmuir* 2014, *30* (46), 13987–13993.

(10) Lattuada, M.; Wu, H.; Hasmy, A.; Morbidelli, M. Estimation of Fractal Dimension in Colloidal Gels. *Langmuir* 2003, *19* (15), 6312–6316.

(11) SasView. SasView for Small Angle Scattering Analysis. 2017.

Chapter 3
Radical Induced Supramolecular Gelation

Work in this chapter published in: Mulvee, M.; Vasiljevic, N.; Mann, S.; Patil, A. J., *Soft Matter* **2018**, *14* (29), 5950–5954.

Chapter Outline:

Herein, the use of radicals to form a supramolecular hydrogel is reported, thereby expanding the available synthetic methodologies. Utilising the photolysis (λ = 254 nm) of sodium nitroprusside, in this work nitric oxide radicals were generated capable of dephosphorylating the water soluble fluorenylmethyloxycarbonyl tyrosine phosphate to form the less soluble fluorenylmethyloxycarbonyl tyrosine, demonstrated *via* NMR. The resulting hydrogelator self-assembles into high-aspect ratio nanofilaments which entangle to form a viscoelastic hydrogel. Interconnecting nanofilaments were visualised with cryo-TEM, high-resolution AFM, and CD, demonstrated periodic twisting of these fibrils of opposing chirality, compared to the same hydrogels formed *via* conventional means. Thus, the use of sodium nitroprusside (SNP) to trigger gelation has unexpected implications on the self-assembly process of the hydrogelator molecules. How the use of SNP effects the hydrogel assembly has been further investigated using DSC, rheometry, FT-IR, and fluorimetry.

Introduction

Supramolecular hydrogels are formed through the self-assembly of low-molecular-weight gelators into high aspect ratio, one-dimensional nanofilaments. These filaments laterally associate, entangle and/or branch to form a three-dimensional solid-like network. This acts as a scaffold to immobilise its solvent through surface tension and capillary forces to form a viscoelastic material. [1–3]

This self-assembly occurs due to stimuli lowering the solubility of the gelator, encouraging the growth of and bundling of filaments, shielding from the solvent. These can either be a physical or chemical perturbation to the gelator. The most common stimulus is the lowering of temperature, whereby the gelator is easily dissolved at higher temperatures and cooling results in a supersaturated solution and subsequent hydrogelation.[4–6] Alternatively, solvent switches can be made from a 'good' solvent by dilution with water until the volume fraction increases sufficiently to saturate the solution and induce a phase change for gelation. [7–10]

Chemical changes to the gelators can also trigger gelation. For instance, modulation of the pH results in either protonation or deprotonation, thus, changing the degree of polarization. Pochan and Schneider designed pH-responsive *de novo* proteins that fold into β-hairpins (Figure 3.1a). Below pH 9 the lysine residues of the peptide are positively charged, preventing the folding. Raising the pH removes the charge, encouraging the peptide to fold about the proline kink. These β-hairpins then assemble into filaments to shield the hydrophobic residues (Figure 3.1a), thus forming the hydrogel network. [11,12] Similar charge screening can be achieved through the addition of sodium chloride or cell culture media. [13]

Enzymatic and biomimetic means have also been employed to trigger supramolecular hydrogelation.[14–20] For example, alkaline phosphatase (ALP)[18] and cerium oxide nanoparticles[19] have been used to trigger gelation of fluorenylmethyloxycarbonyl tyrosine phosphate (FMOC tyrosine phosphate, FYP) *via* dephosphorylation of the tyrosine residue. Consequently, the ionic group ($-PO_3^{2-}$

) is converted into a neutral group (–OH), reducing the electrostatic repulsion between molecules and its hydrophilicity, causing bundling of filaments and subsequent gelation.

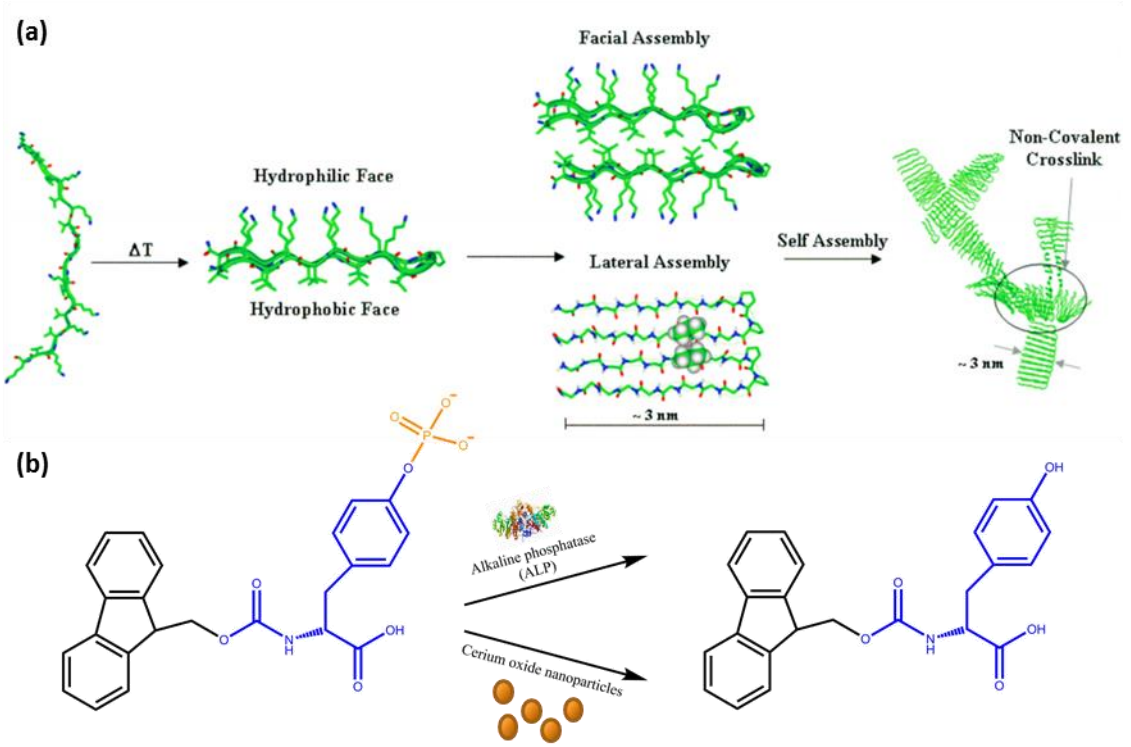

Figure 3.1 Various stimuli to trigger gelation (a) Folding of MAX1 protein to create amphiphilic structure due change in temperature, ionic strength etc. This structure then assembles to form filaments and consequently, a supramolecular hydrogel. Adapted from ref. 11 (b) Scheme for the formation of a supramolecular gelator through dephosphorylation of fluorenylmethyloxycarbonyl-tyrosine-phosphate (FYP) to form fluorenylmethyloxycarbonyl-tyrosine using biogenic (alkaline phosphatase) and abiogenic (CeO_2 nanoparticles) means.

These processes are likely to have a strong kinetic dependence and hence will affect the properties of the hydrogel through determining nucleation process and growth rates. Furthermore, the assemblies formed are a result of balancing attractive forces (*e.g.* hydrophobic interactions, hydrogen bonding *etc.*) against repulsive forces (*e.g.* electrostatics). Thus, the conditions of assembly *e.g.* ionic strength, temperature *etc.*, will affect the strength of these interactions and hence structures formed, resulting in different properties for the hydrogels. Most commonly, this is used to modulate the macroscopic mechanical properties of the gel through enzyme concentration[21], ionic strength[22,23] or even the mode

of agitation[24]. Though gelation time, filament and network structure, and optical properties can also be affected. [20,22,24–29] These can then alter the performance of the gels, such as cell adhesion, survival,[30] and energy transfer through filaments[31].

Since the type of trigger used and experimental conditions can affect the gel properties, an investigation into a novel stimulus and the resulting variation in properties is warranted. For instance, despite radicals being routinely used to crosslink hydrophilic polymers to form hydrogels, they have not been used to form supramolecular hydrogels.[32–37] This unexplored route will be used as a novel stimulus in this chapter. For a proof of concept, it is sensible to first demonstrate the capability of this route using a known system as this allows for easy comparisons between the two triggers. Though there are many routes to generate radicals, *e.g.* electrochemically, [38] photochemically, [39,40] or through the decomposition of peroxides, [41,42] the reported reactivity of nitric oxide against phosphates [43–45] makes it ideal to replicate the activity of alkaline phosphatase against Fmoc-tyrosine-phosphate.

Cleavage of phosphate groups by radicals, has been studied previously due to its relevance to biological systems, such as DNA. [46–52] In these reports, the phosphate ester is bound to a ribose ring or a similar cyclic group. The first stage in the reported mechanism is the abstraction of a proton by the radical from the ring to form a radical. This is followed by elimination of the phosphate group to form a radical carbocation.[46–49,52] This group then reacts with water, producing an alcoholic radical. The final stage is disproportionation with another radical. The reactivity of nitric oxide radicals against phosphorus compounds is determined by solvent polarity, which has been proposed due to the formation of a charged intermediate. [53,54] Thus, a similar mechanism is plausible for nitric oxide to eliminate phosphate from Fmoc-tyrosine-phosphate.

As a therapeutic agent,[55–57] there are many strategies to deliver nitric oxide, though SNP (Figure 3.2a) is an appealing source as it is stable and does not form any products unless irradiated with UV light or the addition of reducing agents (thiols *etc.*) [43,55,58–60]

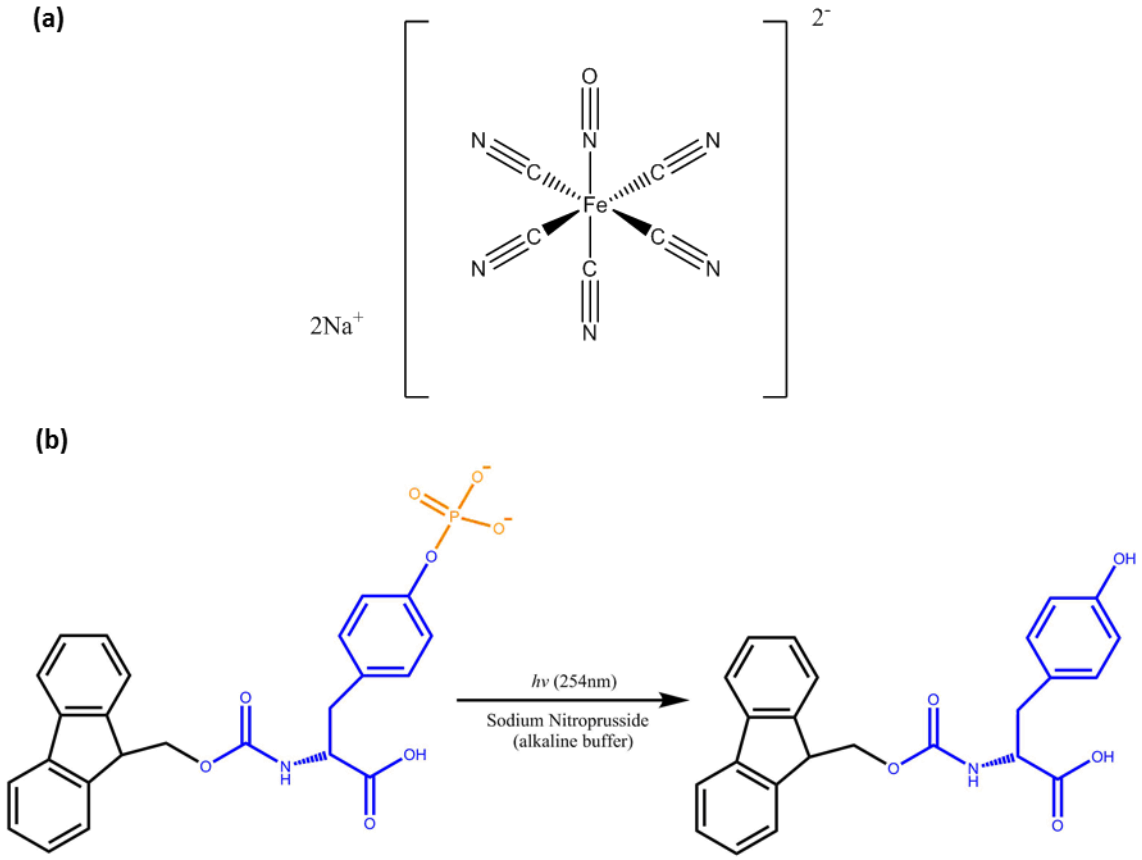

Figure 3.2 (a) Structure of sodium nitroprusside (SNP) and (b) Proposed scheme for the formation of a supramolecular hydrogel through dephosphorylation of fluorenylmethyloxycarbonyl-tyrosine-phosphate (FYP) to form the hydrogelator fluorenylmethyloxycarbonyl-tyrosine via UV irradiation sodium nitroprusside (SNP)

There has been some contention as to which product is formed when SNP is irradiated. For instance, some authors proposed that photolysis of SNP resulted in the photoejection of a nitrosyl cation (NO^+) rather than a nitric oxide radical ($NO^\bullet$)[61–64]. However, the bond cleavage is followed by oxidation of the iron centre which indicates charge transfer to the nitrosyl which would not be the case for the cationic species (NO^+).[55,61,62,65–67] Also, isotopically labelling with ^{18}O ruled out the formation of the nitrosyl cation. [61,68] The photolysis has also been extensively studied, being well reported that irradiation λ>480 nm results in no reaction. [43,60,61,66,69,70] This is because the lowest energy band, associated with the $d_{xy} \rightarrow \pi^*$ (NO) transition is mostly (*ca.* 98%) metal d_{xy} in character so does not interact with the nitrosyl group. [61,66] Thus, it does not sufficiently affect the metal-nitrosyl bond strength to result in bond cleavage. [61] At shorter wavelengths(<400 nm) the transitions overlap but

are centred on the nitrosyl ligand. [61,62] These are molecular bonding orbitals and thus result in a transition to an excited state. The energy is lost through photoemission, vibrational relaxation, or charge transfer to the nitrosyl ligand and subsequent bond cleavage[43,61,62,66] This is followed by oxidation of the metal centre from Fe(II)→Fe(III) and rapid aquation of the pentacyanoferrate(III) intermediate to yield the hydrodrate $(NC)_5Fe^{III}H_2O^{2-}$ (equation 3.1). [43,61,62,66,71]

$$[Fe^{II}(CN)_6(NO)]^{2-} + H_2O \rightarrow [Fe^{III}(CN)_6(H_2O)]^{3-} + NO^{\bullet}$$ (equation 3.1)

Also, irradiation at *ca.* 200 nm, assigned to the d_{xy}→π*(CN) CT transition, may lead to the photoreduction of the central ion, with the ejection of a CN radical ($CN^{\bullet}$)[43,60–62,66,72]. However, cyanide-based products are only observed after an extended period (>3 hours) of photolysis. [43,60,66] Significantly, SNP solutions are stable in the dark and do not form any products, hence UV irradiation will be necessary to trigger supramolecular gelation. [43,58,60]

Thus, SNP is a good source for nitric oxide radicals through UV irradiation, which can be used to cleave phosphorous from Fmoc-tyrosine-phosphate to produce the gelator Fmoc-tyrosine and hence trigger supramolecular gelation (Figure 3.2b). The properties of the resulting hydrogel will be discussed in the following sections and compared to a Fmoc-tyrosine-phosphate hydrogel prepared *via* the alkaline phosphatase mediated phosphate cleavage of FYP,[15] and is referred to as the ALP-FYP gel and the enzymatic route.

Experimental

Preparation

Radical induced FMOC-Tyr hydrogels (SNP-FYP gels): Hydrogels were prepared by first dissolving N-fluorenylmethyloxycarbonyl tyrosine phosphate (FMOC tyrosine phosphate, FYP) (Novabiochem, Merck) in 250 µL of a pH 10.1 alkaline buffer ((50 mM Tris-HCl (Sigma), 50 mM Na_2CO_3 (VWR Life Science), 1 mM $MgCl_2$ (Sigma)) at a concentration of 100 mM. Vortexing and sonication were necessary to aid dissolution. Then, a solution of sodium nitroprusside dihydrate (SNP) (250 µL) (Sigma) was added in varying molar ratios (10:1, 5:1, 2:1 and 1:1), and vortexed, giving a final FYP concentration of 50 mM. Samples were then irradiated with UV light (λ = 254 nm) using a 6W UVP UV Lamp (1290 µW/cm²).

Alkaline phosphatase-mediated FMOC-Tyr Hydrogels (Enzymatic route/ALP-FYP gels): Hydrogels were made in 200 µL of a pH 10.1 alkaline buffer (50 mM Tris-HCl (Sigma), 50 mM Na_2CO_3 (VWR Life Science), 1 mM $MgCl_2$ (Sigma)) at concentrations of 50 mM. Vortexing and sonication were used to aid dissolution. Calf intestine alkaline phosphatase (ALP) (10 µL, 1000 U mL^{-1}) (Calbiochem, Merck) was added to dephosphorylate FYP and trigger gelation. These solutions were heated to 37°C for 6 hours and left to cool to room temperature.

Characterisation

Nuclear magnetic resonance spectroscopy (NMR):

Carbon (^{13}C) and Phosphorous (^{31}P) were recorded respectively at 125.7 and 202.4 MHz. ^{13}C NMR, ^{31}P NMR were performed on the FMOC-Tyr hydrogels to confirm dephosphorylation. Norell Select Series 500 MHz NMR Tubes were used. ^{31}P NMR spectra were reported using 0.01% triethyl phosphate as an internal standard and 10% D_2O. Hydrogels were diluted 4-fold with the reaction buffer to raise the pH and lower the viscosity for analysis. For ^{13}C NMR hydrogels were freeze-dried and redissolved in

deuterated DMSO (d_6DMSO) (Sigma) to aid in solubility as has been reported elsewhere. [73,74] Chemical shifts were recorded in parts per million (ppm).

Differential scanning calorimetry (DSC):

DSC was carried out using a Mettler Toledo TGA/DSC1 Star System at a scan rate of 1 °C min^{-1} with a nitrogen flow of 25 mL min^{-1}.

Rheology:

Rheometry was performed using a Malvern Kinexus fitted with a parallel plate geometry (gap width of 200 µm) at room temperature. Hydrogels, which were aged for one day, were added to the rheometer using a spatula to minimize shear. The top plate was lowered, and the normal force is measured and allowed to reach equilibrium. Further details of the experimental setup, *e.g.* frequency and strain range, are included in the result and discussion section.

Optical and Confocal Laser Scanning Microscopy:

For optical microscopy, hydrogel samples were imaged without any modifications or dilutions by placing a small volume (*ca.* 5 µL) between a microscope slide and a coverslip. Brightfield, phase contrast, and polarized light microscopy were performed on samples. For confocal microscopy, the fluorescent dye Hoechst 33258 (Sigma) was added to both samples prior to gelation such that the final concentration was 200 µM. An excitation wavelength of 405 nm and emission cut off at ## nm was used to visualise Hoechst 33258 within the hydrogel matrix. All images were collected using a Leica SP5-II confocal laser scanning microscope attached to a Leica DMI 6000 inverted epifluorescence microscope

Transmission electron microscopy (TEM), cryogenic-TEM, Scanning Transmission Electron Microscopy (STEM), and energy dispersive X-ray analysis (EDXA):

TEM imaging was performed in bright-field mode using a JEOL TEM 1400 electron microscope and STEM imaging was performed using a JEOL TEM 2010 electron microscope operating at 120 keV. TEM

samples were prepared by drop casting a dilute suspension of hydrogel (5 µL) onto carbon-coated copper TEM grids for three minutes and wicking excess fluid away using filter paper. When negative staining was necessary, an aqueous solution of uranyl acetate (1% w/v, 5 µL) was also drop cast onto the carbon coated TEM grid and wicked off after three minutes. All samples were left to dry overnight at room temperature. Cryo-TEM samples were imaged using an FEI Tecnai Twin Lens electron microscope fitted with an FEI Eagle 4k x4k CCD camera and was operated at 200 keV. Samples were prepared by diluting the hydrogel sample and then drop casting onto glow discharged lacey carbon grids. This was achieved using either FEI Vitrobot™ Mark IV or a Leica GP plunge freezer at 25℃, 90% humidity with a 10-second wait before plunging the samples liquid nitrogen cooled liquid ethane.

All STEM imaging and EDXA were performed by Jonathan Jones. All cryogenic-TEM was performed by Judith Mantell. Samples for cryogenic-TEM were prepared with the assistance of Judith Mantell and Jen Coombs.

Atomic force microscopy (AFM):

AFM tapping mode images were obtained using a Bruker Multimode atomic force microscope with Nanoscope V controller and Picoforce Extender. Samples were prepared by diluting the sample either 10 or 100-fold in deionised water and drop cast on either freshly cleaved mica or carbon-coated TEM grids. All AFM experiments were performed by Dr Robert Harniman in the Chemical Imaging Facility, University of Bristol, with equipment funded by EPSRC under Grant "Atoms to Applications" Grant ref. (EP/K035746/1).

Circular dichroism spectroscopy (CD):

CD spectra were recorded at room temperature using a JASCO J-810 spectrometer through two quartz plates. Samples were prepared by spreading hydrogels (*ca.* 10 µL) between two quartz plates to produce a homogeneous film and to reduce scattering of light by the hydrogel sample. This avoided dilution into a cuvette that could alter the filament environment and concentration.

Attenuated total reflectance Fourier transform infrared spectroscopy (ATR-FTIR):

FMOC-Tyr hydrogels were lyophilized by freezing in liquid nitrogen followed by freeze-drying for at least 24 hours. ATR-FITR was performed using a PerkinElmer Spectrum 100 FTIR spectrometer fitted with a universal attenuated total reflection accessory.

Fluorescence spectroscopy (fluorimetry): Fluorimetry measurements were recorded at room temperature using a Horiba FluoroMax 4 spectrometer. Fluorimetry was carried on supramolecular hydrogels with an excitation wavelength of 265 nm, with excitation bandwidth of 1 nm and emission bandwidth of 5 nm. Samples were prepared by spreading hydrogels (*ca.* 10 µL) between two quartz plates to produce a homogeneous film.

Results and Discussion

Radical triggered gelation was induced by irradiating SNP-FYP solutions with UV light (λ = 254 nm) from a hand-held lamp. Experiments were undertaken for the following ratios (SNP: FYP) 10:1, 5:1, 2:1 and 1:1, indicating the molar ratio of SNP to FYP, with the latter always at a final concentration of 50 mM. Control samples were also prepared with either FMOC tyrosine phosphate, SNP, or UV light exposure absent. For these experiments, we exploited the ability of nitric oxide to cleave phosphoesters to dephosphorylate Fmoc-Tyr-POH *via* non-enzymatic means to form a self-supported Fmoc-tyrosine supramolecular hydrogel (Figure 3.3a).

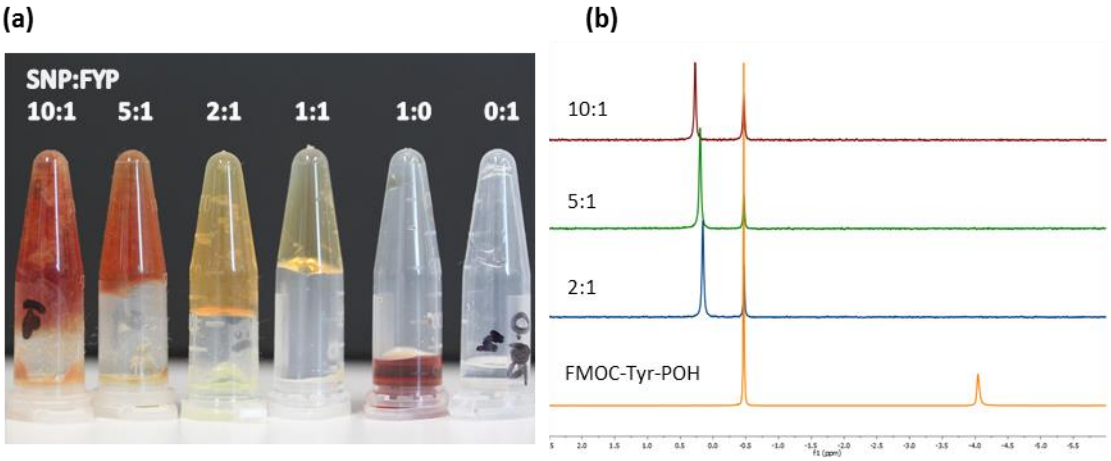

Figure 3.3 (a) Photograph showing self-supported supramolecular hydrogels produced by various SNP:FYP ratios and non-gelating controls. Gelation is observed via vial inversion. (b) ^{31}P NMR, all gelled samples demonstrated total cleavage of Fmoc tyrosine phosphate by loss of the resonance peak at -4.05 ppm, characteristic of an aryl phosphate. This is replaced with a peak a *ca.* 0.20 ppm, indicative of cleaved phosphorous. ^{31}P NMR referenced with triethyl phosphate(0.1% v/v)

Gelation was first observed macroscopically when the material did not flow after inversion. This phenomenon occurs because the entangled nanofilaments form a network that traps the solvent *via* surface tension and capillary forces, preventing flow unless a shear is provided [1,5,75,76]. According to this test (Figure 3.3a), all ratios except 1:1 and the controls (0:1 and 1:0) gelled in under 3 hours.

Furthermore, samples left in the dark did not gel, confirming that the presence of SNP, Fmoc-Tyr-POH and exposure to UV light were all necessary for hydrogelation. The yellow-red colour of the supramolecular hydrogels is due to the iron(III) of the sodium nitroprusside.

Successful dephosphorylation was demonstrated using ^{13}C and ^{31}P NMR spectroscopy. The ^{31}P NMR spectrum (Figure 3.3b) of the Fmoc-Tyr-POH solution gave a resonance peak at -4.05 ppm corresponding to the aryl phosphate ester group,[77,78] which disappeared for gelled samples. Concomitantly, a peak was observed for gelled samples at 0.20 ppm corresponding to cleaved phosphorous. This was slightly higher than would be expected for H_3PO_4 as the pH was increased to disassemble the hydrogel filaments for the NMR experiment. Hence the phosphoric acid will be partially deprotonated. Correspondingly, the ^{13}C spectrum (Figure 3.4) of the Fmoc-Tyr-POH solution had a resonance at 150.59 ppm which is associated with an aryl C-O-P(O)$(OH)_2$ and is absent in all gelled samples. Instead, it is replaced by a peak at 152.87 ppm, corresponding to an aryl C-OH [19,79,80], as observed for FMOC-Tyr. This demonstrates SNP as an effective source of nitric oxide radicals to cleave the phosphate ester bond of the Fmoc-Tyr-POH to form the gelator FMOC-tyrosine.

^{13}C NMR (125 MHz, DMSO-d6) of Fmoc tyrosine phosphate: δC ppm 173.94 (C7), 173.76 (C7), 156.44 (C8), 150.62 (C1), 150.57 (C1), 144.23 (C11), 144.2 (C11'), 141.13 (C16),, 130.51 (C3), 128.1 (C4), 127.54 (C14), 125.74 (C13), 125.69 (C15), 125.49 (C15'), 120.55 (C12), 120.26 (C2), 120.22 (C2), 66.69 (C9), 66.07 (C9) 56.62 (C6), 56.05 (C6), 47.03 (C10), 40.45 (DMSO), 40.29 (DMSO), 40.12 (DMSO), 39.95 (DMSO), 39.79 (DMSO), 39.62 (DMSO), 39.45 (DMSO), 36.44 (C6), 36.08 (C6).
^{13}C NMR (125 MHz, DMSO-d6) of radical triggered Fmoc tyrosine hydrogels: δC ppm: 174.52 (C7), 156.24 (C8), 152.86 (C1), 144.23 (C11'), 141.11 (C16), 131.81 (C3), 129.97 (C4), 128.32 (C≡N, equatorial), 128.13 (C14), 128.11 (C14'), 127.57 (C15), 127.34 (C≡N, axal), 125.77 (C13), 125.7 (C13'), 120.54 (C12), 120.04 (C12'), 119.8 (C2), 66 (C9), 61.51 (Trizma), 59.71 (Trizma), 56.8 (C6), 47.06 (C6), 40.41 (DMSO), 40.24 (DMSO), 40.08 (DMSO), 39.91 (DMSO), 39.74 (DMSO), 39.58 (DMSO), 39.41 (DMSO), 36.61 (C5).

Table 3.1 ^{13}C NMR assignments of Fmoc tyrosine phosphate and radical triggered Fmoc tyrosine hydrogels

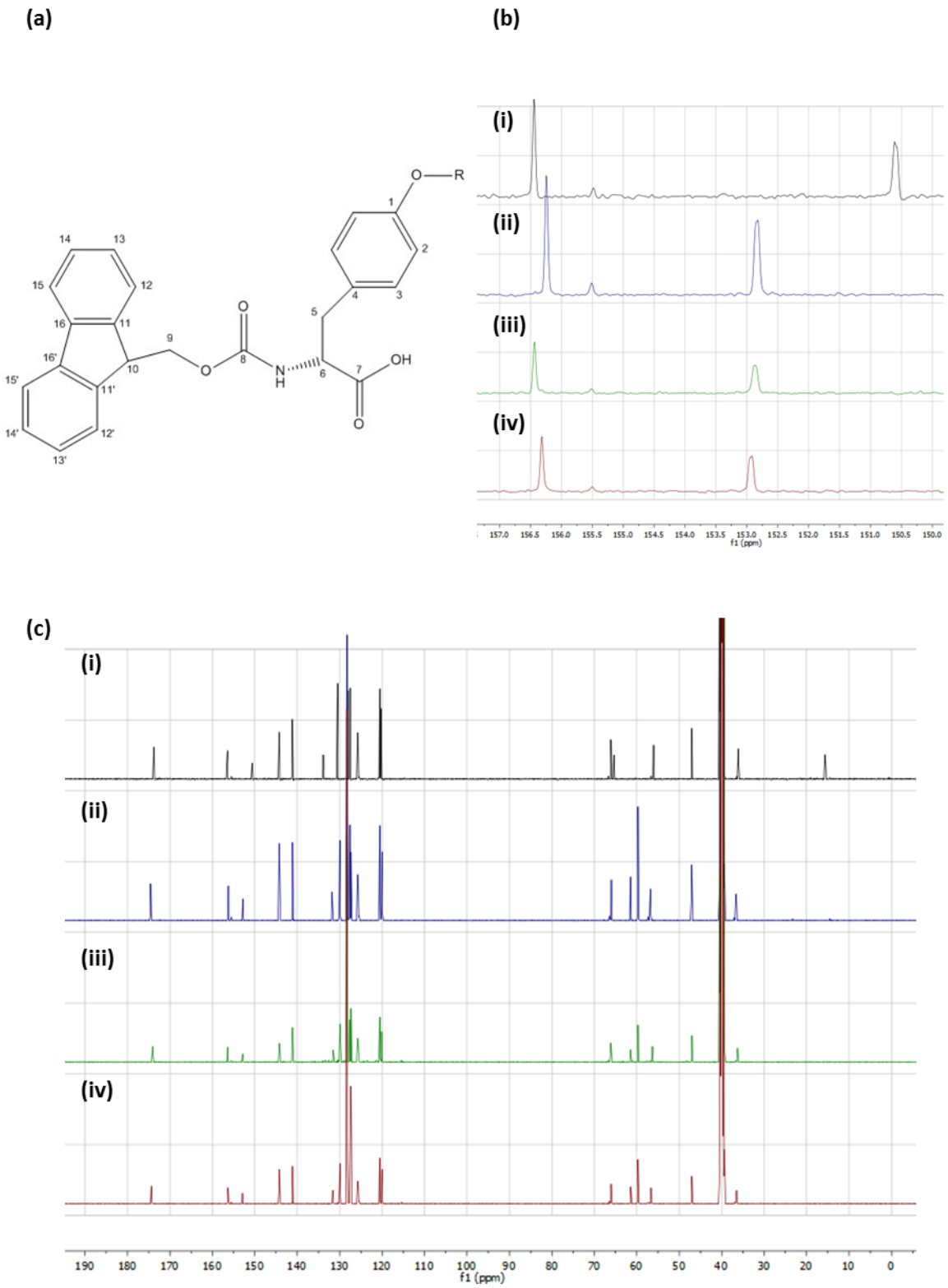

Figure 3.4 (a) Structure of FMOC-tyrosine-R, whereby R refers to either PO_3^{2-} or H. (b) Zoomed in ^{13}C NMR (i) Fmoc tyrosine phosphate, (ii) 2-1 gel, (ii) 5-1 gel, (iii) and 10-1 gel and (c) Full spectra of ^{13}C NMR on (i) Fmoc tyrosine phosphate, (ii) 2-1 gel, (ii) 5-1 gel, (iii) (500 MHz, DMSO-d6)

Next, the structural and mechanical properties of the formed gels were investigated *via* differential scanning calorimetry (DSC) and rheology. This analysis demonstrated that the stoichiometry of sodium nitroprusside to Fmoc-Tyr-POH affected the mechanical properties of the gel. Though, as total cleavage of Fmoc-Tyr-POH is observed through ^{31}P NMR for the gelled samples, this is not due to varying gelator concentration. Firstly, DSC demonstrated a broad endothermic peak for all samples (Figure 3.6a), increasing from *ca.* 51 to 71 °C with increasing SNP: FYP ratio compared to *ca.* 45 °C for the ALP-FYP. These peaks correspond to the breaking of the noncovalent crosslinkages of the supramolecular hydrogel which causes a gel to sol transition. [19,81,82] This variation in gel-sol transition temperature due to SNP stoichiometry indicates that its presence affects the hydrogel network formed.

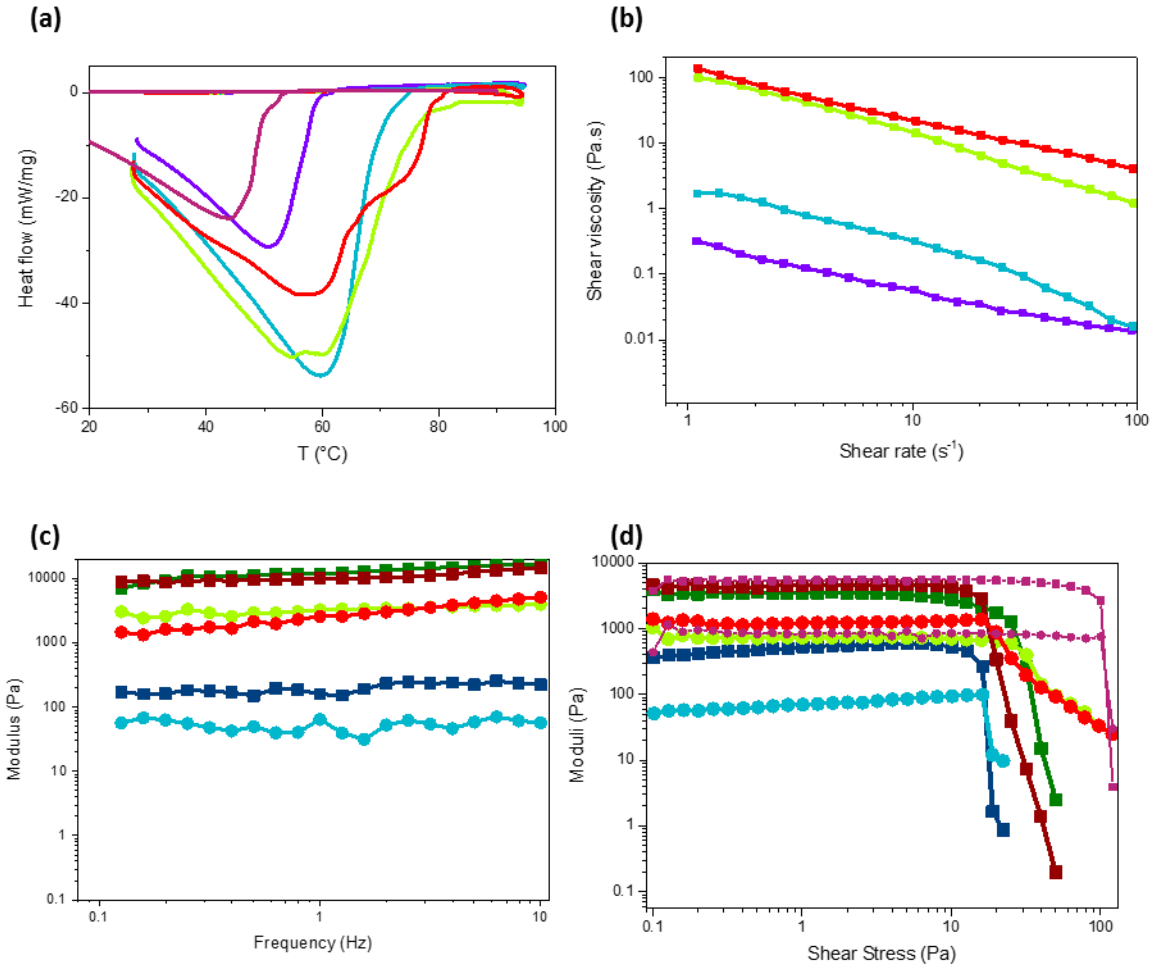

Figure 3.5 In all cases SNP: FYP ratios of 1:1 (purple), 2:1 (blue), 5:1 (green), 10:1 (red) and ALP-FYP gel (maroon). (a) DSC thermogram of supramolecular hydrogels prepared from fmoc tyrosine phosphate (50 mM) showing broad gel to sol transition temperatures, increasing with increasing SNP: FYP molar ratios. (b) Viscosity profile of hydrogels prepared at different SNP:FYP molar ratios, demonstrating shear-thinning behaviour. (c) Oscillatory frequency sweep, moduli demonstrating an indifference to frequency, typical of supramolecular hydrogels and (d) oscillatory amplitude sweeps at a constant frequency (1Hz) . All gels exhibited a linear viscoelastic regime and the stiffness was affected by SNP:FYP ratio. In oscillatory experiments, ▪ refer to G' and ● refer to G", the storage modulus and viscous modulus, respectively.

Rheological analysis (Figure 3.5) was undertaken to determine the mechanical properties of the supramolecular hydrogels. At minimal shear, the viscosity of the hydrogels (Figure 3.5b) increased from 0.3 to 137 Pa.s with increasing molar ratio. The viscosity then decreased for all samples with increasing shear rates (known as shear-thinning), typical of supramolecular hydrogels.[83–86] The applied shear can overcome the weak physical interactions responsible for the hydrogel network allowing the sample to flow more easily, corresponding to a lower viscosity.[86]

Oscillatory amplitude sweeps (Figure 3.5d) at a constant frequency (1 Hz) demonstrated a linear viscoelastic region (LVR) [87,88] in which the storage (elastic) G' modulus is approximately an order of magnitude higher than the loss (viscous) G" modulus for all stoichiometries except 1:1 (not shown). This observation is indicative of a solid-like network throughout the gel [23,87–91] for all stoichiometries except the 1:1 molar ratio which likely has an insufficient network of nanofilaments for hydrogelation.

Increasing the SNP: FYP stoichiometry resulted in an increase in the storage modulus at low strains from 430 to 3500 and then to 4700 Pa, indicating that stoichiometry determines the stiffness of the resulting gel. At increased strains, the viscous moduli (G") increased and at a crossover point, there is a concomitant sharp decrease in the storage moduli (G') indicating a transition from an elastic gel to a viscous fluid. [19,28,81,92] Oscillatory frequency sweeps (Figure 3.6c) at a fixed amplitude demonstrated that G', arising from the elastic network, was higher than G" across all frequencies, which is characteristic of the presence of a solid-like network of filaments in the viscoelastic gel. [18,91] Rheological analysis revealed very little difference in the properties of hydrogels formed at 5:1 and 10:1 molar ratios, thus it is likely that raising the molar ratio above 5:1 has minimal impact on the resulting structure. Hence, it has been demonstrated that increasing the molar ratio of SNP: FYP up to 5:1 impacts the rheological properties of the gel. These increased viscosities and changes in storage and viscous moduli are consistent with observed molar ratio dependence of the gel to sol transition temperature.

It is proposed that the increased SNP ratio aids in further crosslinking the hydrogel network, as has been shown previously, to produce a denser network and consequently a stiffer hydrogel.[23,93,94] In fact, adding a concentrated solution of SNP (50 μL, 1M) to the top of a gel formed through the enzymatic route resulted in a stiffer gel (Figure 3.6), despite the obvious dilution factor, further supporting this assertion. When accounting for the dilution of the gelator concentration, the measured storage modulus of the prepared ALP gel 108.5 Pa mM^{-1}) roughly doubles for the doped gel (180.5 Pa mM^{-1}).

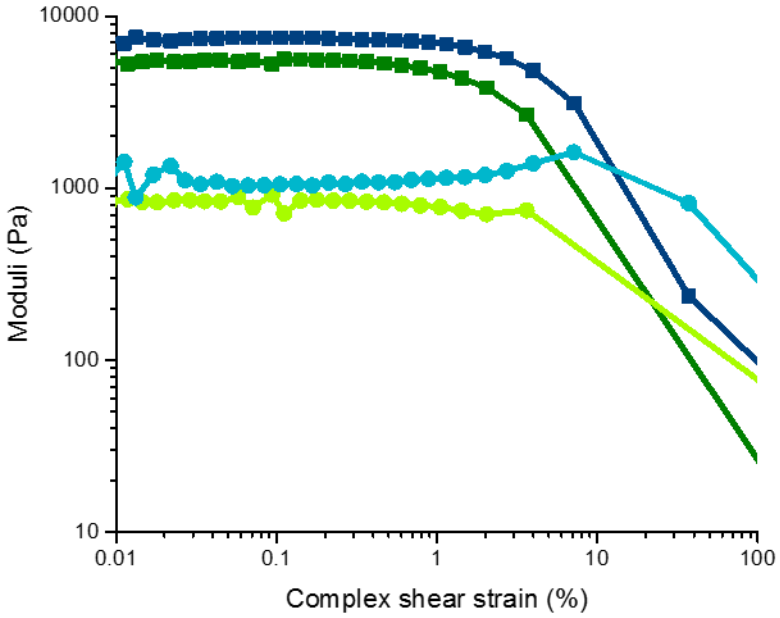

Figure 3.6 Oscillatory amplitude sweep at a constant frequency (1Hz) for gel formed using ALP; without the addition of SNP(green) and with SNP solution (1M) drop cast onto a preformed gel (blue), exhibiting higher G' values, despite the dilution of gelator. In all cases ▪ refer to G' (elastic moduli) and ● refer to G" (viscous moduli)

DSC and rheological analysis demonstrate that the stoichiometry of SNP affects the bulk properties of the hydrogels, despite total cleavage of FYP, meaning that these observations are not due to gelator concentration. However, these are bulk properties of the hydrogel, therefore additional techniques are necessary to determine further information about how the use of sodium nitroprusside affects the hydrogel network. Next optical, electron and atomic force microscopy were used to image the hydrogel network and filament structure.

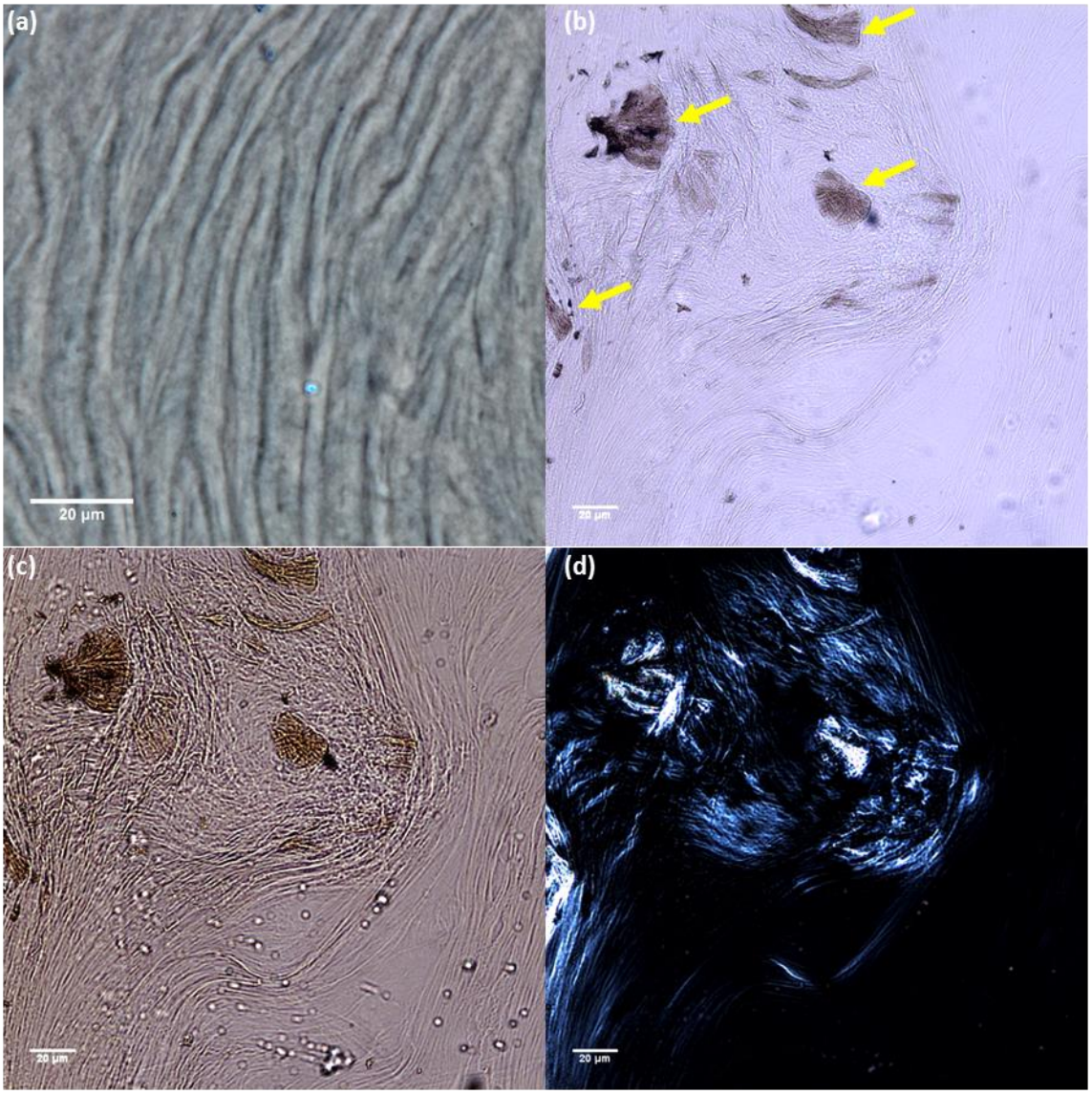

Figure 3.7 Optical microscopy images of enzyme-triggered hydrogel (a) and radical triggered gels (b, c and d). Phase contrast image of ALP-FYP gel demonstrating a sheet like morphology structure around SNP (arrows). A bright field image (b), polarized microscopy image (c) and cross-polarized image displaying sheet-like nematic birefringence (d) of the 2:1 gel. All scale bars are 20 µm

Optical and fluorescence microscopy demonstrated differing network structure for the two types of the gels (Figure 3.7 and Figure 3.8). For instance, phase contrast microscopy images of the ALP-FYP revealed striations resulting from the fibril bundles. Here, the contrast originates from differences in the refractive index due to the density of bundles against the lower density background. This sheet-like morphology is also observed for SNP-FYP hydrogels, however, rather than just uninterrupted isotropic filaments, there is a more matted and entangled network, as well as regions of dense

filaments around what is presumed to be SNP (yellow arrows in Figure 3.8b). The orange colour of these solids indicates that they are indeed SNP. The observation of anisotropic structures around the SNP demonstrates its role in directing the supramolecular ordering of nanofilaments. This is clearer under polarising microscopy (Figure 3.7d), which revealed domains displaying nematic birefringence, indicating ordering of the filaments. Birefringence was not observed for enzyme-triggered gels with samples under crossed-polarizers, instead appearing isotropic.

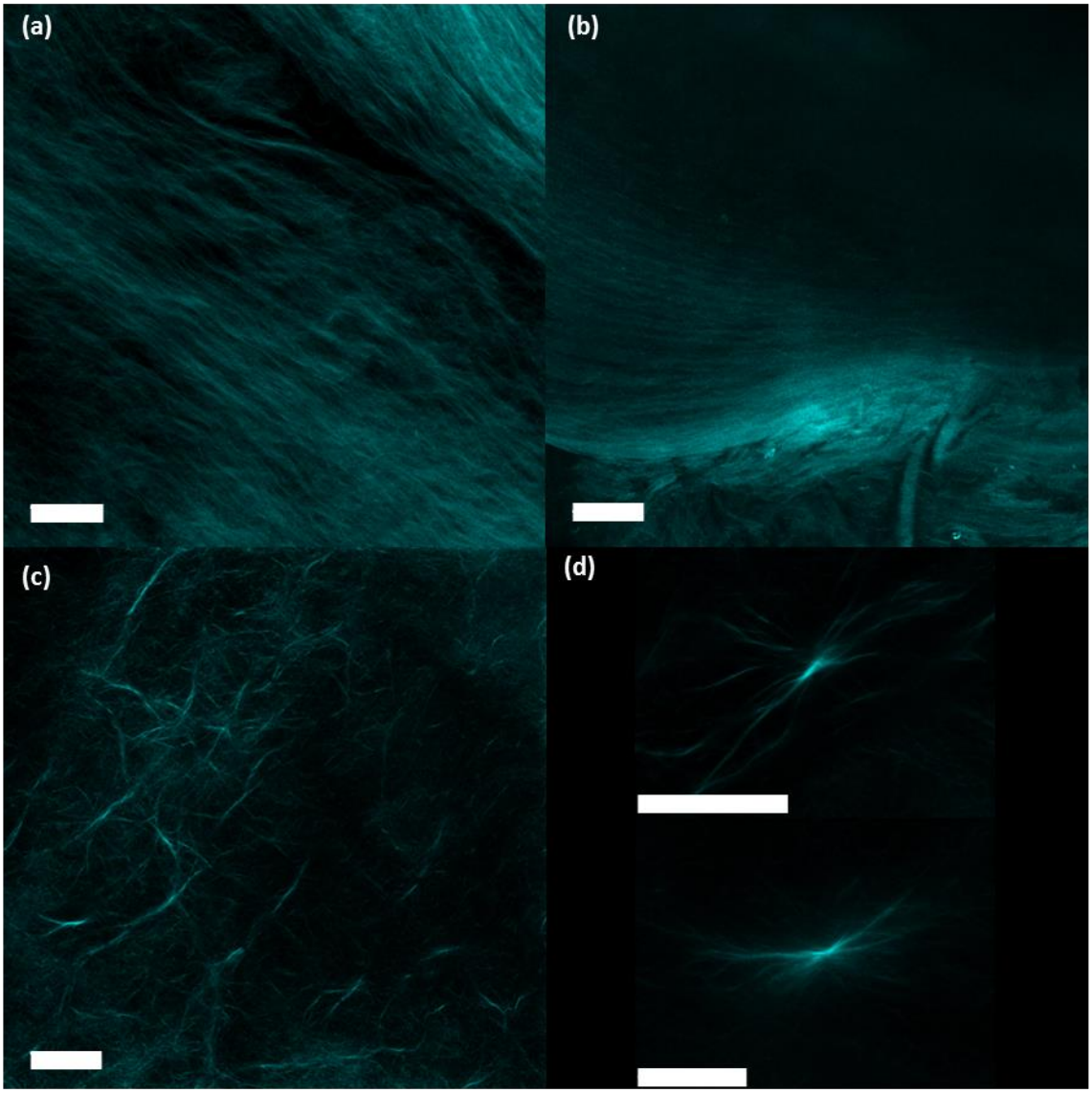

Figure 3.8 Confocal images of hydrogels displaying different network structures for ALP-FYP gel (a) and SNP gels 2-1 (b) 5-1 (c) with cropped images focussing on dense junctions from which filaments protrude from (d). All scale bars are 20 μm

The differences in hydrogel network are obvious when imaging hydrogel samples stained with Hoechst 33258 using confocal microscopy (Figure 3.8). As before, the ALP-triggered gels show a dense network of filaments. Bundled filaments are also observed for radical-triggered gels however a more entangled network is observed with dense regions from which filaments are seen to be protruding. These differences were observed without drying and therefore these artefacts were avoided.[95,96] Thus, radical-triggered gels form a different and denser network, agreeing with observations from the rheology data. Hence, it was necessary to study the differing hydrogel network further with higher resolution techniques, *e.g.* transmission electron microscopy (TEM) and high-resolution atomic force microscopy (AFM).

The supramolecular nanofilaments of the hydrogel were imaged using TEM and AFM. Due to the low electron density of the carbon-based filaments, negative staining with uranyl acetate was used to discern individual filaments *via* TEM. Although samples at the 1:1 ratio did not gel, only appearing slightly more viscous, high-aspect-ratio filaments were still observed (Figure 3.9a). Therefore, it is likely that at this stoichiometry, insufficient filaments are formed for there to be a critical density of filaments to provide a sufficient scaffold for water gelation. Also, another consideration is the inevitable concentrating effect that results from drying the hydrogel suspension on the TEM grids and therefore the density of nanofilaments isn't necessarily representative of the bulk sample.

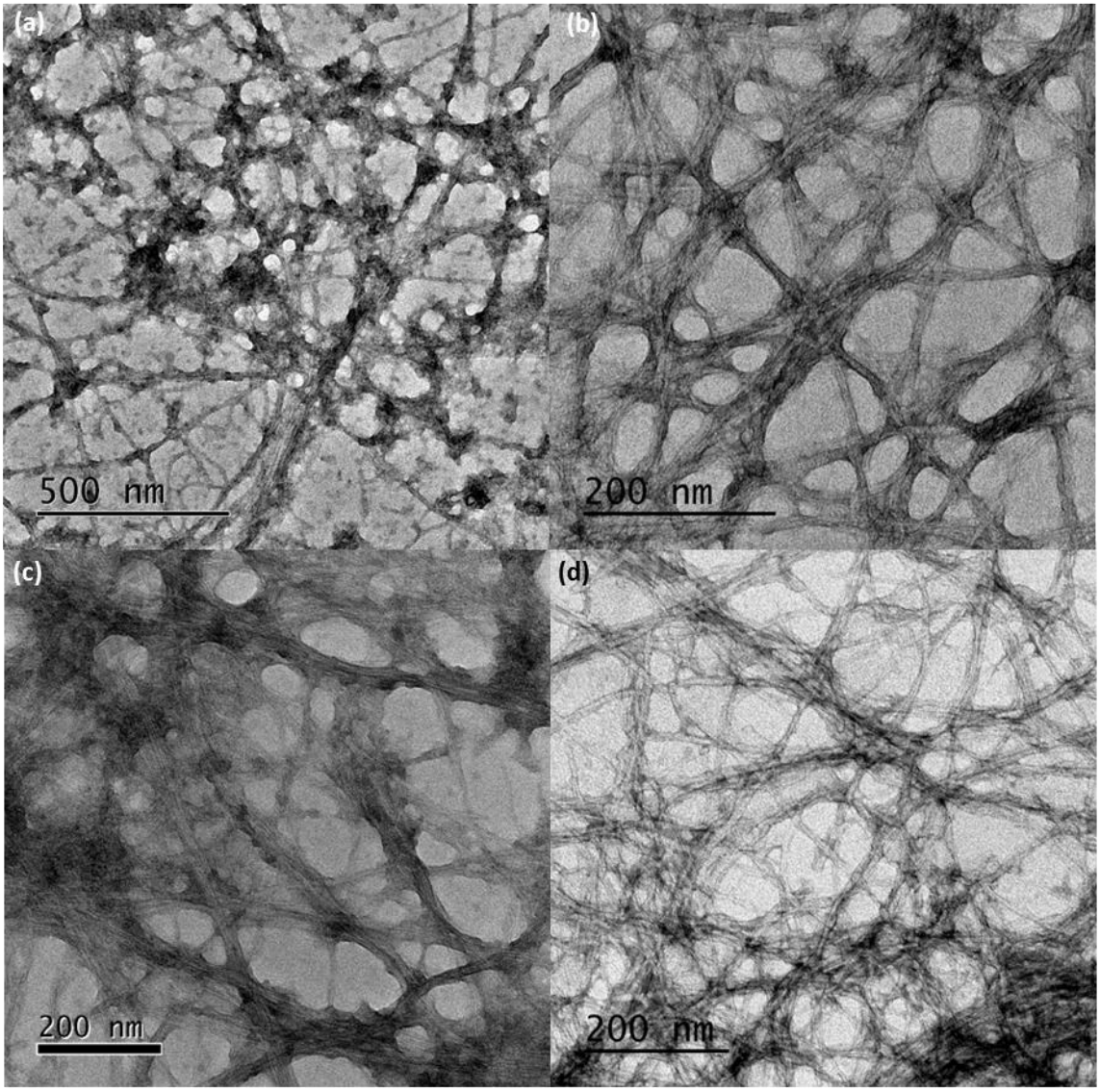

Figure 3.9 TEM images of negatively stained radical-triggered Fmoc-tyrosine hydrogels displaying an entangled network at different SNP:FYP ratios (a) 1:1, (b) 2:1, (c) 5:1 and (d) 10:1. Scale bar= 200 nm.

For higher ratios, it is possible to observe the high density of nanofilaments, which twist together to form bundles and extend to form the network acting as the scaffold for hydrogelation. At higher dilutions, it is possible to discern individual filaments and bundles against the substrate. In such cases, it has been shown that the filaments are 2-4 nm in width. These filaments are much smaller than those formed by the enzymatic route which are *ca.* 14 nm wide, indicating that the radical-triggered gels have a different filament structure as well as variable mechanical and network properties.

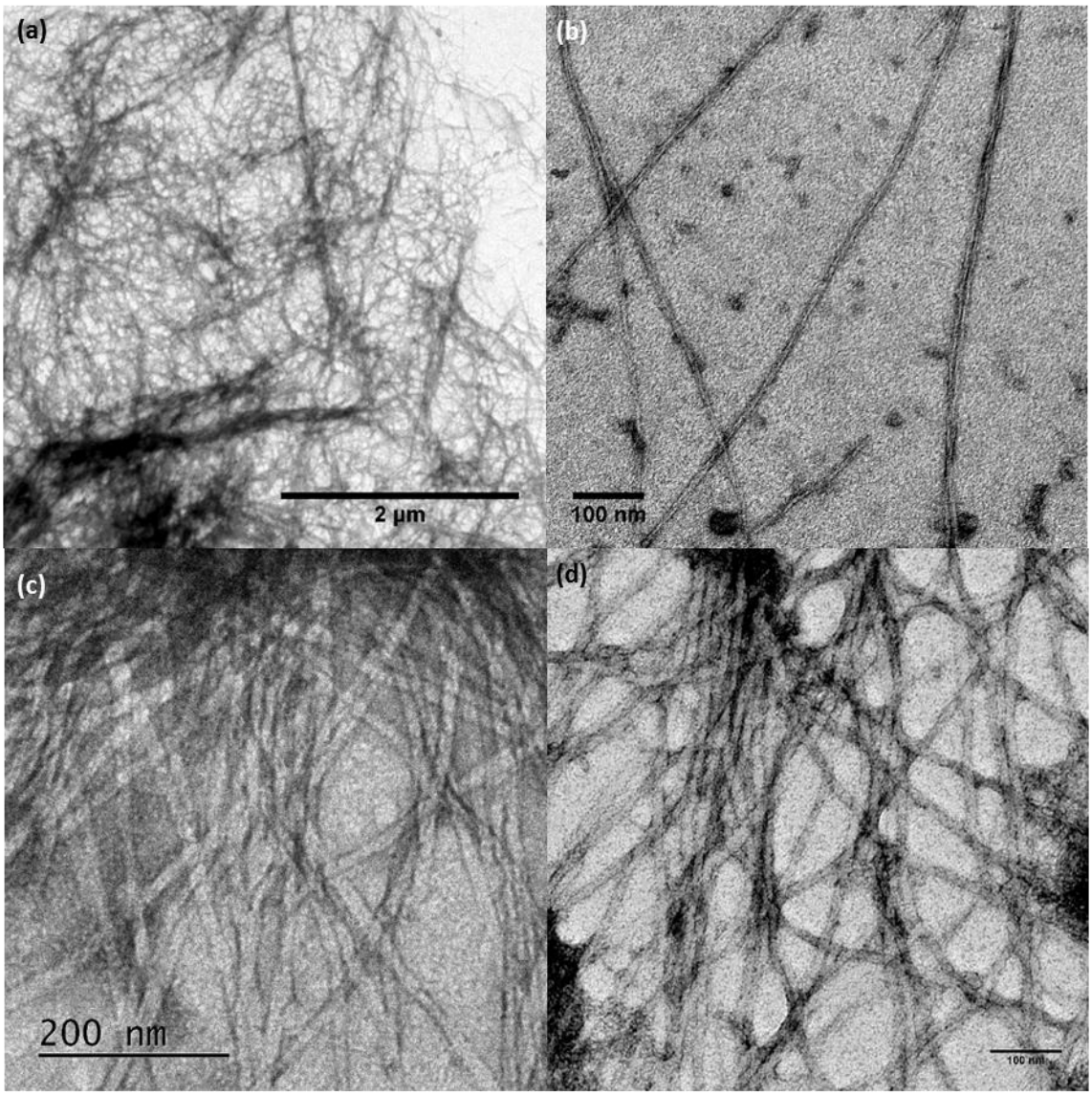

Figure 3.10 TEM images of a negatively stained samples (a) low magnification of diluted SNP-FYP hydrogel network, (b) individual filaments of SNP-FYP sample and (c) and (d) images of ALP-FYP filaments.

As observed with optical measurements, radical-triggered gels form a different network. Radical-triggered gels form more entwinned filaments (Figure 3.10b), whereas the enzymatic-triggered gels are formed of flat tape filaments that appear to be less entwinned (Figure 3.10c and d). It is not possible to rule out drying artefacts affecting network morphology, however, these observations agree with confocal microscopy images which did not require any dilution or drying. Also, unstained images reveal that this differing network is due to SNP salt, as conjectured earlier. For instance, for unstained samples (Figure 3.11), it is possible to visualise salts decorating the hydrogel filaments and

acting as junction points around which the filaments entangle to form a denser network. Energy dispersive X-ray spectroscopy (Figure 3.11) demonstrated localization of SNP (*via* the Fe atom), on filaments (locations ii and iii) at least on the TEM grid. Small amounts of iron were detected at location i, between filaments, due to iron present in the sample holder. These observations support the hypothesis that SNP is integrated into the hydrogel structure to form a more extensively cross-linked network. The metal salts were also observed to be forming along the hydrogel filaments (Figure 3.11b).

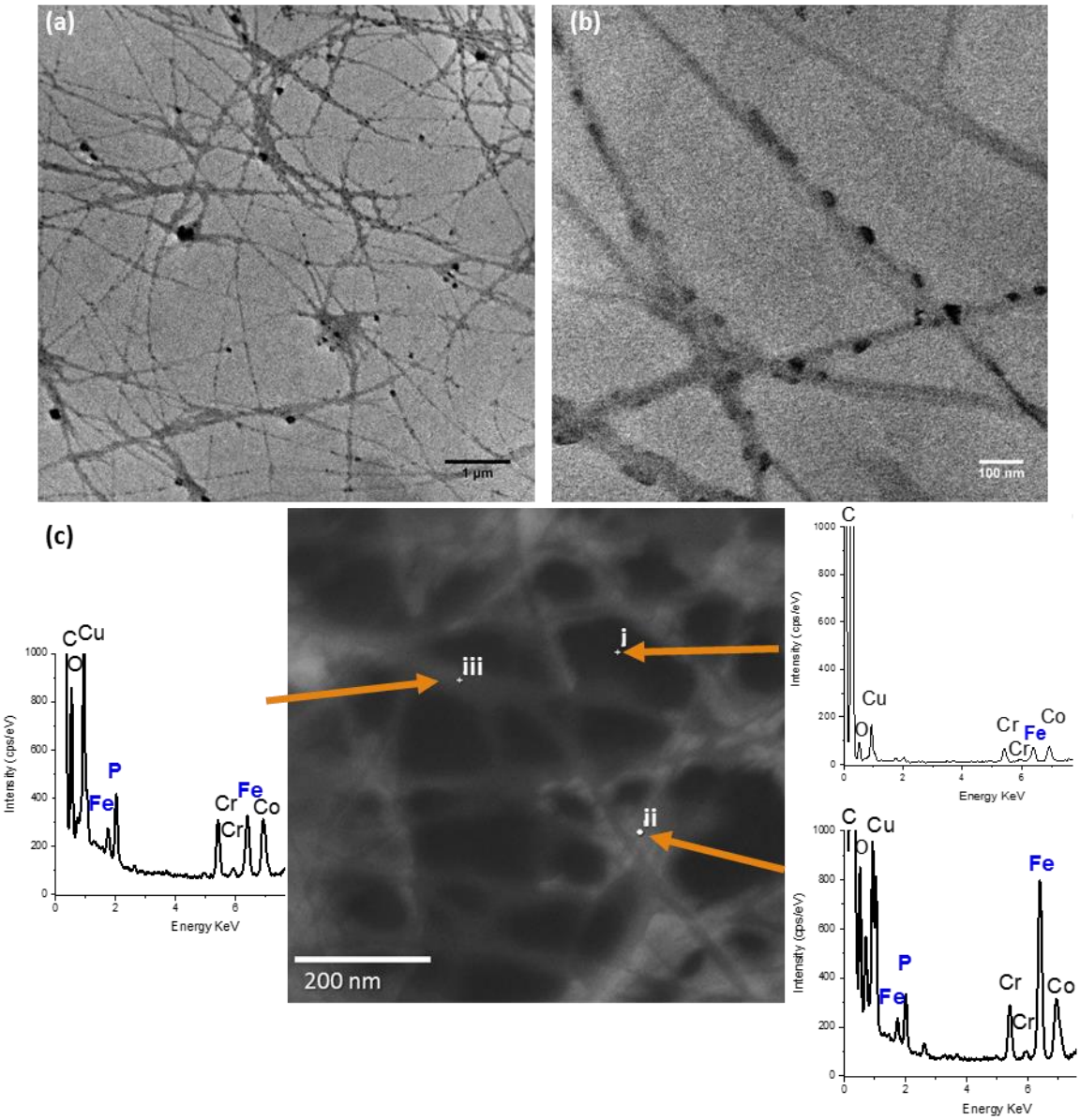

Figure 3.11 (a) unstained TEM image of SNP-FYP hydrogel nanofilaments, (b) decorated with SNP salts and (c) STEM image of SNP-FYP hydrogel; insets shows the energy-dispersive X-ray (EDX) spectra data. Locations: (i) carbon coated copper TEM grid. (ii) Junction zone of entangled filament and (iii) entangled filaments.

The differences in the filament structures were further investigated using cryogenic-TEM, as this technique preserves the native structure in the hydrated state by rapid freezing.[97] Once again, much narrower filaments were observed for the SNP-FYP gel (Figure 3.13a) when compared to the ALP-FYP gel (Figure 3.13b). Interestingly, twisted filaments were observed for both, but the SNP gel (yellow arrows Figure 3.13a) had a much narrower pitch between twists, *ca.* 130 nm compared to *ca.* 220 nm. Twisting in amino acid based fibril assemblies have been shown to be enhanced due to electrostatic

repulsion between the amino acids[98], thus, such electrostatic repulsion could arise from the anionic sodium nitroprusside ions decorating the nanofilaments leading to an increase in twisting. SNP-FYP samples were prepared at a lower pH than the ALP samples due to the higher starting concentration of FYP, a weak acid, and the SNP solution being prepared at a neutral pH. However, these narrower filaments were not due to the lower pH, as if FY was first dissolved at a higher pH and the gelled through the lowering of the pH, wider filaments are still observed (12.1 $\pm$3.3 nm) (Figure 3.12), comparable to the ALP-FYP filaments.

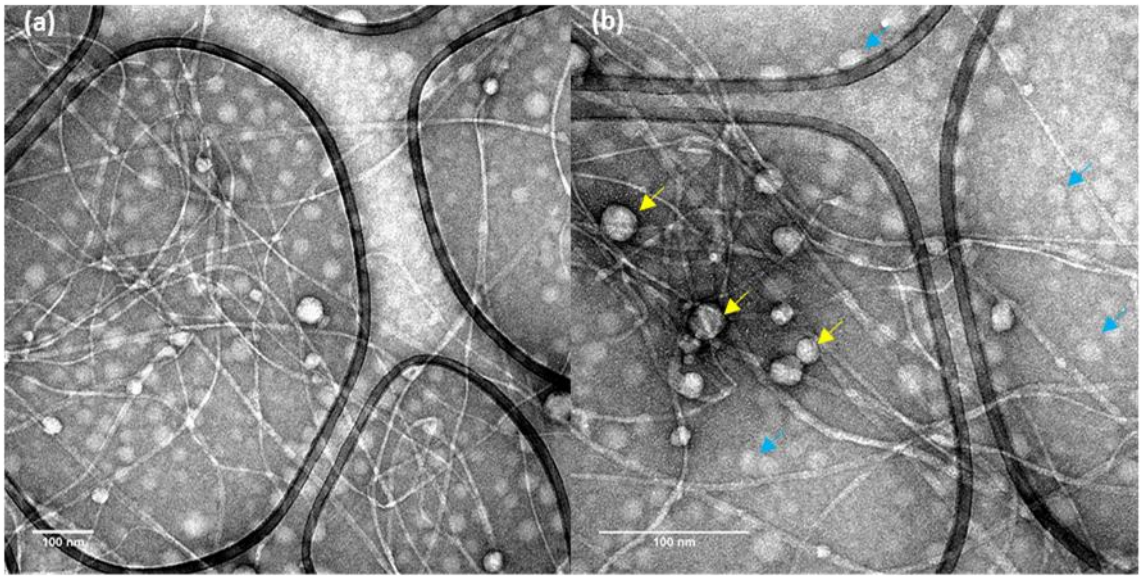

Figure 3.12 (a) Stained TEM image of hydrogel filaments at low pH (*ca.* pH 4) still exhibiting a wide tape structure not observed in SNP-FYP samples. (b) Stained spherical structures (yellow arrows) are presumably spherical micelles formed from FY with a fainter outline are instead an artefact of the uranyl acetate staining (blue arrows).

Also, for the SNP-FYP gel only, the unravelling of these twisted nanofilaments into much wider tapes (*ca.* 52 nm) is observed (Figure 3.14a). These tapes have striations which are visible in the direction of the tape, and these are potentially individual protofilaments.[91] Presumably, this unravelling is the reverse of the assembly process by which the filaments form. This likely occurs through the shearing and dilution necessary for the sample preparation. These are unlikely to be observed with conventional TEM, owing to the low contrast of the carbon-based filaments against the carbon coating of the TEM grid.

The observation of sheets is in agreement with the coiling tape mechanism of filament growth, whereby twist is imparted on the filament due to the curvature arising from the H-bonding between chiral gelators. [99] This curvature results in the formation of metastable twisted structures, preventing indefinite 2D lateral growth into sheets, instead favouring 1D growth in the direction of the filament to eventually form more twisted helical ribbons (Figure 3.14b). [100,101] For instance, Fmoc-SF-OMe assembles into 2D sheets producing a colloidal suspension that does not gel. Yet, simply substituting the serine for threonine induces twists into the supramolecular structure to minimise water contact with the methyl group. Also, the additional chiral centre promotes chiral assembly, both effects encourage 1D assembly over 2D sheets. [102]

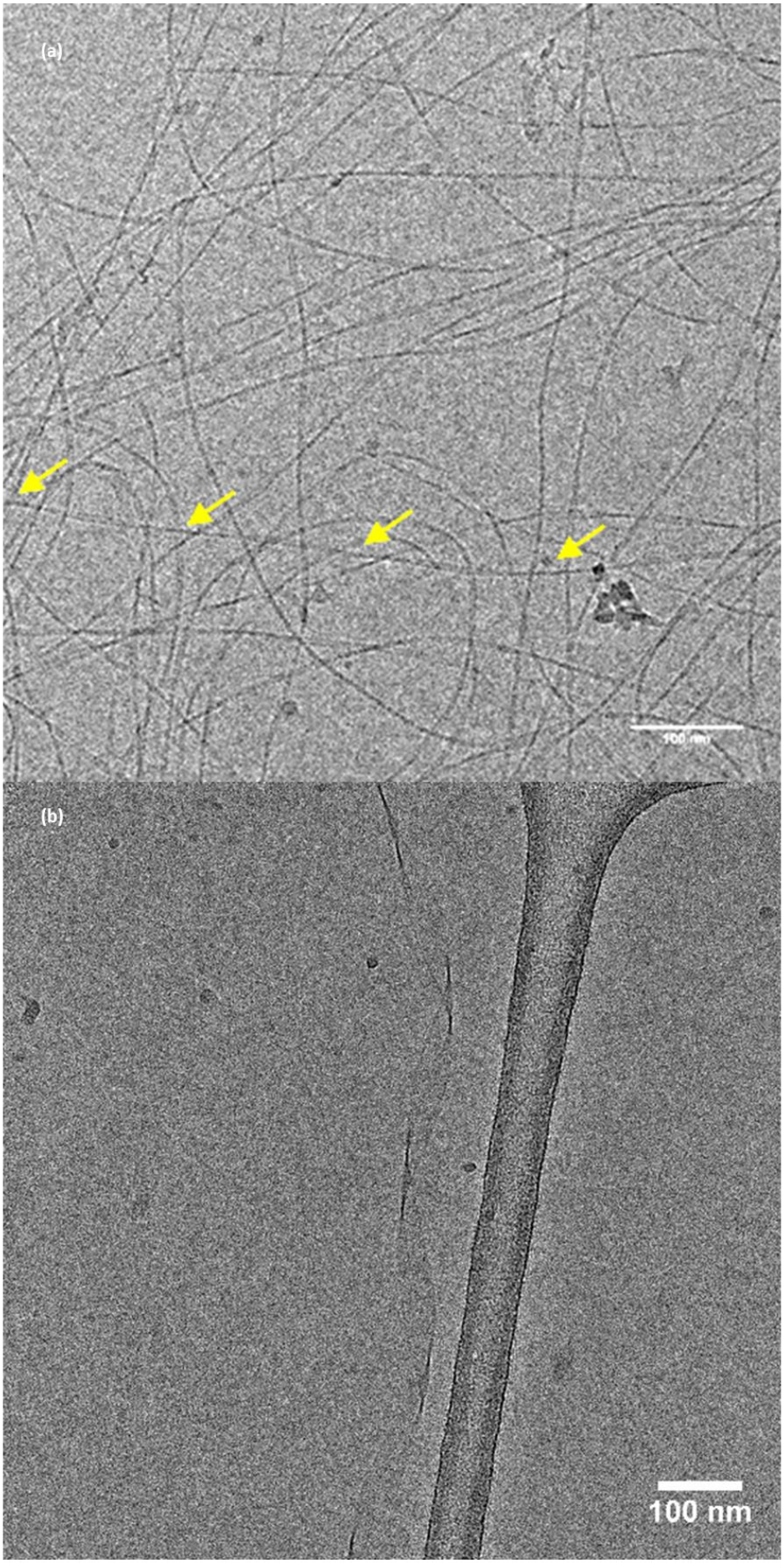

Figure 3.13 (a) Cryo-TEM image of SNP-FYP hydrogel showing narrow and twisted filaments (arrows indicate location of twisting) (b) Cryo-TEM image of ALP-FYP hydrogel showing wider and twisted filaments

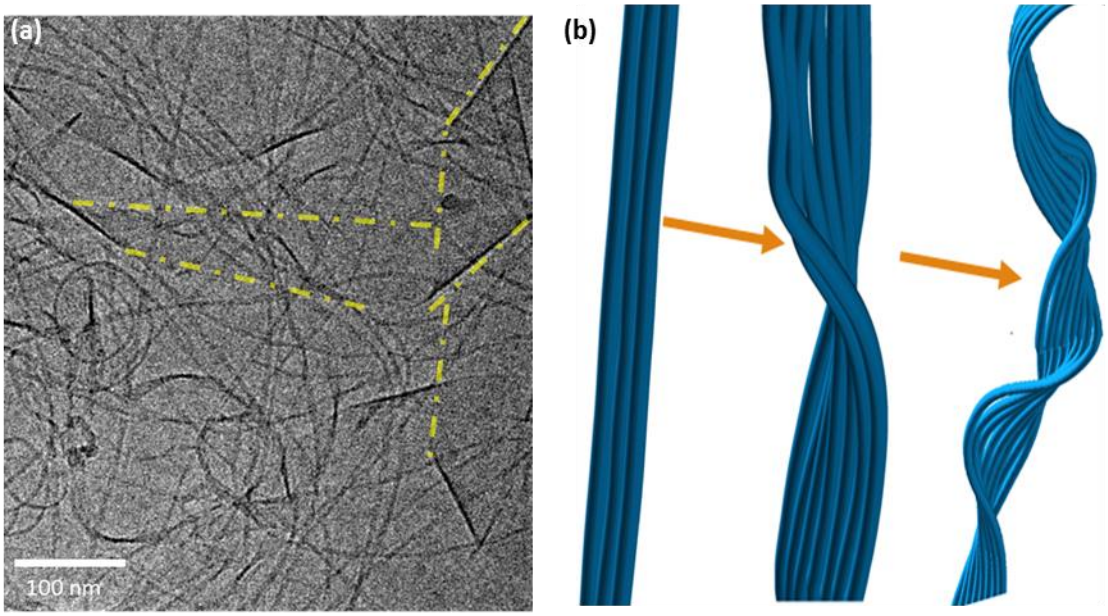

Figure 3.14 (a) cryo-TEM image of unravelled SNP-FYP nanofilaments with striations along the filament axis. (b) Coiling of a flat filament into a twisted ribbon and then into a helical ribbon.

The different filament structure was apparent from TEM. However, as the images obtained by TEM are projections, high-resolution AFM was employed to visualise 3D profiles of filaments. For the gel formed through the enzymatic route, large bundles of filaments were observed, from which smaller bundles were seen to be branching out to form the hydrogel network. There appear to be a large amount of filaments which may be an artefact of the drying process. [103]

Individual filaments were observed against freshly cleaved mica with a twisted ribbon morphology. These filaments (Figure 3.15b) had a wide tape structure 13.19 (±1.25 nm) (blue arrows) that narrowed at the twists 10.49 (±0.89 nm) (red arrows). The 3D image shows the flattening of the tape against the substrate, though the height changes for individual filaments are very subtle.

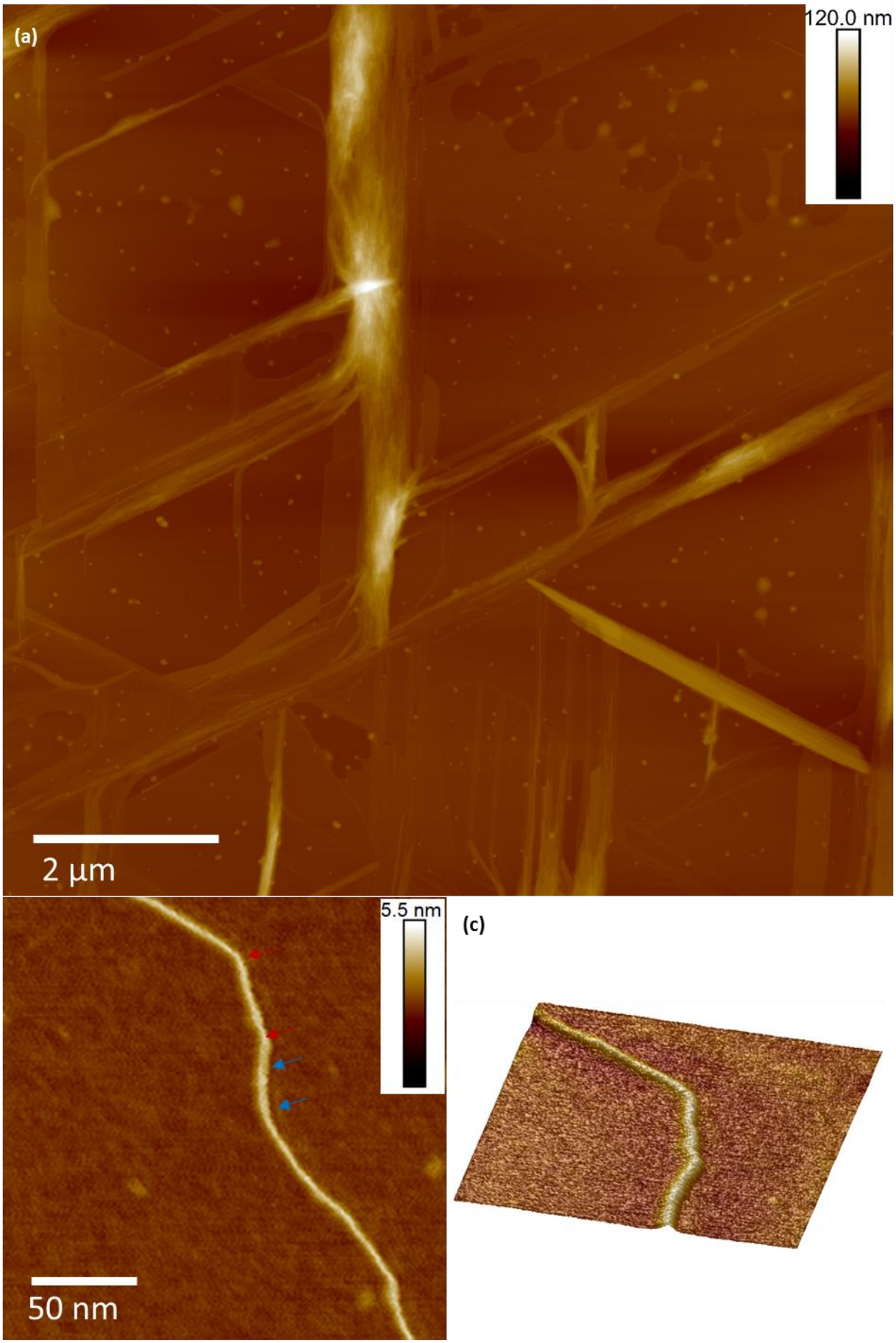

Figure 3.15 AFM data of ALP-FYP: (a) Height scan (retrace), drop cast on bare freshly cleaved mica, (b) height scan showing the twisting of an individual nanofilaments (arrows indicate location of twisting) and (c) 3D image demonstrating flattening of ribbon between two kinks. (Z-axis aspect ratio increased by a factor of two for clarity.)

For the radical induced hydrogels, the highly entangled network of supramolecular nanofilaments (Figure 3.16a) is observed in line with TEM images. At higher dilutions, individual, periodically twisted filaments (Figure 3.16b), attributed to the chiral packing of the dephosphorylated hydrogelator molecules, are imaged. Significantly, this demonstrated that left-handed helical nanofilaments were formed rather than right-handed helical nanofilaments (arrows indicate the location of twisting), as would be expected from previous studies involving FMOC-L-tyrosine. [18,19,21,73,88,104,105] This is also demonstrated by the height profile measured along the deposited nanofilament (Figure 3.16c). Thus, the use of sodium nitroprusside as nitric oxide source has unexpected implications on the self-assembly process of the hydrogelator molecules.

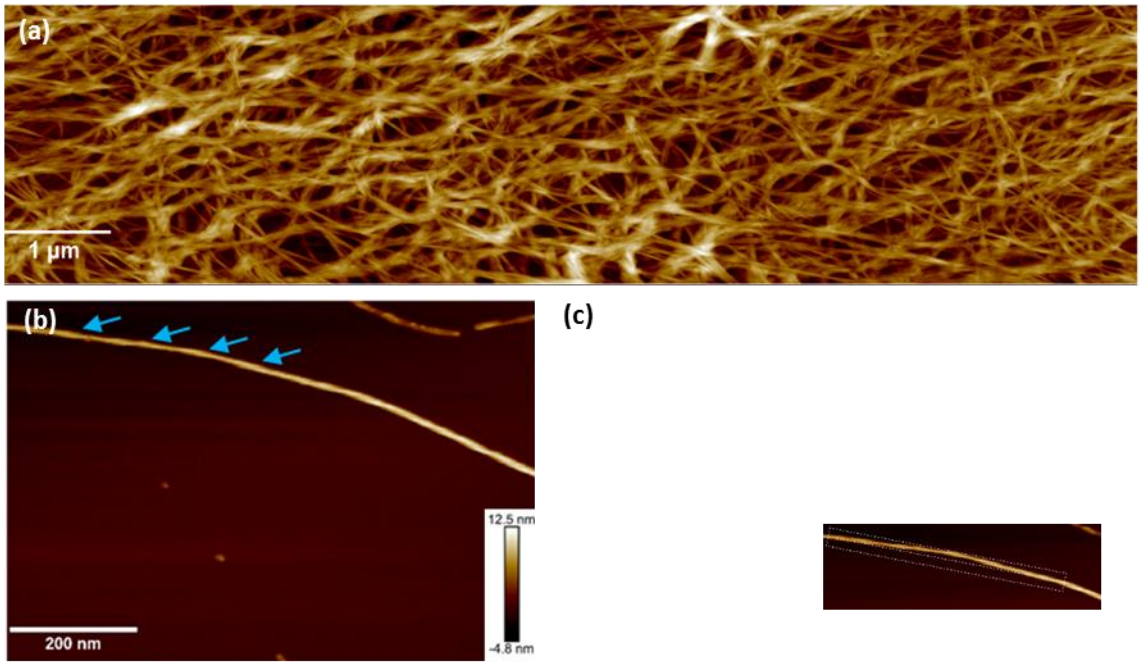

Figure 3.16 AFM data of SNP-FYP hydrogel: (a) Height scan (retrace), drop cast on bare freshly cleaved mica, (b) height scan showing the twisting of an individual nanofilament (arrows indicate location of twisting) and (c) height profile of nanofilament across nanofilament.

The unexpected chirality of the hydrogels was studied further using circular dichroism (CD) spectrometry (Figure 3.17). There was no observed chirality arising from either SNP or FYP solutions, although the former gave a low signal-to-noise ratio at low wavelengths, presumably due to absorbance and scattering from SNP. The absorptions observed at *ca.* 270 – 310 nm and 210 nm were

attributed to offset stacking of the fluorenyl moieties and π – π interactions between the phenyl side chains, respectively. [7,8,106] The peak at 304 nm has been attributed to π–π* transition induced by interactions of fluorenyl groups in the supramolecular assembly. [107–111] Remarkably, all radically induced supramolecular hydrogels had the opposite ellipticity when compared to the hydrogels formed when using alkaline phosphatase. Both hydrogels were formed using L-amino acid derivatives, and therefore it is expected that the opposite ellipticity must be due to opposite chirality inherent to the fibrillar assemblies.[8,106]

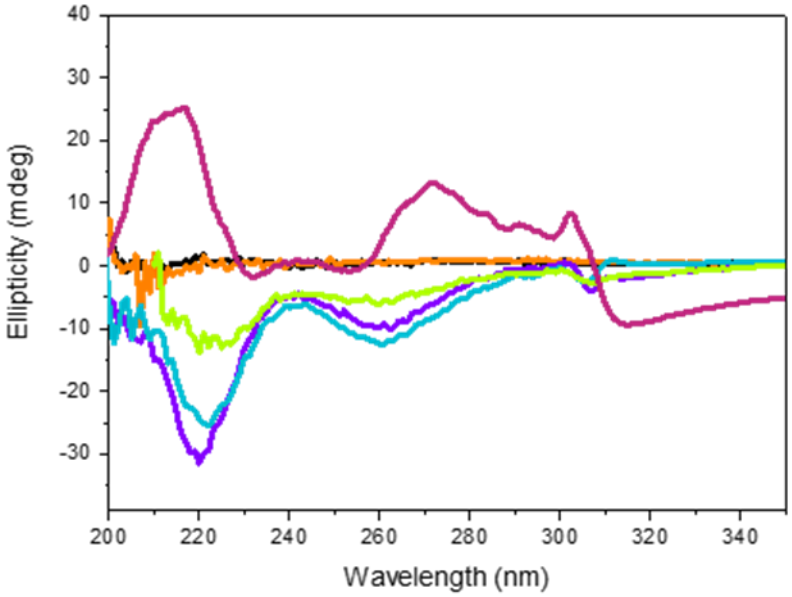

Figure 3.17 In all cases SNP: FYP ratios of 1:1 (purple), 2:1 (blue), 5:1 (green) and 10:1 (red) as well as FYP solution (black), SNP solution (orange) and ALP-FYP gel (magenta). (a) CD spectra hydrogels prepared at varying molar ratios accompanied with FYP (black) and SNP (orange) solutions and supramolecular hydrogel formed using alkaline phosphatase (maroon).

As was mentioned previously the chirality of the nanofilaments originates from hydrogen bonding between chiral amino acids and is inherently dependent on the stereochemistry of these gelators. Therefore, it was considered whether any unintended molecules were generated because of the UV irradiation and/or the use of radicals, that could disrupt the normal stacking of the gelators. This was a concern because chemical additives have been shown to affect the chirality of supramolecular

structures.[111–114] These chiral additives can stack between achiral units or bind to pendant functional groups to perturb interactions along the filament to alter supramolecular chirality.

Thus, it was considered how the use of UV irradiation and generation of radicals could result in unintended chemical modifications to the gelator. For instance, many radicals (*e.g.* superoxide radical ($O_2^{\bullet-}$), hydroxyl radical ($HO^{\bullet}$), hydroperoxyl radical ($^{\bullet}OOH$) *etc.*), colloquially referred to as reactive oxygen species, can oxidize and damage macromolecules.[42,115–119] In particular, the one-electron oxidation of tyrosine through such radicals has been widely studied, owing to such damage being associated with Alzheimer's, Parkinson's and Huntington's diseases, and atherosclerosis.[41,42,117–122]

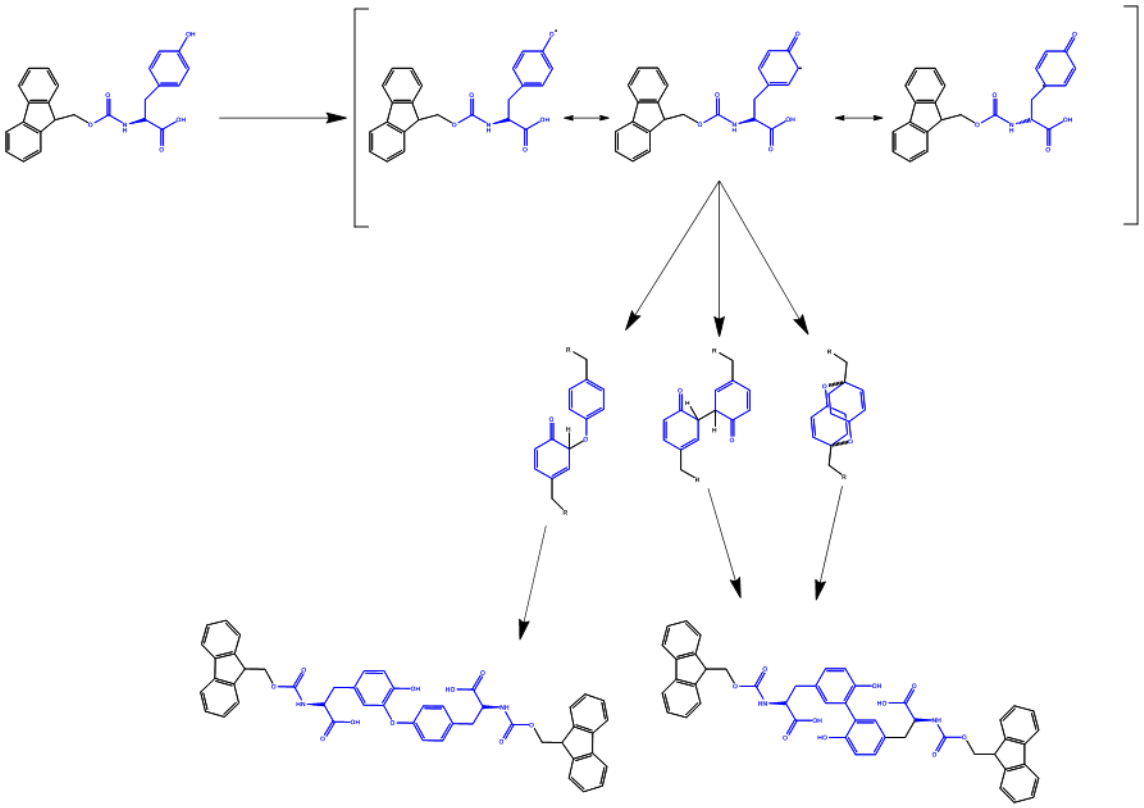

Figure 3.18 Pathways for tyrosine pathway achieved via the stacking of the tyrosyl radical

Commonly, tyrosyl radicals are formed through the abstraction of the hydrogen atom from the hydroxyl group of tyrosine. Of the many possible products, ab initio studies demonstrated that dimerization of two tyrosyl radicals to form either dityrosine or isodityrosine are major products. This is due to strong electron correlation between the two tyrosyl moieties, which is stabilised when the

two are stacked, as the highest energy occupied molecular orbital electron pair is highly delocalised. It is plausible that the tyrosine residues will be in close proximity throughout the gelation process for stacking to occur (Figure 3.18). Furthermore, oxidising agents such as potassium ferricyanide and other iron containing compounds have been used to catalyse the oxidation of tyrosine leading to the formation of dityrosine.[115,116,119,123]

Also, tyrosyl radicals are also formed as a result of the photoexcitation of the tyrosine by UV irradiation followed by the abstraction of the hydroxyl proton *via* electron ejection.[124,125] Both of these conditions mentioned are met and could lead to the formation of dityrosine or isodityrosine (Figure 3.19).

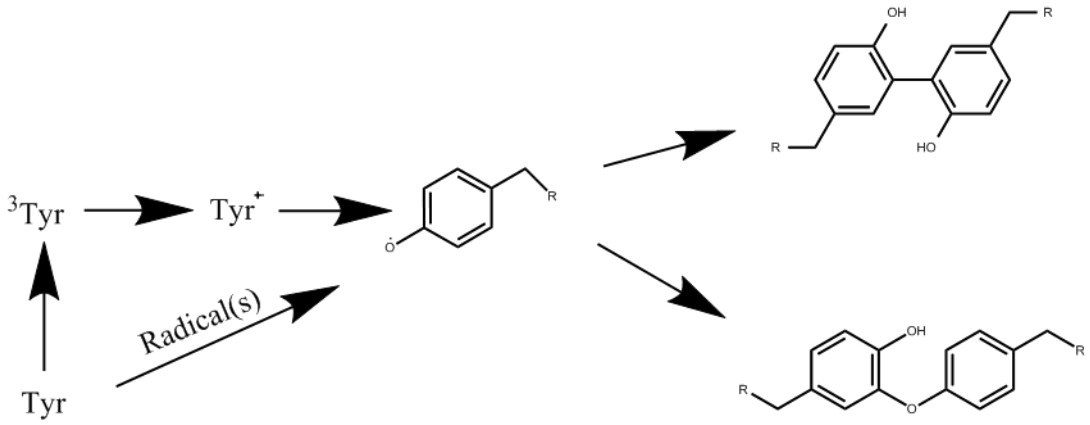

Figure 3.19 Reported pathways leading to the oxidation of tyrosine to form an unintended product

Dityrosine is thought to stabilise assembles of amyloid β-protein into oligomer filaments and trigger Alzheimer's disease. [116,118–120,122,124,126–129] Dityrosine affects the assembly process of peptides into Amyloidβ fibrils and has been shown to affect the conformation of β-sheet assemblies. [116,118] Obviously, the assembly process between peptides and protected single-amino acids is not interchangeable. However, it is plausible that any unexpected formation of dityrosine could perturb assembly between gelators in a similar way to produce unanticipated filament structures.

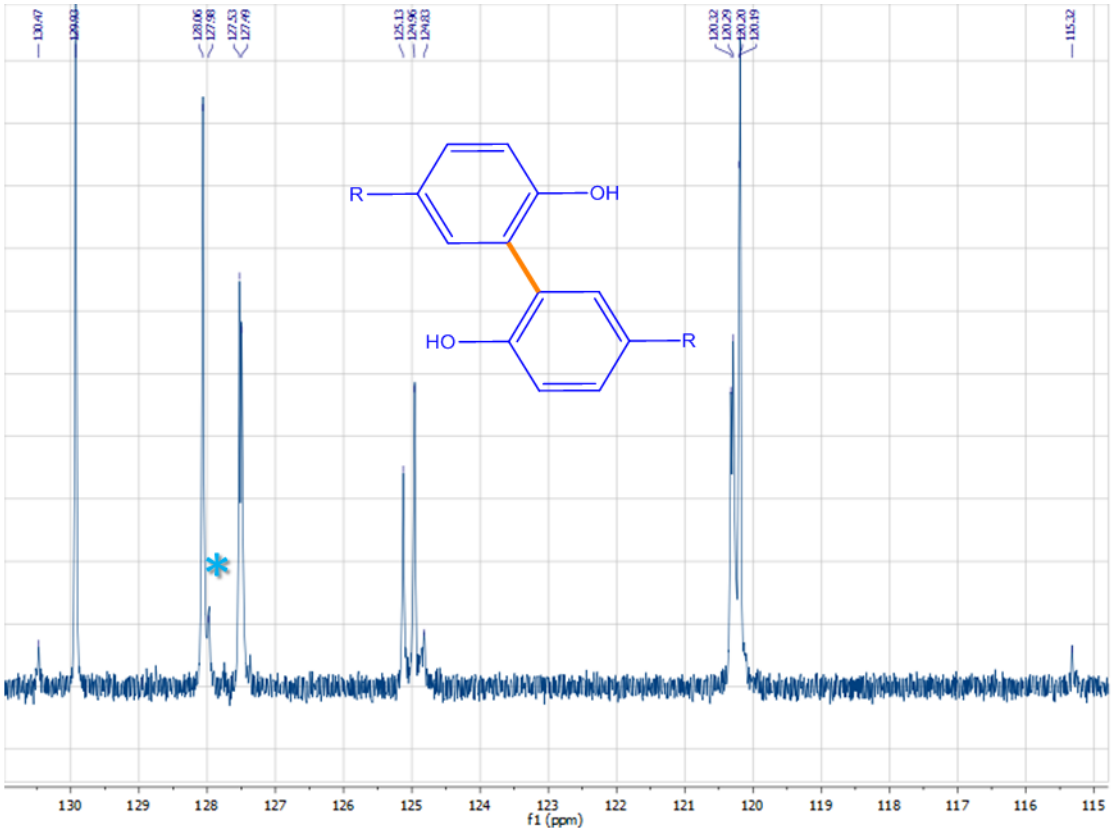

Figure 3.20 ^{13}C NMR of 2-1 Gel (500 MHz, D_2O) exhibiting a resonance peak (*) at 127.98 ppm associated with the carbon-carbon bond formed between the two tyrosyl moieties, illustrated above peak.

Indeed, ^{13}C NMR spectroscopy (Figure 3.20) demonstrated that small amounts of dityrosine were in fact formed, as identified by the resonance peak at several resonance peaks associated with formation of dityrosine, at 115.32, 127.98 and 130.47 ppm corresponding to the perturbed tyrosine ring.[119,130] Significantly, increasing the stoichiometry of SNP increased the intensity of peak associated with dityrosine formed indicating that SNP played a significant role in the formation of dityrosine rather than the UV irradiation.

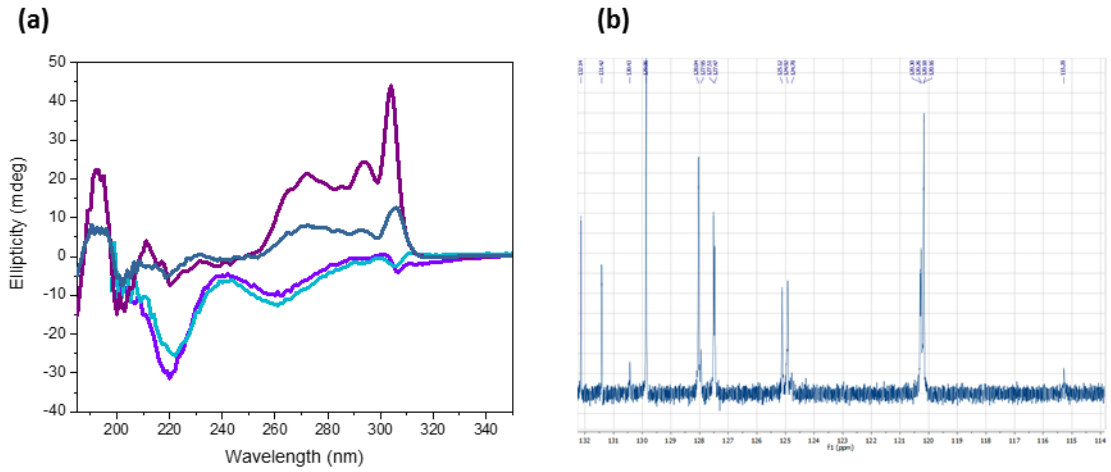

Figure 3.21 (a) CD spectra of hydrogels before and after melting, demonstrating that the chirality of the SNP-FYP can be reversed to the expected chirality after a heating and cooling cycle. 1-1 (before: light purple, after: dark purple) and 2-1 (before: light blue, after: dark blue). (b) ^{13}C NMR of melted 2-1 Gel displaying a resonance at 115 ppm associated with dityrosine. (500 MHz, d_6DMSO)

However, on investigating the stability of the supramolecular chirality to melting, it was observed that melting and then cooling the gel caused it to reform with the expected chirality (Figure 3.21). Significantly, the resonance peak at 128 pm associated with the carbon-carbon bond between the tyrosine moieties of dityrosine was retained. This indicated that the formation of dityrosine was not the cause of the unexpected chirality. Rather, the unexpected chirality is the result of kinetically trapped structures formed in the gelation process but after the heating and cooling cycle, a more thermodynamically favoured state is reached,[20] with chirality in line with what would be expected.

The filaments formed in the presence of SNP are less stable compare to the filaments formed through the enzymatic cleavage due to the different curvatures for the different structures. Work by Oda *et al.* demonstrated that twisted ribbons, like those formed in the enzymatic route, are thermodynamically more stable compare to helical ribbons, formed by the SNP route.[114,131] This can be explained due to geometric reasons, as the interlayer coordination favours a saddle-like curvature, resulting in the formation of twisted ribbons, over the formation of cylindrical sheets, forming helical ribbons. This is because for the later the contact area varies for each layer with the outermost layer twisting the most.

Heating has been shown to allow for the rearrangement of kinetically trapped structures through the disassembly of such assemblies and subsequent assembly into more thermodynamically favoured fibril morphologies. [30,132–134] Thus, it is necessary to consider the environment in which the FMOC-tyrosine self-assembles and how this differs between the two routes. Most obviously, the high stoichiometries of sodium nitroprusside appear to be affecting the network structure and to be interacting with the nanofilaments. Therefore, it was considered that the presence of the SNP could be affecting the chirality.

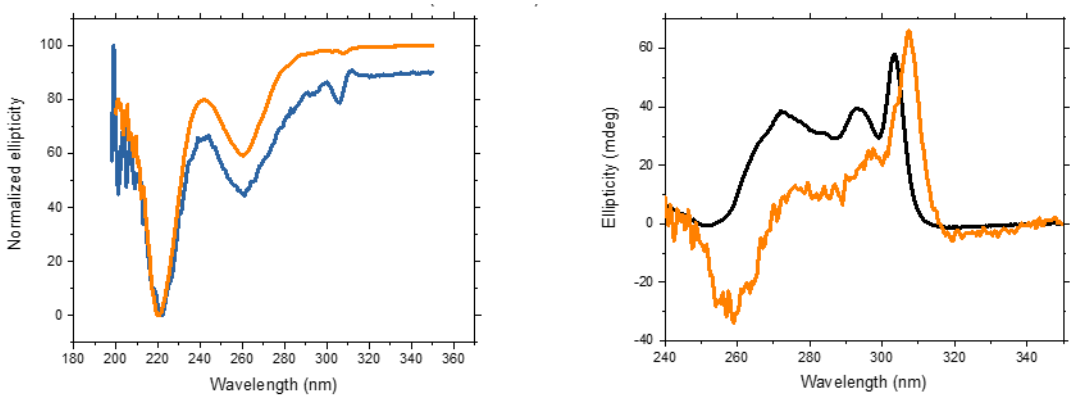

Figure 3.22 CD spectra of doped control gels (a) Fmoc tyrosine-phosphate (50mM) mixed with ALP (1kU/mL) at 37 °C (In tin foil) in the presence of SNP (250 mM) (orange) and SNP-FYP gel at the 2:1 ratio (blue), (b) Fmoc tyrosine-OH (50mM) gelled in the dark via through a lowering of the pH via the hydrolysis of glucono delta lactone (3 mg) in the presence of SNP (100 mM) (orange) and in the absence of SNP (black)

Hence, experiments were set up whereby SNP was present in solution but not used to trigger gelation in order to determine whether its presence in solution was sufficient to affect the supramolecular chirality. This was possible because SNP does not spontaneously release nitric oxide radicals and is stable in the dark,[58,60] rather, it is widely reported that either irradiation with light or one-electron reduction by reducing agents (*e.g.*, thiols, hemoproteins, ascorbate) present in most biological tissues is necessary for the production of nitric oxide radicals. [55,58,59]

Therefore, SNP was doped into an enzymatically- triggered gel and a pH-triggered gel. Both of which were prepared and gelled in the dark. These experiments demonstrated (Figure 3.22) that the supramolecular chirality of the hydrogels, again observed *via* CD, could be affected when SNP was

present in the gelling solution but not used to trigger the gelation. This demonstrates that it is the presence of the sodium nitroprusside affecting the supramolecular chirality.

It has previously been shown that anionic salts can polarize the water molecules to affect the hydrogen bonding to peptides or have direct interactions with the amides of gelators themselves to affect their assembly. [20,22,94,98,135,136]

Yang *et al.* proposed that Fmoc-tyrosine hydrogen bonds with solvent molecules as part of its supramolecular packing[18,73] and interactions between similar salts, *i.e.* potassium ferricyanide and peptides have been shown,[136] it possible that either of these effects could alter the hydrogen bonding and therefore the supramolecular packing of Fmoc-tyrosine.

As mentioned, the supramolecular chirality observed in the CD spectrum, TEM and AFM arises from the curvature of the H-bonding between the chiral gelators. Thus, it is unsurprising that FT-IR demonstrates that the SNP-FYP gels exhibit a different hydrogen bonding network compared to the ALP gels. Both gels exhibit peaks between 1600-1700 cm^{-1} arising from the carbonyl hydrogen bonding (Figure 3.23a), indicative of a β-sheet-like assembly.[91,137–139] Unfortunately, part of the region is masked by OH bend vibrations of water weakly associated with SNP,[67] though it is possible to integrate other peaks. The broad band at 1565 cm^{-1} only present for the ALP FYP gel corresponds to the unprotonated carboxylic acid, arising due to the higher pH of this gel and is not indicative of different packing.[22,139] It may also be that the presence of the enzyme in the ALP-FYP samples contributes to the signal in this region. However, the peak associated with hydrogen bonding originating from the carbamate is significantly red shifted by 20 cm^{-1}. This shift to a higher frequency indicates a weakening of the intermolecular hydrogel bonding for the SNP gels compared to the ALP gels.[138,140,141] Also, at lower wavenumbers, with contributions from N-H bending vibrations[141–143], also demonstrated shifts.

At higher wavenumbers, it is possible to probe how the hydroxyl groups of the carboxylic acid and phenyl residue are affected. First, consider the peaks at 2143 and 2157 cm^{-1} that are associated to equatorial C≡N IR stretching bands and then the band at 2174 cm^{-1} corresponding to the axial C≡N

stretch.[61,66,144] For, the radical-triggered gel sample, there is also a new peak at 2122 cm^{-1} indicating that these groups are forming a new interaction in the gels. Notably, these are not present for irradiated SNP dissolved in the buffer. There is a very small peak at 2100 cm^{-1} which is assigned to free ejected $C{\equiv}N^-$ and thus the peak at 2122 cm^{-1} is not indicative of ejected $C{\equiv}N^-$.[66]

Therefore, this new peak is likely a result of interactions with the gelator instead. Concomitantly there are changes in peaks from 2800-3400 cm^{-1} associated with hydrogen bonded hydroxyl groups of the pendant carboxylic acid and the phenyl residue. Thus, as with the carbonyl peaks, this may be associated with these groups hydrogen bonding to polarised solvent molecules. Additionally, the nitrogen of cyanide has been reported as a hydrogen bond acceptor,[145–147] which may allow for direct interactions with the gelator through hydrogen bonding with the pendant carboxylic acid and the phenol moiety, both of which will be protonated. The two peaks at 3546 and 3628 cm^{-1} are antisymmetric OH stretches for water solvating the sodium nitroprusside. [67]

Previously, peptide-based fibrils formed through a β-sheet hydrogen bonding network have shown variations in chirality due to assembly conditions, indicating that such a motif is sufficiently versatile to allow filaments of either handedness to form.[148–150] Hence, a perturbed hydrogen bonding arrangement could conceivably affect the curvature and consequently the supramolecular chirality of the hydrogel filaments.

Another consideration is that the hydroxyl group is an electron donating group and therefore polarises the π-system of the phenyl residue; different hydrogen bonding for the SNP-FYP gel would affect the electronics of the aromatic ring relative to the enzyme-mediated system. Indeed shifts are observed relative to ALP-FYP gel, at 1402 cm^{-1} to 1413 cm^{-1} and 1446 cm^{-1} to 1438 cm^{-1}, associated with the hydroxyl (C-O-H) bending vibration of the tyrosine and ring vibrations, respectively. [151,152]

It is known that the electronic nature of aromatic rings, determined by substituents, can tune the strength and geometry of intermolecular aromatic interactions. [153–156] Thus, alongside hydrophobic and Van der Waals, the electrostatic component is a key contribution to aromatic-aromatic

interactions. The electrostatics arise, in part due to the quadrupole moment of aromatic rings, resulting from the positively charged σ-framework between two regions of negatively charged π-electron density, which is present on the face of the ring. [153,156,157] The geometries for intermolecular π-π interactions are, partly, determined by the quadrupole moment and therefore any perturbation could conceivably encourage different arrangements. [153] Finally, the different aromatic stacking arrangements were investigated below.

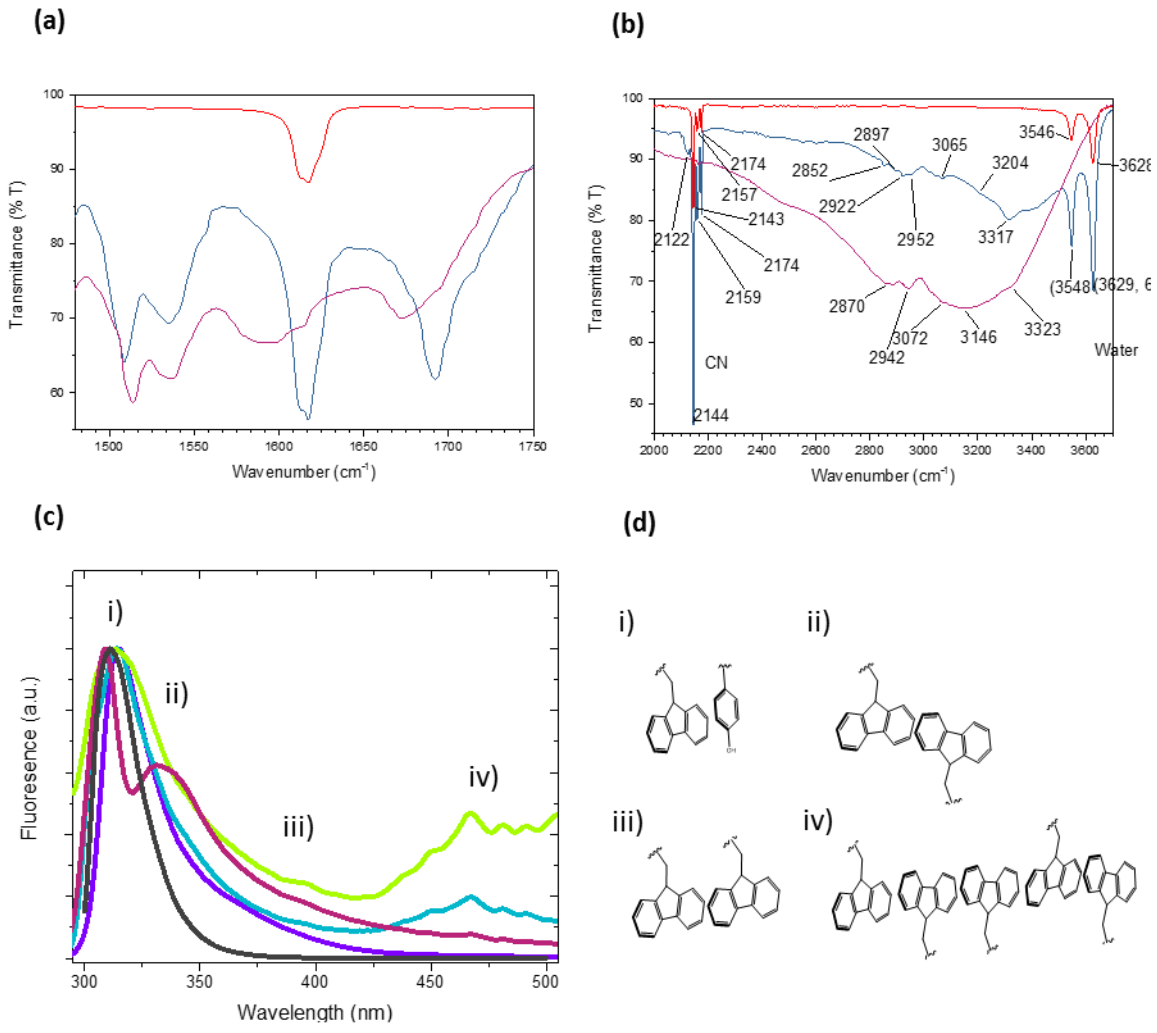

Figure 3.23 (a) and (b) FT-IR of representative SNP-FYP hydrogel and gel achieved through enzymatic route, (c) emission spectra of hydrogels prepared at varying molar ratios accompanied with SNP (black) solution In all cases SNP: FYP ratios of 1:1 (purple), 2:1 (blue), 5:1 (green) and 10:1 (red), supramolecular hydrogel formed using alkaline phosphatase (maroon), (d) as well as FYP solution (black), SNP solution (orange) and ALP-FYP gel (magenta)(d) different aromatic packing arrangements

Beyond hydrogen bonding, another key driving force for the assembly of amphiphilic gelators is the π-π stacking and hydrophobic interactions between the aromatic residues. These give rise to a series of different stacking modes for the aromatic residues[18,100] (Figure 3.23c). Unfortunately, the crystallinity of the SNP excludes powder x-ray diffraction and wide-angle x-ray scattering as useful techniques, yet fluorimetry yields an insight into these assemblies. Figure 3.#c shows the emission spectra for FMOC tyrosine phosphate solution and hydrogel samples. The solution exhibited an emission at 311 nm and all other samples showed a slight red-shift in their emission indicative of inefficient π–π stacking[73,158] which has been attributed to Fmoc-phenyl stacking (Figure 3.23d(i)). At higher wavelengths, differences between the two samples are evident. For instance, the ALP-FYP gel exhibits a peak at 331 nm, indicative of anti-parallel stacking of the Fmoc residues[18] (Figure 3.23d (ii)), which is absent in the SNP-FYP gels. Although there is significant broadening for all SNP-FYP gels there is instead a peak at 395 nm, associated with parallel stacking of Fmoc residues[18] (Figure 3.23d (iii)). Most significantly of all, however, is that with increasing SNP: FYP ratios there is an increase in intensity for substantially red-shifted emission peaks, attributed to excimer formation as a result of extended and conjugated π– π stacking interactions. [73,89,91,100,139] Thus, the increased amounts of SNP present in solution encourage extended aromatic stacking. This is in line with previous reports that observed that hydrophobic interactions become dominant when anionic salts are involved in the assembly process. [94,159]

Conclusions

To conclude, herein is the first ever use, to the best of the author's knowledge, of radicals to form a supramolecular hydrogel, thereby expanding the synthetic methodologies available. The formed hydrogelator self-assembles into high-aspect ratio nanofilaments that entangle to form a self-supported viscoelastic hydrogel. The mechanical properties of this network are affected by the stoichiometry of SNP used. The interconnecting nanofilaments were visualised *via* TEM and high-resolution AFM with the latter, surprisingly, revealing periodically twisted fibres with left-handed chirality, which was corroborated by CD analysis. We envisage that this methodology should open new routes to altering the molecular packing of gelator molecules to construct novel chiral supramolecular architectures.

Future Work

In this chapter, the use of nitric oxides radicals as a trigger for gelation, through dephosphorylation of Fmoc-tyrosine, has been demonstrated. However, it would be advantageous to pursue alternative means of nitric oxide release. Beyond the toxicity issues arising from using sodium nitroprusside, [59] its presence has proved problematic when trying to image individual nanofilaments, particularly when using sensitive techniques such as AFM.

Thankfully, owing to the extensive use of nitric oxide as a therapeutic agent, there has been extensive research into alternative nitric oxide donors. [55–57,59,160–176] For instance, one of the most common classes of donors are S-Nitrosothiols which dissociate, when appropriately triggered, *e.g.*, photolysis, to form nitric oxide and their corresponding disulphide. [163,165–168,177] However, these are not an appropriate replacement to SNP owing to their relatively low solubility and high cost. Instead, amine-derived diazeniumdiolates are a more promising alternative, being both cheaper and more soluble than S-nitrosothiols.

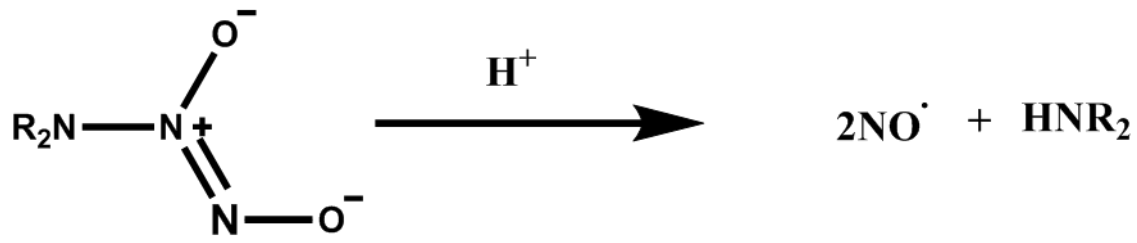

Figure 3.24 Dissociation of amine-derived diazeniumdiolate via protonation of the amino nitrogen to produce two equivalents of nitric oxide.

Dissociation of the anion provides two equivalents of nitric oxide radicals and has been shown to occur *via* the protonation of the amino nitrogen, making the rate of dissociation pH dependent.[57,59,174,176] Interestingly, the dissociation rate can also be carefully modulated *via* a choice of the R- group, which could affect the rate of dephosphorylation and gelation which could then have consequences to the mechanical properties of resulting supramolecular gel.[178,179] For instance, the work by Adams *et al.*

demonstrated that by utilizing the slow hydrolysis of glucono-δ-lactone to gluconic acid resulted in a uniform pH change and produced more uniform and reproducible hydrogels. [90,180]

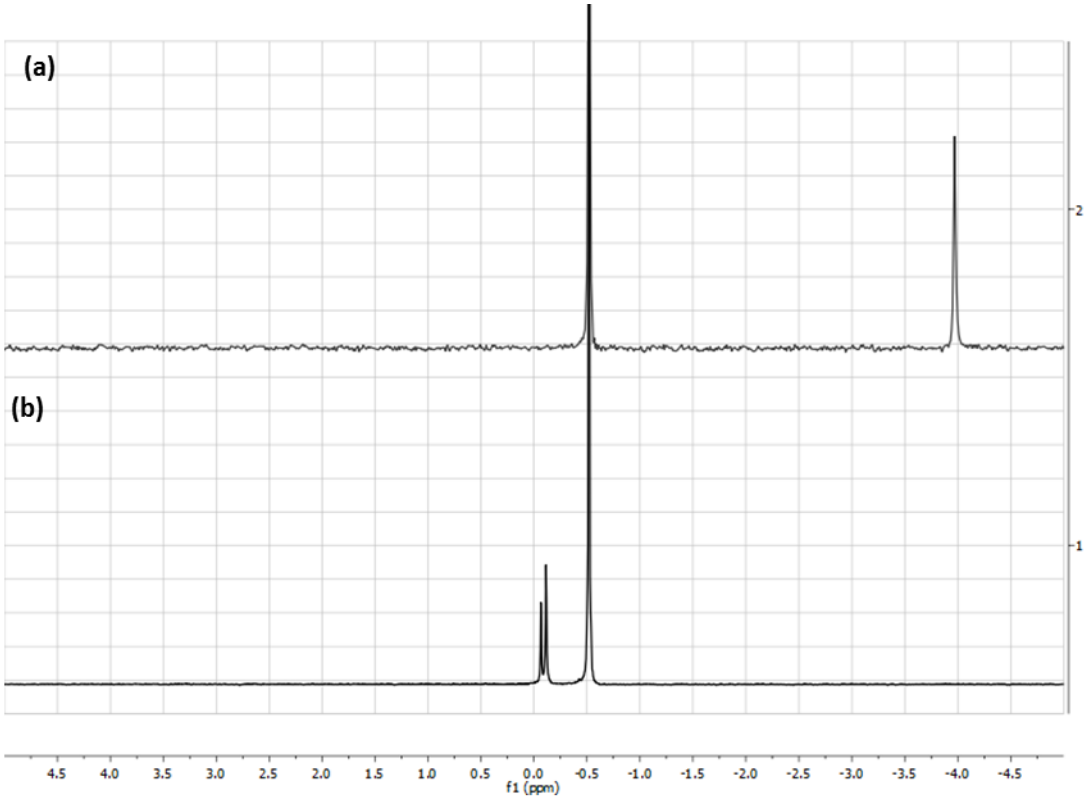

Figure 3.25 ^{31}P NMR spectra of dephosphorylation experiment of FYP via DETA. a) Aqueous FMOC-Tyr-POH displaying resonances at -3.96 ppm and -0.52 ppm for the aryl phosphate ester groups and triethyl phosphate (internal standard), respectively and b) dephosphorylated FYP displaying resonances at -0.06, -0.11 and -0.52 ppm associated with triethyl phosphate and cleaved phosphate group, respectively. Total dephosphorylation demonstrated by disappearance of resonance for the phosphate ester groups associated at -3.96 ppm

The diazeniumdiolate, 2,2'-(Hydroxynitrosohydrazono)bis-ethanimine (DETA), has been shown to be a promising candidate as it is capable of completely dephosphorylating FYP, as shown by NMR studies (Figure 3.25).

The use of photo irradiation to trigger gelation could also be used pattern hydrogel structure. Initial studies demonstrated localised gelation. Spatial resolution could be improved by undertaking such experiments within an existing hydrogel network. For instance, Cornwell *et al.* demonstrated that convection and diffusion of the gelation trigger could be limited in an existing gel to better localise gelation at the point of irradiation. [180]

References

(1) Estroff, L. a; Hamilton, A. D. Water Gelation by Small Organic Molecules. *Chem. Rev.* 2004, *104* (3), 1201–1217.

(2) Weiss, R. G.; Terech, P. *Molecular Gels*; Weiss, R. G., Terech, P., Eds.; Springer Netherlands: Dordrecht, 2006.

(3) Ramachandran, S.; Flynn, P.; Tseng, Y.; Yu, Y. B. Electrostatically Controlled Hydrogelation of Oligopeptides and Protein Entrapment. *Chem. Mater.* 2005, *17* (26), 6583–6588.

(4) Peters, G. M.; Davis, J. T. Supramolecular Gels Made from Nucleobase, Nucleoside and Nucleotide Analogs. *Chem. Soc. Rev.* 2016, *45* (11), 3188–3206.

(5) Sangeetha, N. M.; Maitra, U. Supramolecular Gels: Functions and Uses. *Chem. Soc. Rev.* 2005, *34* (10), 821.

(6) George, M.; Weiss, R. G. Molecular Organogels. Soft Matter Comprised of Low-Molecular-Mass Organic Gelators and Organic Liquids. *Acc. Chem. Res.* 2006, *39* (8), 489–497.

(7) Ryan, D. M.; Doran, T. M.; Nilsson, B. L. Stabilizing Self-Assembled Fmoc–F 5 –Phe Hydrogels by Co-Assembly with PEG-Functionalized Monomers. *Chem. Commun.* 2011, *47* (1), 475–477.

(8) Ryan, D. M.; Anderson, S. B.; Senguen, F. T.; Youngman, R. E.; Nilsson, B. L. Self-Assembly and Hydrogelation Promoted by F 5 -Phenylalanine. *Soft Matter* 2010, *6* (3), 475–479.

(9) Ryan, D. M.; Doran, T. M.; Nilsson, B. L. Complementary π–π Interactions Induce Multicomponent Coassembly into Functional Fibrils. *Langmuir* 2011, *27* (17), 11145–11156.

(10) Dudukovic, N. A.; Zukoski, C. F. Gelation of Fmoc-Diphenylalanine Is a First Order Phase Transition. *Soft Matter* 2015, *11* (38), 7663–7673.

(11) Rajagopal, K.; Lamm, M. S.; Haines-Butterick, L. A.; Pochan, D. J.; Schneider, J. P. Tuning the PH Responsiveness of β-Hairpin Peptide Folding, Self-Assembly, and Hydrogel Material Formation. *Biomacromolecules* 2009, *10* (9), 2619–2625.

(12) Schneider, J. P.; Pochan, D. J.; Ozbas, B.; Rajagopal, K.; Pakstis, L.; Kretsinger, J. Responsive Hydrogels from the Intramolecular Folding and Self-Assembly of a Designed Peptide. *J. Am. Chem. Soc.* 2002, *124* (50), 15030–15037.

(13) Salick, D. A.; Kretsinger, J. K.; Pochan, D. J.; Schneider, J. P. Inherent Antibacterial Activity of a Peptide-Based β-Hairpin Hydrogel. *J. Am. Chem. Soc.* 2007, *129* (47), 14793–14799.

(14) Qin, X.; Xie, W.; Tian, S.; Cai, J.; Yuan, H.; Yu, Z.; Butterfoss, G. L.; Khuong, A. C.; Gross, R. A. Enzyme-Triggered Hydrogelation via Self-Assembly of Alternating Peptides. *Chem. Commun.* 2013, *49* (42), 4839.

(15) Yang, Z.; Liang, G.; Xu, B. Enzymatic Hydrogelation of Small Molecules. *Acc. Chem. Res.* 2008, *41* (2), 315–326.

(16) Krishna Kumar, R.; Yu, X.; Patil, A. J.; Li, M.; Mann, S. Cytoskeletal-like Supramolecular Assembly and Nanoparticle-Based Motors in a Model Protocell. *Angew. Chemie Int. Ed.* 2011, *50* (40), 9343–9347.

(17) Kumar, R. K.; Li, M.; Olof, S. N.; Patil, A. J.; Mann, S. Artificial Cytoskeletal Structures Within Enzymatically Active Bio-Inorganic Protocells. *Small* 2013, *9* (3), 357–362.

(18) Yang, Z.; Gu, H.; Fu, D.; Gao, P.; Lam, J. K.; Xu, B. Enzymatic Formation of Supramolecular Hydrogels. *Adv. Mater.* 2004, *16* (16), 1440–1444.

(19) Patil, A. J.; Kumar, R. K.; Barron, N. J.; Mann, S. Cerium Oxide Nanoparticle-Mediated Self-Assembly of Hybrid Supramolecular Hydrogels. *Chem. Commun.* 2012, *48* (64), 7934.

(20) Roy, S.; Javid, N.; Sefcik, J.; Halling, P. J.; Ulijn, R. V. Salt-Induced Control of Supramolecular Order in Biocatalytic Hydrogelation. *Langmuir* 2012, *28* (48), 16664–16670.

(21) Thornton, K.; Smith, A. M.; Merry, C. L. R.; Ulijn, R. V. Controlling Stiffness in Nanostructured Hydrogels Produced by Enzymatic Dephosphorylation. *Biochem. Soc. Trans.* 2009, *37* (Pt 4), 660–664.

(22) Carrick, L. M.; Aggeli, A.; Boden, N.; Fisher, J.; Ingham, E.; Waigh, T. A. Effect of Ionic Strength on the Self-Assembly, Morphology and Gelation of PH Responsive β-Sheet Tape-Forming Peptides. *Tetrahedron* 2007, *63* (31), 7457–7467.

(23) Ozbas, B.; Kretsinger, J.; Rajagopal, K.; Schneider, J. P.; Pochan, D. J.; Bulent Ozbas, Salt-Triggered Peptide Folding and Consequent Self-Assembly into Hydrogels with Tunable Modulus. *Macromolecules* 2004, *37* (19), 7331–7337.

(24) Helen, W.; de Leonardis, P.; Ulijn, R. V.; Gough, J.; Tirelli, N. Mechanosensitive Peptide Gelation: Mode of Agitation Controls Mechanical Properties and Nano-Scale Morphology. *Soft Matter* 2011, *7* (5), 1732–1740.

(25) Greenfield, M. A.; Hoffman, J. R.; Olvera de la Cruz, M.; Stupp, S. I. Tunable Mechanics of Peptide Nanofiber Gels. *Langmuir* 2010, *26* (5), 3641–3647.

(26) Raeburn, J.; Zamith Cardoso, A.; Adams, D. J. The Importance of the Self-Assembly Process to Control Mechanical Properties of Low Molecular Weight Hydrogels. *Chem. Soc. Rev.* 2013, *42* (12), 5143.

(27) Ding, B.; Li, Y.; Qin, M.; Ding, Y.; Cao, Y.; Wang, W. Two Approaches for the Engineering of Homogeneous Small-Molecule Hydrogels. *Soft Matter* 2013, *9* (18), 4672.

(28) Chen, L.; Raeburn, J.; Sutton, S.; Spiller, D. G.; Williams, J.; Sharp, J. S.; Griffiths, P. C.; Heenan, R. K.; King, S. M.; Paul, A.; Furzeland, S.; Atkins, D.; Adams, D. J. Tuneable Mechanical Properties in Low Molecular Weight Gels. *Soft Matter* 2011, *7* (20), 9721.

(29) Poolman, J. M.; Boekhoven, J.; Besselink, A.; Olive, A. G. L.; Esch, J. H. Van; Eelkema, R.; van Esch, J. H.; Eelkema, R. Variable Gelation Time and Stiffness of Low-Molecular-Weight Hydrogels through Catalytic Control over Self-Assembly. *Nat. Protoc.* 2014, *9* (4), 977–988.

(30) Tantakitti, F.; Boekhoven, J.; Wang, X.; Kazantsev, R. V.; Yu, T.; Li, J.; Zhuang, E.; Zandi, R.; Ortony, J. H.; Newcomb, C. J.; Palmer, L. C.; Shekhawat, G. S.; De La Cruz, M. O.; Schatz, G. C.; Stupp, S. I. Energy Landscapes and Functions of Supramolecular Systems. *Nat. Mater.* 2016, *15* (4), 469–476.

(31) Ardoña, H. A. M.; Draper, E. R.; Citossi, F.; Wallace, M.; Serpell, L. C.; Adams, D. J.; Tovar, J. D. Kinetically Controlled Coassembly of Multichromophoric Peptide Hydrogelators and the Impacts on Energy Transport. *J. Am. Chem. Soc.* 2017, *139* (25), 8685–8692.

(32) Naghash, H. J.; Okay, O. Formation and Structure of Polyacrylamide Gels. *J. Appl. Polym. Sci.* 1996, *60* (7), 971–979.

(33) Saka, Y.; Zetterlund, P. B.; Okubo, M. Gel Formation and Primary Chain Lengths in Nitroxide-Mediated Radical Copolymerization of Styrene and Divinylbenzene in Miniemulsion. *Polymer (Guildf).* 2007, *48* (5), 1229–1236.

(34) Sanson, N.; Rieger, J. Synthesis of Nanogels/Microgels by Conventional and Controlled Radical Crosslinking Copolymerization. *Polym. Chem.* 2010, *1* (7), 965.

(35) Hild, G.; Okasha, R. Kinetic Investigation of the Free Radical Crosslinking Copolymerization in the Pre-gel State, 1. Styrene/M- and P-divinylbenzene Systems. *Die Makromol. Chemie* 1985, *186* (1), 93–110.

(36) Zetterlund, P. B.; Saka, Y.; Okubo, M. Gelation and Hollow Particle Formation in Nitroxide-Mediated Radical Copolymerization of Styrene and Divinylbenzene in Miniemulsion. *Macromol. Chem. Phys.* 2008, *210* (2), NA-NA.

(37) Ide, N.; Fukuda, T. Nitroxide-Controlled Free-Radical Copolymerization of Vinyl and Divinyl Monomers. 2. Gelation. *Macromolecules* 1999, *32* (1), 95–99.

(38) Oturan, M. A. Electrochemically Generated Hydroxyl Radicals for in Situ Destruction of Organic Pollutants. *J. Appl. Electrochem.* 2000, *30* (4), 475–482.

(39) Butler, J. A.; Conway, B. E. The Action of Photochemically Generated Radicals from Hydrogen Peroxide on Deoxyribonucleic Acid and Simple Model Substances. *Proc. R. Soc. London. Ser. B, Biol. Sci.* 1953, *141* (905), 562–580.

(40) Brame, J.; Long, M.; Li, Q.; Alvarez, P. Trading Oxidation Power for Efficiency: Differential Inhibition of Photo-Generated Hydroxyl Radicals versus Singlet Oxygen. *Water Res.* 2014, *60*, 259–266.

(41) Gracanin, M.; Hawkins, C. L.; Pattison, D. I.; Davies, M. J. Singlet-Oxygen-Mediated Amino Acid and Protein Oxidation: Formation of Tryptophan Peroxides and Decomposition Products. *Free Radic. Biol. Med.* 2009, *47* (1), 92–102.

(42) Wright, A.; Bubb, W. A.; Hawkins, C. L.; Davies, M. J. Singlet Oxygen-Mediated Protein Oxidation: Evidence for the Formation of Reactive Side Chain Peroxides on Tyrosine Residues. *Photochem Photobiol* 2002, *76* (1), 35–46.

(43) Tafesse, F.; Enemchukwu, M. Nitric Oxide Assisted Hydrolysis of Nitrophenylphosphate. *Nitric Oxide* 2008, *18* (4), 274–278.

(44) Orth, E. S.; Medeiros, M.; Bortolotto, T.; Terenzi, H.; Kirby, A. J.; Nome, F. Dephosphorylation Reactions with Deferoxamine, a Potential Chemical Nuclease. *J. Org. Chem.* 2011, *76* (24), 10345–10348.

(45) Kuhn, L. P.; Doali, J. O.; Wellman, C. The Reaction of Nitric Oxide with Triethyl Phosphite. *J. Am. Chem. Soc.* 1960, *82* (18), 4792–4794.

(46) Schuchmann, H. P.; Wagner, R.; von Sonntag, C. γ-Radiolysis of 2'-Deoxycytidine-5'-Phosphate in Deoxygenated Aqueous Solutions. OH Radical-Induced Alterations at the Sugar Moiety. *Zeitschrift fur Naturforsch. - Sect. B J. Chem. Sci.* 1983, *38* (10), 1213–1220.

(47) Stelter, L.; Von Sonntag, C.; Schulte-Frohlinde, D. Phosphate Ester Cleavage in Ribose-5-Phosphate Induced by OH Radicals in Deoxygenated Aqueous Solution: The Effect of Fe(II) and Fe(III) Ions. *Int. J. Radiat. Biol.* 1976, *29* (3), 255–269.

(48) Zegota, H.; von Sonntag, C. *Radical-Induced Dephosphorylation of Fructose Phosphates in Aqueous Solution+*; 1981; Vol. 36.

(49) Dizdaroglu, M.; Jaruga, P. Mechanisms of Free Radical-Induced Damage to DNA. *Free Radic. Res.* 2012, *46* (4), 382–419.

(50) von Sonntag, C. The Chemistry of Free-Radical-Mediated DNA Damage. In *Basic life sciences*;

Springer US: Boston, MA, 1991; Vol. 58, 287-317; discussion 317-21.

(51) Samuni, A.; Neta, P. Hydroxy Radical Reaction with Phosphate Esters and the Mechanism of Phosphate Cleavage. *J. Phys. Chem.* 1973, *77* (20), 2425–2429.

(52) Dizdaroglu, M.; von Sonntag, C.; Schulte-Frohlinde, D. Strand Breaks and Sugar Release by _g_amma-Irradiation of DNA in Aqueous Solution_. *Zeitschrift für Naturforsch. C* 1975, *97* (11–12), 2277–2278.

(53) Brown, J. F. The Reaction of Nitric Oxide with Isobutylene. *J. Am. Chem. Soc.* 1957, *79* (10), 2480–2488.

(54) Lim, M. D.; Lorkovic, I. M.; Ford, P. C. Kinetics of the Oxidation of Triphenylphosphine by Nitric Oxide. *Inorg. Chem.* 2002, *41* (4), 1026–1028.

(55) Wang, P. G.; Xian, M.; Tang, X.; Wu, X.; Wen, Z.; Cai, T.; Janczuk, A. J. Nitric Oxide Donors: Chemical Activities and Biological Applications. *Chem. Rev.* 2002, *102* (4), 1091–1134.

(56) Yang, Y.; Qi, P.; Yang, Z.; Huang, N. Nitric Oxide Based Strategies for Applications of Biomedical Devices. *Biosurface and Biotribology* 2015, *1*, 1–25.

(57) Keefer, L. K. Progress Towards Clinical Application of NO Releasing Diazeniumdiolates. *Annu. Rev. Pharmacol. Toxicol.* 2003, *43* (1), 585–607.

(58) Butler, A. R.; Flitney, F. W.; Williams, D. L. H. NO, Nitrosonium Ions, Nitroxide Ions, Nitrosothiols and Iron-Nitrosyls in Biology: A Chemist's Perspective. *Trends Pharmacol. Sci.* 1995, *16* (1), 18–22.

(59) Keefer, L. K.; Saavedra, J. E. Nitrogen-Based Diazeniumdiolates: Versatile Nitric Oxide-Releasing Compounds for Biomedical Research and Potential Clinical Applications. *J. Chem. Educ.* 2002, *79* (12), 1427.

(60) Van Loenen, A. C.; Hofs-Kemper, W. Stability and Degradation of Sodium Nitroprusside. *Pharm. Weekbl.* 1979, *1* (1), 424–436.

(61) Wolfe, S. K.; Swinehart, J. H. Photochemistry of Pentacyanonitrosylferrate(2-), Nitroprusside. *Inorg. Chem.* 1975, *14* (5), 1049–1053.

(62) Shishido, S. M.; De Oliveira, M. G. Photosensitivity of Aqueous Sodium Nitroprusside Solutions: Nitric Oxide Release versus Cyanide Toxicity. *Prog. React. Kinet. Mech.* 2001, *26* (2–3), 239–261.

(63) Mitra, R. P.; Jain, D. V. S.; Banerjee, A. K.; Chari, K. V. R. Photolysis of Sodium Nitroprusside and Nitroprussic Acid. *J. Inorg. Nucl. Chem.* 1963, *25* (10), 1263–1266.

(64) Mitra, R. P.; Sharma, B. K.; Mittal, S. P. Photolysis of Sodium Nitroprusside in the Presence and Absence of Air. *J. Inorg. Nucl. Chem.* 1972, *34* (12), 3919–3920.

(65) Butler, A. R.; Glidewell, C. Recent Chemical Studies of Sodium Nitroprusside Relevant to Its Hypotensive Action. *Chem. Soc. Rev.* 1987, *16*, 361.

(66) de Oliveira, M. G.; Langley, G. J.; Rest, A. J. Photolysis of the $[Fe(CN)_5(NO)]^{2-}$ Ion in Water and Poly(Vinyl Alcohol) Films: Evidence for Cyano Radical, Cyanide Ion and Nitric Oxide Loss and Redox Pathways. *J. Chem. Soc. Dalt. Trans.* 1995, No. 12, 2013.

(67) Soria, D. B.; Aymonino, P. J. Vibrational and ^{13}C NMR Spectra and Thermal Behaviour of Sodium Pentacyanocarbonilferrate(II) Dihydrate, $Na_3[Fe(CN)_5CO] \cdot 2H_2O$. *Spectrochim. Acta Part A Mol. Biomol. Spectrosc.* 1999, *55* (6), 1243–1253.

(68) Wolfe, S. K.; Andrade, C.; Swinehart, J. H. Kinetic Studies of the Pentacyanonitrosylferrate(2-) Azide and -Hydroxylamine Reactions. *Inorg. Chem.* 1974, *13* (11), 2567–2572.

(69) Swinehart, J. The Nitroprusside Ion. *Coord. Chem. Rev.* 1967, *2* (4), 385–402.

(70) Leeuwenkamp, O. R.; van der Mark, E. J.; van Bennekom, W. P.; Bult, A. Investigation of the Photochemical and Thermal Degradation of Aqueous Nitroprusside Solutions Using Liquid Chromatography. *Int. J. Pharm.* 1985, *24* (1), 27–41.

(71) Tafesse, F.; Enemchukwu, M. Nitric Oxide-Triggered Bis-Trimethylenediaminecobalt(III)-Mediated Hydrolysis of Nitrophenylphosphate/Sodium Pyrophosphate. *Water. Air. Soil Pollut.* 2010, *207* (1–4), 203–212.

(72) Kruszyna, H.; Kruszyna, R.; Rochelle, L. G.; Smith, R. P.; Wilcox, D. E. Effects of Temperature, Oxygen, Heme Ligands and Sulfhydryl Alkylation on the Reactions of Nitroprusside and Nitroglycerin with Hemoglobin. *Biochem. Pharmacol.* 1993, *46* (1), 95–102.

(73) Yang, Z.; Liang, G.; Wang, L.; Xu, B. Using a Kinase/Phosphatase Switch to Regulate a Supramolecular Hydrogel and Forming the Supramolecular Hydrogel in Vivo. *J. Am. Chem. Soc.* 2006, *128* (9), 3038–3043.

(74) Skilling, K. J.; Kellam, B.; Ashford, M.; Bradshaw, T. D.; Marlow, M. Developing a Self-Healing Supramolecular Nucleoside Hydrogel. *Soft Matter* 2016, *12* (43), 8950–8957.

(75) Du, X.; Zhou, J.; Shi, J.; Xu, B. Supramolecular Hydrogelators and Hydrogels: From Soft Matter to Molecular Biomaterials. *Chem. Rev.* 2015, *115* (24), 13165–13307.

(76) Dong, R.; Pang, Y.; Su, Y.; Zhu, X. Supramolecular Hydrogels: Synthesis, Properties and Their Biomedical Applications. *Biomater. Sci.* 2015, *3* (7), 937–954.

(77) Johnson, B. B.; Ivanov, A. V.; Antzutkin, O. N.; Forsling, W. 31 P Nuclear Magnetic Resonance Study of the Adsorption of Phosphate and Phenyl Phosphates on γ-Al 2 O 3. *Langmuir* 2002, *18* (4), 1104–1111.

(78) Pedrosa, M. S.; Silva, J. F. C. Da. Ab-Initio Calculations of 31p Nmr Chemical Shifts of Substituted Aryl Dialkyl Phosphates. *Phosphorus. Sulfur. Silicon Relat. Elem.* 2001, *170* (1), 233–246.

(79) Fischer, M. R.; De Groot, H. J. M.; Raap, J.; Winkel, C.; Hoff, A. J.; Lugtenburg, J. Carbon-13 Magic Angle Spinning NMR Study of the Light-Induced and Temperature-Dependent Changes in Rhodobacter Sphaeroides R26 Reaction Centers Enriched in [4'-13C]Tyrosine. *Biochemistry* 1992, *31* (45), 11038–11049.

(80) Herzfeld, J.; Das Gupta, S. K.; Farrar, M. R.; Harbison, G. S.; McDermott, A. E.; Pelletier, S. L.; Raleigh, D. P.; Smith, S. O.; Winkel, C. Solid-State Carbon-13 NMR Study of Tyrosine Protonation in Dark-Adapted Bacteriorhodopsin. *Biochemistry* 1990, *29* (23), 5567–5574.

(81) Dash, J.; Patil, A. J.; Das, R. N.; Dowdall, F. L.; Mann, S. Supramolecular Hydrogels Derived from Silver Ion-Mediated Self-Assembly of 5'-Guanosine Monophosphate. *Soft Matter* 2011, *7* (18), 8120.

(82) Raeburn, J.; Adams, D. J. Multicomponent Low Molecular Weight Gelators. *Chem. Commun.* 2015, *51* (25), 5170–5180.

(83) Chen, G.; Hoffman, A. S. Graft Copolymers That Exhibit Temperature-Induced Phase Transitions over a Wide Range of PH. *Nature* 1995, *373* (6509), 49–52.

(84) Mahler, A.; Reches, M.; Rechter, M.; Cohen, S.; Gazit, E. Rigid, Self-Assembled Hydrogel Composed of a Modified Aromatic Dipeptide. *Adv. Mater.* 2006, *18* (11), 1365–1370.

(85) Huang, R.; Qi, W.; Feng, L.; Su, R.; He, Z. Self-Assembling Peptide–polysaccharide Hybrid Hydrogel as a Potential Carrier for Drug Delivery. *Soft Matter* 2011, *7*, 6222.

(86) Guvendiren, M.; Lu, H. D.; Burdick, J. a. Shear-Thinning Hydrogels for Biomedical Applications. *Soft Matter* 2012, *8* (2), 260.

(87) Zuidema, J. M.; Rivet, C. J.; Gilbert, R. J.; Morrison, F. a. A Protocol for Rheological Characterization of Hydrogels for Tissue Engineering Strategies. *J. Biomed. Mater. Res. - Part B Appl. Biomater.* 2014, *102* (5), 1063–1073.

(88) Thornton, K.; Abul-Haija, Y. M.; Hodson, N.; Ulijn, R. V. Mechanistic Insights into Phosphatase Triggered Self-Assembly Including Enhancement of Biocatalytic Conversion Rate. *Soft Matter* 2013, *9* (39), 9430.

(89) Birchall, L. S.; Roy, S.; Jayawarna, V.; Hughes, M.; Irvine, E.; Okorogheye, G. T.; Saudi, N.; De Santis, E.; Tuttle, T.; Edwards, A. A.; Ulijn, R. V. Exploiting CH-π Interactions in Supramolecular Hydrogels of Aromatic Carbohydrate Amphiphiles. *Chem. Sci.* 2011, *2* (7), 1349.

(90) Adams, D. J.; Butler, M. F.; Frith, W. J.; Kirkland, M.; Mullen, L.; Sanderson, P. A New Method for Maintaining Homogeneity during Liquid–hydrogel Transitions Using Low Molecular Weight Hydrogelators. *Soft Matter* 2009, *5* (9), 1856.

(91) Smith, A. M.; Williams, R. J.; Tang, C.; Coppo, P.; Collins, R. F.; Turner, M. L.; Saiani, A.; Ulijn, R. V. Fmoc-Diphenylalanine Self Assembles to a Hydrogel via a Novel Architecture Based on Π–π Interlocked β-Sheets. *Adv. Mater.* 2008, *20* (1), 37–41.

(92) Pai, V.; Srinivasarao, M.; Khan, S. a. Evolution of Microstructure and Rheology in Mixed Polysaccharide Systems. *Macromolecules* 2002, *35* (5), 1699–1707.

(93) Knerr, P. J.; Branco, M. C.; Nagarkar, R.; Pochan, D. J.; Schneider, J. P. Heavy Metal Ion Hydrogelation of a Self-Assembling Peptide via Cysteinyl Chelation. *J. Mater. Chem.* 2012, *22* (c), 1352.

(94) Li, J.; Fan, K.; Niu, L.; Li, Y.; Song, J. Effects of Salt on the Gelation Mechanism of a D-Sorbitol-Based Hydrogelator. *J. Phys. Chem. B* 2013, *117* (19), 5989–5995.

(95) Colquhoun, C.; Draper, E. R.; Schweins, R.; Marcello, M.; Vadukul, D.; Serpell, L. C.; Adams, D. J.; Yang, Z.; Ding, D.; Kong, D.; Liu, J.; Atkins, D.; Adams, D. J.; Schatz, G. C.; Stupp, S. I. Controlling the Network Type in Self-Assembled Dipeptide Hydrogels. *Soft Matter* 2017, *13* (9), 1914–1919.

(96) Mears, L. L. E.; Draper, E. R.; Castilla, A. M.; Su, H.; Zhuola; Dietrich, B.; Nolan, M. C.; Smith, G. N.; Doutch, J.; Rogers, S.; Akhtar, R.; Cui, H.; Adams, D. J. Drying Affects the Fiber Network in Low Molecular Weight Hydrogels. *Biomacromolecules* 2017, acs.biomac.7b00823.

(97) Dubochet, J.; Adrian, M.; Chang, J. J.; Homo, J. C.; Lepault, J.; McDowall, A. W.; Schultz, P. Cryo-Electron Microscopy of Vitrified Specimens. *Q. Rev. Biophys.* 1988, *21* (2), 129–228.

(98) Hu, Y.; Lin, R.; Zhang, P.; Fern, J.; Cheetham, A. G.; Patel, K.; Schulman, R.; Kan, C.; Cui, H. Electrostatic-Driven Lamination and Untwisting of β-Sheet Assemblies. *ACS Nano* 2016, *10* (1), 880–888.

(99) Smith, A. M.; Collins, R. F.; Ulijn, R. V.; Blanch, E. Raman Optical Activity of an Achiral Element in a Chiral Environment. *J. Raman Spectrosc.* 2009, *40* (9), 1093–1095.

(100) Fleming, S.; Ulijn, R. V. Design of Nanostructures Based on Aromatic Peptide Amphiphiles. *Chem. Soc. Rev.* 2014, *43* (23), 8150–8177.

(101) Pashuck, E. T.; Stupp, S. I. Direct Observation of Morphological Tranformation from Twisted

Ribbons into Helical Ribbons. *J. Am. Chem. Soc.* 2010, *132* (26), 8819–8821.

(102) Hughes, M.; Xu, H.; Frederix, P. W. J. M.; Smith, A. M.; Hunt, N. T.; Tuttle, T.; Kinloch, I. A.; Ulijn, R. V.; Kale, L.; Schulten, K.; Popelier, P. L. A.; Turner, M. L.; Xiao, P.; Kinloch, I. A.; Ulijn, R. V. Biocatalytic Self-Assembly of 2D Peptide-Based Nanostructures. *Soft Matter* 2011, *7* (21), 10032.

(103) Hashemnejad, S. M.; Kundu, S. Probing Gelation and Rheological Behavior of a Self-Assembled Molecular Gel. *Langmuir* 2017, *33* (31), 7769–7779.

(104) Sadownik, J. W.; Leckie, J.; Ulijn, R. V. Micelle to Fibre Biocatalytic Supramolecular Transformation of an Aromatic Peptide Amphiphile. *Chem. Commun.* 2011, *47* (2), 728–730.

(105) Hirst, A. R.; Roy, S.; Arora, M.; Das, A. K.; Hodson, N.; Murray, P.; Marshall, S.; Javid, N.; Sefcik, J.; Boekhoven, J.; van Esch, J. H.; Santabarbara, S.; Hunt, N. T.; Ulijn, R. V. Biocatalytic Induction of Supramolecular Order. *Nat. Chem.* 2010, *2* (12), 1089–1094.

(106) Ryan, D. M.; Anderson, S. B.; Nilsson, B. L. The Influence of Side-Chain Halogenation on the Self-Assembly and Hydrogelation of Fmoc-Phenylalanine Derivatives. *Soft Matter* 2010, *6* (14), 3220.

(107) Zhang, Y.; Gu, H.; Yang, Z.; Xu, B. Supramolecular Hydrogels Respond to Ligand-Receptor Interaction. *J. Am. Chem. Soc.* 2003, *125* (45), 13680–13681.

(108) Adhikari, B.; Nanda, J.; Banerjee, A. Multicomponent Hydrogels from Enantiomeric Amino Acid Derivatives: Helical Nanofibers, Handedness and Self-Sorting. *Soft Matter* 2011, *7* (19), 8913.

(109) Eckes, K. M.; Mu, X.; Ruehle, M. A.; Ren, P.; Suggs, L. J. β Sheets Not Required: Combined Experimental and Computational Studies of Self-Assembly and Gelation of the Ester-Containing Analogue of an Fmoc-Dipeptide Hydrogelator. *Langmuir* 2014, *30* (18), 5287–5296.

(110) Shao, H.; Parquette, J. R. A π-Conjugated Hydrogel Based on an Fmoc-Dipeptide Naphthalene Diimide Semiconductor. *Chem. Commun.* 2010, *46* (24), 4285.

(111) Deng, M.; Zhang, L.; Jiang, Y.; Liu, M. Role of Achiral Nucleobases in Multicomponent Chiral Self-Assembly: Purine-Triggered Helix and Chirality Transfer. *Angew. Chemie Int. Ed.* 2016, *55* (48), 15062–15066.

(112) Ogoshi, T.; Akutsu, T.; Yamafuji, D.; Aoki, T.; Yamagishi, T. Solvent- and Achiral-Guest-Triggered Chiral Inversion in a Planar Chiral Pseudo [1]Catenane. *Angew. Chemie Int. Ed.* 2013, *52* (31), 8111–8115.

(113) Kumar, M.; Jonnalagadda, N.; George, S. J. Molecular Recognition Driven Self-Assembly and Chiral Induction in Naphthalene Diimide Amphiphiles. *Chem. Commun.* 2012, *48* (89), 10948.

(114) Oda, R.; Huc, I.; Schmutz, M.; Candau, S. J.; MacKintosh, F. C. Tuning Bilayer Twist Using Chiral Counterions. *Nature* 1999, *399* (6736), 566–569.

(115) Fry, S. C. Isodityrosine, a Diphenyl Ether Cross-Link in Plant Cell Wall Glycoprotein: Identification, Assay, and Chemical Synthesis. *Methods Enzymol.* 1984, *107* (C), 388–397.

(116) Al-Hilaly, Y. K.; Williams, T. L.; Stewart-Parker, M.; Ford, L.; Skaria, E.; Cole, M.; Bucher, W. G.; Morris, K. L.; Sada, A. A.; Thorpe, J. R.; Serpell, L. C. A Central Role for Dityrosine Crosslinking of Amyloid-β in Alzheimer's Disease. *Acta Neuropathol. Commun.* 2013, *1*, 83.

(117) Capeillere-Blandin, C.; Delaveau, T.; Descamps-Latscha, B. Structural Modifications of Human Beta 2 Microglobulin Treated with Oxygen-Derived Radicals. *Biochem. J.* 1991, *277 (Pt 1*, 175–182.

(118) Zhang, S.; Fox, D. M.; Urbanc, B. Insights into Formation and Structure of Aβ Oligomers Cross-Linked via Tyrosines. *J. Phys. Chem. B* 2017, *121* (22), 5523–5535.

(119) Lee, D.-I.; Hwang, S.; Choi, J. Y.; Ahn, I.-S.; Lee, C.-H. A Convenient Preparation of Dityrosine via Mn(III)-Mediated Oxidation of Tyrosine. *Process Biochem.* 2008, *43* (9), 999–1003.

(120) Souza, J. M.; Giasson, B. I.; Chen, Q.; Lee, V. M.-Y.; Ischiropoulos, H. Dityrosine Cross-Linking Promotes Formation of Stable α-Synuclein Polymers. *J. Biol. Chem.* 2000, *275* (24), 18344–18349.

(121) Amadò, R.; Aeschbach, R.; Neukom, H. Dityrosine: In Vitro Production and Characterization. *Methods Enzymol.* 1984, *107* (C), 377–388.

(122) Shamovsky, I. L.; Riopelle, R. J.; Ross, G. M. Ab Initio Studies on the Mechanism of Tyrosine Coupling. *J. Phys. Chem. A* 2001, *105* (6), 1061–1070.

(123) Va, P.; Va, P. Synthesis of a Dityrosine-Linked Protein G Peptide Dimer. *UCI Undergratuate Res. J.* 2001, 61–68.

(124) Malencik, D. A.; Anderson, S. R. Dityrosine as a Product of Oxidative Stress and Fluorescent Probe. *Amino Acids* 2003, *25* (3–4), 233–247.

(125) Joschek, H.-I.; Miller, S. I. Photooxidation of Phenol, Cresols, and Dihydroxybenzenes. *J. Am. Chem. Soc.* 1966, *88* (14), 3273–3281.

(126) DiMarco, T.; Giulivi, C. Current Analytical Methods for the Detection of Dityrosine, a Biomarker of Oxidative Stress, in Biological Samples. *Mass Spectrom. Rev.* 2007, *26* (1), 108–120.

(127) Pattison, D. I.; Rahmanto, A. S.; Davies, M. J. Photo-Oxidation of Proteins. *Photochem. Photobiol. Sci.* 2012, *11* (1), 38–53.

(128) Wang, J.; Liu, K.; Xing, R.; Yan, X. Peptide Self-Assembly: Thermodynamics and Kinetics. *Chem. Soc. Rev.* 2016, *45* (20), 5589–5604.

(129) Fichman, G.; Gazit, E. Self-Assembly of Short Peptides to Form Hydrogels: Design of Building Blocks, Physical Properties and Technological Applications. *Acta Biomater.* 2014, *10* (4), 1671–1682.

(130) Hutton, C. A.; Skaff, O. A Convenient Preparation of Dityrosine via Miyaura Borylation–Suzuki Coupling of Iodotyrosine Derivatives. *Tetrahedron Lett.* 2003, *44* (26), 4895–4898.

(131) Oda, R.; Huc, I.; Homo, J. C.; Heinrich, B.; Schmutz, M.; Candau, S. Elongated Aggregates Formed by Cationic Gemini Surfactants. *Langmuir* 1999, *15* (7), 2384–2390.

(132) Korevaar, P. A.; Newcomb, C. J.; Meijer, E. W.; Stupp, S. I. Pathway Selection in Peptide Amphiphile Assembly. *J. Am. Chem. Soc.* 2014, *136* (24), 8540–8543.

(133) Barker, E. C.; Martin, A. D.; Garvey, C. J.; Goh, C. Y.; Jones, F.; Mocerino, M.; Skelton, B. W.; Ogden, M. I.; Becker, T. Thermal Annealing Behaviour and Gel to Crystal Transition of a Low Molecular Weight Hydrogelator. *Soft Matter* 1006, *13* (13), 1006–1011.

(134) Otero, R.; Schöck, M.; Molina, L. M.; Laegsgaard, E.; Stensgaard, I.; Hammer, B.; Besenbacher, F. Guanine Quartet Networks Stabilized by Cooperative Hydrogen Bonds. *Angew. Chemie Int. Ed.* 2005, *44* (15), 2270–2275.

(135) Cao, M.; Wang, Y.; Ge, X.; Cao, C.; Wang, J.; Xu, H.; Xia, D.; Zhao, X.; Lu, J. R. Effects of Anions on Nanostructuring of Cationic Amphiphilic Peptides. *J. Phys. Chem. B* 2011, *115* (41), 11862–11871.

(136) Caplan, M. R.; Moore, P. N.; Zhang, S.; Kamm, R. D.; Lauffenburger, D. A. Self-Assembly of a β-Sheet Protein Governed by Relief of Electrostatic Repulsion Relative to van Der Waals Attraction. *Biomacromolecules* 2000, *1* (4), 627–631.

(137) Tang, C.; Smith, A. M.; Collins, R. F.; Ulijn, R. V.; Saiani, A. Fmoc-Diphenylalanine Self-Assembly Mechanism Induces Apparent PKa Shifts. *Langmuir* 2009, *25* (16), 9447–9453.

(138) Fleming, S.; Frederix, P. W. J. M.; Ramos Sasselli, I.; Hunt, N. T.; Ulijn, R. V.; Tuttle, T. Assessing the Utility of Infrared Spectroscopy as a Structural Diagnostic Tool for β-Sheets in Self-Assembling Aromatic Peptide Amphiphiles. *Langmuir* 2013, *29* (30), 9510–9515.

(139) Fleming, S.; Debnath, S.; Frederix, P. W. J. M.; Hunt, N. T.; Ulijn, R. V. Insights into the Coassembly of Hydrogelators and Surfactants Based on Aromatic Peptide Amphiphiles. *Biomacromolecules* 2014, *15* (4), 1171–1184.

(140) Sukul, P. K.; Malik, S. Removal of Toxic Dyes from Aqueous Medium Using Adenine Based Bicomponent Hydrogel. *RSC Adv.* 2013, *3* (6), 1902–1915.

(141) Baral, A.; Basak, S.; Basu, K.; Dehsorkhi, A.; Hamley, I. W.; Banerjee, A. Time-Dependent Gel to Gel Transformation of a Peptide Based Supramolecular Gelator. *Soft Matter* 2015, *11* (24), 4944–4951.

(142) Hayashi, T.; Mukamel, S. Vibrational−Exciton Couplings for the Amide I, II, III, and A Modes of Peptides. *J. Phys. Chem. B* 2007, *111* (37), 11032–11046.

(143) Baral, A.; Roy, S.; Ghosh, S.; Hermida-Merino, D.; Hamley, I. W.; Banerjee, A. A Peptide-Based Mechano-Sensitive, Proteolytically Stable Hydrogel with Remarkable Antibacterial Properties. *Langmuir* 2016, *32* (7), 1836–1845.

(144) Chaco´n Villalba, M. E.; Varetti, E. L.; Aymonino, P. J. Cyanide Infrared Stretching Bands of the 13C Isotopomers of Sodium Nitroprusside Dihydrate. *Vib. Spectrosc.* 1992, *4* (1), 109–113.

(145) Nihei, M.; Yanai, Y.; Hsu, I.-J.; Sekine, Y.; Oshio, H. A Hydrogen-Bonded Cyanide-Bridged [Co 2 Fe 2] Square Complex Exhibiting a Three-Step Spin Transition. *Angew. Chemie Int. Ed.* 2017, *56* (2), 591–594.

(146) White, S. C.; Thompson, H. W. Hydrogen Bonding Between Phenols and Cyanides. *Proc. R. Soc. London A Math. Phys. Eng. Sci.* 1966, *291* (1427).

(147) Ramabhadran, R. O.; Hua, Y.; Flood, A. H.; Raghavachari, K. C vs N: Which End of the Cyanide Anion Is a Better Hydrogen Bond Acceptor? *J. Phys. Chem. A* 2014, *118* (35), 7418–7423.

(148) Rubin, N.; Perugia, E.; Wolf, S. G.; Klein, E.; Fridkin, M.; Addadi, L. Relation between Serum Amyloid A Truncated Peptides and Their Suprastructure Chirality. *J. Am. Chem. Soc.* 2010, *132* (12), 4242–4248.

(149) Hoyer, W.; Antony, T.; Cherny, D.; Heim, G.; Jovin, T. M.; Subramaniam, V. Dependence of α-Synuclein Aggregate Morphology on Solution Conditions. *J. Mol. Biol.* 2002, *322* (2), 383–393.

(150) Volpatti, L. R.; Vendruscolo, M.; Dobson, C. M.; Knowles, T. P. J. A Clear View of Polymorphism, Twist, and Chirality in Amyloid Fibril Formation. *ACS Nano* 2013, *7* (12), 10443–10448.

(151) Fichman, G.; Guterman, T.; Adler-abramovich, L.; Gazit, E. Synergetic Functional Properties of Two-Component Single Amino Acid-Based Hydrogels. *CrystEngComm* 2015, *17* (42), 8105–8112.

(152) Berthomieu, C.; Hienerwadel, R. Fourier Transform Infrared (FTIR) Spectroscopy. *Photosynth. Res.* 2009, *101* (2–3), 157–170.

(153) Liyanage, W.; Nilsson, B. L. Substituent Effects on the Self-Assembly/Coassembly and Hydrogelation of Phenylalanine Derivatives. *Langmuir* 2016, *32* (3), 787–799.

(154) Wheeler, S. E. Understanding Substituent Effects in Noncovalent Interactions Involving Aromatic Rings. *Acc. Chem. Res.* 2013, *46* (4), 1029–1038.

(155) Cockroft, S. L.; Perkins, J.; Zonta, C.; Adams, H.; Spey, S. E.; Low, C. M. R.; Vinter, J. G.; Lawson, K. R.; Urch, C. J.; Hunter, C. A. Substituent Effects on Aromatic Stacking Interactions. *Org. Biomol. Chem.* 2007, *5* (7), 1062.

(156) Cozzi, F.; Ponzini, F.; Annunziata, R.; Cinquini, M.; Siegel, J. S. Polar Interactions between Stackedπ Systems in Fluorinated 1,8-Diarylnaphthalenes: Importance of Quadrupole Moments in Molecular Recognition. *Angew. Chemie Int. Ed. English* 1995, *34* (9), 1019–1020.

(157) Carver, F. J.; Hunter, C. A.; Carver, F. J.; Seward, E. M. Structure–activity Relationship for Quantifying Aromatic Interactions†. *Chem. Commun.* 1998, No. 7, 775–776.

(158) Yang, Z.; Liang, G.; Ma, M.; Abbah, A. S.; Lu, W. W.; Xu, B. D-Glucosamine-Based Supramolecular Hydrogels to Improve Wound Healing. *Chem. Commun.* 2007, *0* (8), 843–845.

(159) Kabiri, M.; Unsworth, L. D. Application of Isothermal Titration Calorimetry for Characterizing Thermodynamic Parameters of Biomolecular Interactions: Peptide Self-Assembly and Protein Adsorption Case Studies. *Biomacromolecules* 2014, *15* (10), 3463–3473.

(160) Srinivasan, A.; Kebede, N.; Saavedra, J. E.; Nikolaitchik, A. V.; Brady, D. A.; Yourd, E.; Davies, K. M.; Keefer, L. K.; Toscano, J. P. Chemistry of the Diazeniumdiolates. 3. Photoreactivity. *J. Am. Chem. Soc.* 2001, *123* (23), 5465–5472.

(161) Pavlos, C. M.; Cohen, A. D.; D'Sa, R. A.; Sunoj, R. B.; Wasylenko, W. A.; Kapur, P.; Relyea, H. A.; Kumar, N. A.; Hadad, C. M.; Toscano, J. P. Photochemistry of 1-(N,N-Diethylamino)Diazen-1-Ium-1,2-Diolate: An Experimental and Computational Investigation. *J. Am. Chem. Soc.* 2003, *125* (48), 14934–14940.

(162) Hughes, M. N. Relationships between Nitric Oxide, Nitroxyl Ion, Nitrosonium Cation and Peroxynitrite. *Biochim. Biophys. Acta - Bioenerg.* 1999, *1411* (2–3), 263–272.

(163) Butler, A. R.; Rhodes, P. Chemistry, Analysis, and Biological Roles of S-Nitrosothiols. *Anal. Biochem.* 1997, *249* (1), 1–9.

(164) Thomas, C. E.; Darley-Usmar, V. Forum : Therapeutic Applications of Reactive Oxygen and Nitrogen Species in Human Disease. *Free Radic. Biol. Med.* 2000, *28* (10), 1478–1486.

(165) Williams, D. L. H. The Chemistry of S-Nitrosothiols. *Acc. Chem. Res.* 1999, *32* (10), 869–876.

(166) Gaston, B. Nitric Oxide and Thiol Groups. *Biochim. Biophys. Acta - Bioenerg.* 1999, *1411* (2–3), 323–333.

(167) Al-Sa'doni, H.; Ferro, a. S-Nitrosothiols: A Class of Nitric Oxide-Donor Drugs. *Clin. Sci. (Lond).* 2000, *98* (5), 507–520.

(168) Singh, R. J.; Hogg, N.; Joseph, J.; Kalyanaraman, B. Mechanism of Nitric Oxide Release from S -Nitrosothiols. *J. Biol. Chem.* 1996, *271* (31), 18596–18603.

(169) Bahnson, E. S.; Kassam, H. A.; Moyer, T. J.; Jiang, W.; Morgan, C. E.; Vercammen, J. M.; Jiang, Q.; Flynn, M. E.; Stupp, S. I.; Kibbe, M. R. Targeted Nitric Oxide Delivery by Supramolecular Nanofibers for the Prevention of Restenosis after Arterial Injury. *Antioxid. Redox Signal.* 2015, 401–419.

(170) Wink, D. a; Cook, J. a; Pacelli, R.; DeGraff, W.; Gamson, J.; Liebmann, J.; Krishna, M. C.; Mitchell, J. B. The Effect of Various Nitric Oxide-Donor Agents on Hydrogen Peroxide-Mediated Toxicity: A Direct Correlation between Nitric Oxide Formation and Protection. *Arch. Biochem. Biophys.* 1996, *331* (2), 241–248.

(171) Fitzhugh, A. L.; Keefer, L. K. Diazeniumdiolates: Pro- and Antioxidant Applications of the "NONOates." *Free Radic. Biol. Med.* 2000, *28* (10), 1463–1469.

(172) Keefer, L. K. Fifty Years of Diazeniumdiolate Research. from Laboratory Curiosity to Broad-Spectrum Biomedical Advances. *ACS Chem. Biol.* 2011, *6* (11), 1147–1155.

(173) Konter, J.; Abuo-Rahma, G. E. D. A.; El-Emam, A.; Lehmann, J. Synthesis of Diazen-1-Ium-1,2-Diolates Monitored by the "NOtizer" Apparatus: Relationship between Formation Rates, Molecular Structure and the Release of Nitric Oxide. *European J. Org. Chem.* 2007, No. 4, 616–624.

(174) Shaikh, N.; Valiev, M.; Lymar, S. V. Decomposition of Amino Diazeniumdiolates (NONOates): Molecular Mechanisms. *J. Inorg. Biochem.* 2014, *141* (1), 28–35.

(175) Lymar, S. V.; Shafirovich, V. Photoinduced Release of Nitroxyl and Nitric Oxide from Diazeniumdiolates. *J. Phys. Chem. B* 2007, *111* (24), 6861–6867.

(176) Davies, K. M.; Wink, D. A.; Saavedra, J. E.; Keefer, L. K. Chemistry of the Diazeniumdiolates. 2. Kinetics and Mechanism of Dissociation to Nitric Oxide in Aqueous Solution. *J. Am. Chem. Soc.* 2001, *123* (23), 5473–5481.

(177) Stamler, J. S.; Simon, D. I.; Osborne, J. A.; Mullins, M. E.; Jaraki, O.; Michel, T.; Singel, D. J.; Loscalzo, J. S-Nitrosylation of Proteins with Nitric Oxide: Synthesis and Characterization of Biologically Active Compounds. *Proc. Natl. Acad. Sci. U. S. A.* 1992, *89* (1), 444–448.

(178) Cardoso, A. Z.; Alvarez Alvarez, A. E.; Cattoz, B. N.; Griffiths, P. C.; King, S. M.; Frith, W. J.; Adams, D. J. The Influence of the Kinetics of Self-Assembly on the Properties of Dipeptide Hydrogels. *Faraday Discuss.* 2013, *166*, 101.

(179) Jamieson, S. A.; Tong, K. W. K.; Hamilton, W. A.; He, L.; James, M.; Thordarson, P. Small Angle Neutron Scattering (SANS) Studies on the Structural Evolution of Pyromellitamide Self-Assembled Gels. *Langmuir* 2014, *30* (46), 13987–13993.

(180) Cornwell, D. J.; Daubney, O. J.; Smith, D. K. Photopatterned Multidomain Gels: Multi-Component Self-Assembled Hydrogels Based on Partially Self-Sorting 1,3:2,4-Dibenzylidene- d -Sorbitol Derivatives. *J. Am. Chem. Soc.* 2015, *137* (49), 15486–15492.

Chapter 4
Multicomponent Nucleotide-Peptide Hydrogel

Chapter Outline:

This fourth chapter of the work highlights the design and construction of a nucleotide-amino acid multicomponent hydrogel. Multicomponent hydrogels are a growing area of research owing to the possibility to impart a higher information content into assemblies, thus allowing researchers to build more complex materials. Current approaches often rely on gelation due to a single stimulus for all components. Herein, one stimulus is used to trigger gelation of one component and this gelation process triggers the gelation of the second component. This is achieved through the addition of silver nitrate to a guanosine monophosphate (GMP) *N*-fluorenylmethyloxycarbonyl tyrosine (FY) solution. This results in the formation of silver-guanosine dimers stabilised through the enol tautomerisation and subsequent proton abstraction. The associated drop in pH then triggers the gelation of the second gelator, FY, through protonation of its pendant carboxylic acid.

As observed in the previous chapter, the process of gelation can be heavily kinetically dependent. The assembly process is highly sensitive to environmental conditions such as, but not limited to, ionic strength and temperature. Alterations in the supramolecular structure due to the assembly conditions are also observed here, with the ratio of Ag: GMP affecting the assembly kinetics, the resulting supramolecular organisation and mechanical properties of the hydrogel. These gels were formed at two Ag: GMP ratios, 2:1 and 1:1. The higher stoichiometries resulted in almost instantaneous gelation with non-orthogonal assembly between the gelators. However, at lower stoichiometries, this disruptive assembly is avoided and the second component, FY, can be selectively disassembled through the raising of pH. This demonstrates the possibility of creating a hydrogel with adaptable network density and mechanical properties. Such a strategy may be advantageous to many applications e.g., drug delivery, tissue engineering, wound dressing *etc.*

Introduction:

This chapter will focus on the formation of a multicomponent gelation system, a rapidly growing area of research. This self-assembly is more akin to biological assembly in which different components (e.g. nucleosides, lipids and amino acids) must self-sort or combine to assemble into a myriad of structures. For example, the cytoskeleton of cells is made up of microtubules and actin filaments which undergo orthogonal assembly and disassembly resulting in varied mechanical properties. Other biological systems form assemblies with multifunctional behaviour with different responses to different stimuli. Such complex biological systems are emergent, and the result of incremental, evolutionary steps. Thus, the assembly of more complex abiotic systems can inform origin of life studies and researchers wishing to engineer more sophisticated self-assembled structures over different length scales.[1–3] For instance, the design of multicomponent systems can produce gels with a higher information content as gelators with different functionality and responsiveness can be combined, e.g. modulating mechanical strength or having only one gelator susceptible to a stimulus.

In an excellent review, Buerkle and Rowan outlined three classifications of multicomponent supramolecular gels. [4] They are as follows (Figure 4.1):

1. A supramolecular gel formed from two (or more) compounds which do not gel individually.
2. A supramolecular gel formed from a gelator plus an additive that does not gel but modulates some property of the gel.
3. A supramolecular gel formed from two (or more) gelators that do gel individually.

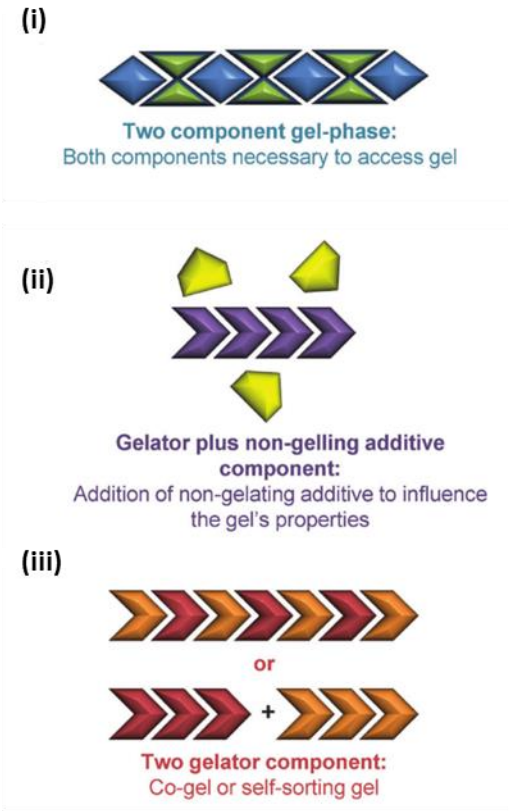

Figure 4.1 Multicomponent hydrogels classifications: (i) gelation through two non-gelators, (ii) gelation of a gelator co-assembling with an additive, or (iii) gelation of two components that could gel individually. Adapted from ref. 4

The first classification is perhaps the most studied, particularly for organogels (gels formed through an organic solvent) and involves the combination of non-gelators. These can then assemble via complementary interactions, e.g. hydrogen bonding, metal-ligand or donor acceptor interactions.[4] A common strategy is to couple components with complementary hydrogen bonding interactions to encourage co-operative assembly. The first report within this classification by Hanabusa *et al.* exploited well-known interactions between barbituric acid and pyrimidine units. These motifs were functionalised to encourage hydrogen bonding between each other and with alkyl chains to induce steric constraints, both of which promote one-dimensional assembly.[5] Also, Xu *et al.* demonstrated that two amino acids, based on a class of anti-inflammatory agents, gelled when both were present upon the addition of Na_2CO_3, which solubilised the amino acids and was proposed to be involved in hydrogen bonding between two components.[6] Owing to the prevalence of aromatic groups to encourage self-assembly, donor-acceptor interactions can promote assembly between two normally

non-gelating components. For instance, Rao *et al.* demonstrated the gelation of a coronene derivative and a dodecyl-functionalized methyl viologen derivative through π-π, charge-transfer, and electrostatic interactions.[7] This resulted in an assembly of alternating stacks of the two components to form one-dimensional filaments and subsequent gelation. The authors proposed that such an assembly of chromophores may have relevance to sensing applications.

The second classification has also been widely researched and refers to the combination of an additive and a gelator to modulate mechanical properties, to enhance the stability of the gel or to use the gel as a scaffold for crystallisation. Work by Van Esch's group highlights some interesting consequences of combining gelators with surfactants. [8,9] The gelators (derivatives of 1,3,5-cyclohexyltrisamide) were either mixed with a micelle-forming surfactant, cetyltrimethylammonium tosylate (CTAT), or vesicle forming surfactant, 1,2-dioleoyl-sn-glycerol-3-phosphocholine (DOPC). Gelation in the presence of CTAT resulted in gel fibres and cylindrical micelles, which increased the T_{gel} value, presumably due to the surfactant creating a more entangled network. The orthogonal assembly also occurred in the presence of DOPC, with vesicles forming alongside hydrogel filaments, as confirmed with cryo-TEM (Figure 4.2a). Though, if the gel network was disassembled and then reassembled inside the DOPC vesicles and therefore constrained filament length (Figure 4.2b).

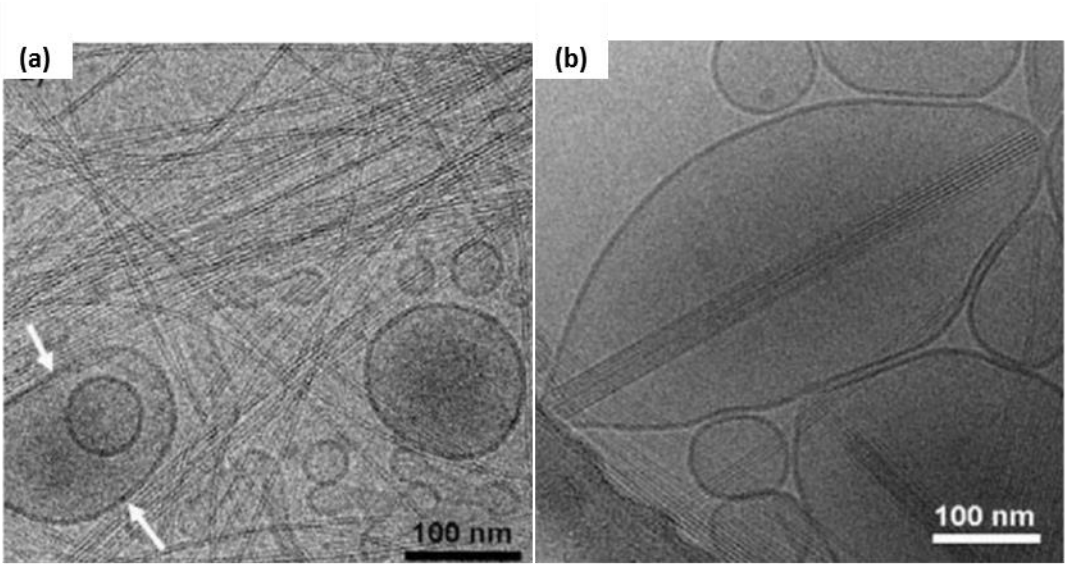

Figure 4.2 Cryo-TEM images of (a) unilamellar DOPC vesicles coexisting with a network of hydrogel fibres and (b) DOPC vesicles deformed by the growth of gel fibres directly contained in their aqueous compartment. Adapted from ref. 8.

Furthermore, Fuhrhop *et al.* demonstrated that gelation in the presence of sodium dodecyl sulfate (SDS) would increase the long-term stability of gels that are susceptible to gel-crystal transformations which gradually disassembled the gel network.[10] This occurs because gelators exist in both the gel and sol phases and the latter act as a nucleation point for crystallisation.[11–14] This effectively lowers the concentration of gelators in solution, promoting gelators to move from the gel to the sol phase. It was conjectured that the SDS would solubilise the gelator nuclei preventing further macroscopic crystallisation and thus averting network disassembly. Yu *et al.* demonstrated that the gelation of the insoluble nucleoside guanosine (G) in the presence of its more soluble analogue, guanosine monophosphate (GMP), resulted in stable hydrogels.[15] Unlike individual G gels, this binary mixture exhibited thermoassociative behaviour (gelling as the temperature is raised), attributed to the solubilisation of G into GMP aggregates existing prior to heating. This reduced the repulsion between anionic GMP stabilising further aggregation and gelation.

An alternative approach under this second classification is to use the supramolecular gel to promote the crystallisation of the second component under non-equilibrium conditions. Simply put, crystallisation occurs through an unenergetically favourable nucleation step, followed by an

energetically favourable crystal phase growth. However, this explanation is an oversimplification as there are kinetic and thermodynamic aspects involved and hence metastable structures are common and polymorphism is prevalent in crystallisation.[1] The study of different crystal forms is extremely valuable owing to their different bioavailability and solubility, which also affects processing, with obvious consequences to applications of pharmaceutical agents.[1] The gel network can affect the crystallisation process by modulating diffusion of reactants, preventing convection currents and sedimentation and reducing the number of nucleation sites.[1] The gel can also selectively act as a nucleating point through interactions with the crystallising material. The synthetic and structural versatility of LMWGs allows for specific interactions with the crystallising material thus making molecular gels particularly attractive as crystallisation scaffolds. For instance, Estroff *et al.* demonstrated that the carboxylate groups of a bis-urea dicarboxylic acid-based gelator functioned as calcium binding domain, to grow calcite crystals.[16] The gelator itself was occluded into the crystalline lattice which is expected to affect crystal properties.

Daly *et al.* demonstrated the formation of single-crystal halide nanowires from supramolecular gel surfaces.[17] The supramolecular gel stabilizes the growth of these wires by facilitating a diffusion-driven base growth mechanism. Though the mechanism wasn't fully understood the authors proposed that the supramolecular gel was key to directing anisotropic growth. In addition, Pandoli *et al.* demonstrated that GMP hydrogels could be used to produce chiral silver nanoparticles templated by the helical supramolecular GMP assemblies.[18] These reports demonstrate that supramolecular gels have a role in controlling the morphology of crystallising material.

Finally, the third classification concerns the formation of a multicomponent supramolecular hydrogel using two gelators which are capable of gelling individually and is the focus of experimental work reported in this chapter. Such systems can increase the information content by mixing gelators with different properties or to functionalise the same gelator differently.

These gelators can orthogonally 'self-sort' into separate narcissistic filaments or co-assemble into mixed filaments.[4,13,19–22] If mixed filaments form, there are several ways for the gelators to order in the filaments: alternating or mixed in an ordered or random way. Additionally, these filaments may then self-sort or entangle together. Finally, the co-assembly of the gelators can be disruptive such that the properties are hampered, e.g. either the mechanical properties or a disordered supramolecular assembly. This often occurs through a mismatch in the alignment of the gelators such that the ordering of the intermolecular interactions is perturbed, relative to how the individual gelators assemble.[13] It is also possible for a mixture of these assemblies to occur.

Multicomponent hydrogels are relevant to forming more complex hydrogel scaffolds with a higher information content, e.g. multiple synergistic functional groups which affect tissue growth.[23] For instance, Horgan *et al.* combined two Fmoc-protected peptides functionalized with different biologically active epitopes.[24] This produced a scaffold more chemically and physically similar to the extracellular matrix suitable for tissue engineering applications. Also, the co-assembled gel induced changes in the cells not achieved when either of the individual gelators was used separately. Another key focus is using mixed systems for optoelectronics.[25–29] For instance, through the formation of 'self-sorted' filaments it should be possible to generate bulk p-n heterojunctions.[30] Indeed, Sugiyasu *et al.* successfully demonstrated a gel capable of photoelectrical conversion through the self-sorting of p-type oligothiophene and n-type perylene derivatives.[31] Such an approach produces a solution-processible material that showed promising photoelectrical conversion by visible light irradiation.

The co-assembly of different gelators allows for different responses to various stimuli e.g. light, heat, pH changes *etc.* For instance, Draper *et al.* could selectively remove the fibres of one gelator by a light-triggered gel-to-sol transition.[32] Irradiation of the gel with 365 nm light induced a trans-cis isomerisation in a stilbene-based gelator, with the latter isomer being a poor gelator. The second,

naphthalene-amino acid gelator was unaffected, leaving a hydrogel network intact with rheological properties comparable to the naphthalene-amino acid gelator gelling by itself. As opposed to "negative etching" (removing one component), Cornwell *et al.* demonstrated "positive writing" by forming a multicomponent gel using two different proton sources to trigger the assembly of two DBS (1,3:2,4-dibenzyldene-D-sorbitol) derivatives with different pKas (Figure 4.3).[33] The first gelator (DBS-CO_2H), gels due to the hydrolysis of glucono-δ-lactone (GdL) and the associated pH drop. Then the second gelator (DBS-Gly), with a lower pKa can be selectively gelled using a mask and photoactivation of diphenyl iodonium nitrate (DPIN). Doing this in a preformed gel network lowers convection and diffusion effects, thus enhancing spatial resolution. Gels with tuneable network properties are attracting interest owing to numerous applications such as determining cargo release and affecting the mechanical properties of tissue culture scaffolds. [34,35]

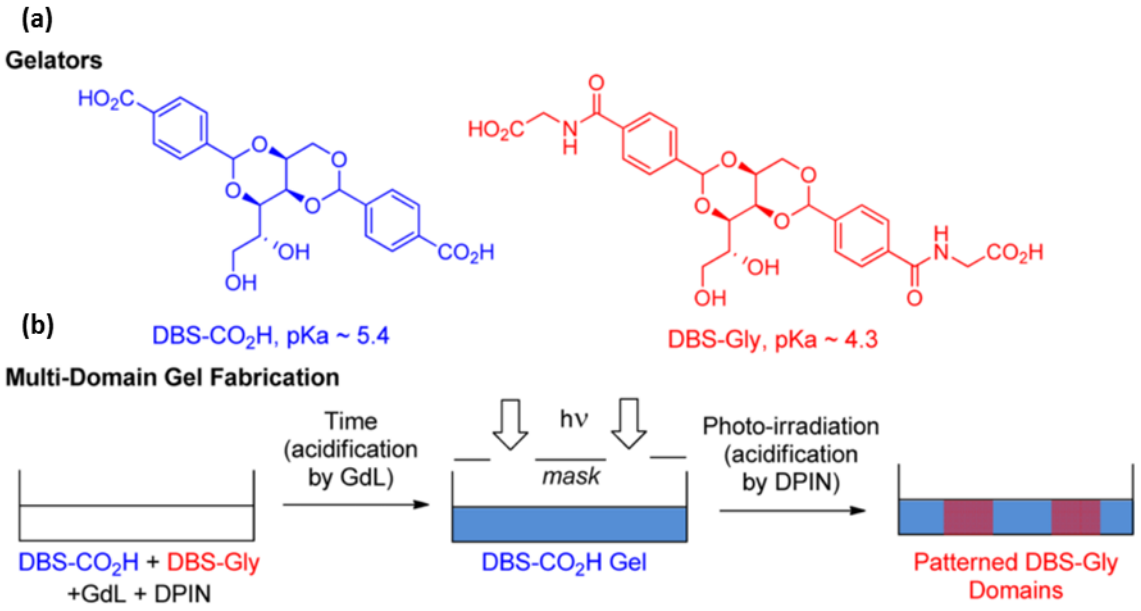

Figure 4.3 a) DBS-based gelators. b) Scheme for spatially resolved multicomponent hydrogel through formation of DBS-CO_2H gel network and photoactivation of diphenyl iodonium nitrate (DPIN) under a mask subsequently patterns DBS-Gly domains. Adapted from ref. 33.

Further elegant work has been reported by Singh *et al.,* who produced a bola-amphiphilic hydrogelator capable of catalysing the formation of a second trishydrazone hydrogelator from a trishydrazide and

benzaldehyde. [36] The formation of the second gelator is enhanced by acid catalysis and it was proposed the fibres of the first gel have acidic interfaces resulting in local decrease in the pH.

Herein, is reported the gelation of one component producing the trigger for the gelation of the second component. This is achieved through the addition of silver nitrate to a GMP and FY solution, which lowers the pH, through abstraction of a proton from the guanine residue of GMP. [18,37–39] Silver-GMP dimers are formed which stack into nanofilaments through π-stacking and hydrogen bonding. The drop in pH then triggers the gelation of FY, which is soluble at high pH (*ca.* >pH 8) but protonation of the pendant carboxylic acid lowers its hydrophilicity and electrostatic repulsion. (Figure 4.3) This promotes one-dimensional assembly and entanglement of these filaments to form the hydrogel network. Doing so produces a multicomponent hydrogel of which one component is more pH sensitive and can be disassembled. The ratio of silver to GMP determines the kinetics of assembly and hence the process of assembly and properties of the gel across multiple length scales, e.g. supramolecular packing, mechanical properties will be discussed below.

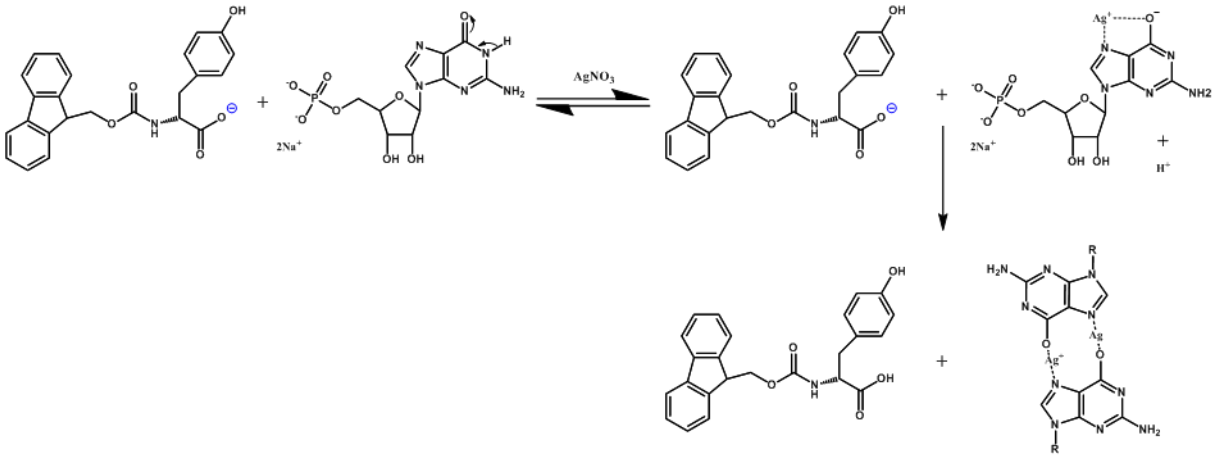

Figure 4.4 Scheme for the formation of multicomponent nucleotide-peptide hydrogel through the addition of a silver to a Fmoc-tyrosine and guanosine monophosphate solution.

Experimental

Preparation

Single component hydrogels: Silver nitrate ($AgNO_3$) (Alfa Aesar) and guanosine 5'-monophosphate sodium salt (Na_2GMP) (Signma) were used as received and all solutions prepared using Milli-Q ™ water. Ag-GMP hydrogels with $AgNO_3$: GMP molar ratios of 1:1 and 2:1 were prepared at room temperature by adding an appropriate concentration of aqueous $AgNO_3$ (25-100 mM) to an aqueous solution of Na_2GMP (25-50 mM) whilst vortexing (1,000 rpm) to aid dissolution of the silver salt for homogenous gelation.

N-Fluorenylmethyloxycarbonyl tyrosine (Fmoc tyrosine, FY) (Novabiochem, Merck) was dissolved in 25 mM NaOH with the aid of sonication and vortexing. Aliquots of NaOH (1 M) were also added to raise the pH of the solution to 9, above the pKa of the pendant carboxylic acid. The solutions were filtered through a 0.44 μm polyethersulfone syringe filter to remove any undissolved solid. Then glucono-δ-lactone (GdL) (3 mg/mL) was dissolved in the Fmoc-tyrosine solution.

Multicomponent hydrogels: Fmoc-tyrosine solutions were prepared as above and were then used to dissolve GMP. Multicomponent hydrogels were formed adding an appropriate concentration of aqueous $AgNO_3$ (25-100 mM) to an aqueous solution of Na_2GMP (25-50 mM) and FY (25-50 mM) whilst vortexing (1,000 rpm) to aid dissolution of the silver salt for homogenous gelation. Gels were left to form in the dark. These gels were formed at a 2:1 or 1:1 molar ratio relative to the GMP concentration. The samples were prepared such that either the GMP and Fmoc-tyrosine were the same concentration (25 mM), or that one gelator was at a lower concentration (12.5 mM). This resulted in nine samples (three single component samples and six multicomponent samples). The ratios are listed here and summarised again in the next section. 1:1 AgGMP (25 mM) Fmoc-tyrosine (25 mM) (A), 1:1 AgGMP (25 mM) Fmoc-tyrosine (12.5 mM) (B), and 1:1 AgGMP (12.5 mM) Fmoc-tyrosine (25 mM) (C), 2:1

AgGMP (25 mM) Fmoc-tyrosine (25 mM) (D), 2:1 AgGMP (25 mM) Fmoc-tyrosine (12.5 mM) (E) and 2:1 AgGMP (12.5 mM) Fmoc-tyrosine (25 mM) (F),

Characterisation

Differential scanning calorimetry (DSC): DSC was carried out using a Mettler Toledo TGA/DSC1 Star System at a scan rate of 2 °C min^{-1} with a nitrogen flow of 25 mL min^{-1}. All experiments were carried out with the assistance of Maddy Nichols.

Rheology: Rheometry was performed using a Malvern Kinexus fitted with a parallel plate geometry (gap width of 200 μm) at room temperature. Hydrogels, which were aged for one day, were added to the rheometer using a spatula to minimise shear. The top plate was lowered, and the normal force was measured and allowed to reach equilibrium. For oscillatory amplitude sweeps, a constant frequency was maintained for all experiments and the sweep runs from 0.01-500% strain. To measure gelation, samples were prepared as normal and loaded as above. Then a constant strain (0.1 %) was applied at a constant frequency (1 Hz) and the moduli were recorded every 10 seconds. The specimen chamber was kept slightly humid to prevent drying of the sample. These measurements were followed by the aforementioned oscillatory amplitude sweep to demonstrate that mechanically equivalent gels were formed. Further details of the experimental setup e.g. frequency and strain range are included in the result and discussion section.

Transmission electron microscopy (TEM), Scanning transmission electron microscopy (STEM) and energy dispersive X-ray analysis (EDXA): TEM imaging was performed in bright-field mode using a JEOL TEM 1400 electron microscope and STEM imaging was performed using a JEOL TEM 2010 electron microscope operating at 120 keV. TEM samples were prepared by drop casting a dilute suspension of hydrogel (5 μL) onto carbon-coated copper TEM grids for three minutes and wicking excess fluid away using filter paper. When negative staining was necessary, an aqueous solution of uranyl acetate (1% w/v, 5 μL) were also dropcast onto the carbon coated TEM grid and wicked off after three minutes. All

samples were left to dry overnight at room temperature. STEM imaging and EDX data collection was undertaken by Dr Jean-Charles Eloi.

Circular dichroism spectroscopy (CD): CD spectra were recorded at room temperature using a JASCO J-810 spectrometer through two quartz plates. Samples were prepared by spreading hydrogels (*ca.* 10 µL) between two quartz plates to produce a homogeneous film and to reduce scattering of light by the hydrogel sample. This avoided dilution into a cuvette that could alter the filament environment and concentration.

Attenuated total reflectance Fourier transform infrared spectroscopy (ATR-FTIR): Fmoc-Tyr hydrogels were lyophilized by freezing in liquid nitrogen followed by freeze-drying for at least 24 hours. ATR-FITR was performed using a PerkinElmer Spectrum 100 FTIR spectrometer fitted with a universal attenuated total reflection accessory.

Fluorescence spectroscopy (fluorimetry): Fluorimetry measurements were recorded at room temperature using a Horiba FluoroMax 4 spectrometer. Fluorimetry was carried on supramolecular hydrogels with an excitation wavelength of 265 nm, with excitation bandwidth of 1nm and emission bandwidth of 5 nm. Samples were prepared by spreading hydrogels (*ca.* 10 µL) between two quartz plates to produce a homogeneous film, as for CD.

Results and Discussion

Single component supramolecular hydrogels were formed as reported previously to act as controls for multi-component hydrogels.[34,38,40,41] The first class of these gels were formed by adding silver nitrate (50mM or 100mM) at an equal volume to give a guanosine monophosphate (GMP) aqueous solution (50 mM) to a final concentration of 25 mM. This gives the two Ag-GMP ratios that will be used for the multi-component hydrogels. The 2:1 molar ratio forms an opaque self-supporting hydrogel almost instantaneously, but the 1:1 molar ratio forms a viscous solution which is not self-supporting after vial inversion (Figure 4.7 (a) (ii)). The second gelator, *N*-fluorenylmethyloxycarbonyl tyrosine (Fmoc-tyrosine, FY), is first dissolved at a high pH to deprotonate the pendant carboxylic acid which aids dissolvation as the sodium salt is more soluble.[40,42] This then forms a gel after lowering of pH through protonation of the terminal carboxylic acid. As the protonated form is less soluble than the sodium salt, its hydrophilicity and electrostatic repulsion are lowered, allowing for kinetically trapped nanofilaments to grow and entangle. These then form the scaffold to immobilise the aqueous solvent to form a supramolecular hydrogel.

Lowering of pH can be achieved via addition of mineral acids (i.e. HCl) or through the hydrolysis of glucono-δ-lactone (GdL), forming gluconic acid (Figure 4.4a). It has been reported that gelation tends to occur on shorter timescales than it takes to adequately dissolve mineral acids which causes very localised gelation, resulting in irreproducible gels. [40,42,43] Alternatively, GdL is more soluble and thus allows for a homogenous pH change for consistent gelation throughout the sample (Figure 4.4b). Also, as the rate of hydrolysis is determined by the starting OH^- concentration and temperature, this allows for reproducible gelation.[27,40,42,44] This method was used to trigger gelation of Fmoc-tyrosine gels and produced slightly turbid self-supporting supramolecular hydrogels (Figure 4.6 (a) (iii)).

(a)

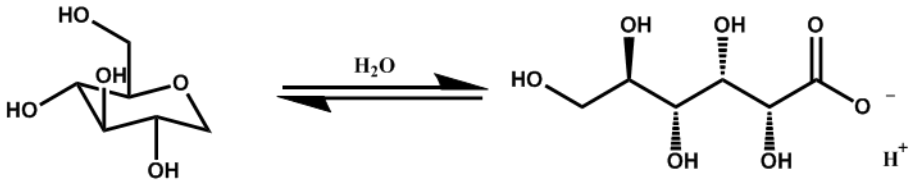

(b)

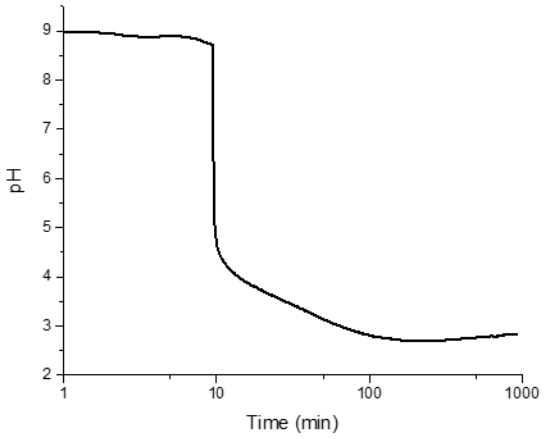

Figure 4.5: (a) Scheme demonstrating the hydrolysis of glucono-δ-lactone (GdL) to form gluconic acid and (b) measuring the pH change achieved through the hydrolysis in pure Milli-Q water.

In the Fmoc-tyrosine solution (Figure 4.5a), there is a rapid pH drop after the addition of GdL (at *ca.* 10 minutes) as the hydrolysis of GdL is base catalysed. [27,40,42,44] Surprisingly, the Fmoc-tyrosine solution gels, despite the final pH being above that of the predicted pKa for *N*-protected amino acids of 3.2-3.7.[45] This can be understood by a transition at *ca.* pH 7.10 and the plateau observed at pH *ca.* 5.6. This plateau indicates a region of buffering by the Fmoc-tyrosine well above expected pKa, characteristic of a shift in apparent pKa of the carboxylic acid. [46–49] Similar shifts of apparent pKas have been widely reported for other carboxylic acids, such as amino acids in hydrophobic environments and fatty acids. [50–52]

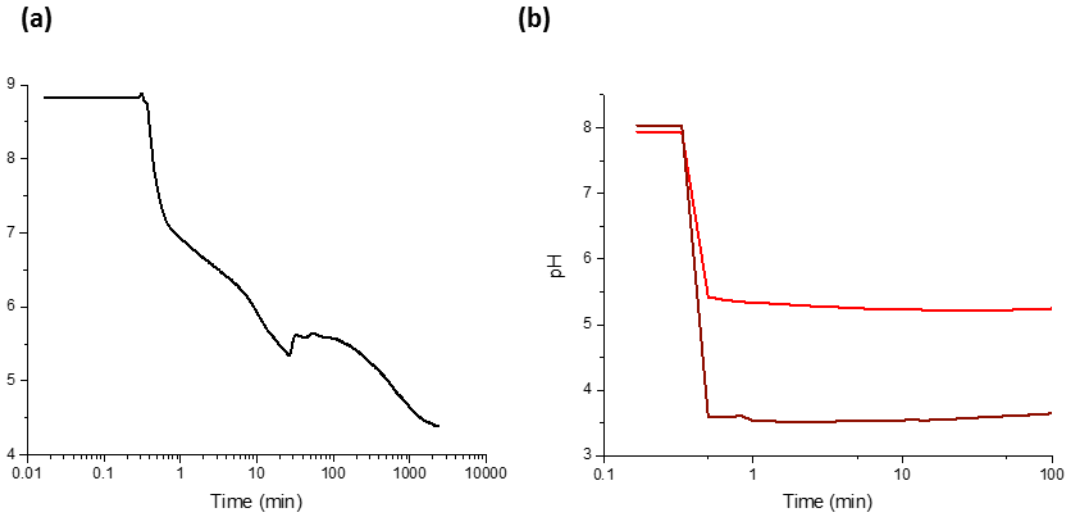

Figure 4.6 pH measurements of single component gels (a) FY gel (b) 2-1 AgGMP (dark red) and 1-1 AgGMP (red)

These shifts are associated with structural behaviours dependent on the pH, whereby the assemblies are stabilised through interactions such as hydrogen bonding with the carboxylic acid. As such, this disfavours deprotonation of the carboxylic acid resulting in a shift in the apparent pKa. Due to the amphiphilic nature of the gelators at high pHs, the gelators act as surfactants and therefore can self-assemble into spherical or worm-like micelles. [25,46,48,53–56] These assemblies result in the observed shift of apparent pKa, relative to what would be predicted for well dissolved individual monomer units.

Thus, the two observations can be understood by protonation of the FY molecules at *ca.* pH 7.1 encouraging self-assembly. With a further drop in pH, further FY molecules will be protonated, lowering the degree of ionisation allowing for the lateral association of these filaments and subsequent entanglement of these filaments to form a 3D network and gel. [46]

Addition of silver nitrate to a GMP solution (Figure 4.5b) results in a stark pH drop, not observed when added to just water (Figure 4.5b). This is in line with the proposed model of Ag-GMP dimerization that results in the abstraction of the proton from the guanine residue through the enolate tautomerization (Figure 4.3). [18,37–39]

Multicomponent gels were formed by adding silver nitrate at equal volumes to a FY GMP solution at either a 2:1 or 1:1 molar ratio relative to the GMP concentration. The samples were prepared such that either the GMP and Fmoc-tyrosine were the same concentration (25 mM), or that one gelator was at a lower concentration (12.5 mM), producing six multicomponent samples. A summary of the three single component gels and six multicomponent samples are listed in Table 4.1. The multicomponent samples are abbreviated to one letter codes for clarity and listed alongside their colour code that are kept constant for all figures. Any alterations to these will be referred to in the figure captions.

Sample		Sample Label	Type	Legend	Result
FY			Solution		Solution
GMP			Solution		Solution
FY-GMP			Solution		Solution
FY 25mM GdL			Single component		Gel
1-1 AgGMP 25 mM			Single component		Viscous solution
2-1 AgGMP 25mM			Single component		Gel
1-1 AgGMP FY	GMP 25 FY 25	A	Multicomponent		Gel
	GMP 25 FY 12.5	B	Multicomponent		Gel
	GMP 12.5 FY 25	C	Multicomponent		Solution
2-1 AgGMP FY	GMP 25 FY 25	D	Multicomponent		Gel
	GMP 25 FY 12.5	E	Multicomponent		Gel
	GMP 12.5 FY 25	F	Multicomponent		Gel

Table 4.1 Summary of gels prepared with their associated label and legend colour.

The different ratios of the GMP and FY gelators showed interesting behaviour in the gel formation. For the 2:1 gels, samples D gelled after a few minutes, E gelled almost instantly despite a lower gelator concentration, and then F gelled after several hours. The quicker gelation time of E was surprising and indicated non-orthogonal assembly between GMP and Fmoc-tyrosine which was lessened by lowering the Fmoc-tyrosine concentration. Then for the 1:1 gels, A and B gelled overnight, and C failed to gel (Figure 4.3 (c). This can be understood with the pH measurements, as all the gels are below pH 7 except C and thus cannot sufficiently protonate the carboxylic acid of Fmoc-tyrosine to promote gelation. Additionally, sample C, is below critical gelation concentration to promote AgGMP gelation. Significantly, neither GMP-FY solutions nor addition of silver to FY resulted in gelation (Figure 4.5b). Thus, indicating that all three components must be necessary for FY molecules to gel water and therefore form a multicomponent hydrogel.

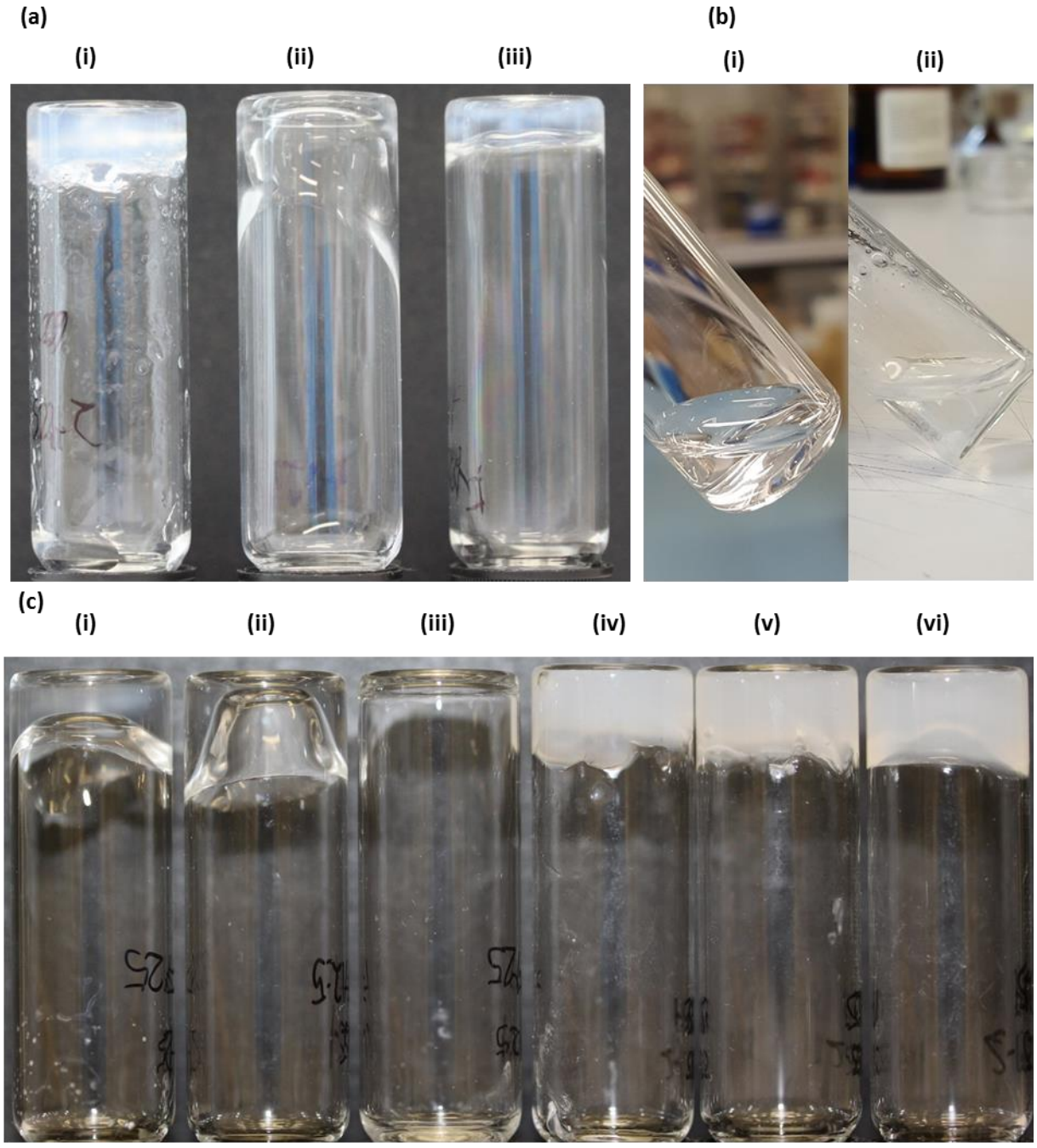

Figure 4.7 (a) Photo of single component samples; (i) 2-1 AgGMP, (ii) 1-1 AgGMP, and (iii) FY gel. (b) Photos demonstrating that no gelation occurs unless all three components are present. (i) FY-GMP solution demonstration no gelation occurs without the addition of silver and (ii) no gelation upon the addition of silver to a FY solution. Some precipitation does occur, possibly complexation between the silver salt and FY, which is explored later. Lastly, multicomponent nucleotide-peptide hydrogels (c) 1-1 AgGMP stoichiometry and varying molar ratios; samples: (i) A, (ii) B, and (iii) C, and at 2-1 AgGMP stoichiometry and vary molar ratios; samples: (iv) D, (v) E, and (vi) F.

Sample		pH
FY		9.00
GMP		7.93
FY-GMP		8.51
FY 25mM GdL		
1-1 AgGMP 25 mM		5.64
2-1 AgGMP 25mM		3.25
1-1 AgGMP FY	GMP 25 mM FY 25 mM **(A)**	6.73
	GMP 25 mM FY 12.5 mM **(B)**	6.37
	GMP 12.5 mM FY 25 mM **(C)**	7.16
2-1 AgGMP FY	GMP 25 mM FY 25 mM **(D)**	5.66
	GMP 25 mM FY 12.5 mM **(E)**	5.02
	GMP 12.5 mM FY 25 mM **(F)**	6.99

Table 4.2 pH measurements of solutions, single component gels, and multicomponent gels.

The nanofilament network of these hydrogels can be visualised using transmission electron microscopy. Due to the low electron density of the carbon-based filaments of the Fmoc-tyrosine gels, negative staining with uranyl acetate was used to discern individual filaments. For all samples, it is possible to observe the high density of nanofilaments which entangle to form the scaffold for hydrogelation. FY filaments had a flat tape morphology with filaments of 12.1 $\pm$3.3 nm (Figure 4.8a). Ag-GMP filaments could be observed without staining due to electron-dense silver nanoparticles present in the filaments as confirmed by EDX analysis (Figure 4.8b). Filaments of 3-8 nm and 3-10 nm were imaged for 1:1 and 2:1 molar ratios, respectively.

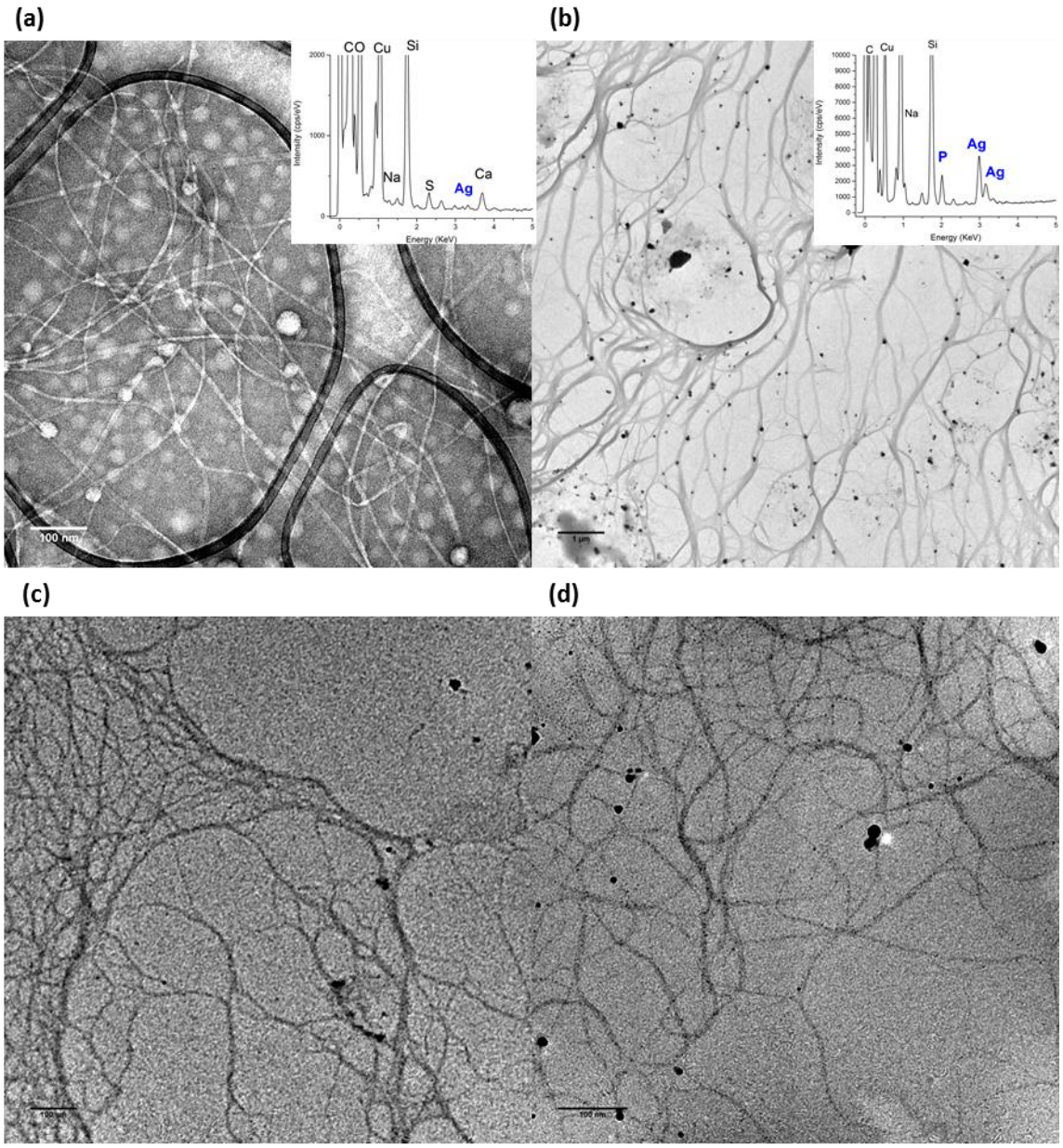

Figure 4.8 TEM images of single component hydrogels. (a) Image of FY filaments (inset EDX of sample), negatively stained with uranyl acetate and Ag-GMP gels at (b and c) 2:1 ratio (inset of B is EDX of sample demonstrating significant P and Ag) and (d) 1:1 ratio. Scale bar 100 nm except b (1 µm).

High-aspect-ratio filaments were observed for all multicomponent samples, including sample C. This isn't surprising as filaments are still expected for this sample and their density may be increased due to the concentrating effects of the sample preparation. It appears that there is significant disorder around the filaments, most clearly observed for sample A, though it is not clear whether this is an artefact of the sample preparation. Interesting observations are made in filament widths for samples A and B. Both have narrower filaments present 2-8 nm and 2-6 nm, respectively and wider filaments

9-16 nm and 8-13 nm, respectively. The smaller filaments may be, at least predominantly, Ag-GMP filaments and the wider filaments may be FY filaments as these filament widths are in line with single component widths. Sample C also has a spread of filament widths from 4-9 nm. Samples prepared at the 2:1 ratio also demonstrated a breadth of widths; D (3-14 nm), E (3-11 nm), and F (4-14 nm). Electron-dense silver nanoparticles, confirmed by EDX, are also observed for the multicomponent samples at both Ag:GMP ratios. There are a large number of these observed at the 2:1 ratio as the silver is in excess, relative to GMP. However, as gelators are in equilibrium between the filaments and the solution, silver ions will be available to form silver nanoparticles.

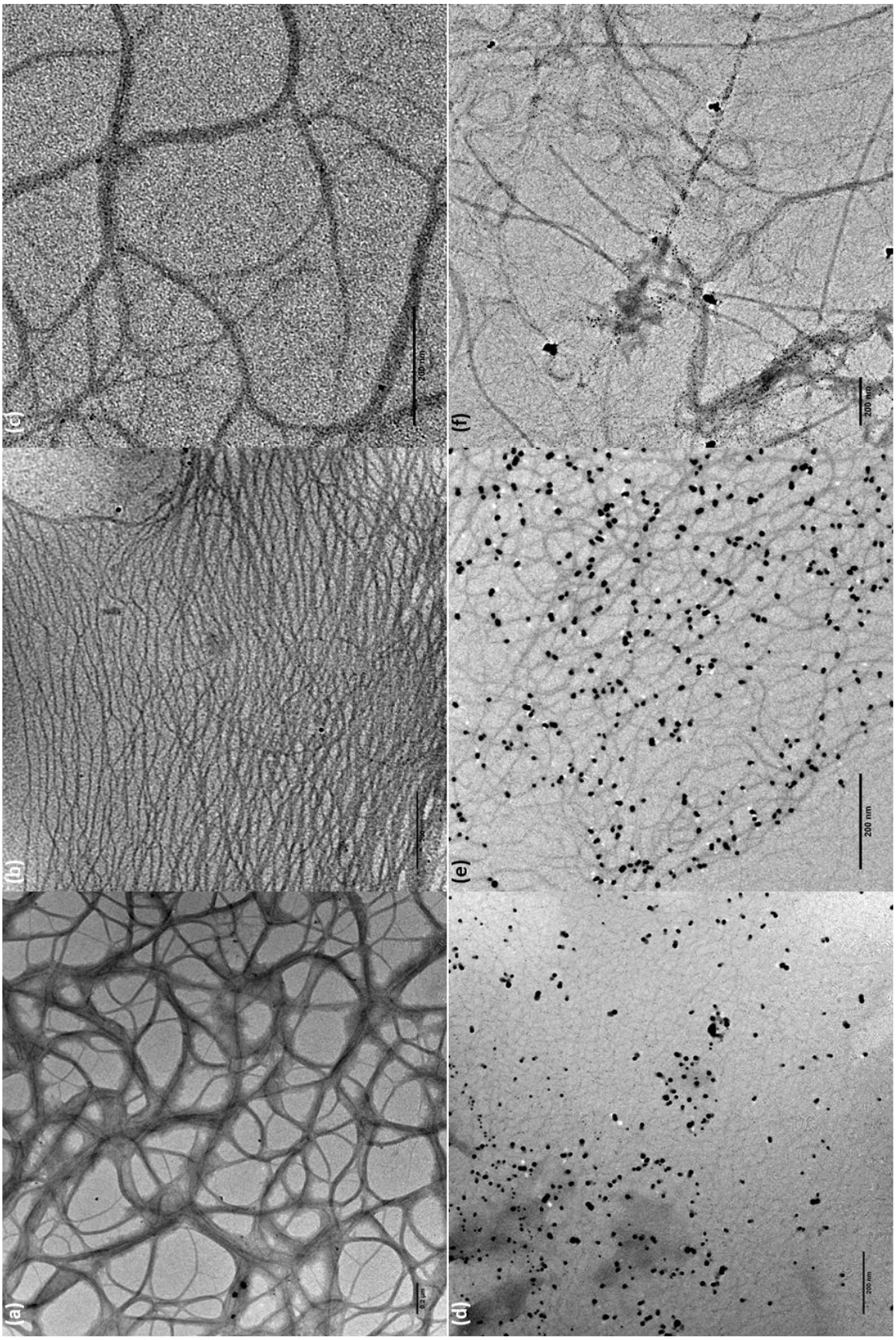

Figure 4.9 TEM images of multicomponent samples at 1-1 AgGMP stoichiometry and varying molar ratios; samples: (a) A, (b) B, and (c) C, and at 2-1 AgGMP stoichiometry and vary molar ratios; samples: (d) D, (e) E, and (f) F.

Although others have demonstrated self-sorting through the observation of very different widths, [57,58] in this case it is not reliable as the filament widths are relatively comparable between the two gelators. Also, the work detailed in Chapter 3 demonstrates that the same gelator can form filaments with different widths depending on how they are prepared. Also, Mears *et al.* demonstrated that measurements of dry filaments by electron microscopy were wider than measurements of wet filaments by cryo-TEM and small angle neutron scattering.[59]

Since the GMP gelator has phosphorus and potentially higher levels of silver present energy-dispersive X-ray spectroscopy (EDXS) was employed to determine whether any filaments could be imaged without these elements present, which would indicate that the filament was composed just FY corresponding to self-sorting. However, this was not achieved (Figure 4.10) and therefore, spectroscopic analysis was undertaken to better understand the assembly of the two gelators in the multicomponent systems.

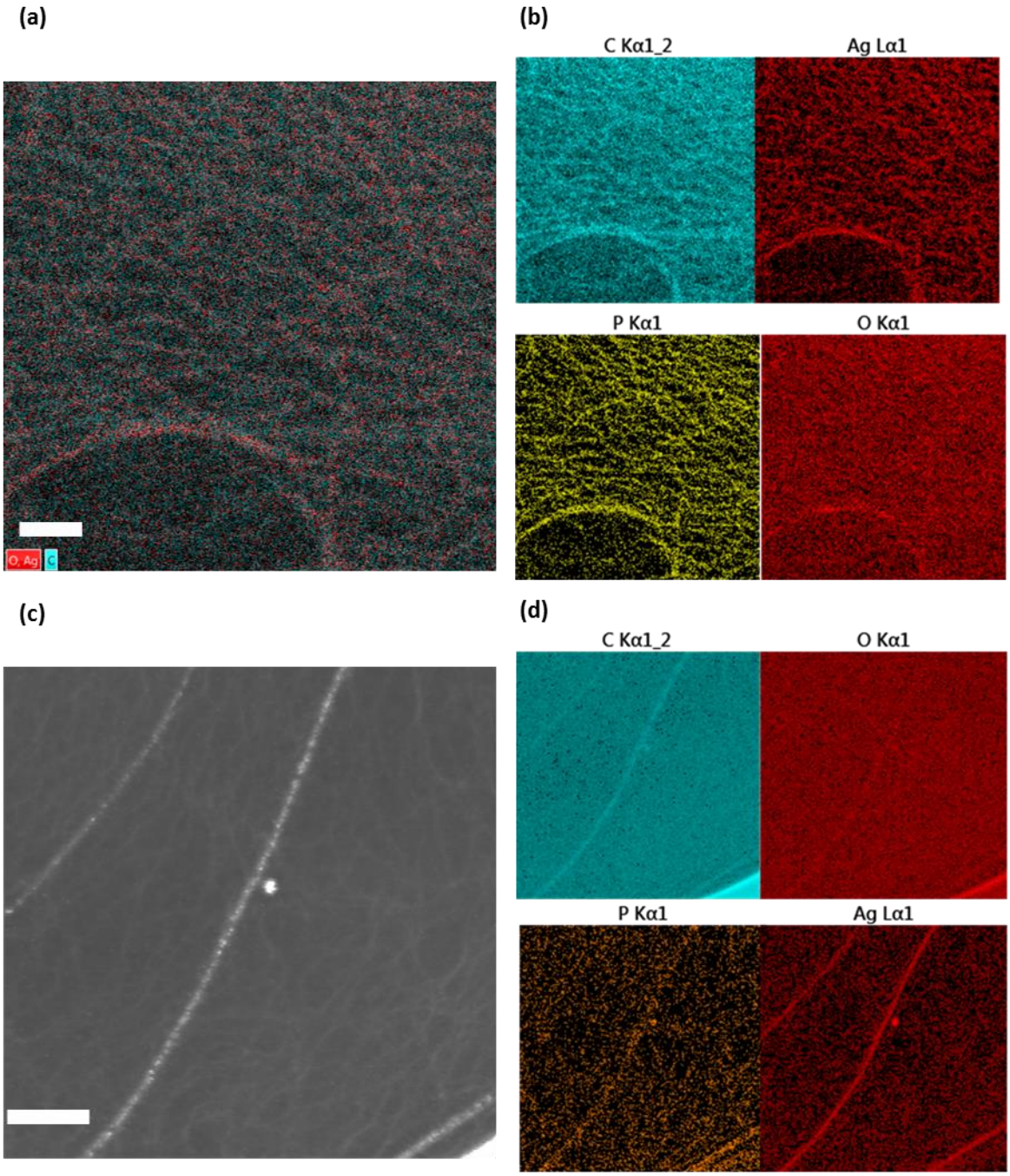

Figure 4.10 STEM images (a and c) and corresponding EDX maps (c and d) for sample B. C, Ag, P, and O refer to carbon, silver, phosphorus, and oxygen, respectively.

As it is not possible to differentiate the filament structures of each gelator via TEM other techniques were employed to characterise the hydrogel and understand the assembly. Firstly, a series of spectroscopic methods were used to understand the supramolecular organisation of the gelators, comparing their assembly to the single component gels.

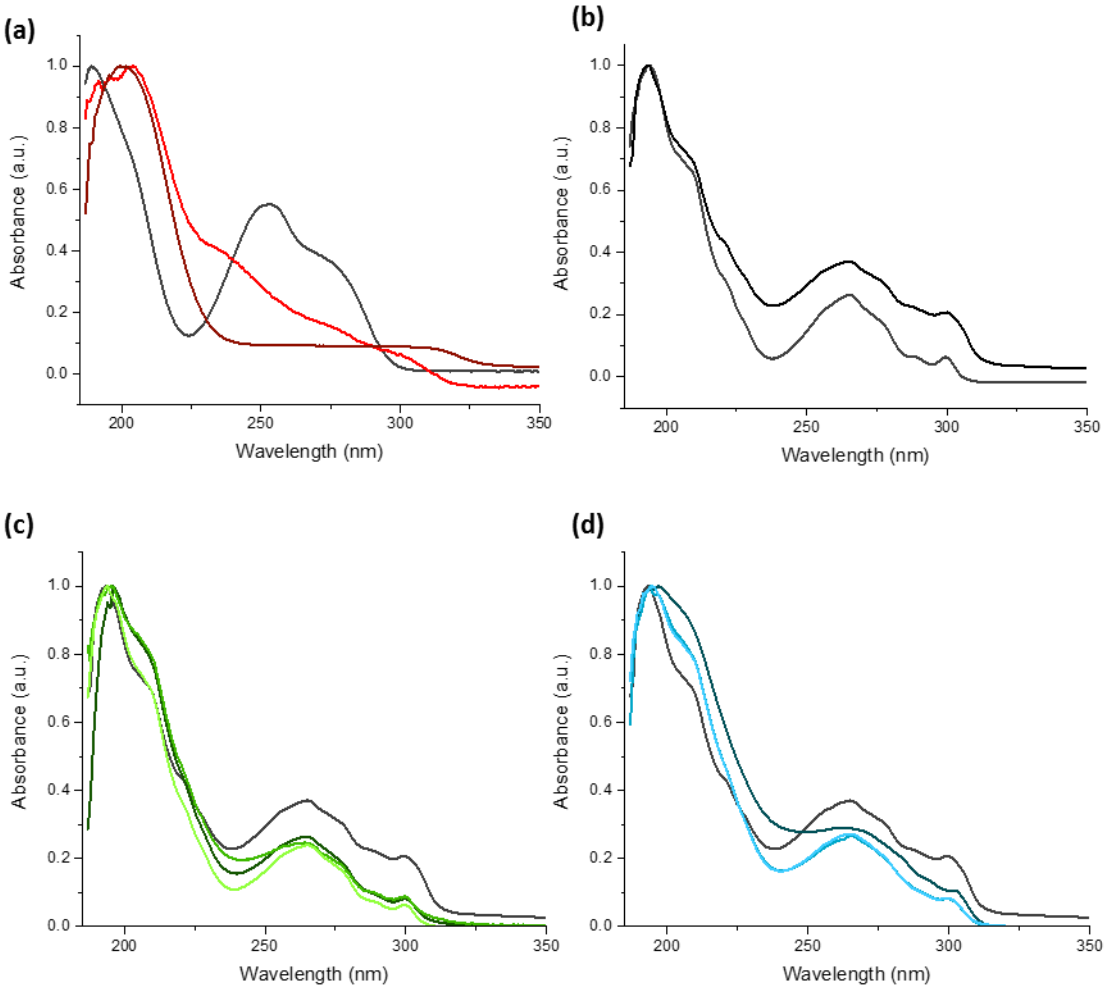

Figure 4.11 UV-Vis spectra of individual hydrogels and then multicomponent nucleotide-peptide hydrogels. (a) Na_2GMP solution and AgGMP hydrogel at varying AgGMP stoichiometries 1-1(red) 2-1 (maroon), (b) Fmoc-Tyr solution (grey) and then pH triggered Fmoc-Tyr supramolecular hydrogel through the hydrolysis of GdL (black). Multicomponent samples (c) 1-1 AgGMP stoichiometry and varying molar ratios; samples: A (—), B (—), and C(—), and (d) at 2-1 AgGMP stoichiometry and vary molar ratios; samples:D(—), E(—), and F(—).

UV-vis spectroscopy (Figure 4.8) of the hydrogels exhibited multiple peak maxima, as the spectra were collected from samples between quartz plates the path length was variable and thus the data was normalised. Also, the different gelator concentration between samples would inevitably lead to different absorbance values. Thus, exact absorbance values were not informative. Though hypochromicity was observed for all samples because of gelation. This can be understood when considering the two different environments for the gelators prior to and post gelation. Before gelation,

in solution, the gelators are relatively free to rotate allowing for unhindered transitions. In contrast, after gelation, these molecules are confined in nanofilaments that bundle and entangle together. This relatively confined, and more rigid assembly reduces rotation such that electron transitions are less favourable. This observation is analogous to the hyperchromic effect that occurs with denaturing of the DNA helix, which disrupts the bonding between nucleobases, allowing for freer rotation of its aromatic groups and increased absorbance values.[60]

Substantial peaks shifts are observed for the AgGMP gelation, Na_2GMP solution exhibited peaks at 196, 252 and 276 nm. The absorbance peak at 196 nm undergoes a bathochromic shift to 200 nm, as well as significant shifts for other peaks, indicative of aromatic stacking. The Fmoc-tyrosine solution exhibited absorbance at around 210nm and then 265, 288 and 299 nm with peaks around 210 nm previously being attributed to fluorenyl $n \rightarrow \pi^*$ transitions and absorbances between 265 to 300 being attributed to the tyrosine and fluorenyl $\pi \rightarrow \pi^*$.[61,62] Less significant shifts are observed due to Fmoc-tyrosine gelation, indicating similar assemblies for the aromatic residues before and after gelation. For the multicomponent hydrogels, hypochromocity is also observed, characteristic of supramolecular gelation. [38,63,64] As both gelators absorb within the same wavelengths, there is broadening of the peaks. The absorbance peaks are somewhat similar to the single component hydrogels, perhaps indicating self-sorting into separate filaments. Fluorimetry and circular dichroism were used to study the molecular arrangements of the gelators further.

Circular dichroism (CD) was employed to further understand the supramolecular organisation and how it differs in the multi-component hydrogels (Figure 4.10). The Fmoc-tyrosine solution (Figure 4.12a) did exhibit peaks prior to gelation, indicating that there is already some supramolecular organisation in solution. Fmoc-tyrosine and structurally similar gelators have been shown to form micelles, and at the concentrations used here, often worm-like in nature. [13,41,53,54,62] Thus they are expected to exhibit supramolecular chirality. Upon the gelation of the Fmoc-tyrosine solution (Figure 4.12b), the ellipticity and hence supramolecular chirality is substantially increased, attributed to extended filament growth

and bundling. [61,62] The absorptions observed at *ca.* 210 nm characteristic of fluorenyl the n→π* transitions and absorbances between 265 to 300 being attributed to the tyrosine and fluorenyl π→π* transitions.[61,62] Then the peak at 304 nm has been attributed to π–π* transition induced by interactions of fluorenyl groups in the supramolecular assembly. [13,61,62,65]

The GMP aqueous solution exhibits relatively low ellipticity (Figure 4.12a), with a negative band at 196 nm arising from the chiral ribose moiety, a positive band centred at 219nm, due to a n → π * transition and two weak negative bands at 250 and 253 nm appear, due to π → π * transitions originating from the guanine chromophore. [66–68] At 25 mM and pH 8, GMP can exist as monomers, dimers and tetramer stacks which would give rise to a CD signal. [68,69] The Ag-GMP hydrogel spectra (Figure 4.12c) have a marked increase in ellipticity and a red-shift for the π → π * transition, indicative of an overlap between the aromatic moieties contributing to exciton coupling. [37,70–73]

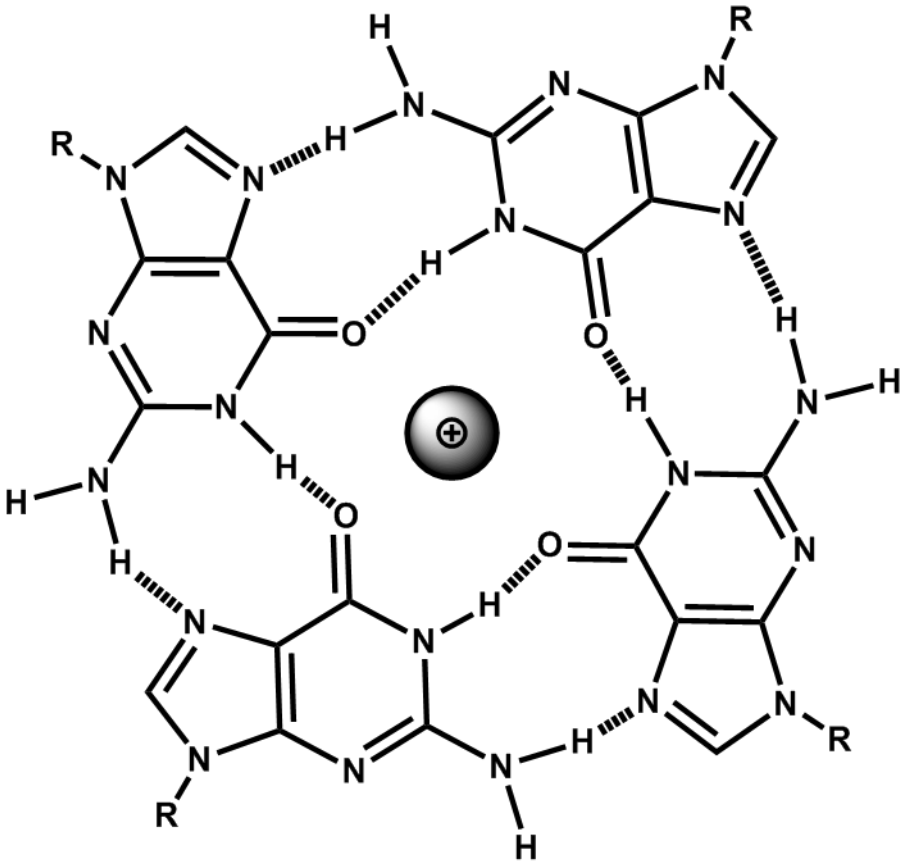

Figure 4.12 Structure of guanosine tetramer, known as G-quartets, is stabilised by the presence of a monovalent cation. For GMP the R refers to the ribose and phosphate.

Also, included is the CD spectra for GMP tetramers that can assemble (Figure 4.13c), known as G-quartets, due to various stimuli such as lowering of pH, for GMP this from 2-6 and therefore is an alternative assemble that could conceivably form. [15,67,74,75] The GMP tetramers assemble through Hoogsteen style hydrogen bonding between the guanine bases (Figure 4.12) and monovalent cations can stabilise the electron density allowing for stacking. [67,76–83] For GMP, the protonation of the phosphate groups lowers electrostatic repulsion between the tetramers, promoting stacking and hydrogen bonding interactions between the phosphate groups and the sugar moieties. [18,68,75] These structures have characteristic peaks at 213 nm and 272 nm typical of a left-handed superhelix.[67,84]

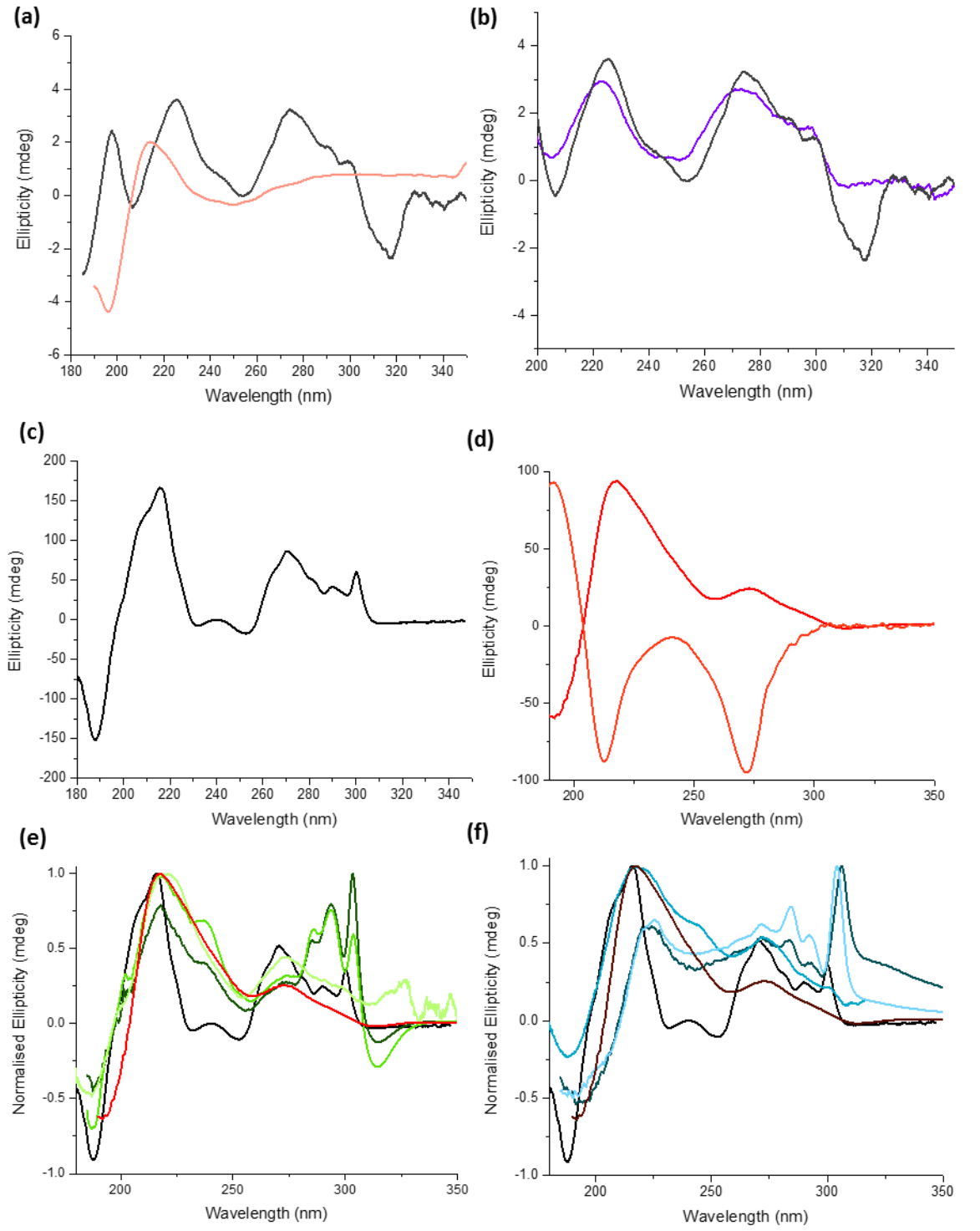

Figure 4.13 Circular dichroism spectra of (a), (b), solutions, (c), (d), single component gels, and (e),(f), multicomponent gels. Solutions: (a) FY (grey) and GMP (pink) and (b) FY (grey) and FY-GMP (purple). Single component hydrogels: (c) FY gel through hydrolysis of GdL and (d) Ag-GMP gel (red) and GMP G-quartet (peach). Normalised CD spectra of multicomponent samples (e) 1-1 AgGMP stoichiometry and varying molar ratios; samples: A (—), B (—), and C(—), and (f) at 2-1 AgGMP stoichiometry and vary molar ratios; samples: D(—), E(—), and F(—).

Significantly, for the multi-component hydrogels, the CD signal of both gelators appear in the spectra (Figure 4.12c and d.), indicating both components gel. Also, the characteristic peaks for G-quartets are not observed indicating that these are not formed at a significant level in this system.

For the 1:1 ratio, samples A and B exhibit a split cotton effect with a negative and positive peak at 315 and 304 nm, respectively. This is characteristic of extended helical arrangements of the fluorenyl groups. [85,86] These are red-shifted relative to the Fmoc-tyrosine gel, which is not too surprising as these filaments are likely to be in a different environment in the multicomponent system, potentially bundling with GMP filaments. This could occur as the tyrosine has previously been reported to intercalate between GMP stacks. [83,87] Thus, they could potentially form self-sorted filaments but mixed bundles. However, shifts for turbid samples have also been attributed to chiral scattering and therefore may not necessarily be indicative of different assembly relative to the single component samples. [88] This spilt cotton effect is notably absent from sample C and is instead dominated by noise, indicating that there isn't sufficient filament formation by Fmoc-tyrosine to generate a sufficient CD signal. This agrees with the pH measurement and observation that this sample doesn't gel. For samples A and B, peaks at 285 and 293 nm associated with Fmoc-tyrosine gelation are observed. Surprisingly, the peak structure at 270 nm, characteristic of Fmoc-tyrosine gelation is not present, the reason for this is not known though it may indicate that at this ratio an insufficient amount of FY gels to present a sufficient FY signal. However, the peak at 275 nm associated with Ag-GMP gelation is present.

At shorter wavelengths (*ca.* 190-250 nm), the broad peak is characteristic of Ag-GMP gelation (221 nm) causes significant broadening than would be expected for just Fmoc-tyrosine gelation, indicating both have gelled. There is also a shoulder peak at *ca.* 200 nm associated with Fmoc-tyrosine gelation. For C, as observed at longer wavelengths only peaks associated with GMP are observed for this sample.

Interestingly for the 2:1 ratio gels, the split Cotton effect is absent for all samples, despite all gelling, this may be related to the turbidity of the sample but may also indicate disruption to the FY assembly. For samples D and F, there was a significant bathochromic shift for the 300 nm peak to 306 nm and 304 nm, respectively. Other peaks between 250-300 nm, associated with fluorenyl and phenyl π- π* transitions, are also present. The peak at 270 nm is particularly prominent for these samples, potentially due to the lower pH achieved at this ratio, thus promoting more Fmoc-tyrosine gelation.[46] For sample E, these peaks are present as well as the broad peak at 217 nm associated with AgGMP gelation and the peaks as a shoulder peak at 209 nm and a negative peak at 188 nm, indicating Fmoc-tyrosine gelation. Whereas, when the Fmoc-tyrosine concentration is the same as GMP or higher, as with samples D and F, the most prominent peak is significantly shifted to *ca.* 220 nm and the shoulder peak at *ca.* 200 nm and the associated negative at *ca.* 190 nm is not observed for D and F. This cotton effect is characteristic of helical assembly,[12,89,90] and its absence further indicates disruption to the supramolecular assembly of FY.

As well as the chiral environments, CD measurements are sensitive to the electronic environments but these are comparable between samples. [91–93] Thus, these observations indicate that there is significant disruption to the supramolecular organisation of the gelators in the multicomponent system. Fourier-transform infrared spectroscopy (FT-IR) (Figures 4.11 and 4.12) was employed to understand this further.

Firstly, there are numerous peak shifts associated with the gelation of GMP compared to the GMP powder (Figure 4.13 a and b). Most notably, the carbonyl vibration of the guanine residue shifts sustainably from its conjugated keto form (1669 cm^{-1}),[39,94,95] to a lower wavenumber in its enolate form (1606 cm^{-1} and 1605 cm^{-1}, for ratios 1:1 and 2:1, respectively), in line with previous reports. [39,96] This hypsochromic shift is indicative of a higher energy bond formation, relative to the conjugated keto carbonyl. Loo *et al.* reported that this binding resulted in a large negative enthalpic change

through isothermal calorimetry measurements and therefore, the electrostatic bond between the enolate and the silver ion as a dimer is likely stronger than the original carbonyl.[37]

Many of the guanine ring stretches in this region observed in the powder are masked by this strong enol vibration. However, the C=C vibration (1537 cm^{-1}) is slightly shifted to a higher vibration (1524 cm^{-1}), possibly a consequence of disrupting the disrupting the conjugated π-orbital system of the guanine ring. [39] Also, the NH_2 scissoring bend peak (1491 cm^{-1}) broadens and shifts to 1477 cm^{-1} upon gelation, indicative of becoming involved in hydrogen bonding. [49,97] In conjunction with this, at higher wavenumbers, are new peaks are observed at 3320 cm^{-1} and 3440 cm^{-1} characteristic of symmetric and asymmetric stretches, respectively, for hydrogen bonded amine residues.[95] The broad peaks at 1321 and 1341 cm^{-1} for the 2:1 and 1:1 ratio, respectively, are associated with the full dissociated NO_3^- stretch, with the shoulder peak due to the vibrational mode for the ionic pair separated by one water molecule. [98]

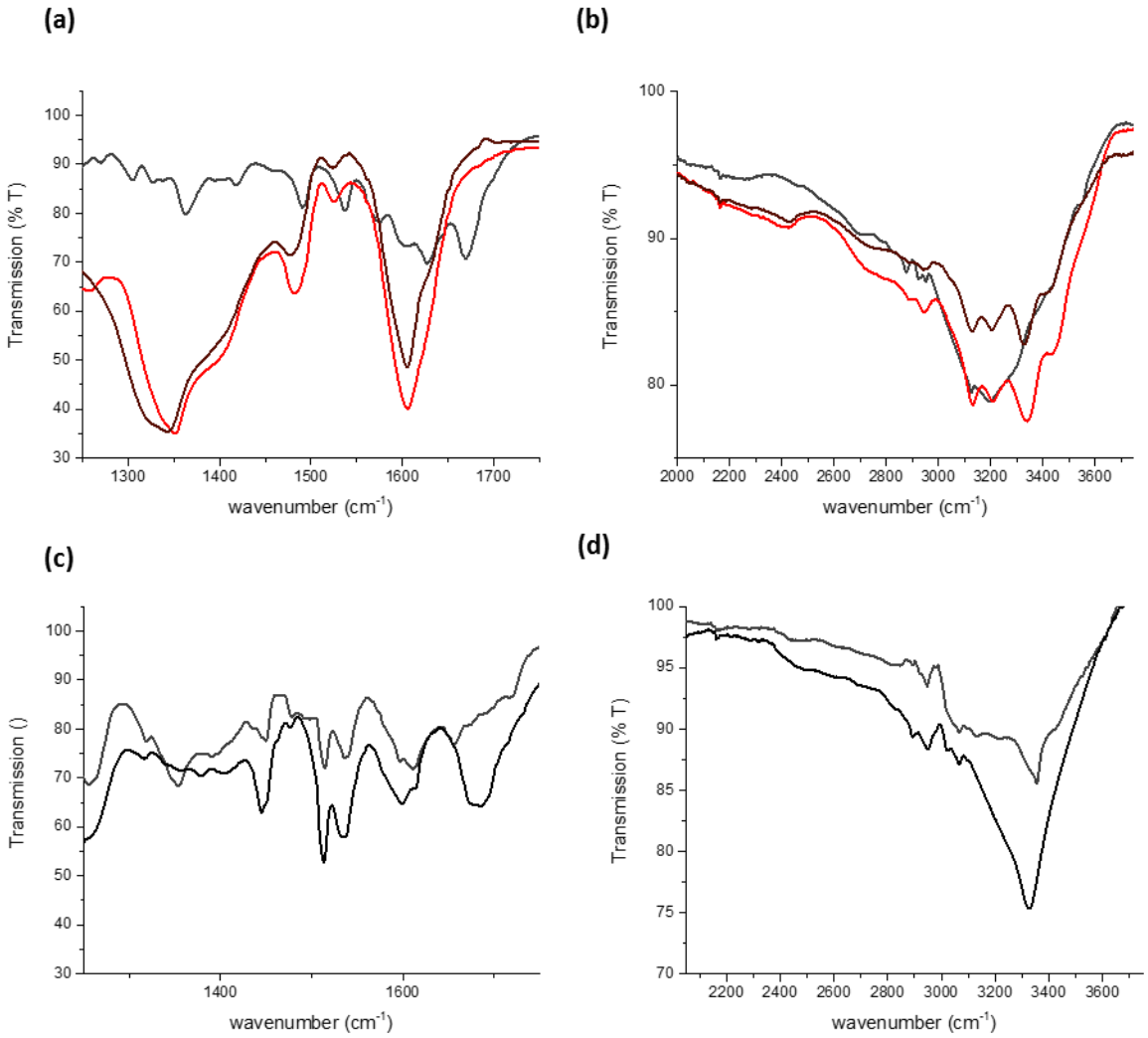

Figure 4.13 FT-IR spectra of lyophilised single component hydrogels (a, b, c & d) . Spectra of Fmoc-tyrosine powder (grey) and hydrogel (black) through hydrolysis of GdL (a &b). Spectra of GMP powder and AgGMP hydrogel; 1-1 (red) and 2-1 (maroon).

FTIR of Fmoc-tyrosine (Figure 4.13 c and d) shows several key differences between the gelled sample and the Fmoc-tyrosine powder. These mainly originate from the Amide I regions, associated with carbonyl stretches, Amide II related to N-H bends and Amide A associated with hydrogen-bonded amine and hydroxyl groups. Gelation results in the disappearance of the 1656 cm^{-1}, associated with disordered or unstacked carbonyl groups. [13,49] This indicates more ordered assembly, which would be expected in the nanofilament formation. Gelation of Fmoc-tyrosine is also marked by a slight bathochromic shift in the amide I region for the pendant carbonyl (1611 cm^{-1}) to 1614 cm^{-1} indicating more extended hydrogen bonding, as would be expected as electrostatic repulsion is lowered through

protonation. [49,99,100] A broad non-Gaussian peak also emerges with two minima at 1675 and at 1685 cm^{-1} characteristic of the carbamate carbonyl group, indicating that this group becomes involved in the hydrogen bonding network as a result gelation.[13,49,101] The former peak is associated with disordered carbamate hydrogen bonding and some disorder is to be expected for such small gelators. [49,102,103] The peak at 1599 cm^{-1} is the asymmetric stretching of the carboxylate anion indicating a proportion of the terminal carboxylic acid groups remain deprotonated. [13,48,49] Also, associated with gelation is a broad peak at 3321 cm^{-1} characteristic of hydrogen-bonded hydroxyl groups. [104,105]

For the multicomponent gels (Figure 4.14), the spectra are rather complicated owing to similar functional groups being present in each gelator, but important observations can still be made. For instance, at the 1:1 ratio (Figure 4.14a and b), the carbamate peak is observed for all samples at 1693 cm^{-1}, indicating that this gelator has assembled due to hydrogen bonding. Also, the prominent enol-peak (*ca.* 1610 cm^{-1}), indicating the formation of the GMP dimer via the silver has occurred [96] and not through the formation of G-quartets. This supports the observations via CD analysis that both gelators gel in the multicomponent system.

However, for all multicomponent gels, the enol-Ag^{+} peak is at a slightly higher wavenumber (1608-1610 cm^{-1}) relative to single component Ag-GMP gels in the absence of FY, indicating a slightly less strong bond. This indicates non-orthogonal assembly between Fmoc-tyrosine and GMP, supported by the observation that this shift is less perturbed when the Fmoc-tyrosine concentration is lower than GMP e.g. sample B. Also, there is a disruption to the amide II region (*ca.* 1515-1550 cm^{-1}). Furthermore, the NH_2 scissoring bend peak of GMP involved in hydrogen bonding is effectively absent, except when the Fmoc-tyrosine concentration is lower than GMP. Further indicating that hydrogen bonding involved in the GMP supramolecular assembly is perturbed. Also, at higher wavelengths, the stretching bands associated with hydrogen bonded amines of the guanine are less pronounced (Figure 4.13 b) when Fmoc-tyrosine is at the same or higher concentration than GMP. However, at the 1:1 Ag-GMP ratio the 1675 cm^{-1} characteristic of disordered carbamate arrangements is absent and

therefore, the slow assembly of these gels perhaps allows ordered hydrogen bonding with carbamate moiety.

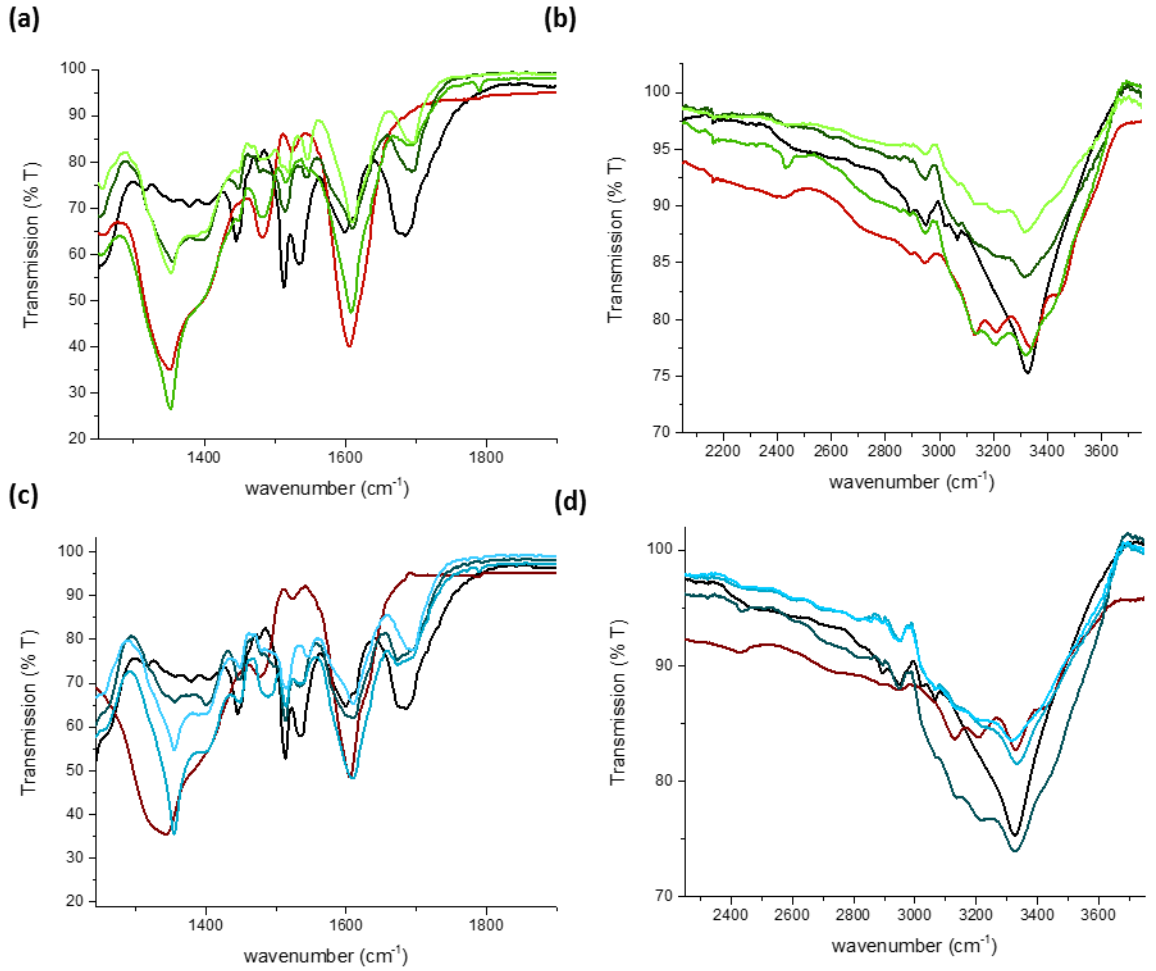

Figure 4.15 FT-IR spectra of lyophilised multicomponent hydrogels (a, b, c & d). Multicomponent samples (a) and (b) 1-1 AgGMP stoichiometry and varying molar ratios; samples: A (—), B (—), and C(—), (c) and (d) at 2-1 AgGMP stoichiometry and varying molar ratios; samples: D(—), E(—), and F(—).

Similar observations are made for multicomponent hydrogels formed at the 2:1 ratio. Again, a broad peak is observed for all ratios at 1694 cm^{-1} attributed to the carbamate associated in hydrogen bonding was identified. This is red-shifted relative to the 1:1 ratio gels, perhaps due to the lower pH achieved promoting gelation further and therefore a more extended hydrogen bonding network. However, there is also a peak at 1672 cm^{-1}. As the enol-Ag^{+} peak was observed, it was not attributed to the keto carbonyl of the guanine ring (1669 cm^{-1}). Rather, this peak is attributed to disordered carbamate

assembly which is likely a consequence of the fast kinetics of gelation as this is not observed for sample F which gels much slower. The kinetics of gelation has been shown to determine hydrogel ordering at the microscale, with slower gelation often producing a more homogenous gel network. [40,106–108]

As for the 1:1 Ag-GMP ratio gels, a slight bathochromic shift, relative to the single component gels, is observed for the enolate-Ag^+ of 3-5 cm^{-1}. As before, this is less shifted when the Fmoc-tyrosine concentration is less than the GMP concentration, again indicating more orthogonal assembly as the FY concentration is lowered. Also, the hydrogen-bonded NH_2 scissoring bend peak at *ca.* 1478 cm^{-1} is most prominent at this ratio.

For all samples, peaks in amide II region (*ca.* 1515-1550 cm^{-1}), associated with hydrogen bonded amines are more prominent than samples prepared at the 1:1 Ag: GMP ratio. Thus, the lower pH likely encourages filament formation due to protonation of the terminal carboxylic acid, resulting in more extensive hydrogen bonding than at the 1:1 ratio. In addition, at higher wavenumbers (Figure 4.15d), peaks associated with the hydrogen bonding for both gelator systems are observed. Though, as with the 1:1 gels, these peaks exhibit some broadening due to overlapping peaks from the two gelators.

The observed non-orthogonal assembly can be understood if there is binding of the silver ions to both Fmoc-tyrosine and GMP. This would perturb the assembly of the GMP and thus also affect the pH drop required for Fmoc-tyrosine to gelate. Indeed there are reports of amino acids binding silver and these are capable of reducing Ag^+ to form silver nanoparticles. [90,109–113] Above the pKa of tyrosine (*ca.* 10.1) the hydroxyl group is deprotonated and subsequent electron transfer to the silver salt results in the reduction of silver salts to form silver nanoparticles and a quinone structure. [111] However, Selvakannan *et al.* demonstrated that this does not occur below the pKa and therefore is not expected to occur in this system as after addition of the GMP to the Fmoc-tyrosine the solution pH is *ca.* 8.5. This was verified by ^{13}C NMR which demonstrated that no quinone had been formed (Figure 4.16a), due to the absence of a resonance peak at *ca.* 186 ppm [114], with the peak at 156. ppm associated with the tyrosine hydroxyl group. The peak 174.6 ppm is characteristic of the pendant carboxylic acid. Instead, as

previously reported, interactions between the carboxylate anion (with a predicted pKa of *ca.* 3.2-3.7[45], though this likely to be sustainably shifted[46]) and the silver salt are expected. This would result in a stretching vibration at 1601 cm^{-1}. This region is masked in the multicomponent system by the enol peak but may explain the broader peaks for samples D and E. Also, gelation of Fmoc-tyrosine in the presence of silver resulted in a perturbed hydrogen bonding (Figure 4.16b). The peak at 1672 cm^{-1} was absent, indicating that previous observations were not due to the formation of a quinone silver bond. Instead, there is an additional peak at 1579 cm^{-1} associated with the carboxylate anion and may indicate binding with the silver ion resulting in the formation of a new peak.

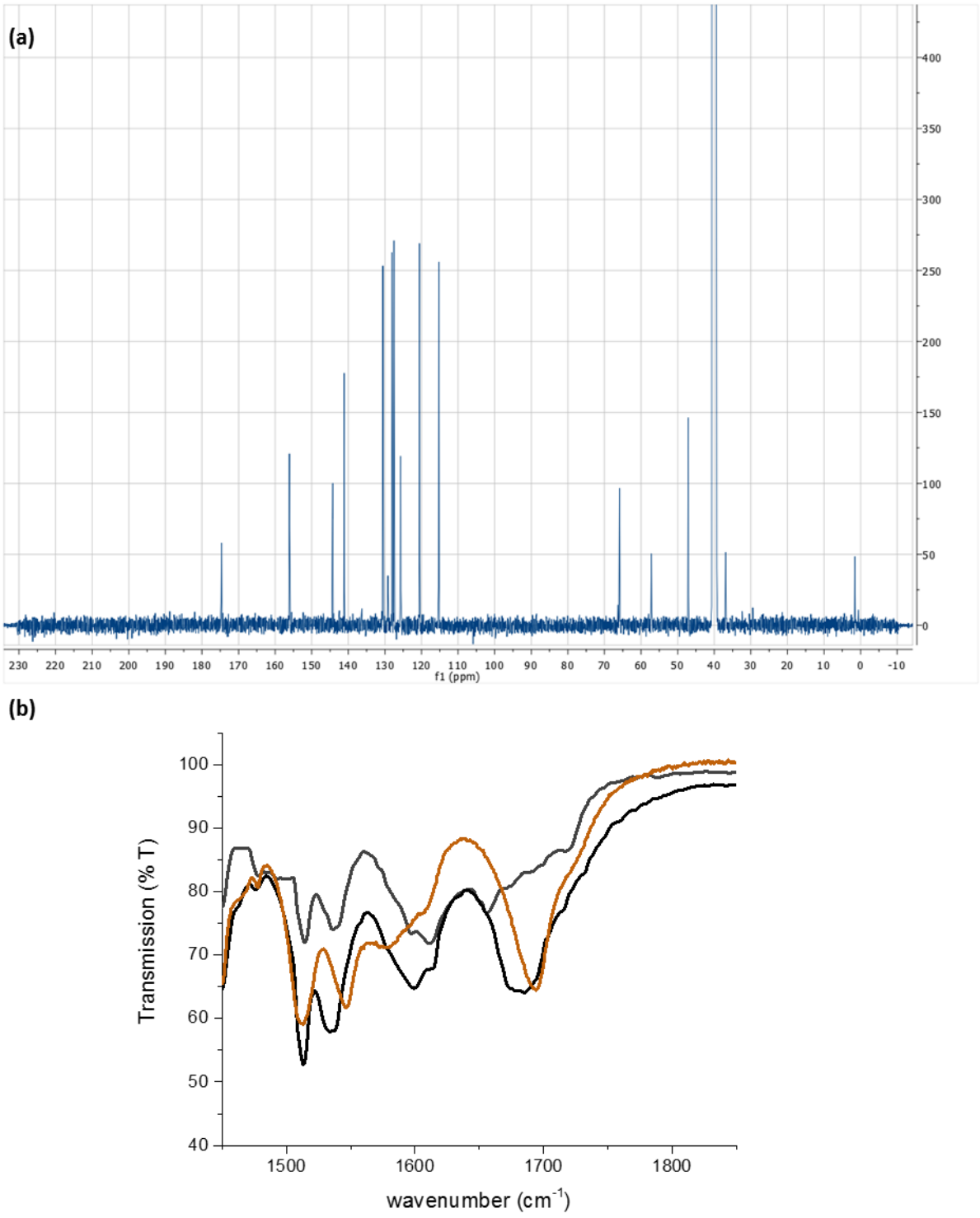

Figure 4.16 (a) ^{13}C NMR spectrum (500 MHz, DMSO-d6) of sample D which exhibits resonance peak at 156 ppm characteristic of a tyrosine hydroxyl carbon and (b) FT-IR spectrum demonstrating perturbed hydrogen bonding when Fmoc-tyrosine gels in the presence of Ag (orange) versus in the absence (black).

The consequences of this non-orthogonal assembly on the macroscopic properties of the gels were studied using via differential scanning calorimetry (DSC) and oscillatory rheology (Figure 4.17). A broad endothermic peak was observed for all samples, corresponding to the breaking of the non-covalent

crosslinks of the supramolecular hydrogel which causes a gel to sol transition.[30,38,64] For the single component gels, the Fmoc-tyrosine gel there is a broad minimum at 40.1 °C with a broad shoulder from 48-60 °C. For the Ag-GMP gels, the 1:1 AgGMP gel, the broad melting peak is centred at 46.8 °C. At the 2:1 ratio, the melting peak is very broad with a minimum at 39.7 °C, with a smaller peak at 52.2 °C and a shoulder at 55.9-74.4 °C. This indicates heterogeneity in the gelation, which may be a consequence of the relatively slow dissolution of the silver salt relative to the gelation. This is analogous to using mineral salts to lower the pH as a trigger for gelation.

Sample	$T_{gel-sol}$ (°C)	Comment
FY	40.1	broad shoulder (48-60 °C)
Ag:GMP 1:1	46.8	
Ag:GMP 2:1	39.7	smaller peak (52.2 °C) and shoulder (55.9-74.4 °C)
Ag:GMP 1:1 25 mM FY 25 mM	44.8	
Ag:GMP 1:1 25 mM FY 12.5 mM	41.2	
Ag:GMP 1:1 12.5 mM FY 25 mM	36.2 and 40.4	
Ag:GMP 2:1 25 mM FY 25 mM	35.5 and 40.2	
Ag:GMP 2:1 25 mM FY 12.5 mM	42.3 and 44.7	Broad peak(s)
Ag:GMP 2:1 12.5 mM FY 25 mM	46.1	

Table 4.2 Reported moduli and yield strains for hydrogel samples for single and multicomponent hydrogel samples and associated comments

For the multicomponent hydrogels, interesting observations can be made that demonstrate non-orthogonal assembly for the two components. Firstly, for multicomponent hydrogels at the 1:1 Ag: GMP ratio, samples have a decreasing $T_{gel-sol}$ for samples A, B and C (Table 4.2). This is in line with a lower total gelator concentration for samples B and C and thus, likely a lower network density, then the lower pH drop achieved for sample C will result in less gelation for both components. More interestingly though, this relationship does not hold true for multicomponent hydrogels prepared at the 2:1 ratio. For instance, two endothermic peaks were observed for samples D and E, indicative of

heterogenous gelation. Though not sample F, presumably due to the slower gelation processes allowing for more homogeneous gelation. Also, the endothermic peaks for sample E are higher than the peaks observed for sample D, despite the lower total gelator concentration. This indicates non-orthogonal assembly as a the $T_{gel\text{-}sol}$ is expected to increase with increasing gelator concentration.[115] This unexpected observation was probed further using rheology (Figure 4.13 c and d).

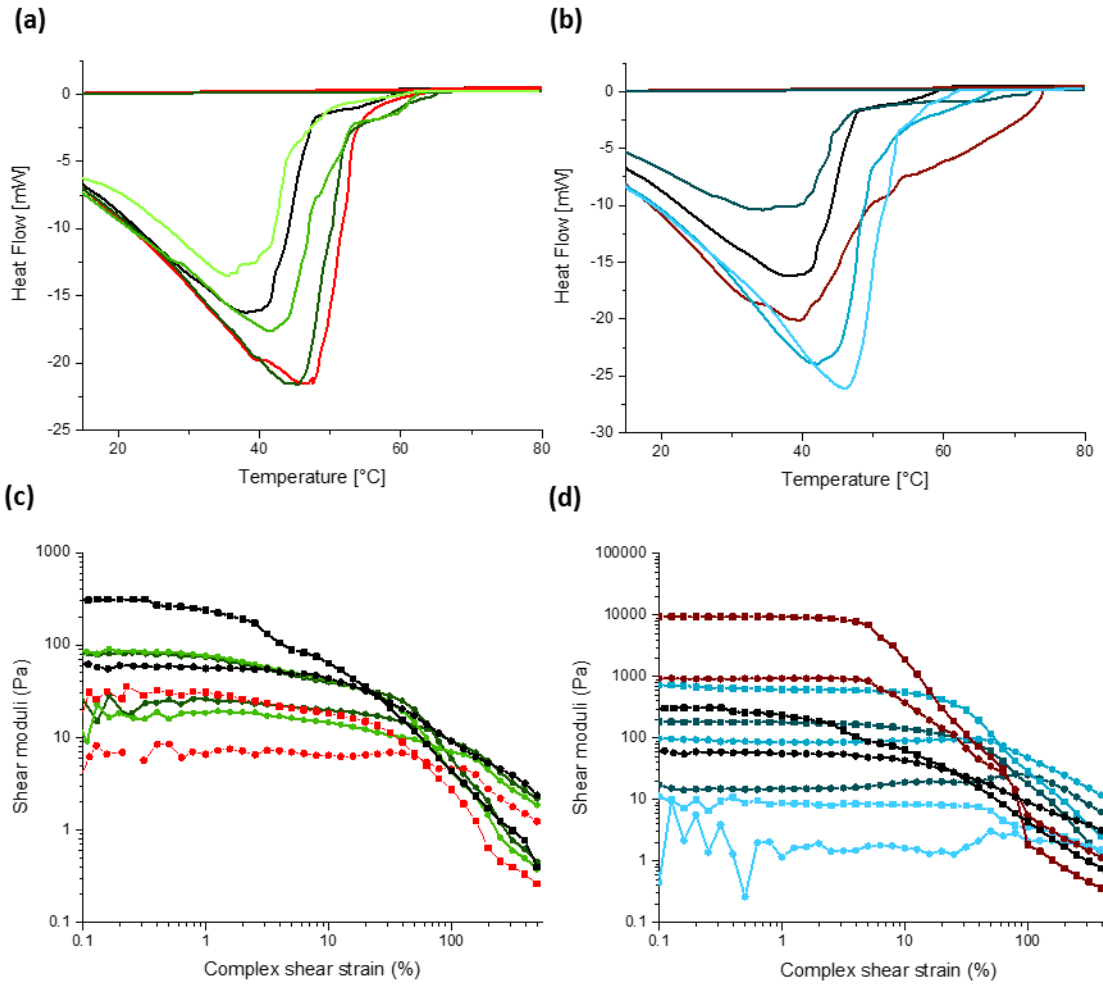

Figure 4.17 DSC thermograms (a) and (b) of multicomponent supramolecular hydrogel alongside single component hydrogels. Oscillatory amplitude sweeps at a constant frequency (1Hz) (c) and (d). All gels exhibited a linear viscoelastic regime. In oscillatory experiments, ▪ refer to G' and ● refer to G", the storage modulus and viscous modulus, respectively. For all figures, Multicomponent samples -1 AgGMP stoichiometry and varying molar ratios; samples: A (—), B (—), and C(—), and at 2-1 AgGMP stoichiometry and vary molar ratios; samples: D(—), E(—), and F(—). Red lines refer to the AgGMP samples.

Rheological analysis (Figure 4.13 c and d) was undertaken to determine the mechanical properties of the multicomponent supramolecular hydrogels. Oscillatory amplitude sweeps at a constant frequency

(1 Hz) demonstrated a linear viscoelastic region (LVR) for all gelled samples, in which the storage (elastic) G' moduli are roughly an order of magnitude higher than the loss (viscous) G" moduli. This is indicative of an elastic solid-like network of the gel throughout a viscous solvent.[38,40,61,116] At increasing strains, there is a crossover of the moduli with a sharp decrease of the storage moduli (G') such that it is lower than the viscous moduli (G''), indicating a transition from an elastic gel to a viscous fluid.[38,64,117,118] At low strain, the Fmoc-tyrosine gel had an elastic modulus of *ca.* 310 Pa and had a yield strain of *ca.* 25%. For the 1:1 gel, the elastic moduli (*ca.* 30 Pa) was not at least roughly an order magnitude higher than the viscous moduli (*ca.* 7 Pa) and hence is not classified as a gel, rather a viscous solution. Though a yield strain of *ca.* 50% was observed, as the filaments formed could still be sheared. For the 2:1 gel, within the LVR the elastic modulus is *ca.* 9500 Pa and has a yield stress of *ca.* 63%.

Some key observations can be made for the multicomponent gels. For instance, the multicompetent gels at the 1:1 ratio, the gelled samples were stiffer than the AgGMP 1:1 gel by itself but were noticeably less stiff than the Fmoc-tyrosine gel. This is likely due to the fact the higher pH resulted in lower gelation of the FY molecules. Sample C was too soft to give meaningful data. The multicomponent gels also had enhanced yield stress against the single component hydrogels which is not too surprising considering the enhanced gelator concentration. Similar observations were made for the gels at the 2:1 ratios. However, most significantly of all is that at both ratios, when the Fmoc-tyrosine concentration is lower than the GMP concentration the measured elastic moduli is higher. This supports observations of the non-orthogonal assembly through CD and FT-IR analysis. Significantly, all 2:1 multicomponent gels were less stiff than the 2:1 Ag-GMP which makes sense if there is competition for silver ion binding between Fmoc-tyrosine and GMP.

This non-orthogonally assembly was tracked using rheological analysis. The gels were prepared as before and transferred to the rheometer instantly after vortexing. A very low shear strain (0.1%) at a constant frequency (1 Hz) was applied throughout the measurement. This allowed for the elastic and viscous moduli and phase angle to be measured in real-time to track gelation. The applied strain was

well within the LVR, thus it should not have any significant impact on the gelation characteristics.[20,26,61,119] Indeed, this was confirmed by undertaking oscillatory amplitude strain sweeps (Figure 4.15) after the measurement which demonstrated similar moduli and yield strain to gels formed normally.

The moduli for Fmoc-tyrosine rises very quickly within the first 90 minutes or so before beginning to plateau. At the 1:1 ratio, the elastic moduli for the single component gel rise very slowly, rising about the viscous moduli at *ca.* 170 minutes. In comparison, the multicomponent gels at this ratio, the elastic moduli rise above the viscous moduli within *ca.* 40 minutes. This is since the other gelator, Fmoc-tyrosine can assemble much quicker, as observed for the single component gel.

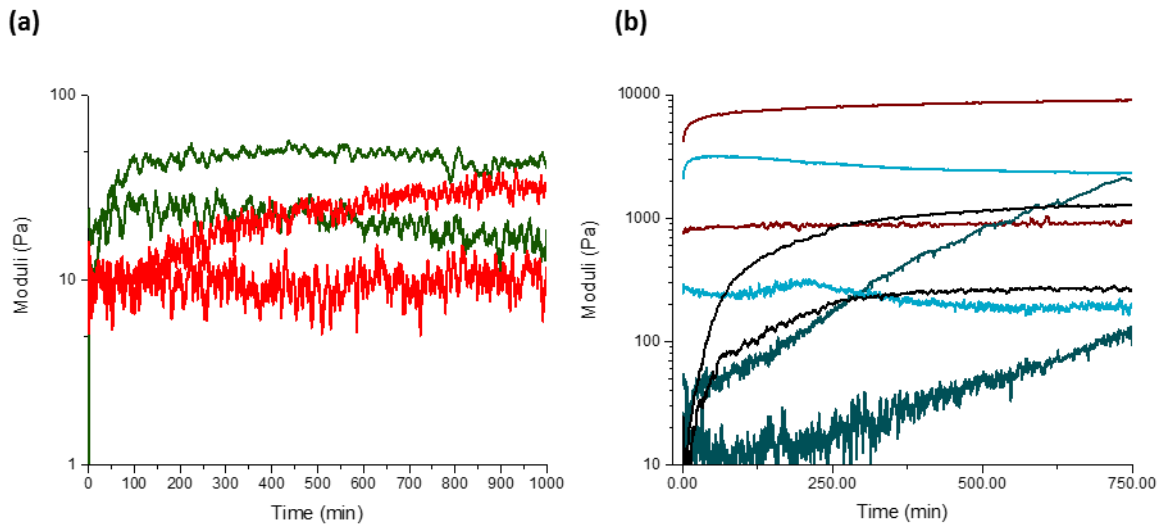

Figure 4.17 Probing gelation through measuring moduli changes with a timed oscillatory study at a constant strain (0.1%) and frequency (1 Hz). (a) hydrogels formed at a 1:1 Ag:GMP ratio and (b) hydrogels formed at a 2:1 Ag:GMP ratio.

Unlike the 1:1 gel, at the 2:1 ratio, for the single component gel, there is instantly a very fast increase in moduli and within *ca.* 30 minutes the moduli begin to plateau. Significantly, this is also observed at this ratio when the Fmoc-tyrosine concentration is lower than that of GMP. A slight reduction of elastic moduli of roughly 780 Pa is observed after 90 minutes as well as a slight increase and then a reduction in the viscous moduli is observed at *ca.* 210 minutes. As these observations are absent from either of the single component gels, these could represent some supramolecular reorganisation. As the

filament structures are non-covalent assemblies, gelators can equilibrate between sol and gel state,[11,14,120] this can allow for the transformation of the supramolecular structures.[30,115,119–122] For instance, Stupp *et al.* demonstrated the conversion of metastable twisted ribbon structures into thermodynamically stable helical ribbon structures without the need for any external stimuli.[123]

A similar reduction in moduli has also been made for oligophenylene vinylene and perylene bisimide based gelators. [27,124] These also assemble through protonation of pendant carboxylic acids which result in the bundling of filaments after a reduction in negative charge, thus these bundles become more hydrophobic. This causes a contraction of the gel network and expulsion of the aqueous solvent, known as syneresis. Consequently, there is a weaker contact between the plates of the rheometer and the gel, causing an apparent decrease in the mechanical properties.[124] For sample E no expulsion was observed but very small expulsion may not be noticeable. Castilla *et al.* reported as much as 60% volume loss and much more abrupt changes in moduli were observed. Therefore, this may not be the case for this sample. Instead, the possibility of structural rearrangement was considered. CD spectroscopy was used to measure supramolecular assembly over time as the single and multicomponent samples assembled *via* changes in the ellipticity (Figure 4.18).

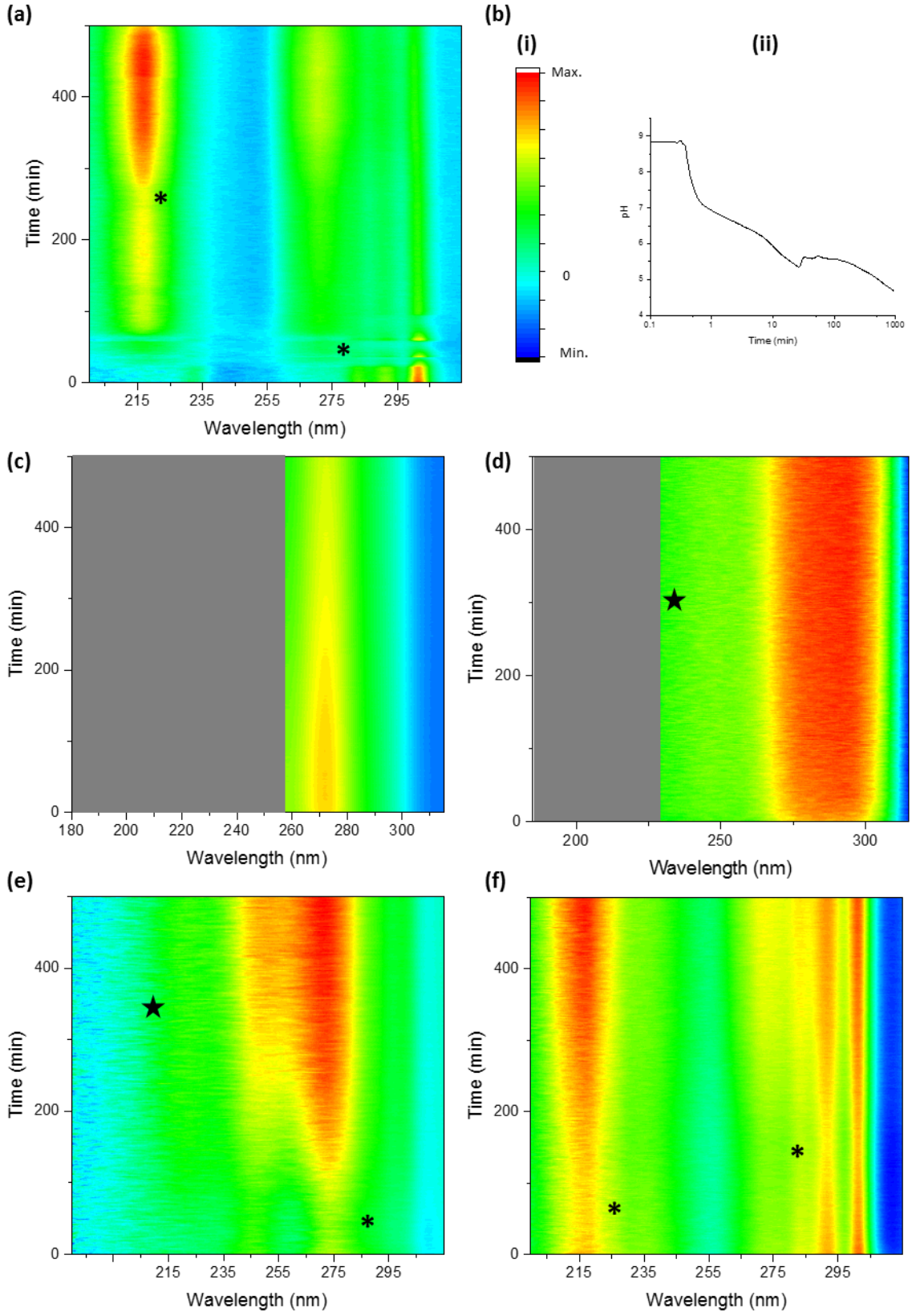

Figure 4.19 CD spectra of single component spectra (a) FY 25 mM, (c) AgGMP 1:1 and (d) AgGMP 2:1. (b) (i) Scale used for CD spectra. (ii) Also included is pH measurements of FY gelled through the hydrolysis of GdL, demonstrating plateaus at *ca.* 1 minute and *ca.* 100 minutes. CD spectra of multicomponent hydrogels at 2-1 AgGMP stoichiometry at varying molar ratios; (e) GMP 25 mM Fmoc Tyr 25 mM and (f) GMP 25 mM Fmoc Tyr 12 5 mM. All spectra do not include all wavelengths as HT values exceeded threshold value. When the threshold is exceeded no ellipticity is measure, e.g. at star of (e). Asterisks indicate drops and then increases in ellipticity for all samples with FY present.

Samples were prepared as before but transferred into slightly wider sandwich cells to allow for gelation to occur inside the spectrometer. (Samples placed between two plates did not gel and just dried up.) Consequently, this increased the absorbance values compared to spectra reported earlier (Figure 4.18). As a result, over time, particularly at shorter wavelengths, the HT threshold was exceeded which resulted in extremely low ellipticity values measured but this does not correspond to suppression of supramolecular chirality: see star symbol in figure 4.18e as an example. Also, inevitably the sample loading takes a minute or two and each scan takes roughly a minute. Therefore, taken together, the spectra should be used to provide an indication of processes occurring rather precise quantitative information of exactly when certain process occur.

Bearing this in mind some key observations can be made. For instance, the single component AgGMP gels appear to demonstrate an increase in ellipticity overtime, with no fluctuations (Figure 4.18c and d). (Though the 1:1 sample exhibits a decrease associated with increasing HT values.) However, the FY sample exhibits fluctuations to the ellipticity at the start of the measurement and then a gradual decrease followed by a gradual increase again over time at *ca.* 177 minutes (Figure 4.18a). This could be associated with the rearrangements reported by Tang *et al.*[46] for a similar gelator (Fmoc-FF) and appears to coincide with to the plateaus observed in the pH decrease (Figure 4.18b), discussed earlier in this chapter. Similar observations are made for samples D and E, with decreasing and then increasing ellipticity values at *ca.* 30 minutes and 125 minutes. It is not understood what is causing these changes, but it could perhaps indicate structural reorganisation which could correspond to different rheological properties throughout the gelation process. It also appears that for sample D there is a delay in the increase of ellipticity value but then a very sudden increase and plateau of these values.

Referring to the rheological analysis again. In contrast, to sample E, for sample D with an equimolar concentration of Fmoc-tyrosine and GMP for the sample, the rise in elastic moduli is greatly retarded. Which is in agreement with the CD observations during the gelling process. At this ratio, there is no

sharp increase in elastic moduli, indicative of fast gelation. Rather there is a gradual increase despite the higher total gelator concentration, for which faster gelation would be expected.[13] This verifies that there is non-orthogonal assembly between the two gelators as the increased Fmoc-tyrosine concentration perturbs the gelation.

Rheology has previously been used to infer whether co-assembly or self-sorting has occurred in the assembly process. When the assembly of two gelators is suitably slow and separated by enough time i.e., large differences in pKa, self-sorting gelators exhibit a plateau in the shear moduli between the sequential growth stages.[20,26,27,32] This is not observed here but this likely due to the very fast gelation for both gelators in the system, and thus sequential gelation would not be observed regardless of whether co-assembly or self-sorting occurred. Instead, experiments were undertaken to selectively remove one of the gelator networks, as this should be possible if self-sorted filaments and self-sorted network assembly had occurred.

Since the gelation of Fmoc-tyrosine is heavily pH-responsive it was investigated whether one of the gelators could be selectively removed by raising the pH. Regardless of trying to determine whether self-sorting has occurred, the ability to selectively remove individual gelators is advantageous for numerous reasons, such as modulating the mechanical properties of the gel and lowering the network density which should affect diffusion of cargo *e.g.* therapeutics or result in different cell differentiation if acting as tissue culture scaffold.[34,35,101,125–128] To achieve this, ammonia gas was passively added by flowing the gas from the ammonia solution (*ca.* 18 M) into the vial containing the supramolecular hydrogel (Figure 4.19a). This gradually increased the pH of the gel over several hours and was left to do so until the pH raised to 8.5, above the pKa of Fmoc-tyrosine, causing deprotonation of the terminal carboxylic acid and disassembly of the hydrogel filaments. At this pH there will be no further deprotonation of the guanine residue as the most labile proton, which has a pKa of 9.2[37] has already been abstracted in the formation of the dimer. This raising of pH was monitored using a pH probe, demonstrating a gradual increase in pH over a few hours. It is important to note that the pH is

increased gradually through the sample over time as the ammonia diffuses through the sample and discussed below. Therefore, apparent drops in pH over time, such as the AgGMP 1:1 gel is due the difficulty in measuring the pH at exactly the same location each time and doing so inevitably perturbs the network and may affect the raising of the pH.

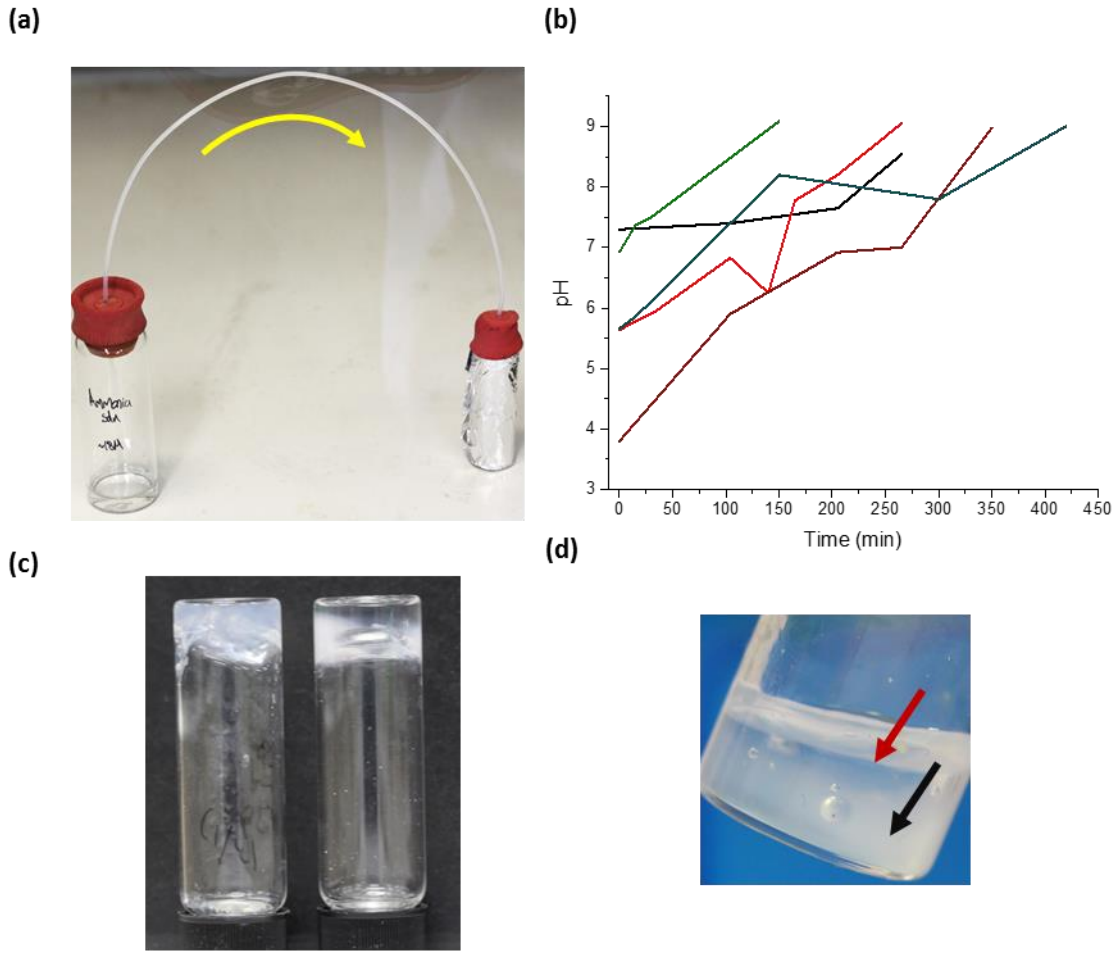

Figure 4.19 Disassembly of multi-component hydrogels. (a) Photo of set up to raise pH whereby ammonia gas flows from the left through the tubing to gradually raise the pH of the supramolecular hydrogel. (b) pH plots of raising pH over time. (c) Photos of single component hydrogels. At ca. 8.5 AgGMP samples are still gels but Fmoc-tyrosine sample forms a viscous solution. (d) Photo demonstrating change in turbidity down the hydrogel indicating disassembly of supramolecular aggregates. (Red arrow shows transparent area of gel and black arrow shows opaque region.)

For the single component hydrogels, only the Fmoc-tyrosine gel was dissembled by raising the pH to *ca.* 8.5. However, raising the pH above *ca.* 9.5 also results in the disassembly of the AgGMP gels, presumably due to deprotonation of the guanine residue and therefore disruption to the hydrogen bonding network. At an elevated pH, the AgGMP gels still exhibited rheology behaviour characteristic

prior to raising the pH (an LVR) and supramolecular chirality indicative of gelation (Figure 4.20b and c). For the multicomponent hydrogels at the 1:1 ratio, gels were retained after raising the pH. Interestingly, a separation between a turbid gel at the bottom and a transparent gel at the top. This is due to the ammonia gas diffusing through the top of the hydrogel and thus causing the gradual disassembly of the Fmoc-tyrosine filaments throughout the sample leaving the AgGMP filaments intact (Figure 4.19d). This leaves the transparent 1:1 AgGMP gel intact, as with the single component gel. This indicates that at the 1:1 ratio the two networks formed must be independent, analogous to interpenetrating polymer hydrogels, whereby two networks exist in sharp contrast to one another.[32,129,130]

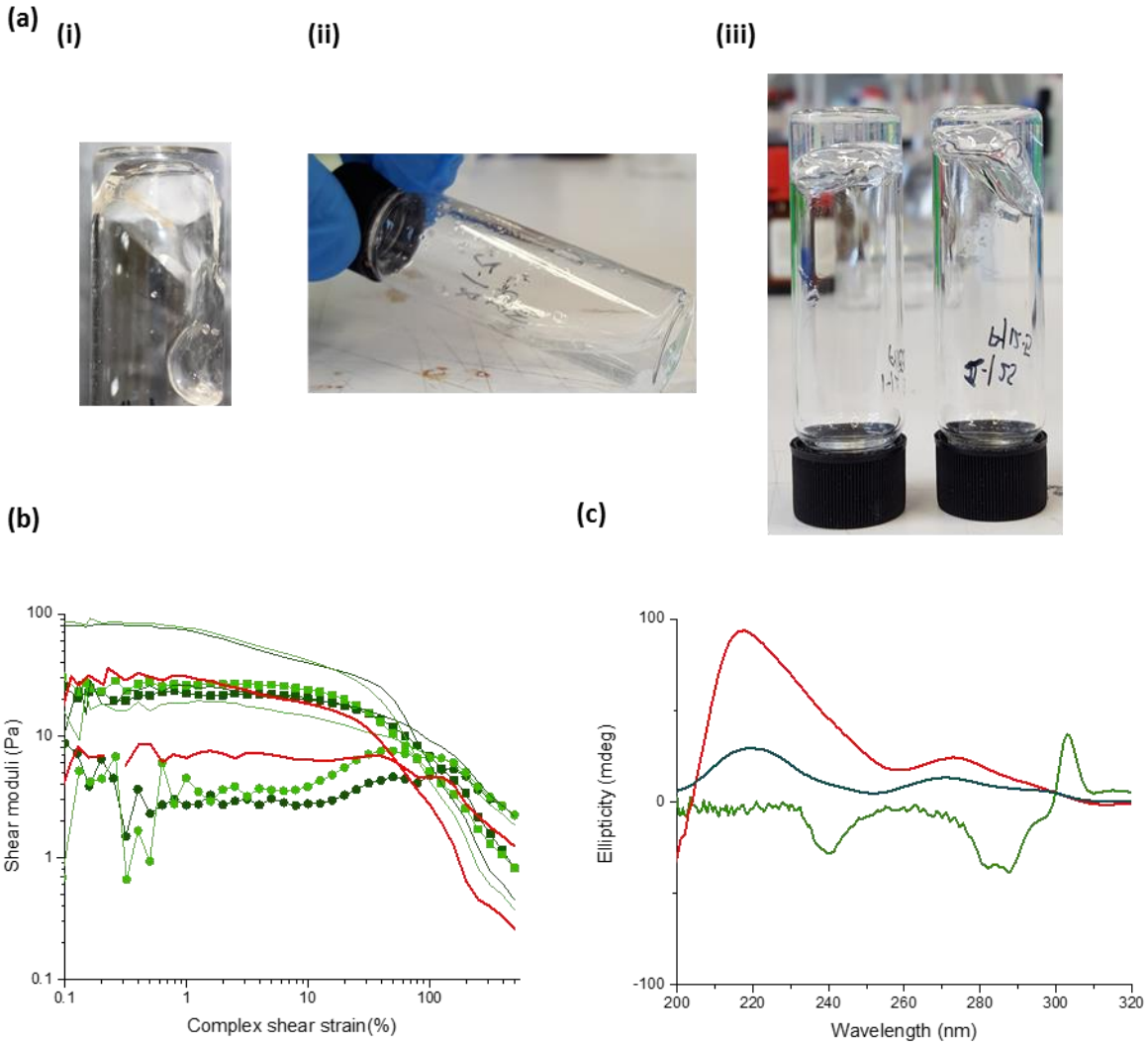

Figure 4.20 (a) Photos of the raising the pH for multicomponent hydrogels. (i) Sample D clear viscous solution at pH # and (ii) then clear solution formed at pH 8.5 (iii) self supporting hydrogel retained for sample A and B (b) Rheology experiments demonstrating a gel retained after raising pH. Thin line plots indicate moduli prior to raising pH and the line and symbol plots post raising pH. For both, ▪ refer to G' and ● refer to G", the storage modulus and viscous modulus, respectively. (c) CD spectra for gels at elevated pH, 1-1 AgGMP (red), 1-1 AgGMP 25 FY 25 (navy) and 2-1 AgGMP 25 FY 25.

Significantly, for this sample the CD signal attributed to Fmoc-tyrosine gelation was absent and the spectra were instead dominated by ellipticity characteristic to AgGMP, demonstrating that filaments of the gelator were intact. Rheological analysis demonstrated that a hydrogel persisted after raising the pH and was comparable moduli to the single component 1:1 AgGMP gel. The multi-component gels have a higher yield stress (120 % and 80 %) for samples A and B, respectively, vs *ca.* 55% prior to raising the pH). This discrepancy isn't surprising as self-assembly conditions are widely reported to affect mechanical properties. Further, surfactants are routinely used as additives to manipulate

mechanical properties of gels. [8–10,131] These surfactants can form micelles which entangle within the hydrogel network to provide mechanical support to the gel filaments. By raising the pH, the amphiphilic FY molecules will act as a surfactant perhaps forming a more entangled network. Hence, the yield strain is higher when the Fmoc-tyrosine concentration is higher, despite this not correlating to higher elastic moduli before raising the pH. Indeed, a highly entangled network was imaged *via* TEM for samples are the pH had been raised.

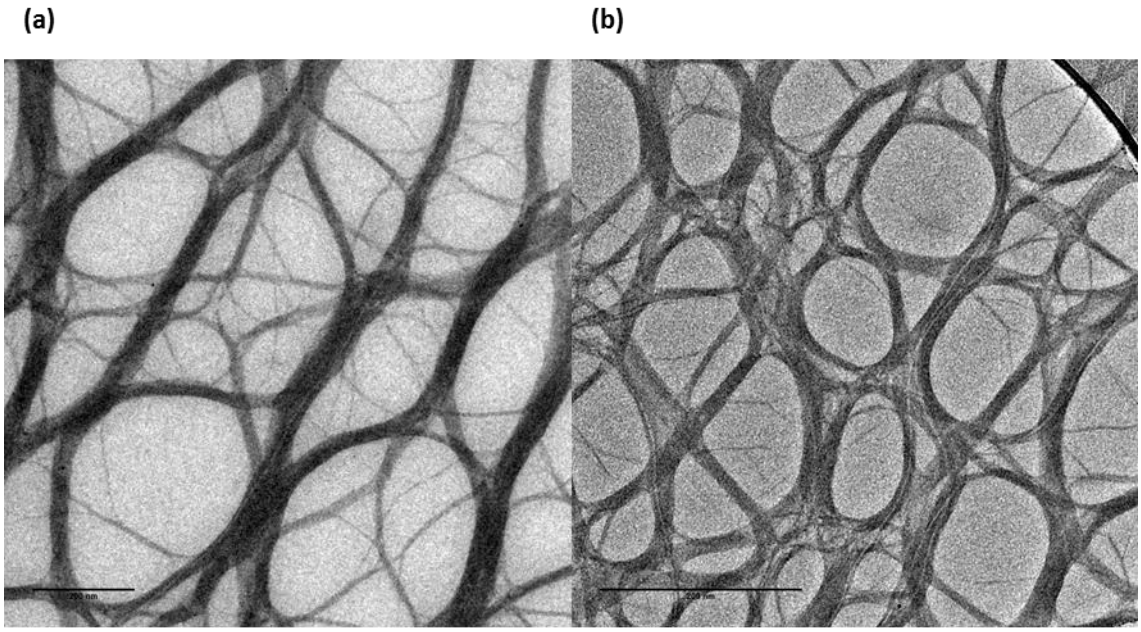

Figure 4.21 (a) and (b) TEM images of sample A after pH raised to 8.7, clearly demonstrating that filaments are intact. Scale bars are 200 nm.

Conversely, even though the single component AgGMP at the 2:1 ratio did not disassemble at pH 8.5, multi-component hydrogels at this ratio fully disassembled. Again, this disassembly could be observed through the gel sample as the ammonia gas diffuses through the gel. The transparent solution on top of the turbid gel indicates disrupting of both the Fmoc-tyrosine and GMP assembly, as an opaque would be expected to remain if the 2:1 AgGMP gel remained. As the pH of 8.5 is reached throughout the sample, a clear solution results, indicating disassembly of the self-assembled structures. This indicates that at this ratio, separate self-sorted filaments have not been formed and therefore it is not possible to selectively remove Fmoc-tyrosine nanofilaments without also disrupting the AgGMP

structures. This does not definitely prove that only co-assembled filaments formed. For instance, self-sorted filaments could assemble that then form mixed bundles, as the tyrosine has previously been reported to intercalate GMP stacks. [83,87] As a result, the Fmoc-tyrosine filaments cannot be removed without also disassembling the GMP stacks too. The CD spectra for this sample showed peaks not associated with Fmoc-tyrosine or AgGMP gelation, confirming that both these filaments were disassembled. Interactions between ammonia and silver are well known with the nitrogen acting as a lone pair donor, forming a $Ag(NH3)^{2+}$ complex.[132,133] Thus, such complexes would cause the disassembly of the Ag-GMP dimers. Thus, the peaks observed could instead be due to the formation of G-quartets.[67,84]

Further characterisation of the degree of mixing and self-sorting by the gelators in filaments and the filaments themselves is necessary and though has proven challenging to numerous researchers owing to the differences between crystal and filament structures, as mentioned in chapter 1.[59] For instance, information from traditional crystallographic studies, i.e. powder x-ray diffraction may be misleading owing to the different packing in the crystal and gel state with the latter considered to be significantly amorphous.[41,134] Instead, alternative *in-situ* methods are recommended and are discussed in Chapter 6.

Conclusions and Future Work

Presented is a novel example of the gelation of one gelator used to trigger the gelation of the second gelator which is used to form the construction of nucleotide-amino acid multicomponent hydrogels. The second gelator is more susceptible to pH and thus it possible to selectively remove one gelator. It is also demonstrated that the kinetics of assembly dramatically affects the properties of the resulting hydrogel.

Beyond this proof-of-concept study and the further characterisation recommended later in chapter 6, it would be interesting to apply this process for other pH-responsive gelators with specific functions. For instance, the second component could be a lysine, arginine and/or histidine contacting peptide, which has been shown exhibit antibacterial properties. [135–137] The cationic charges are thought to enable interaction with bacterial membranes.[137] Thus, both components, i.e. the silver and the peptide, would have anti-bacterial properties and would allow for low concentrations of both. Also, multicomponent technologies have been proposed to lower the likelihood of developing resistance.

Alternatively, the Ag-GMP hydrogel can be combined with catalytically active gelators [57] or with gelators that demonstrate optoconductivity, as the alignment of the silver ions and guanosine residues may result in interesting conductivity. [138,139] For instance, guanosine analogues are good candidates for conductivity due to their sufficient delocalization for the transport of charge along the molecule. [140] Thus, Livshits *et al.* demonstrated that guanine stacks imposed sufficient rigidity for reproducible charge transport in these stacks adsorbed on a mica substrate. [139]

The selective removal of one gelator through the raising of pH is a promising strategy to affect network properties which could lead to a range of applications as already discussed. However, the use of concentrated ammonia may not be applicable to many applications owing to the serious health concerns of using concentrated ammonia (e.g. being corrosive and toxic to aquatic organisms). Therefore, alternative means of increasing the pH are necessary. One promising candidate which would the use of photobases, which raise the pH due to photo-irradiation. [141] This could allow for the

raising of the pH in a spatially controlled manner which could allow for the creation of multidomain materials. Further, the presence of the AgGMP network should lessen the convection and diffusion of species in the gel which could increase spatial resolution. [33]

References

(1) Kumar, D. K.; Steed, J. W. Supramolecular Gel Phase Crystallization: Orthogonal Self-Assembly under Non-Equilibrium Conditions. *Chem. Soc. Rev.* 2014, *43* (7), 2080–2088.

(2) Sarikaya, M.; Tamerler, C.; Jen, A. K.-Y.; Schulten, K.; Baneyx, F. Molecular Biomimetics: Nanotechnology through Biology. *Nat. Mater.* 2003, *2* (9), 577–585.

(3) Sanchez, C.; Arribart, H.; Guille, M. M. G. Biomimetism and Bioinspiration as Tools for the Design of Innovative Materials and Systems. *Nat. Mater.* 2005, *4* (4), 277–288.

(4) Buerkle, L. E.; Rowan, S. J. Supramolecular Gels Formed from Multi-Component Low Molecular Weight Species. *Chem. Soc. Rev.* 2012, *41* (18), 6089.

(5) Hanabusa, K.; Miki, T.; Taguchi, Y.; Koyama, T.; Shirai, H. Two-Component, Small Molecule Gelling Agents. *J. Chem. Soc. Chem. Commun.* 1993, No. 18, 1382.

(6) Yang, Z.; Gu, H.; Zhang, Y.; Wang, L.; Xu, B. Small Molecule Hydrogels Based on a Class of Antiinflammatory Agents. *Chem. Commun.* 2004, No. 2, 208.

(7) Rao, K. V.; Jayaramulu, K.; Maji, T. K.; George, S. J. Supramolecular Hydrogels and High-Aspect-Ratio Nanofibers through Charge-Transfer-Induced Alternate Coassembly. *Angew. Chemie* 2010, *122* (25), 4314–4318.

(8) Brizard, A. M.; Stuart, M. C. A.; van Esch, J. H. Self-Assembled Interpenetrating Networks by Orthogonal Self Assembly of Surfactants and Hydrogelators. *Faraday Discuss.* 2009, *143* (0), 345.

(9) Brizard, A.; Stuart, M.; van Bommel, K.; Friggeri, A.; de Jong, M.; van Esch, J. Preparation of Nanostructures by Orthogonal Self-Assembly of Hydrogelators and Surfactants. *Angew. Chemie Int. Ed.* 2008, *47* (11), 2063–2066.

(10) Fuhrhop, J. H.; Svenson, S.; Boettcher, C.; Roessler, E.; Vieth, H. M. Long-Lived Micellar N-Alkylaldonamide Fiber Gels. Solid-State NMR and Electron Microscopic Studies. *J. Am. Chem. Soc.* 1990, *112* (11), 4307–4312.

(11) Adams, D. J.; Morris, K.; Chen, L.; Serpell, L. C.; Bacsa, J.; Day, G. M. The Delicate Balance between Gelation and Crystallisation: Structural and Computational Investigations. *Soft Matter* 2010, *6* (17), 4144.

(12) Fleming, S.; Ulijn, R. V. Design of Nanostructures Based on Aromatic Peptide Amphiphiles. *Chem. Soc. Rev.* 2014, *43* (23), 8150–8177.

(13) Fleming, S.; Debnath, S.; Frederix, P. W. J. M.; Hunt, N. T.; Ulijn, R. V. Insights into the Coassembly of Hydrogelators and Surfactants Based on Aromatic Peptide Amphiphiles. *Biomacromolecules* 2014, *15* (4), 1171–1184.

(14) Peters, G. M.; Davis, J. T. Supramolecular Gels Made from Nucleobase, Nucleoside and Nucleotide Analogs. *Chem. Soc. Rev.* 2016, *45* (11), 3188–3206.

(15) Yu, Y.; Nakamura, D.; DeBoyace, K.; Neisius, A. W.; McGown, L. B. Tunable Thermoassociation of Binary Guanosine Gels. *J. Phys. Chem. B* 2008, *112* (4), 1130–1134.

(16) Estroff, L. A.; Addadi, L.; Weiner, S.; Hamilton, A. D. An Organic Hydrogel as a Matrix for the Growth of Calcite Crystals. *Org. Biomol. Chem.* 2004, *2* (1), 137.

(17) Daly, R.; Kotova, O.; Boese, M.; Gunnlaugsson, T.; Boland, J. J. Chemical Nano-Gardens: Growth

of Salt Nanowires from Supramolecular Self-Assembly Gels. *ACS Nano* 2013, *7* (6), 4838–4845.

(18) Pandoli, O.; Massi, A.; Cavazzini, A.; Spada, G. P.; Cui, D. Circular Dichroism and UV-Vis Absorption Spectroscopic Monitoring of Production of Chiral Silver Nanoparticles Templated by Guanosine 5'-Monophosphate. *Analyst* 2011, *136* (18), 3713–3719.

(19) Draper, E. R.; Adams, D. J. Supramolecular Fibres: Self-Sorting Shows Its True Colours. *Nat. Chem.* 2016, *8* (8), 737–738.

(20) Morris, K. L.; Chen, L.; Raeburn, J.; Sellick, O. R.; Cotanda, P.; Paul, A.; Griffiths, P. C.; King, S. M.; O'Reilly, R. K.; Serpell, L. C.; Adams, D. J.; O'Reilly, R. K.; Serpell, L. C.; Adams, D. J. Chemically Programmed Self-Sorting of Gelator Networks. *Nat. Commun.* 2013, *4*, 1480.

(21) Onogi, S.; Shigemitsu, H.; Yoshii, T.; Tanida, T.; Ikeda, M.; Kubota, R.; Hamachi, I. In Situ Real-Time Imaging of Self-Sorted Supramolecular Nanofibres. *Nat. Chem.* 2016, *8* (8), 743–752.

(22) Hirst, A. R.; Smith, D. K. Two-Component Gel-Phase Materials—Highly Tunable Self-Assembling Systems. *Chem. - A Eur. J.* 2005, *11* (19), 5496–5508.

(23) Liyanage, W.; Vats, K.; Rajbhandary, A.; Benoit, D. S. W.; Nilsson, B. L. Multicomponent Dipeptide Hydrogels as Extracellular Matrix-Mimetic Scaffolds for Cell Culture Applications. *Chem. Commun.* 2015, *51* (56), 11260–11263.

(24) Horgan, C. C.; Rodriguez, A. L.; Li, R.; Bruggeman, K. F.; Stupka, N.; Raynes, J. K.; Day, L.; White, J. W.; Williams, R. J.; Nisbet, D. R. Characterisation of Minimalist Co-Assembled Fluorenylmethyloxycarbonyl Self-Assembling Peptide Systems for Presentation of Multiple Bioactive Peptides. *Acta Biomater.* 2016, *38*, 11–22.

(25) Draper, E. R.; Dietrich, B.; Adams, D. J. Self-Assembly, Self-Sorting, and Electronic Properties of a Diketopyrrolopyrrole Hydrogelator. *Chem. Commun.* 2017, *53* (11), 1864–1867.

(26) Ardoña, H. A. M.; Draper, E. R.; Citossi, F.; Wallace, M.; Serpell, L. C.; Adams, D. J.; Tovar, J. D. Kinetically Controlled Coassembly of Multichromophoric Peptide Hydrogelators and the Impacts on Energy Transport. *J. Am. Chem. Soc.* 2017, *139* (25), 8685–8692.

(27) Castilla, A. M.; Draper, E. R.; Nolan, M. C.; Brasnett, C.; Seddon, A.; Mears, L. L. E.; Cowieson, N.; Adams, D. J. Self-Sorted Oligophenylvinylene and Perylene Bisimide Hydrogels. *Sci. Rep.* 2017, *7* (1), 8380.

(28) Nozik, A. J. Nanoscience and Nanostructures for Photovoltaics and Solar Fuels. *Nano Lett.* 2010, *10* (8), 2735–2741.

(29) Draper, E. R.; Lee, J. R.; Wallace, M.; Jäckel, F.; Cowan, A. J.; Adams, D. J. Self-Sorted Photoconductive Xerogels. *Chem. Sci.* 2016, *7* (10), 6499–6505.

(30) Raeburn, J.; Adams, D. J. Multicomponent Low Molecular Weight Gelators. *Chem. Commun.* 2015, *51* (25), 5170–5180.

(31) Sugiyasu, K.; Kawano, S.-I.; Fujita, N.; Shinkai, S. Self-Sorting Organogels with p−n Heterojunction Points. *Chem. Mater.* 2008, *20* (9), 2863–2865.

(32) Draper, E. R.; Eden, E. G. B.; McDonald, T. O.; Adams, D. J. Spatially Resolved Multicomponent Gels. *Nat. Chem.* 2015, *7* (10), 848–852.

(33) Cornwell, D. J.; Daubney, O. J.; Smith, D. K. Photopatterned Multidomain Gels: Multi-Component Self-Assembled Hydrogels Based on Partially Self-Sorting 1,3:2,4-Dibenzylidene- d -Sorbitol Derivatives. *J. Am. Chem. Soc.* 2015, *137* (49), 15486–15492.

(34) Sutton, S.; Campbell, N. L.; Cooper, A. I.; Kirkland, M.; Frith, W. J.; Adams, D. J. Controlled Release from Modified Amino Acid Hydrogels Governed by Molecular Size or Network Dynamics. *Langmuir* 2009, *25* (17), 10285–10291.

(35) Drury, J. L.; Mooney, D. J. Hydrogels for Tissue Engineering: Scaffold Design Variables and Applications. *Biomaterials* 2003, *24* (24), 4337–4351.

(36) Singh, N.; Maity, C.; Zhang, K.; Angulo-Pachón, C. A.; van Esch, J. H.; Eelkema, R.; Escuder, B. Synthesis of a Double-Network Supramolecular Hydrogel by Having One Network Catalyse the Formation of the Second. *Chem. - A Eur. J.* 2017, *23* (9), 2018–2021.

(37) Loo, K.; Degtyareva, N.; Park, J.; Sengupta, B.; Reddish, M.; Rogers, C. C.; Bryant, A.; Petty, J. T. Ag + -Mediated Assembly of 5′-Guanosine Monophosphate. *J. Phys. Chem. B* 2010, *114* (12), 4320–4326.

(38) Dash, J.; Patil, A. J.; Das, R. N.; Dowdall, F. L.; Mann, S. Supramolecular Hydrogels Derived from Silver Ion-Mediated Self-Assembly of 5′-Guanosine Monophosphate. *Soft Matter* 2011, *7* (18), 8120.

(39) Tu, A. T.; Reinosa, J. A. The Interaction of Silver Ion with Guanosine, Guanosine Monophosphate, and Related Compounds. Determination of Possible Sites of Complexing. *Biochemistry* 1966, *5* (10), 3375–3383.

(40) Adams, D. J.; Butler, M. F.; Frith, W. J.; Kirkland, M.; Mullen, L.; Sanderson, P. A New Method for Maintaining Homogeneity during Liquid–hydrogel Transitions Using Low Molecular Weight Hydrogelators. *Soft Matter* 2009, *5* (9), 1856.

(41) Draper, E. R.; Morris, K. L.; Little, M. A.; Raeburn, J.; Colquhoun, C.; Cross, E. R.; McDonald, T. O.; Serpell, L. C.; Adams, D. J. Hydrogels Formed from Fmoc Amino Acids. *CrystEngComm* 2015, *17* (42), 8047–8057.

(42) Aufderhorst-Roberts, A.; Frith, W. J.; Donald, A. M. Micro-Scale Kinetics and Heterogeneity of a PH Triggered Hydrogel. *Soft Matter* 2012, *8* (21), 5940–5946.

(43) Wang, H.; Yang, Z.; Adams, D. J. Controlling Peptide Based Hydrogelation. *Mater. Today* 2012, *15* (11), 500–507.

(44) Pocker, Y.; Green, E. Hydrolysis of D-Glucono-δ-Lactone. I. General Acid-Base Catalysis, Solvent Deuterium Isotope Effects, and Transition State Characterization. *J. Am. Chem. Soc.* 1973, *95*, 113–119.

(45) Ulijn, R. V; Moore, B. D.; Janssen, A. E. M.; Halling, P. J. A Single Aqueous Reference Equilibrium Constant for Amide Synthesis–hydrolysis. *J. Chem. Soc. Perkin Trans. 2* 2002, No. 5, 1024–1028.

(46) Tang, C.; Smith, A. M.; Collins, R. F.; Ulijn, R. V.; Saiani, A. Fmoc-Diphenylalanine Self-Assembly Mechanism Induces Apparent PKa Shifts. *Langmuir* 2009, *25* (16), 9447–9453.

(47) Draper, E. R.; Wallace, M.; Schweins, R.; Poole, R. J.; Adams, D. J. Nonlinear Effects in Multicomponent Supramolecular Hydrogels. *Langmuir* 2017, *33* (9), 2387–2395.

(48) Abul-Haija, Y. M.; Roy, S.; Frederix, P. W. J. M.; Javid, N.; Jayawarna, V.; Ulijn, R. V. Biocatalytically Triggered Co-Assembly of Two-Component Core/Shell Nanofibers. *Small* 2014, *10* (5), 973–979.

(49) Fleming, S.; Frederix, P. W. J. M.; Ramos Sasselli, I.; Hunt, N. T.; Ulijn, R. V.; Tuttle, T. Assessing the Utility of Infrared Spectroscopy as a Structural Diagnostic Tool for β-Sheets in Self-Assembling Aromatic Peptide Amphiphiles. *Langmuir* 2013, *29* (30), 9510–9515.

(50) Kanicky, J. R.; Poniatowski, A. F.; Mehta, N. R.; Shah, D. O. Cooperativity among Molecules at Interfaces in Relation to Various Technological Processes : Effect of Chain Length on the pKa of Fatty Acid Salt Solutions. *Langmuir* 2000, *16* (1), 172–177.

(51) Urry, D. W.; Peng, S. Q.; Parker, T. M.; Gowda, D. C.; Harris, R. D. Relative Significance of Electrostatic- and Hydrophobic-Induced PKa Shifts in a Model Protein: The Aspartic Acid Residue. *Angew. Chemie Int. Ed. English* 1993, *32* (10), 1440–1442.

(52) Stryer, L.; *H Freeman & Co., New York,* 1995 .

(53) Cardoso, A. Z.; Mears, L. L. E.; Cattoz, B. N.; Griffiths, P. C.; Schweins, R.; Adams, D. J. Linking Micellar Structures to Hydrogelation for Salt-Triggered Dipeptide Gelators. *Soft Matter* 2016, *12* (15), 3612–3621.

(54) Adams, D. J.; Draper, E.; Su, H.; Brasnett, C.; Poole, R.; Rogers, S.; Cui, H.; Seddon, A. Opening a Can of Worm(-like Micelle)s: The Effect of Temperature of Solutions of Functionalised Dipeptides. *Angew. Chemie Int. Ed.* 2017.

(55) Lee, O.-S.; Cho, V.; Schatz, G. C. Modeling the Self-Assembly of Peptide Amphiphiles into Fibers Using Coarse-Grained Molecular Dynamics. *Nano Lett.* 2012, *12* (9), 4907–4913.

(56) Vijay, R.; Polavarapu, P. L. FMOC-Amino Acid Surfactants: Discovery, Characterization and Chiroptical Spectroscopy. *J. Phys. Chem. A* 2012, *116* (44), 10759–10769.

(57) Singh, N.; Zhang, K.; Angulo-Pachón, C. A.; Mendes, E.; van Esch, J. H.; Escuder, B. Tandem Reactions in Self-Sorted Catalytic Molecular Hydrogels. *Chem. Sci.* 2016, *7* (8), 5568–5572.

(58) Moffat, J. R.; Smith, D. K. Controlled Self-Sorting in the Assembly of 'Multi-Gelator' Gels. *Chem. Commun.* 2009, No. 3, 316–318.

(59) Mears, L. L. E.; Draper, E. R.; Castilla, A. M.; Su, H.; Zhuola; Dietrich, B.; Nolan, M. C.; Smith, G. N.; Doutch, J.; Rogers, S.; Akhtar, R.; Cui, H.; Adams, D. J. Drying Affects the Fiber Network in Low Molecular Weight Hydrogels. *Biomacromolecules* 2017, acs.biomac.7b00823.

(60) D'Abramo, M.; Castellazzi, C. L.; Orozco, M.; Amadei, A. On the Nature of DNA Hyperchromic Effect. *J. Phys. Chem. B* 2013, *117* (29), 8697–8704.

(61) Thornton, K.; Abul-Haija, Y. M.; Hodson, N.; Ulijn, R. V. Mechanistic Insights into Phosphatase Triggered Self-Assembly Including Enhancement of Biocatalytic Conversion Rate. *Soft Matter* 2013, *9* (39), 9430.

(62) Sadownik, J. W.; Leckie, J.; Ulijn, R. V. Micelle to Fibre Biocatalytic Supramolecular Transformation of an Aromatic Peptide Amphiphile. *Chem. Commun.* 2011, *47* (2), 728–730.

(63) Shao, H.; Parquette, J. R. A π-Conjugated Hydrogel Based on an Fmoc-Dipeptide Naphthalene Diimide Semiconductor. *Chem. Commun.* 2010, *46* (24), 4285.

(64) Patil, A. J.; Kumar, R. K.; Barron, N. J.; Mann, S. Cerium Oxide Nanoparticle-Mediated Self-Assembly of Hybrid Supramolecular Hydrogels. *Chem. Commun.* 2012, *48* (64), 7934.

(65) Raeburn, J.; Zamith Cardoso, A.; Adams, D. J. The Importance of the Self-Assembly Process to Control Mechanical Properties of Low Molecular Weight Hydrogels. *Chem. Soc. Rev.* 2013, *42* (12), 5143.

(66) Zhou, P.; Li, H. Chirality Delivery from a Chiral Copper(Ii) Nucleotide Complex Molecule to Its Supramolecular Architecture. *Dalton Trans.* 2011, *40* (18), 4834.

(67) Panda, M.; Walmsley, J. A. Circular Dichroism Study of Supramolecular Assemblies of

Guanosine 5'-Monophosphate. *J. Phys. Chem. B* 2011, *115* (19), 6377–6383.

(68) Wu, G.; Kwan, I. C. M. Helical Structure of Disodium 5'-Guanosine Monophosphate Self-Assembly in Neutral Solution. *J. Am. Chem. Soc.* 2009, *131* (9), 3180–3182.

(69) Wong, A.; Ida, R.; Spindler, L.; Wu, G. Disodium Guanosine 5'-Monophosphate Self-Associates into Nanoscale Cylinders at PH 8: A Combined Diffusion NMR Spectroscopy and Dynamic Light Scattering Study. *J. Am. Chem. Soc.* 2005, *127* (19), 6990–6998.

(70) Du, X.; Zhou, J.; Shi, J.; Xu, B. Supramolecular Hydrogelators and Hydrogels: From Soft Matter to Molecular Biomaterials. *Chem. Rev.* 2015, *115* (24), 13165–13307.

(71) Yang, Z.; Gu, H.; Fu, D.; Gao, P.; Lam, J. K.; Xu, B. Enzymatic Formation of Supramolecular Hydrogels. *Adv. Mater.* 2004, *16* (16), 1440–1444.

(72) Babu, S. S.; Praveen, V. K.; Ajayaghosh, A. Functional π-Gelators and Their Applications. *Chem. Rev.* 2014, *114* (4), 1973–2129.

(73) Wang, Z.; Medforth, C. J.; Shelnutt, J. a. Porphyrin Nanotubes by Ionic Self-Assembly. *J. Am. Chem. Soc.* 2004, *126* (49), 15954–15955.

(74) Panda, M.; Walmsley, J. A. Circular Dichroism Study of Supramolecular Assemblies of Guanosine 5'-Monophosphate. *J. Phys. Chem. B* 2011, *115* (19), 6377–6383.

(75) Gellert, M.; Lipsett, M. N.; Davies, D. R. Helix Formation by Guanylic Acid. *Proc. Natl. Acad. Sci. U. S. A.* 1962, *48* (12), 2013–2018.

(76) Davis, J. T. G-Quartets 40 Years Later: From 5'-GMP to Molecular Biology and Supramolecular Chemistry. *Angew. Chemie Int. Ed.* 2004, *43* (6), 668–698.

(77) Lena, S.; Masiero, S.; Pieraccini, S.; Spada, G. P. Guanosine Hydrogen-Bonded Scaffolds: A New Way to Control the Bottom-Up Realisation of Well-Defined Nanoarchitectures. *Chem. - A Eur. J.* 2009, *15* (32), 7792–7806.

(78) Davis, J. T.; Spada, G. P. Supramolecular Architectures Generated by Self-Assembly of Guanosine Derivatives. *Chem. Soc. Rev.* 2007, *36* (2), 296–313.

(79) Buerkle, L. E.; Li, Z.; Jamieson, A. M.; Rowan, S. J. Tailoring the Properties of Guanosine-Based Supramolecular Hydrogels. *Langmuir* 2009, *25* (15), 8833–8840.

(80) Sreenivasachary, N.; Lehn, J.-M. Gelation-Driven Component Selection in the Generation of Constitutional Dynamic Hydrogels Based on Guanine-Quartet Formation. *Proc. Natl. Acad. Sci.* 2005, *102*, 5938–5943.

(81) Bimalendu Adhikari, P.; Kraatz, H.-B.; Adhikari, B.; Afzal Shah ac, ab; Shah, A.; Kraatz, H.-B. Self-Assembly of Guanosine and Deoxy-Guanosine into Hydrogels: Monovalent Cation Guided Modulation of Gelation, Morphology and Self-Healing Properties. *J. Mater. Chem. B* 2014, *2* (30), 4802.

(82) Way, A. E.; Korpusik, A. B.; Dorsey, T. B.; Buerkle, L. E.; von Recum, H. A.; Rowan, S. J. Enhancing the Mechanical Properties of Guanosine-Based Supramolecular Hydrogels with Guanosine-Containing Polymers. *Macromolecules* 2014, *47* (5), 1810–1818.

(83) Gupta, A. P.; Taylor, W. J.; McGown, L. B.; Kempf, J. G. NMR Studies of the Chiral Selectivity of Self-Assembled Guanosine Monophosphate. *J. Phys. Chem. B* 2014, *118* (49), 14243–14256.

(84) Zhou, P.; Shi, R.; Yao, J.-F.; Sheng, C.-F.; Li, H. Supramolecular Self-Assembly of Nucleotide–metal Coordination Complexes: From Simple Molecules to Nanomaterials. *Coord. Chem. Rev.*

2015, *292*, 107–143.

(85) Zhang, Y.; Gu, H.; Yang, Z.; Xu, B. Supramolecular Hydrogels Respond to Ligand-Receptor Interaction. *J. Am. Chem. Soc.* 2003, *125* (45), 13680–13681.

(86) Adhikari, B.; Nanda, J.; Banerjee, A. Multicomponent Hydrogels from Enantiomeric Amino Acid Derivatives: Helical Nanofibers, Handedness and Self-Sorting. *Soft Matter* 2011, *7* (19), 8913.

(87) Dong, Y.; McGown, L. B. Chiral Selectivity of Guanosine Media in Capillary Electrophoresis. *Electrophoresis* 2011, *32* (13), 1735–1741.

(88) Deng, M.; Zhang, L.; Jiang, Y.; Liu, M. Role of Achiral Nucleobases in Multicomponent Chiral Self-Assembly: Purine-Triggered Helix and Chirality Transfer. *Angew. Chemie Int. Ed.* 2016, *55* (48), 15062–15066.

(89) Cheng, G.; Castelletto, V.; Moulton, C. M.; Newby, G. E.; Hamley, I. W. Hydrogelation and Self-Assembly of Fmoc-Tripeptides: Unexpected Influence of Sequence on Self-Assembled Fibril Structure, and Hydrogel Modulus and Anisotropy. *Langmuir* 2010, *26* (7), 4990–4998.

(90) Dutta, S.; Shome, A.; Debnath, S.; Das, P. K. Counterion Dependent Hydrogelation of Amino Acid Based Amphiphiles: Switching from Non-Gelators to Gelators and Facile Synthesis of Silver Nanoparticles. *Soft Matter* 2009, *5* (8), 1607.

(91) Liyanage, W.; Nilsson, B. L. Substituent Effects on the Self-Assembly/Coassembly and Hydrogelation of Phenylalanine Derivatives. *Langmuir* 2016, *32* (3), 787–799.

(92) Ryan, D. M.; Doran, T. M.; Nilsson, B. L. Stabilizing Self-Assembled Fmoc–F_5–Phe Hydrogels by Co-Assembly with PEG-Functionalized Monomers. *Chem. Commun.* 2011, *47* (1), 475–477.

(93) Ryan, D. M.; Anderson, S. B.; Senguen, F. T.; Youngman, R. E.; Nilsson, B. L. Self-Assembly and Hydrogelation Promoted by F_5-Phenylalanine. *Soft Matter* 2010, *6* (3), 475–479.

(94) Navarro, R.; Peral, F.; Gallego, E.; Morcillo, J. Studies of the Self-Association of 5′-GMP in Aqueous Solutions by Fourier Transform Infrared Spectroscopy. *J. Mol. Struct.* 1986, *143*, 357–360.

(95) Zhizhina, G. P.; Oleinik, E. F. Infrared Spectroscopy of Nucleic Acids. *Russ. Chem. Rev.* 1972, *41* (3), 258–280.

(96) Tavakol, H. Study of Binding Energies Using DFT Methods, Vibrational Frequencies and Solvent Effects in the Interaction of Silver Ions with Uracil Tautomers. *Arab. J. Chem.* 2013, *10*, S786–S799.

(97) Hashemnejad, S. M.; Kundu, S. Probing Gelation and Rheological Behavior of a Self-Assembled Molecular Gel. *Langmuir* 2017, *33* (31), 7769–7779.

(98) De La Fuente, M.; Hernanz, A.; Navarro, R. IR and Raman Study on the Interactions of the 5′-GMP and 5′-CMP Phosphate Groups with Mg(II), Ca(II), Sr(II), Ba(II), Cr(III), Co(II), Cu(II), Zn(II), Cd(II), Al(III) and Ga(III). *J. Biol. Inorg. Chem.* 2004.

(99) Sukul, P. K.; Malik, S. Removal of Toxic Dyes from Aqueous Medium Using Adenine Based Bicomponent Hydrogel. *RSC Adv.* 2013, *3* (6), 1902–1915.

(100) Baral, A.; Basak, S.; Basu, K.; Dehsorkhi, A.; Hamley, I. W.; Banerjee, A. Time-Dependent Gel to Gel Transformation of a Peptide Based Supramolecular Gelator. *Soft Matter* 2015, *11* (24), 4944–4951.

(101) Singh, V.; Snigdha, K.; Singh, C.; Sinha, N.; Thakur, A. K. Understanding the Self-Assembly of

Fmoc–phenylalanine to Hydrogel Formation. *Soft Matter* 2015, *11* (26), 5353–5364.

(102) Fleming, S.; Debnath, S.; Frederix, P. W. J. M.; Tuttle, T.; Ulijn, R. V. Aromatic Peptide Amphiphiles: Significance of the Fmoc Moiety. *Chem. Commun. (Camb).* 2013, *49*, 10587–10589.

(103) Wang, J.; Liu, K.; Xing, R.; Yan, X. Peptide Self-Assembly: Thermodynamics and Kinetics. *Chem. Soc. Rev.* 2016, *45* (20), 5589–5604.

(104) Metreveli, N. O.; Jariashvili, K. K.; Namicheishvili, L. O.; Svintradze, D. V; Chikvaidze, E. N.; Sionkowska, A.; Skopinska, J. UV–vis and FT-IR Spectra of Ultraviolet Irradiated Collagen in the Presence of Antioxidant Ascorbic Acid. *Ecotoxicol. Environ. Saf.* 2009, *73*, 448–455.

(105) Gerothanassis, I. P.; Birlirakis, N.; Sakarellos, C.; Marraud, M. Solvation State of the Tyr Side Chain in Peptides. An FT-IR and ^{17}O NMR Approach. *J. Am. Chem. Soc.* 1992, *114* (23), 9043–9047.

(106) Nishi, K.; Fujii, K.; Katsumoto, Y.; Sakai, T.; Shibayama, M. Kinetic Aspect on Gelation Mechanism of Tetra-PEG Hydrogel. *Macromolecules* 2014, *47* (10), 3274–3281.

(107) Salzano de Luna, M.; Altobelli, R.; Gioiella, L.; Castaldo, R.; Scherillo, G.; Filippone, G. Role of Polymer Network and Gelation Kinetics on the Mechanical Properties and Adsorption Capacity of Chitosan Hydrogels for Dye Removal. *J. Polym. Sci. Part B Polym. Phys.* 2017, *55* (24), 1843–1849.

(108) Colquhoun, C.; Draper, E. R.; Schweins, R.; Marcello, M.; Vadukul, D.; Serpell, L. C.; Adams, D. J.; Yang, Z.; Ding, D.; Kong, D.; Liu, J.; Atkins, D.; Adams, D. J.; Schatz, G. C.; Stupp, S. I. Controlling the Network Type in Self-Assembled Dipeptide Hydrogels. *Soft Matter* 2017, *13* (9), 1914–1919.

(109) Aslam, M.; Fu, L.; Su, M.; Vijayamohanan, K.; Dravid, V. P. Novel One-Step Synthesis of Amine-Stabilized Aqueous Colloidal, *J. Mater. Chem.* 2004, *14* (12), 1795.

(110) Roy, S.; Banerjee, A. Amino Acid Based Smart Hydrogel: Formation, Characterization and Fluorescence Properties of Silver Nanoclusters within the Hydrogel Matrix. *Soft Matter* 2011, *7* (11), 5300.

(111) Selvakannan, P.; Swami, A.; Srisathiyanarayanan, D.; Shirude, P. S.; Pasricha, R.; Mandale, A. B.; Sastry, M. Synthesis of Aqueous Au Core−Ag Shell Nanoparticles Using Tyrosine as a PH-Dependent Reducing Agent and Assembling Phase-Transferred Silver Nanoparticles at the Air−Water Interface. *Langmuir* 2004, *20* (18), 7825–7836.

(112) Fichman, G.; Guterman, T.; Adler-abramovich, L.; Gazit, E. Synergetic Functional Properties of Two-Component Single Amino Acid-Based Hydrogels. *CrystEngComm* 2015, *17* (42), 8105–8112.

(113) Roy, S.; Das, T. K. Study of Interaction Between Tryptophan, Tyrosine, and Phenylalanine Separately with Silver Nanoparticles by Fluorescence Quenching Method. *J. Appl. Spectrosc.* 2015, *82* (4), 598–606.

(114) Benson, M.; Jurd, L. Carbon-13 NMR of Quinone Methides. *Org. Magn. Reson.* 1984, *22* (2), 86–89.

(115) Yu, G.; Yan, X.; Han, C.; Huang, F. Characterization of Supramolecular Gels. *Chem. Soc. Rev.* 2013, *42* (16), 6697.

(116) Zuidema, J. M.; Rivet, C. J.; Gilbert, R. J.; Morrison, F. a. A Protocol for Rheological Characterization of Hydrogels for Tissue Engineering Strategies. *J. Biomed. Mater. Res. - Part B Appl. Biomater.* 2014, *102* (5), 1063–1073.

(117) Pai, V.; Srinivasarao, M.; Khan, S. a. Evolution of Microstructure and Rheology in Mixed Polysaccharide Systems. *Macromolecules* 2002, *35* (5), 1699–1707.

(118) Chen, L.; Raeburn, J.; Sutton, S.; Spiller, D. G.; Williams, J.; Sharp, J. S.; Griffiths, P. C.; Heenan, R. K.; King, S. M.; Paul, A.; Furzeland, S.; Atkins, D.; Adams, D. J. Tuneable Mechanical Properties in Low Molecular Weight Gels. *Soft Matter* 2011, *7* (20), 9721.

(119) Colquhoun, C.; Draper, E. R.; Eden, E. G. B.; Cattoz, B. N.; Morris, K. L.; Chen, L.; McDonald, T. O.; Terry, A. E.; Griffiths, P. C.; Serpell, L. C.; Adams, D. J. The Effect of Self-Sorting and Co-Assembly on the Mechanical Properties of Low Molecular Weight Hydrogels. *Nanoscale* 2014, *6* (22), 13719–13725.

(120) Veiga, A. S.; Sinthuvanich, C.; Gaspar, D.; Franquelim, H. G.; Castanho, M.A. ; Schneider, J. P. Arginine-Rich Self-Assembling Peptides as Potent Antibacterial Gels. *Biomaterials* 2012, *33* (35), 8907–8916.

(121) McGrath, N.; Patil, A. J.; Watson, S. M. D.; Horrocks, B. R.; Faul, C. F. J.; Houlton, A.; Winnik, M. a.; Mann, S.; Manners, I. Conductive, Monodisperse Polyaniline Nanofibers of Controlled Length Using Well-Defined Cylindrical Block Copolymer Micelles as Templates. *Chem. - A Eur. J.* 2013, *19*, 13030–13039.

(122) Nanda, J.; Biswas, A.; Banerjee, A. Single Amino Acid Based Thixotropic Hydrogel Formation and PH-Dependent Morphological Change of Gel Nanofibers. *Soft Matter* 2013, *9* (16), 4198.

(123) Pashuck, E. T.; Stupp, S. I. Direct Observation of Morphological Tranformation from Twisted Ribbons into Helical Ribbons. *J. Am. Chem. Soc.* 2010, *132* (26), 8819–8821.

(124) Castilla, A. M.; Wallace, M.; Mears, L. L. E.; Draper, E. R.; Doutch, J.; Rogers, S.; Adams, D. J. On the Syneresis of an OPV Functionalised Dipeptide Hydrogel. *Soft Matter* 2016, *12* (37), 7848–7854.

(125) Das, R. N.; Kumar, Y. P.; Pagoti, S.; Patil, A. J.; Dash, J. Diffusion and Birefringence of Bioactive Dyes in a Supramolecular Guanosine Hydrogel. *Chem. - A Eur. J.* 2012, *18* (19), 6008–6014.

(126) Mahler, A.; Reches, M.; Rechter, M.; Cohen, S.; Gazit, E. Rigid, Self-Assembled Hydrogel Composed of a Modified Aromatic Dipeptide. *Adv. Mater.* 2006, *18* (11), 1365–1370.

(127) Hule, R. A.; Nagarkar, R. P.; Hammouda, B.; Schneider, J. P.; Pochan, D. J. Dependence of Self-Assembled Peptide Hydrogel Network Structure on Local Fibril Nanostructure. *Macromolecules* **2009**, *42* (18), 7137–7145.

(128) Qiu, Y.; Park, K. Environment-Sensitive Hydrogels for Drug Delivery. *Adv. Drug Deliv. Rev.* **2001**, *53* (3), 321–339.

(129) Gupta, N.; Srivastava, A. K. Interpenetrating Polymer Networks: A Review on Synthesis and Properties. *Polymer International*. **1994**, 109–118.

(130) Haque, M. A.; Kurokawa, T.; Gong, J. P. Super Tough Double Network Hydrogels and Their Application as Biomaterials. *Polymer.* **2012**, *53* (9), 1805–1822.

(131) Buerkle, L. E.; Galleguillos, R.; Rowan, S. J. Nonionic Surfactant-Induced Stabilization and Tailorability of Sugar-Amphiphile Hydrogels. *Soft Matter* 2011, *7* (15), 6984.

(132) Bruehlman, R. J.; Verhoek, F. H. The Basic Strengths of Amines as Measured by the Stabilities of Their Complexes with Silver Ions. *J. Am. Chem. Soc.* 1948, *70* (4), 1401–1404.

(133) Dubas, S. T.; Pimpan, V. Green Synthesis of Silver Nanoparticles for Ammonia Sensing. *Talanta* 2008, *76* (1), 29–33.

(134) Draper, E. R.; Adams, D. J. Low-Molecular-Weight Gels: The State of the Art. *Chem* 2017, *3* (3), 390–410.

(135) Liu, Y.; Yang, Y.; Wang, C.; Zhao, X. Stimuli-Responsive Self-Assembling Peptides Made from Antibacterial Peptides. *Nanoscale* 2013, *5* (14), 6413.

(136) Laverty, G.; Gorman, S. P.; Gilmore, B. F. The Potential of Antimicrobial Peptides as Biocides. *Int. J. Mol. Sci.* 2011, *12* (12), 6566–6596.

(137) McCloskey, A. P.; Gilmore, S. M.; Zhou, J.; Draper, E. R.; Porter, S.; Gilmore, B. F.; Xu, B.; Laverty, G. Self-Assembling Ultrashort NSAID-Peptide Nanosponges: Multifunctional Antimicrobial and Anti-Inflammatory Materials. *RSC Adv.* 2016, *6* (115), 114738–114749.

(138) Yan, H.; Park, S. H.; Finkelstein, G.; Reif, J. H.; LaBean, T. H. DNA-Templated Self-Assembly of Protein Arrays and Highly Conductive Nanowires. *Science* 2003, *301* (September), 1882–1884.

(139) Livshits, G. I.; Stern, A.; Rotem, D.; Borovok, N.; Eidelshtein, G.; Migliore, A.; Penzo, E.; Wind, S. J.; Di Felice, R.; Skourtis, S. S.; Cuevas, J. C.; Gurevich, L.; Kotlyar, A. B.; Porath, D. Long-Range Charge Transport in Single G-Quadruplex DNA Molecules. *Nat. Nanotechnol.* 2014, *9* (12), 1040–1046.

(140) Bixon, M.; Giese, B.; Wessely, S.; Langenbacher, T.; Michel-Beyerle, M. E.; Jortner, J. Long-Range Charge Hopping in DNA. *Proc. Natl. Acad. Sci. U. S. A.* 1999, *96* (21), 11713–11716.

(141) Driscoll, E. W.; Hunt, J. R.; Dawlaty, J. M. Proton Capture Dynamics in Quinoline Photobases: Substituent Effect and Involvement of Triplet States. *J. Phys. Chem. A* 2017, *121* (38), 7099–7107.

Chapter 5
Investigating the antimicrobial properties of silver-guanosine monophosphate hydrogels

Chapter Outline:

In this final chapter, the research presented in this thesis will move beyond investigating new strategies for constructing supramolecular hydrogels to characterise the anti-bacterial activity of a silver-containing hydrogel.

Introduction:

Recent outbreaks of infectious diseases caused by different pathogenic bacteria and the rise of antibiotic resistance underscore the challenge of design and screening of new drugs.[1–5] Modifications to surgical devices, such as coatings, are often employed to combat infections.[6–9] One strategy is chemical coatings that rely on the elution of drugs but this approach only has short-term antimicrobial effects and could cause cumulative toxicity as well as potentially resulting in antimicrobial resistance.[10] Another strategy is to use cationic polymers[11,12] such as methacrylate[13–16], poly(phenylene ethynylene)[17,18], poly(vinyl-N-hexyl pyridinium)[19,20] *etc.*, which penetrate and disrupt the bacterial cytoplasmic membrane. However, production of these polymers often requires the use of organic solvents and their efficacy relies on sufficient diffusion of the polymers into cell membranes. [10]

Supramolecular hydrogels are an attractive alternative owning to their facile synthesis, aqueous composition (making them applicable for physiological conditions) and porous nature which allows for diffusion of pathogens into the gel network.[10,21–24] Also, their shear-thinning behaviour allows for them to be injected as a viscous liquid and then regel upon the cessation of any shear.[22,25] There is a broad range of possible hydrogel systems that could be used as antibacterial agents. For instance, peptide-based hydrogels with inherent antibacterial activity is a popular approach. Salick *et al.* designed a β-hairpin hydrogel scaffold that gels upon addition the of salt, e.g. DMEM cell culture media.[26] The authors proposed that the activity arises from the positive lysine-rich hydrogel surface interacting and disrupting negatively charged bacterial cell membranes, analogous to cationic polymers. Liu *et al.* also demonstrated the antibacterial potential of a series of lysine-based peptide gels versus polystyrene controls but gave no quantitative measurements. [27]

Similar approaches use arginine-rich peptides to formulate antibacterial hydrogels. [28,29] Arginine content can be modulated to balance hemolytic activity (breakdown of red blood cells) and antibacterial activity. The dephosphorylation of tyrosine-phosphate gelators by phosphatase enzymes has been exploited by Yang *et al.* and Hughes *et al.* for innovative approaches to formulating

antibacterial agents. [30,31] The gelators enter the bacteria via diffusion and then enzyme -regulated dephosphorylation of the gelators results in intracellular self-assembly and subsequent inhibition of cell growth (Figure 5.1a). This accumulation of gelators within the bacteria was confirmed via HPLC analysis. The hydrophobicity of the gelators determined the preference for the small molecules to accumulate either in the media or bacteria.[31] It was hypothesized that the self-assembly affected the viscosity of the cytoplasm, leading to cell stress and subsequent inhibition of bacterial growth.

This approach relied on *E. coli* to overexpress phosphatase, with a 100-fold increase of gelator concentration necessary for bacteria without phosphatase enzymes overexpression. Still, this is undoubtedly an interesting approach and could inspire other strategies that make use of enzyme triggers.

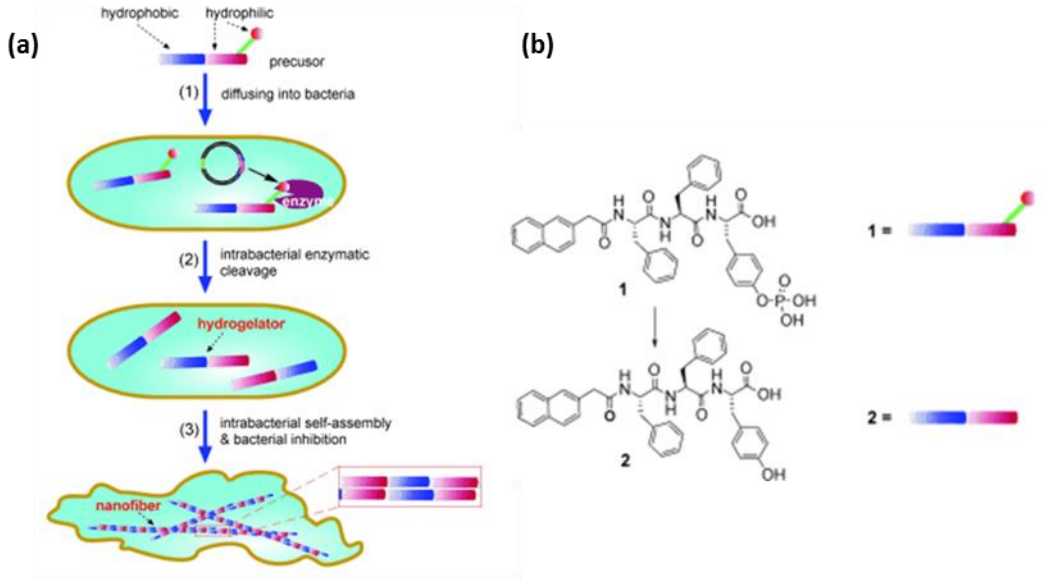

Figure 5.1 a) Schematic representation of intracellular nanofiber formation leading to hydrogelation and the inhibition of bacterial growth. b) The chemical structures and graphic representations of a typical precursor (1) and the corresponding hydrogelator (2). Adapted from ref. 30

Composites of hydrogels and nanoscale materials have also emerged as a promising potential technology they allow for the combination of effective antibacterial nanoscale materials into diverse self-assemblies with tunable properties. [32] Many nanomaterials have demonstrated activity e.g. copper,[33–35] zinc,[36] magnesium,[37] gold,[38,39] and silver.[40–43] Of these, silver nanoparticles have been shown to have the highest antibacterial activity.

The antimicrobial properties of silver have been known since ancient times, having a broad spectrum of activity against bacteria. To this end, silver-containing materials are becoming increasingly more popular due to their broad spectrum of activity and expectations that it'll be harder for bacteria to develop resistance to silver. [1,42,44–53] Metallic silver is inert, whereas ionic silver is highly reactive and binds to many biomolecules.[1,43] Many studies have reported structural and morphological changes to the cell membrane as well as observing electron dense silver granules on and inside the bacteria via electron microscopy.[42,46–49] The silver ions can also interact with DNA, possibly preventing DNA replication[48,54], as well as interacting with the thiols of vital sulphur-containing enzymes which perturbs their structure and inactivates them. [1,44,45,48,50–53] This can interrupt the respiratory system leading to the accumulation of reactive oxygen species which can then cause lipid peroxidation, DNA and protein damage, eventually contributing to cell death. [40,51,53,55–58]

Several groups have used a hydrogel network to template silver nanoparticles[59–62] Whereas, previous researchers in the Mann group exploited the association between silver and the guanine residue [62–64] of guanosine monophosphate to form a supramolecular hydrogel. [65] The silver ions interact with the enolate tautomer leading to the stabilisation of GMP dimer (Scheme 5.1), which stack through aromatic interactions and hydrogen bonding to form one-dimensional filaments which entangle to form the hydrogel network. Excess silver ions can then be photo-reduced to form silver nanoparticles on the nanofilaments. Dash *et al.* demonstrated the enzymatic activity was retained for protein molecules immobilized in the hydrogel, however, given the widely reported antibacterial properties of silver, this hydrogel is a strong candidate as an antibacterial material by combining the advantages of self-assembled hydrogels and nanoscale materials.

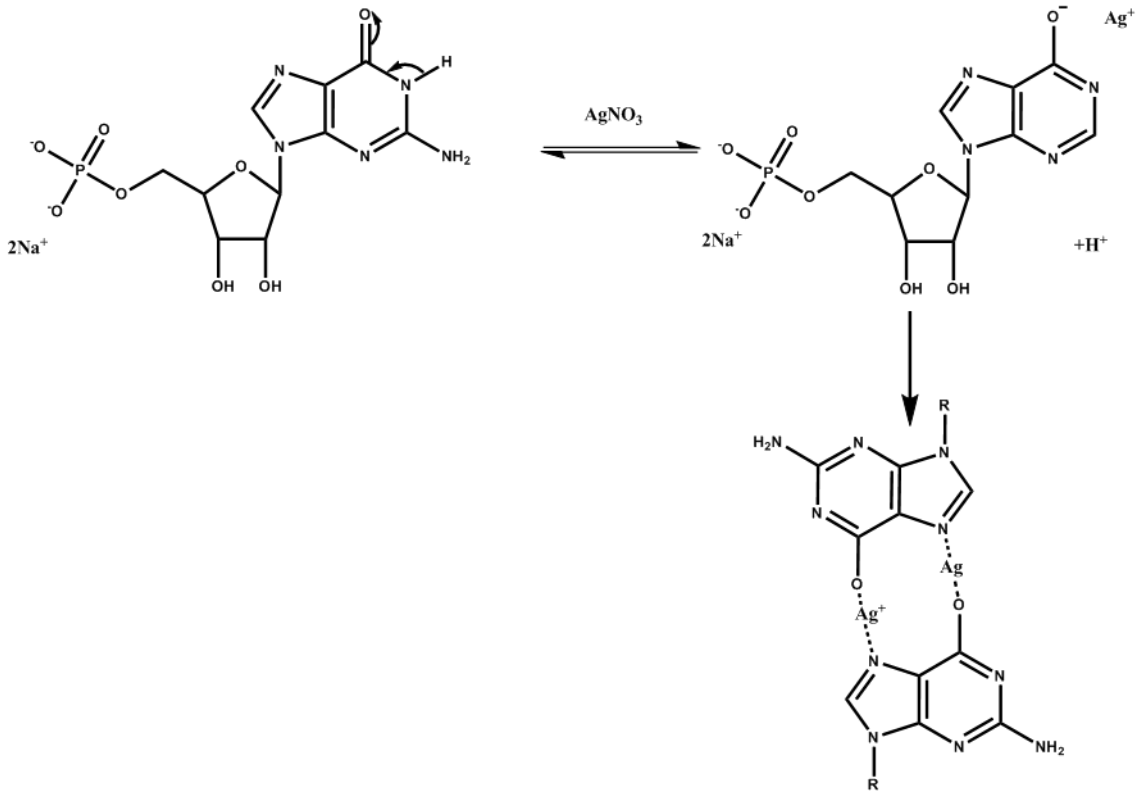

Scheme 5.1 Formation of Ag-GMP supramolecular hydrogels through the addition of Ag+ ions to GMP produces an enolate tautomer and release of a proton from N1, and subsequent formation of a Ag-GMP dimer by binding at N7 and O6. (R groups refer to ribose phosphate moiety and are excluded for clarity.)

Broadly, there are two main divisions of bacteria based on their shape. First, are spherical cocci (*ca.* 1 µm diameter), e.g. *Staphylococcus* (which tend to bunch together) and *Streptococcus* (which tend to adhere into long chains). The second division is rod-shaped bacteria and are usually 1-10 µm and 0.2-1 µm wide.[66] This class is characteristic of the genera *Bacterium, Bacillus* and others. All bacteria are divided into two classes known as Gram-positive and Gram-negative, depending on whether they are stained by the crystal violet-iodine complex in the Gram staining test. This variance is due to different cell wall compositions for Gram-positive and Gram-negative bacteria (Figure 5.2).[67] Usually, the former has a single outer membrane and thick peptidoglycan layer (*ca.* 30 nm), whereas, the latter has a second outer membrane and a lipopolysaccharide layer but a much thinner peptidoglycan layer. (*ca.* 2-3 nm) and are therefore less protected against the penetration of silver ions into the cytoplasm.[1,68,69]

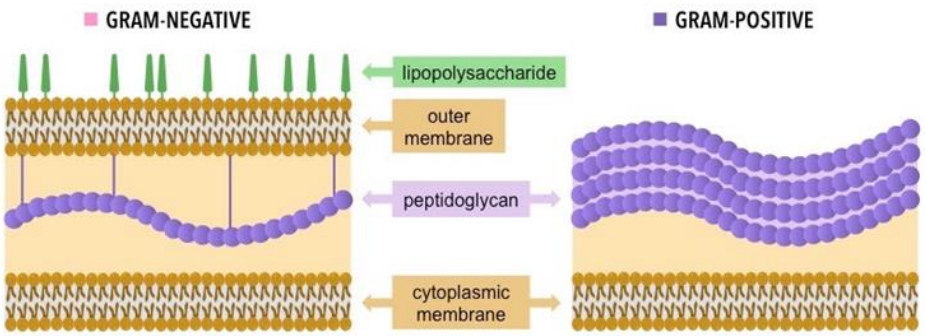

Figure 5.2 A representation of the different cell wall compositions for Gram-negative and Gram-positive bacteria. Adapted from ref. 67

Therefore, the antibacterial properties of this hydrogel will be investigated in this final chapter against a candidate gram-negative bacterium (*E. coli*) and a gram-positive bacterium (*E. faecalis)*. Included is a negative control, silver-free GMP hydrogel. The mechanical properties of the Ag-GMP are dependent on the stoichiometry of Ag:GMP and all gels are shown to have gel-sol transition temperature higher than 37°C, indicating that the gel network is retained when incubated with the bacteria. Significant antibacterial activity is reported over two time scales and preliminary studies are presented to demonstrate the mechanisms responsible for the activity.

Experimental

Silver nitrate ($AgNO_3$) and guanosine 5'-monophosphate sodium salt (Na_2GMP) were used as received and all solutions were made up in sterilised Milli-Q water. Ag-GMP hydrogels with $AgNO_3$: GMP molar ratios of 1:1 and 2:1 were prepared at room temperature by adding an appropriate concentration of aqueous $AgNO_3$ (200-400 mM) to an aqueous solution of Na_2GMP (100 mM) (pH≈ 8). Hydrogels were then formed in well-plates (in a laminar flow cabinet) by adding an equal volume of silver nitrate, at the appropriate concentration) to guanosine monophosphate in the well to final concentration GMP of 100 mM. Silver free, G-quartet, guanosine monophosphate hydrogels were prepared by dissolving glucono delta-lactone (GdL) (10 or 20 mg/mL) with GMP (100 mM) in NaCl (200 mM) and transferring to the well plate. All hydrogels had a final volume of 1 mL and were left to form overnight in the dark.

Characterisation of hydrogels samples

Differential scanning calorimetry (DSC): DSC was carried out using a Mettler Toledo TGA/DSC1 Star System at a scan rate of 1 °C min^{-1} with a nitrogen flow of 25 mL min^{-1}. All experiments were undertaken with Maddy Nichols.

Rheology

Rheometry was performed using a Malvern Kinexus fitted with a parallel plate geometry (gap width of 200 μm) at room temperature. Hydrogels, which were aged for one day, were added to the rheometer using a spatula to minimize shear. The top plate was lowered, and the normal force measured and allowed to reach equilibrium. Further details of the experimental setup e.g. frequency and strain range are included in the result and discussion section.

Optical Microscopy:

Bacteria were imaged using standard Gram-staining procedures. For fluorescence microscopy, excitation of 340-380 nm and emission cut off at 400 nm was used to visualise fluorescent GFP-expressing *E. coli*.

Transmission electron microscopy (TEM)

TEM imaging was performed in bright-field mode using a JEOL TEM 1400 electron microscope and electron microscope operating at 120 keV. TEM samples were prepared by dropcasting a dilute suspension of hydrogel (5 µL) onto carbon-coated copper TEM grids for three minutes and wicking excess fluid away using filter paper. When negative staining was necessary, an aqueous solution of uranyl acetate (1% w/v, 5 µL) also dropped cast onto the carbon coated TEM grid and wicked off after three minutes. All samples were left to dry overnight at room temperature in the dark.

Characterisation of microbiology experiments

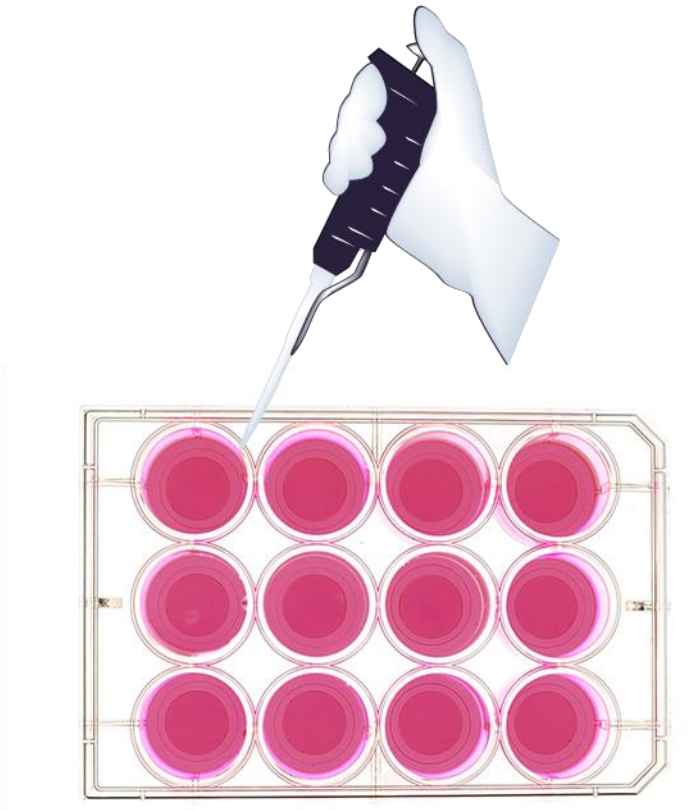

Figure 5.3 Representation of microbiology set-up. Hydrogels (1 mL) are prepared in a 12 well plate and left in the dark overnight. Then an inoculum of a set optical density is added on top and the well plate is sealed with parafilm and transferred to the incubator (37°C).

Growing the Bacteria with the hydrogel

E. faecalis were cultivated on Brain Heart Infusion Yeast Neopeptone (BHYN) agar (37g brain heart infusion broth, 5g yeast, 5 g neopeptone, 15g agar per litre) at 37°C. Suspensions of cultures were growth in BHYN medium (brain heart infusion broth containing 5g/L yeast extract) overnight in an incubator (37 °C), without shaking. The cells are collected by centrifugation (5000 rpm, 7 minutes) washed in phosphate-buffered saline PBS and re-suspended in BHYN broth to an $OD_{600=}$ 0.5 (approximately 1 x $10x^{8}$ cells/mL), thus, allowing a similar number of bacteria to be used for each experiment. The strain of *E. coli* used contained a plasmid responsible for expressing the green

fluorescent protein (GFP). Therefore, all growth media and agar plates also contained the antibiotic erythromycin as there was a cassette in the plasmid which made this strain resistant to the antibiotic. Therefore, this encourages retention of the plasmid and hence the expression of GFP. Lysogeny broth (LB) was inoculated with *Escherichia coli* (*E. coli*) and then grown overnight in an incubator (37 ^{o}C). The cells were washed in phosphate-buffered saline PBS and re-suspended in LB to an $OD_{600=}$ 0.5 (approximately 2 x $10x^{8}$ cells/mL). Microbial suspensions were gently pipetted onto the GMP hydrogel. The plate was incubated (37 ^{o}C) for 2-24 h in an incubator and then collected for analysis.

Gram staining

Gram staining was used to classify bacteria and aid optical microscopy imaging. An aliquot (ca. 10µL) of the inoculum is dried onto a glass slide. Then the first stain, crystal violet (1 mL), is added to slide and left for 1 minute before rinsing with water. Then iodine (1 mL, 1%) is added to fix the crystal violet to the bacterial cell wall. This is then briefly rinsed with acetone and then water. Then the second dye, safranin (1 mL), is added and left for 1 minute before rinsing again.

Measuring colony forming units (CFUs)

The total volume of the well-plate (i.e. microbial suspensions and hydrogel) are collected, washed with PBS and then serially diluted in PBS by an order of magnitude each time before plating (5x 20µL per dilution) onto either BHY or LB agar plates, with sodium thioglycolate. These plates were incubated (37°C) overnight for approximately 18 hours.

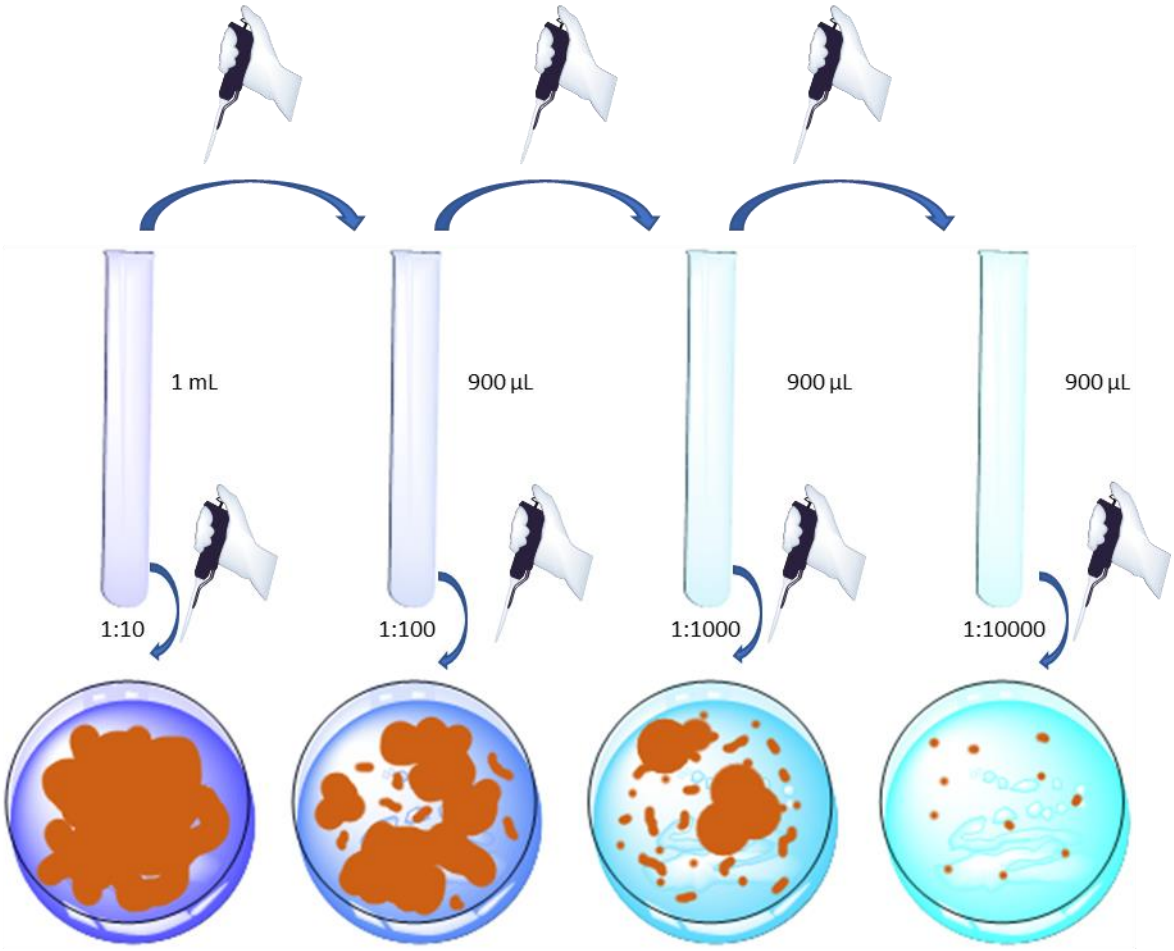

Figure 5.4 Serial dilutions from original inoculum before plating onto agar plates for colony forming units counting

Chromosomal DNA Extraction

Chromosomal DNA was isolated from *E. faecalis* grown in BHYN and *E. faecalis* grown in BHYN, as for previous experiments (in an incubator, 37°C without shaking), on top of Ag GMP hydrogels using a Wizard Genomic DNA Purification kit (Promega, Madison, WI, USA). Broadly, this involved lysing the cells, removing cellular proteins by salt precipitation and finally concentrating and desalting the chromosomal DNA by isopropanol precipitation[70] (Figure 5.5).

Figure 5.5 Threads of DNA suspended in isopropanol

Gel electrophoresis

Agarose gels (0.8 wt%) were prepared in Tris base, boric acid, and ethylenediaminetetraacetic acid (TBE) buffer, loaded with ethidium bromide (final concentration *ca.* 0.5 µg/ml), a nucleic acid stain, for visualization. In all cases, a 1 kb DNA Ladder, a solution with a set of standard fragments was used to estimate approximate sizes of DNA fragments. All other lanes were loaded with DNA solution (10 µL) and gel electrophoresis was performed for ~30 min at 90 V.

Results and Discussion

Ag-GMP supramolecular hydrogels were formed by the addition of aqueous silver nitrate ($AgNO_3$) guanosine monophosphate (GMP) at room temperature to a final concentration of 100 mM (at 20°C). Samples were prepared at two Ag:GMP molar ratios: 1:1 and 2:1. Gelation did not occur for molar ratios less than 1:1. At molar ratios of 1:1 the gelation occurred within roughly 10 minutes and resulted in a transparent hydrogel. At the higher molar ratio, gelation occurred almost instantaneously and produced an opaque hydrogel (Figure 5.6a). The addition of silver nitrate to the GMP solution led to a drop in pH (to values of 5.19, and 3.74 for the 1:1, and 2:1 samples, respectively), which is associated with the abstraction of a proton from the N7 amine in the guanine base as a result of the Ag-GMP dimerization (Scheme 5.1). [63–65,71,72]

(a)

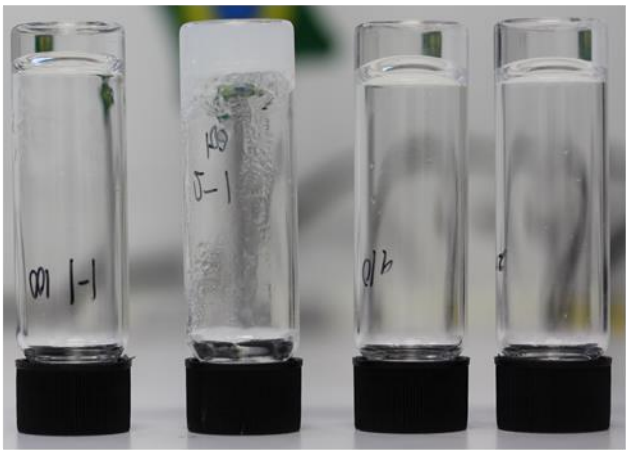

(b)

Ag : GMP	pH reading
GMP solution	8.06
Ag:GMP 1:1	5.19
AgGMP 2:1	3.74
qGMP (GdL, 10 mg/mL)	5.63
qGMP (GdL, 20 mg/mL)	3.80

Figure 5.6 (a) Photo of Ag-GMP and, the silver free, qGMP hydrogels. Both Ag:GMP ratios, (i) 1:1 and (ii) 2:1, form a self-supported hydrogel, with the latter forming an opaque gel which indicates the formation of large structures resulting in the scattering of light. Then photos of the qGMP hydrogels formed through the hydrolysis of different masses of GdL (iii) 10 mg/mL and (iv) 20 mg/mL. (b) Table summarising pH changes upon gelation due to abstraction from the guanine base for gels (i) and (ii) and then the pH drop achieved for the hydrolysis of GdL to gluconic acid.

As mentioned in Chapter 4, GMP is also capable of gelation through the lowering of pH *via* the formation of G-quartets (Figure 5.7c). Thus, two control hydrogels were formed by lowering the pH through the hydrolysis of glucono-δ-lactone (GdL), forming gluconic acid (Figure 5.7a). As the mass of GdL added reproducibly results in the same pH and therefore can be used to form gels with the same

final pH as Ag-GMP hydrogels (Figure 5.6b).[73] These gels are referred to as qGMP (in reference to the quartet structure) and the mass of GdL used to lower the pH, either 10 or 20 mg/mL. The Ag-GMP hydrogel has already been reported by the Mann group[65] and in the previous chapter, thus the characterisation is only briefly summarised to highlight the significance of the Ag:GMP stoichiometry and to compare these samples to the control qGMP hydrogels.

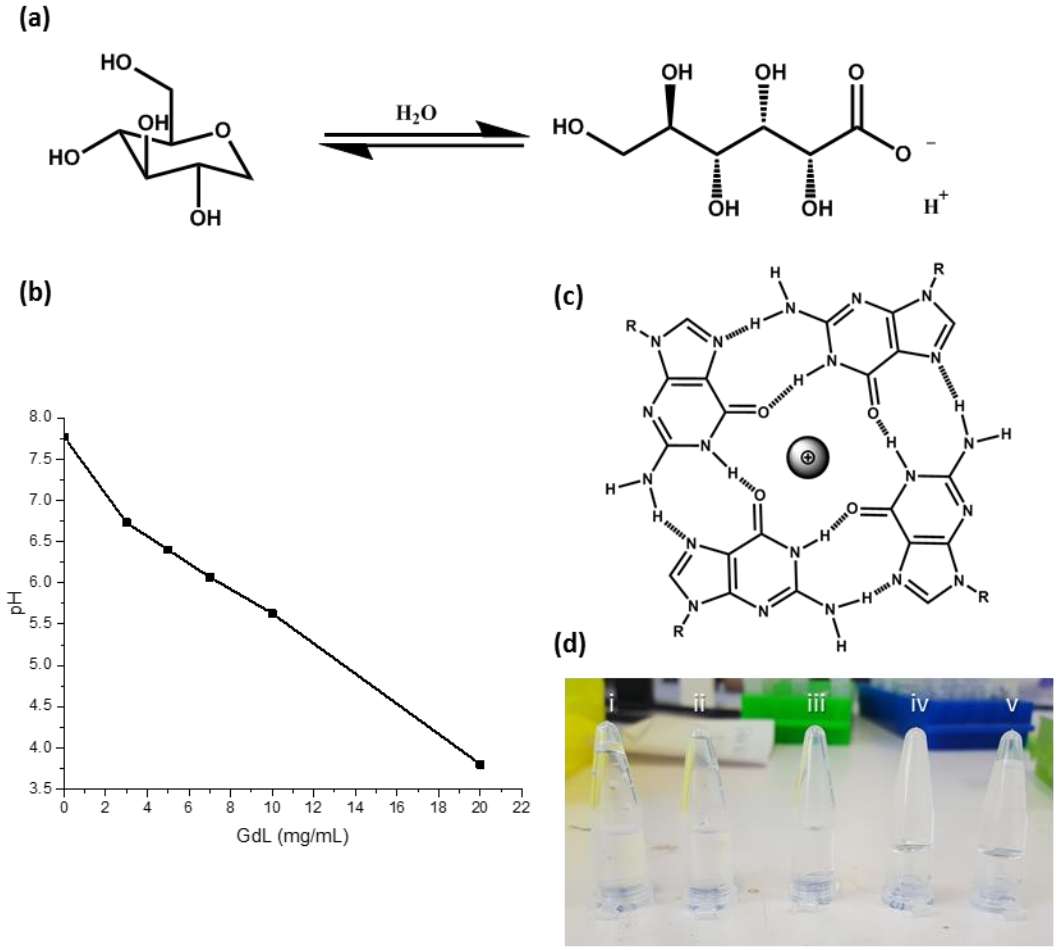

Figure 5.7 (a) Scheme demonstrating the hydrolysis of glucono-δ-lactone (GdL) to form gluconic acid (b) final pH resulting from different masses of GdL added to GMP solution. 10 mg and 20 mg match the pH of the AgGMP gels 1-1 (5.21) and 2-1 (3.74). (c)Hydrogen bonded GMP quartert (R=ribose and phosphate group) and (d) photo of GMP samples after the hydrolysis of GdL (i) 3 mg/mL, (ii) 5 mg /mL, (iii) 7 mg/mL, (iv) 10 mg/mL and 20 mg/mL. Only the final two gelled with (iii) forming a viscous solution.

Transmission electron microscopy (TEM) was used to image an entangled network of nanofilaments for all samples (Figure 5.8). For Ag-GMP samples (Figure 5.8a and b), electron-dense silver nanoparticles were imaged decorating the nanofilaments. Filaments of 2-7 nm and 3-10 nm were imaged for 1:1 and 2:1 molar ratios, respectively. As expected, these nanoparticles were absent for the qGMP gels. Filaments of 2-5 nm and 4-9 nm were imaged for the 10 mg/mL and 20 mg/mL samples, respectively. The wider filaments observed at a lower pH may be due to the increased bundling of

protofilaments as observed for protected amino acid-based filaments. [74] The pH reached of 3.8 would be sufficient to partially protonate the phosphate group and thus reduce the degree of ionisation for the filaments, which would increase the hydrophobicity and promote bundling.

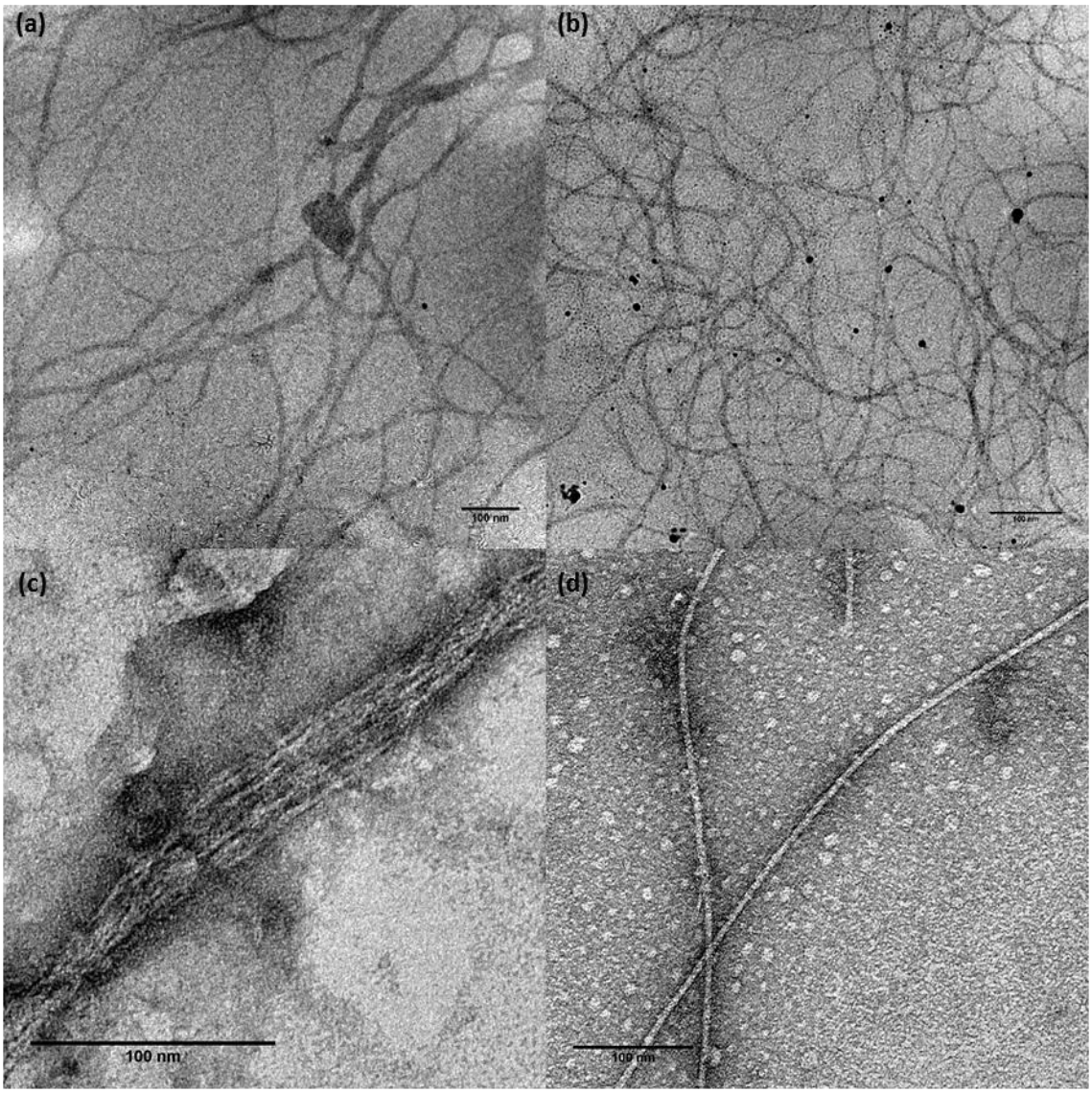

Figure 5.8 TEM images of a GMP supramolecular hydrogels displaying an entangled network Ag-GMP (a) 2:1 and (b) 1:1, qGMP gels (c) 20 mg and (d) 10 mg. Scale bar= 100 nm.

As there are silver ions present in solution, these are capable of reducing to form silver nanoparticles. Their formation could also be observed macroscopically due to the plasmonic resonance of nanosized silver causing a gradual colour change from either transparent or white to pink and then eventually a dark red/brown as the silver nanoparticles grow in size and number (Figure5.9a). [75–77] This observation

is supported by UV analysis which demonstrated a distinct surface plasmon resonance band at 452 nm characteristic of silver nanoparticles (Figure5.9b). [40,43,52,65,75–77]

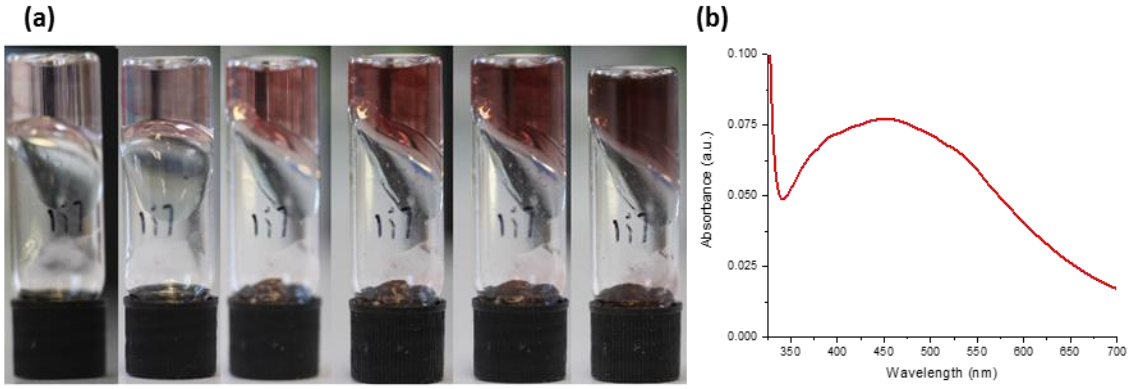

Figure 5.9 (a) Photograph of supramolecular hydrogel exhibiting a gradual colour change due to plasmonic resonance as a result of silver nanoparticles forming b) corresponding UV-Vis spectrum demonstrating a surface plasmon resonance band at 452 nm.

The macroscopic properties of the gels were studied using via differential scanning calorimetry (DSC) and oscillatory rheology (Figure 5.10). A broad endothermic peak was observed for all samples (Figure 5.10a), corresponding to the breaking of the non-covalent crosslinks of the supramolecular hydrogel which causes a gel to sol transition. [65,78,79] Significantly, for all gels, these peaks were above 37°C and therefore the samples will still be gels in the incubator for the microbiology experiments. The Ag-GMP hydrogels exhibited broad endothermic peaks at ca. 46.6 and 48.0 °C for the 1:1 and 2:1 ratio, respectively. The qGMP hydrogels exhibited endothermic peaks at ca. 41.5 and 47.4 °C for the 10 mg/mL and 20 mg/mL, respectively.

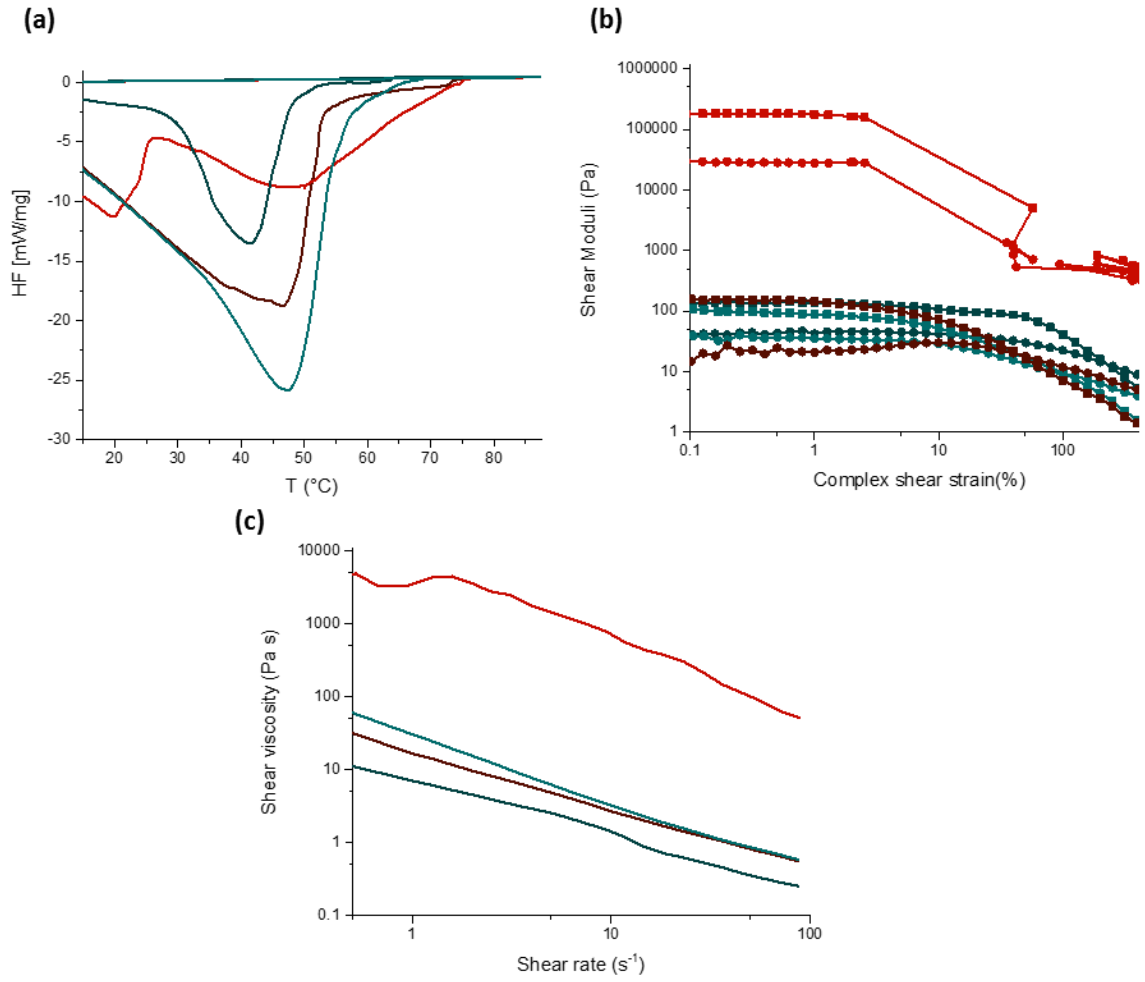

Figure 5.10 In all cases Ag-GMP 2:1 (red) and 1:1 (maroon), qGMP gels 20 mg (blue) and 10 mg (navy). (a) DSC thermogram of supramolecular hydrogels prepared from guanosine monophosphate showing a broad gel to sol transition temperatures, in all cases, well above 37°C. (b) Oscillatory amplitude sweeps at a constant frequency (1Hz) . All gels exhibited a linear viscoelastic regime. In oscillatory experiments, ▪ refer to G' and ● refer to G", the storage modulus and viscous modulus, respectively. (c) Viscosity profile of hydrogels prepared at different SNP:FYP molar ratios, demonstrating shear-thinning behaviour.

Oscillatory amplitude sweeps at a constant frequency (1 Hz) demonstrated a linear viscoelastic region (LVR) for all gelled samples, in which the storage (elastic) G' moduli are roughly an order of magnitude higher than the loss (viscous) G" moduli. This is indicative of an elastic solid-like network of the gel throughout a viscous solvent. [65,73,80,81] All gels exhibited shear-thinning behaviour (Figure 5.10c), with viscosity decreasing with increasing shear rates which overcomes non-covalent interactions between gelators. [82–84,22] For the AgGMP gel at the 2:1 molar ratio, the viscosity plateaus at low shear and behaves like a Newtonian material with viscosity independent of shear.

Importantly, the stoichiometry of the silver can be exploited to impart drastic changes to the rheological properties of the hydrogel. As the silver is embedded within the network of the hydrogel, it is likely that it could be exploited as a functional soft material. Of the many possible properties of silver that could be exploited, e.g. electrical, plasmonic and catalytic,[85,86] its antimicrobial properties are perhaps the most exciting. Therefore, the rest of this report on the antimicrobial properties of the Ag- GMP hydrogel.

Firstly, the gram-positive opportunistic bacteria *Enterococcus faecalis* (*E. faecalis)* was chosen to determine the antibacterial activity of the Ag-GMP hydrogel. *E. faecalis* has previously been responsible for highly antibiotic-resistant, hospital-acquired infections. [87–89] Also, as a gram-positive bacterium, its peptidoglycan layer that comprises the cell wall can be up to ten times larger than those of gram-negative bacteria, which imparts resilience to harsh environmental conditions.[69] Thus, demonstrating antimicrobial activity against *E.faecalis* would provide excellent proof of principle of using a self-assembled silver containing hydrogel as an antibacterial agent.

Often, colourimetric assays, i.e. LIVE/DEAD™ Cell Viability Assays, are employed for assessing cell metabolic activity or live dead stains can be used to evaluate the population of cell death due to some external stimuli.[45,90,91] However, owing to the turbidity of the hydrogels and since the hydrogel will also be stained by the dyes such an approach was not applicable. Instead, alternative means have been used to determine cell death. Colony counts (Figure 5.11) were used to indicate and quantify any killing of bacteria by the Ag-GMP hydrogel. For this, the bacteria are collected from each sample after incubation for a set time and serial dilutions of this inoculum are pipetted onto agar plates and grown for 16 hours. Then, colony forming units (CFU) can be counted and compared between samples.

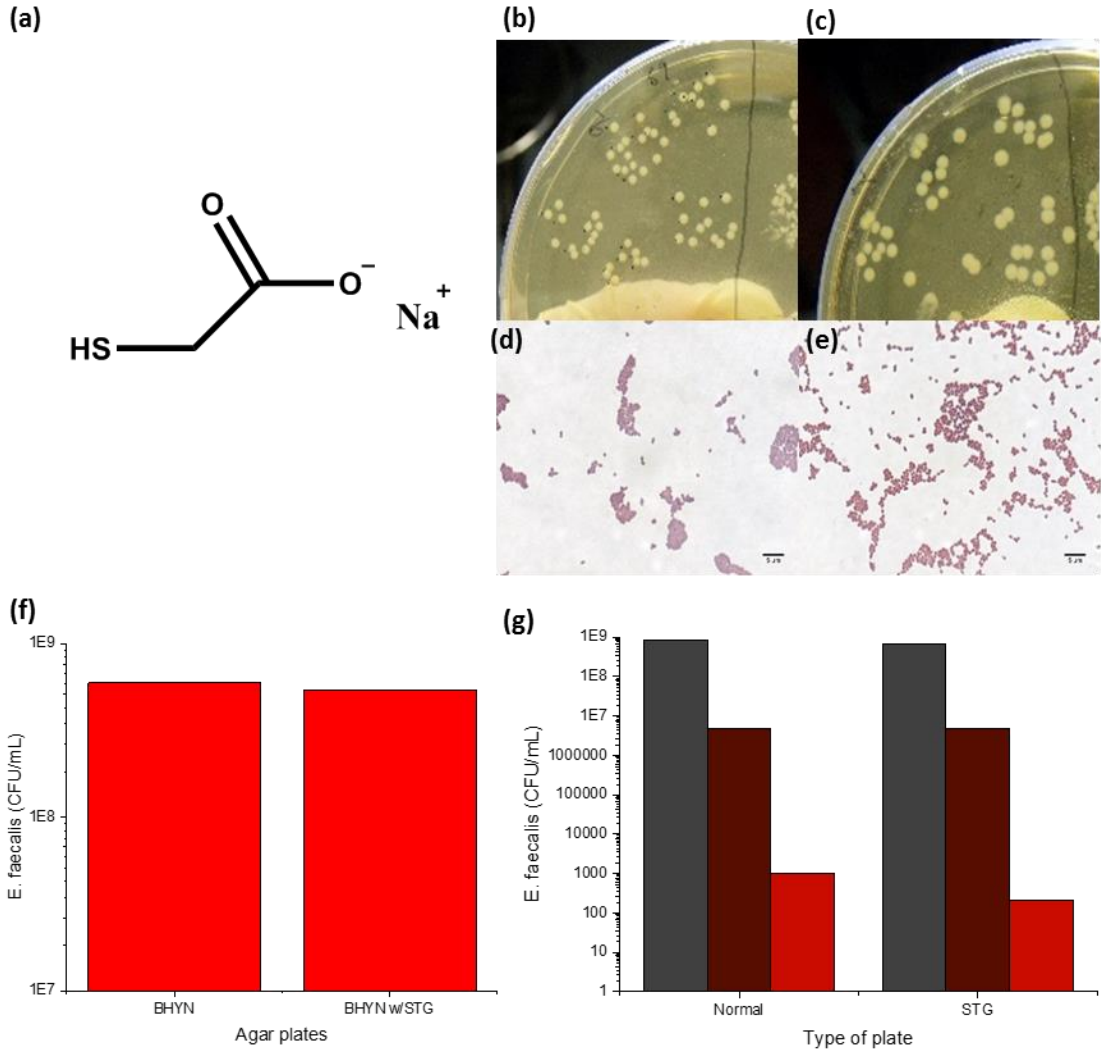

Figure 5.11 a) Structure of sodium thioglycolate (STG). Photos of serial dilutions of *E. faecalis* plated and grown on b) BHY agar c) BHYN with sodium thioglycolate agar and bright-field microscopy images of gram stained *E. faecalis* grown on d) BHYN agar and e) BHYN with STG agar. (f) CFU counts for E. faecalis grown on BHYN and BHYN with STG agar plates (n=1) and (g) CFU counts for E. faecalis grown on BHYN and BHYN with STG agar plates (n=1)

An early concern was whether silver deposited onto the agar plates would affect the growth of the bacteria on the agar plates and then over-represent any activity that was occurring over the initial incubation period. Thus, the composition of the agar plates was modified to include sodium thioglycolate (STG), a strong ligand for silver, which is routinely used to inactivate silver. [49,92,93] Inclusion of STG into the agar plates does not appear to affect the CFU counts for *E. faecalis* only experiments (Figure 5.9f and g), i.e. incubated in the absence of any hydrogel samples.

Although slightly larger colonies grow on the agar plates without STG (Figure 5.11b and c), gram staining these colonies do not appear to reveal any significant difference between the morphology of bacteria grown on the two plates (Figure 5.9d and e). Hence, the inclusion of STG into the agar plates does not seem to interfere with the growth of *E. faecalis* and will be used to inactivate deposited silver, thus making the CFU counts reproducible and reliable. Also, there wasn't a significant difference between CFU/mL counts for *E. faecalis* grown on Ag-GMP hydrogels on BHYN and BHYN with STG agar plates. This indicates that the activity arises from the first incubation period and not from the silver deposited on the agar plates.

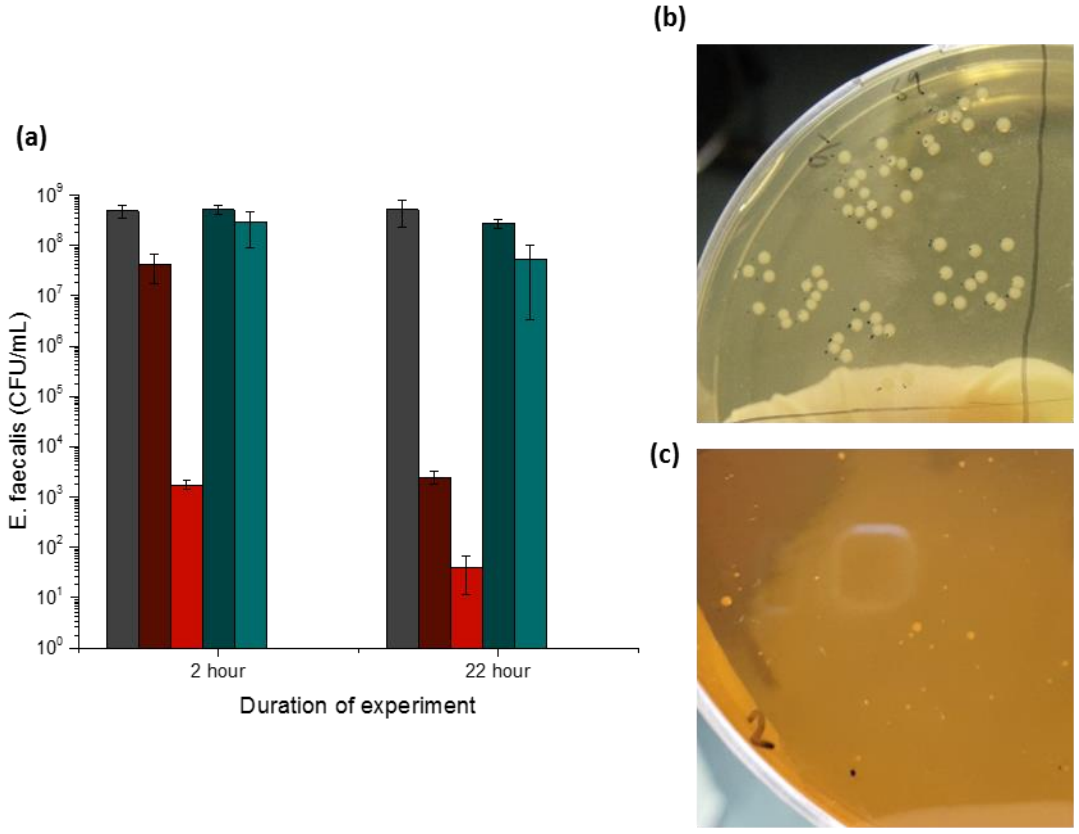

Figure 5.12 a) CFU counts for *E. faecalis* grown on BHYN with STG agar plates (n=3) Ag-GMP gels 1:1 (maroon) and 2:1 (red), qGMP gels 10 mg (navy) and 20 mg (blue). Photographs of colonies formed on an agar plate (10^{-6} dilution and 10^{-2} dilution for *E. faecalis* (b) and *E. faecalis* & 1:1 gel (c), respectively

Thus, further experiments were undertaken with STG-containing agar plates (Figure 5.12). CFU counts revealed that within only two hours a small, yet noticeable decrease in the number of colonies formed is observed for the 1:1 ratio. However, after 22 hours there is a five orders of magnitude reduction in

the CFUs per mL. However, for the 2:1 ratio within 2 hours there is a substantial decrease of 5 orders of magnitude for the CFU counts and within 22 hours this drops to 7 orders of magnitude. Importantly, not only is there a decrease in the colonies formed, but many of the colonies are much smaller than those formed the absence of the silver (Figure 5#b and c). Through gram staining of the bacteria, it was confirmed that these smaller colonies were, in fact, *E. faecalis* and not a contamination. Therefore, this observation is due to a stress mechanism observed in bacteria because of the harsh growth conditions causing the bacteria to go into an almost metabolic stasis causing fewer bacteria to grow and hence forming smaller colonies. Similar observations have been made in the case of *E. coli* grown in the presence of silver nanoparticles. [43,45]

There is a slight reduction in CFU counts between *E. faecalis* incubated on top of the qGMP gels compared to *E. faecalis* only experiments. Viscous media has been shown to affect growth behaviour, with consequences on bacterial dispersal, bacterial mobility and the diffusion of transport molecules. [94,95] Thus, it isn't surprising that over long periods growth isn't optimal. However, the log reduction in qGMP samples is far less substantial than gels containing silver.

As mentioned previously, colourimetric assays are not useful in this case to further understand the impact of the silver on the *E. faecalis* and therefore other methods of analysis are necessary. Previously, silver nanoparticles have been shown to degrade plasmid DNA in vitro [96] and also degrade chromosomal DNA of *Bacillus subtilis.*[97] Therefore, the chromosomal DNA from *E. faecalis* was extracted and gel electrophoresis used to examine the DNA integrity. Briefly, gel electrophoresis is a technique to separate macromolecules through a porous gel according to size, for which smaller molecules will travel faster and therefore further down the gel. [98,99] These results have revealed major degradation of the chromosomal DNA.

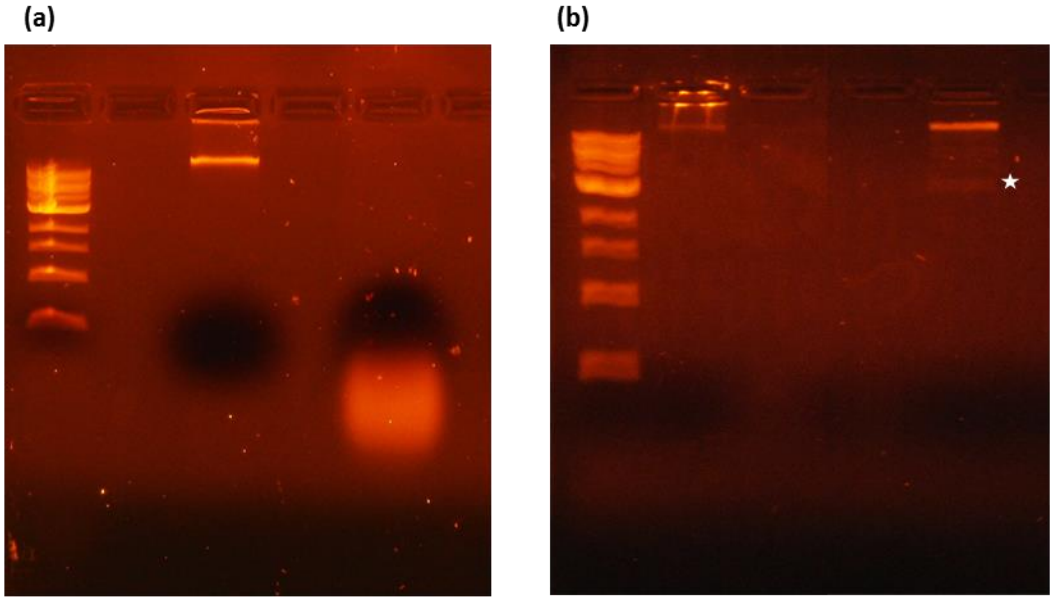

Figure 5.13 Agarose gel electrophoresis on extracted DNA from *E. faecalis* experiments (2 hours). a) Lane 1, 1 kb DNA Ladder. Lane 2, *E. faecalis* only (100x dilution). Lane 3, *E. faecalis* Ag-GMP 2:1 gel. b) Lane 1, 1 kb DNA Ladder. Lane 2, *E. faecalis* only (100x dilution). Lane 3, *E. faecalis* qGMP 10 mg gel. (Ladder separations refer to 10 kb, 8 kb, 6 kb, 5 kb, 4 kb, 3 kb, 2 kb, and 1 kb in descending order.

Gel electrophoresis experiments (Figure 5.13) demonstrated an intact chromosomal band for *E. faecalis* only samples and for *E. faecalis* incubated with the qGMP (10mg/mL) sample. There is also a very faint band at *ca.* 6 kb. From the DNA extraction from the 2-hour Ag-GMP 2:1 sample, there appears to be a total disappearance of the band associated with chromosomal DNA. This coincides with a 'smear' below the DNA ladder indicating that these are small fragments of DNA[97]. Chromosomal DNA extraction is inherently inefficient, and it is highly likely that some intact DNA would be lost or damaged. However, as this 'smear' is not observed to any substantial level for the *E. faecalis* only experiment this is not likely to be the cause of the smear at the bottom of the gel. In support of this, chromosomal DNA extraction was undertaken for the qGMP samples after incubation for 2 hours and these samples exhibited intact chromosomal DNA. Therefore, this 'smear' is not likely caused by any shear used to disassemble the gel network before lysing the cell membrane. Thus, incubating *E. faecalis* with the Ag-GMP hydrogels significantly compromises the integrity of its chromosomal DNA and this is almost certainly a contributing factor to the significant killing of *E. faecalis*. The cause of this damage will be considered in future work.

As mentioned previously, the AgGMP hydrogel network can be used as a scaffold for the photo-reduction of silver nanoparticles. Therefore, the prepared AgGMP and qGMP hydrogels were irradiated with UV light for 90 minutes and left in the dark overnight. These were then incubated with the *E. faecalis* inoculum and collected for CFU counts, as with previous experiments.

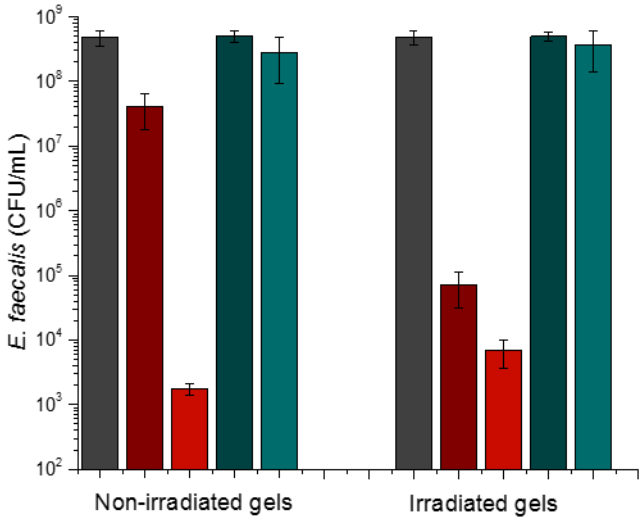

Figure 5.14 CFU counts for *E. faecalis* grown on BHYN with STG agar plates (n=3) and UV irradiated gels Ag-GMP gels 1:1 (maroon) and 2:1 (red), qGMP gels 10 mg (navy) and 20 mg (blue) and non-irradiated gels.

As would be expected, there were no substantial differences between the CFU counts of *E. faecalis* only and *E. faecalis* incubated with the control samples compared between non-irradiated and irradiated hydrogels (Figure 5.14). Unexpectedly, there is a slight increase in the CFU count for the 2:1 sample. One reason that might explain this increase is that the silver nanoparticles formed are produced from excess silver ions in solution. However, this increase from 1.8×10^3 to 6.9×10^3 is not too significant. Therefore, this effectively lowers the concentration of silver in solution. However, there is a three orders of magnitude reduction for the 1:1 sample over the two-hour period comparing the irradiated and non-irradiated gel samples. This can be understood if the bacteria are entangled in the gel network. For the irradiated gel samples, the hydrogel filaments are decorated with silver nanoparticles and therefore the bacteria could conceivably be in direct contact with the silver

nanoparticles. The activity of silver nanoparticles relies on the positive charge to encourage electrostatic attraction with the negatively charged cell membrane of the microorganism. [40]

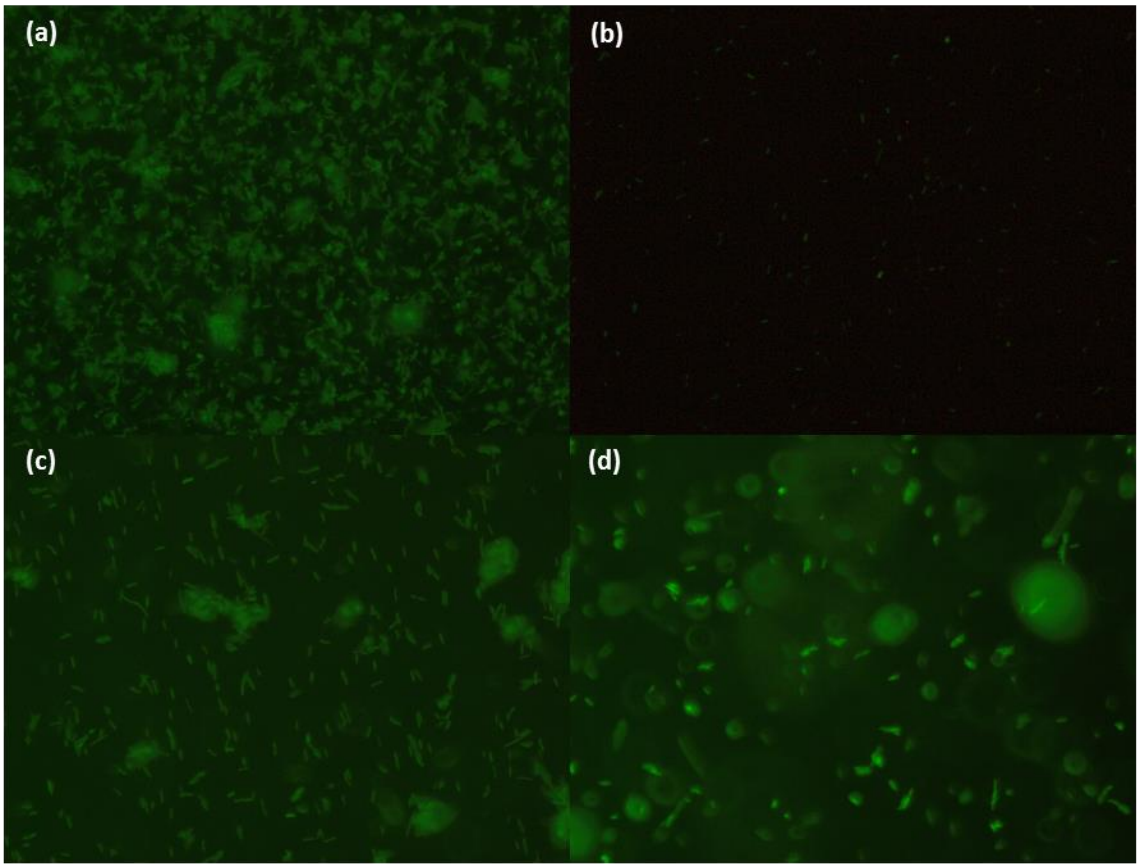

Figure 5.15 Fluorescence images a) *E. faecalis,* b) *E. faecalis 1:1,* c) *E. faecalis* qGMP (10 mg/mL), and d) *E. faecalis* qGMP (20 mg/mL)

The antimicrobial properties of the hydrogels were also tested on *E. coli* to compare the effects between gram-negative and gram-positive bacteria. The experiments were carried out using the same methods used for the gram-positive bacteria, but with some minor modifications (described in the methods section). The *E. coli* strain expressed a green fluorescent protein (GFP) which allowed the cells to be visualised by light microscopy. Images were taken halfway down the gel and showed that that significant numbers of bacteria were present throughout the gel sample *i.e.* not just at either the top or the bottom. Images taken from the AgGMP sample showed low numbers of fluorescent bacteria which is likely due to the significant killing of the *E. coli* prior to imaging.

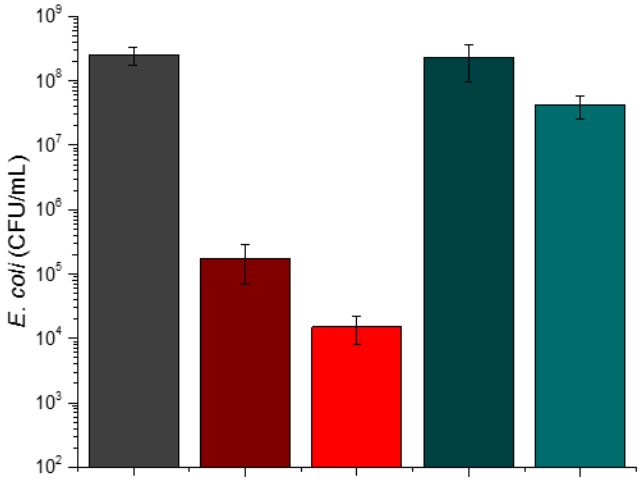

Figure 5.16 CFU counts for *E. coli* grown on LB with STG agar plates (n=3) from incubation with Ag-GMP gels 1:1 (maroon) and 2:1 (red), qGMP gels 10 mg (navy) and 20 mg (blue).

CFU counts were also made for the *E. coli* experiments (Figure 5.16). For *E. coli,* measurements were only made after 2 hours. As expected, there was a significant drop in CFU counts for bacteria incubated with the control hydrogels, though the there was a reduction for the 20 mg/mL sample. However, there was a substantial reduction in both AgGMP samples. There was a three and four orders of magnitude reduction in the CFU count for 1:1 and 2:1 ratio, respectively. This is in line with previous reports demonstrating great effects on gram-negative bacteria.[1,45,49,52] Gram-negative bacteria have a much thinner peptidoglycan cell wall (~2-3 nm vs ~30 nm) and therefore are less protected against the penetration of silver ions into the cytoplasm. [1,69,68]

Conclusion

The binding of silver ions to the guanosine residue of GMP has been utilised to form a supramolecular hydrogel in one step. The stoichiometry of the silver has substantial influence over the rheological properties of the resulting hydrogel. This silver is integral to the formation of the nanofilaments of the hydrogel and can be photo-reduced to form silver nanoparticles embedded within the supramolecular matrix. The Ag-GMP hydrogels demonstrated substantial, and statistically valid, killing of gram-negative bacteria (*E. coli*) and gram-positive bacteria (*E. faecalis)*. Fluorescence experiments demonstrated bacteria throughout the gel network and gel electrophoresis experiments indicated that this activity seems to be, at least in part, due to damage caused to the chromosomal DNA of *E. faecalis.* In contrast, control hydrogels produced by acidifying GMP solutions, in the absence of silver, did not show antibacterial activity. These findings clearly indicate the activity is related to the presence of the silver in the AgGMP gels. These gels could be irradiated with UV light to promote the formation of photo-reduced silver nanoparticles. This resulted in increased killing of *E. faecalis* at for the 1:1 AgGMP sample for CFU counts at 2 hours, thus indicating that the antibacterial activity was at least in part due to the silver nanoparticles formed on the hydrogel filaments and not just dissolved silver ions.

Future Work

As demonstrated via gel electrophoresis, there are severe degradations to the chromosomal DNA of *E. faecalis* when they are incubated with the Ag-GMP hydrogel. DNA damage has previously been attributed to the generation of reactive oxygen species (ROS) by silver. [51,53] ROS are highly reactive and potentially destructive oxidants such as superoxide-radical (O_2^-), hydroxyl radical ($^{\cdot}OH$), hydrogen peroxide (H_2O_2), and singlet oxygen ($^1O_2$).[51,53,55–57,100–103] These species are generated naturally as part of the normal aerobic mechanism and may be involved in messenger pathways, but levels are kept low by cellular antioxidants. [51,56] However, silver has been shown to increase these species either acting as a catalytic site to produce ROS or by inactivating enzymes in the respiratory chain via interactions with thiols, thereby preventing them from removing ROS, causing an imbalance known as oxidative stress. [45,49,51,104–106] This burden allows for the accumulation of these reactive species which can then go on to either react directly with DNA or react with lipids to produce malondialdehyde which would then go on to react with DNA. [53,97,100,107,108]

To check whether these species are responsible for the DNA degradation and consequently the significant killing of *E. faecalis,* it is necessary to determine whether these species are present at higher levels when incubated with the Ag-GMP hydrogel. Stress-specific reporter strains that express reporter genes in response to elevated ROS levels, have been used previously [49,51] but would complicate the experiments further by introducing new strains. Instead, fluorescent probes can be used to detect ROS levels. [53,56–58,106,109] For instance, dichlorodihydrofluorescein diacetate is non-fluorescent and passively diffuses through the cellular membrane but is sensitive to oxidation. As a result, it can react with ROS to form the fluorescent dichlorofluorescein which is then trapped in cells and can be detected via fluorimetry or fluorescence microscopy. Thus, the fluorescence levels are proportional to the ROS levels and can then be correlated to the antimicrobial levels of the Ag-GMP hydrogel. This experiment can be run with positive controls such as paraquat and Norfloxacin, which are well-known to increase intracellular ROS levels. [58,110]

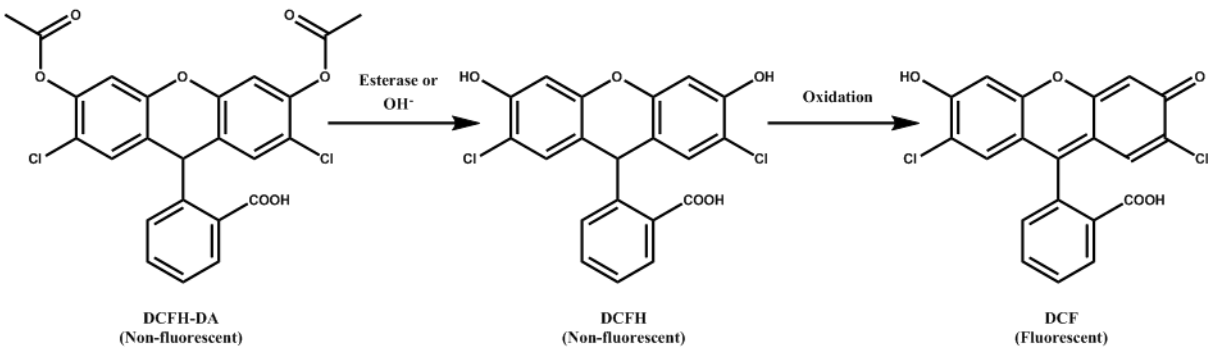

Figure 5.# Scheme of dichlorodihydrofluorescein diacetate (DCFH-DA) de-esterification to dichlorodihydrofluorescein (DCFH), and further oxidation to fluorescent dichlorofluorescein (DCF) by ROS (adapted from 164).

Further, ROS levels could be suppressed in the presence of an antioxidant (e.g. N-acetylcysteine, L-cysteine, L-methionine) and the DNA integrity evaluated after incubation with the Ag-GMP hydrogel and an applicable antioxidant to corroborate the fluorescent probe experiments.[48,53,105,111]

Beyond this, electron microscopy will be used to determine structural changes to *E. faecalis* and in conjunction with energy-dispersive X-ray spectroscopy to detect silver species. This could elucidate other mechanisms, other than DNA damage, responsible for the killing of *E.faecalis.*

References

(1) Rai, M.; Yadav, A.; Gade, A. Silver Nanoparticles as a New Generation of Antimicrobials. *Biotechnol. Adv.* 2009, *27* (1), 76–83.

(2) Kyriacou, S. V.; Brownlow, W. J.; Xu, X.-H. N. Using Nanoparticle Optics Assay for Direct Observation of the Function of Antimicrobial Agents in Single Live Bacterial Cells †. *Biochemistry* 2004, *43* (1), 140–147.

(3) Tenover, F. C. Mechanisms of Antimicrobial Resistance in Bacteria. *Am. J. Med.* 2006, *119* (6), S3–S10.

(4) Wise, R.; Hart, T.; Cars, O.; Streulens, M.; Helmuth, R.; Huovinen, P.; Sprenger, M. Antimicrobial Resistance. Is a Major Threat to Public Health. *BMJ* 1998, *317* (7159), 609–610.

(5) Cohen, M. L. Epidemiology of Drug Resistance: Implications for a Post--Antimicrobial Era. *Science.* 1992, *257* (5073), 1050–1055.

(6) Yu, Q.; Wu, Z.; Chen, H. Dual-Function Antibacterial Surfaces for Biomedical Applications. *Acta Biomaterialia*. 2015, 1–13.

(7) Vasilev, K.; Cook, J.; Griesser, H. J. Antibacterial Surfaces for Biomedical Devices. *Expert Rev. Med. Devices* 2009, *6* (5), 553–567.

(8) Bazaka, K.; Jacob, M. V.; Chrzanowski, W.; Ostrikov, K. Anti-Bacterial Surfaces: Natural Agents, Mechanisms of Action, and Plasma Surface Modification. *RSC Adv.* 2015, *5* (60), 48739–48759.

(9) DiTizio, V.; Ferguson, G. W.; Mittelman, M. W.; Khoury, A. E.; Bruce, A. W.; DiCosmo, F. A Liposomal Hydrogel for the Prevention of Bacterial Adhesion to Catheters. *Biomaterials* 1998, *19* (20), 1877–1884.

(10) Li, P.; Poon, Y. F.; Li, W.; Zhu, H.-Y.; Yeap, S. H.; Cao, Y.; Qi, X.; Zhou, C.; Lamrani, M.; Beuerman, R. W.; Kang, E.-T.; Mu, Y.; Li, C. M.; Chang, M. W.; Jan Leong, S. S.; Chan-Park, M. B. A Polycationic Antimicrobial and Biocompatible Hydrogel with Microbe Membrane Suctioning Ability. *Nat. Mater.* 2011, *10* (2), 149–156.

(11) Carmona-Ribeiro, A. M.; de Melo Carrasco, L. D. Cationic Antimicrobial Polymers and Their Assemblies. *Int. J. of Mol. Scis*. 2013, 9906–9946.

(12) Strassburg, A.; Kracke, F.; Wenners, J.; Jemeljanova, A.; Kuepper, J.; Petersen, H.; Tiller, J. C. Nontoxic, Hydrophilic Cationic Polymers - Identified as Class of Antimicrobial Polymers. *Macromol. Biosci.* 2015, *15* (12), 1710–1723.

(13) Laverty, G.; Gorman, S. P.; Gilmore, B. F. Antimicrobial Peptide Incorporated Poly(2-Hydroxyethyl Methacrylate) Hydrogels for the Prevention of Staphylococcus Epidermidis-Associated Biomaterial Infections. *J. Biomed. Mater. Res. Part A* 2012, *100A* (7), 1803–1814.

(14) Locock, K. E. S.; Michl, T. D.; Stevens, N.; Hayball, J. D.; Vasilev, K.; Postma, A.; Griesser, H. J.; Meagher, L.; Haeussler, M. Antimicrobial Polymethacrylates Synthesized as Mimics of Tryptophan-Rich Cationic Peptides. *ACS Macro Lett.* 2014, *3* (4), 319–323.

(15) Locock, K. E. S.; Michl, T. D.; Valentin, J. D. P.; Vasilev, K.; Hayball, J. D.; Qu, Y.; Traven, A.; Griesser, H. J.; Meagher, L.; Haeussler, M. Guanylated Polymethacrylates: A Class of Potent Antimicrobial Polymers with Low Hemolytic Activity. *Biomacromolecules* 2013, *14* (11), 4021–4031.

(16) Locock, K. E. S. Bioinspired Polymers: Antimicrobial Polymethacrylates. *Aust. J. Chem*. 2016, 69, 717–724.

(17) Wang, Y.; Canady, T. D.; Zhou, Z.; Tang, Y.; Price, D. N.; Bear, D. G.; Chi, E. Y.; Schanze, K. S.; Whitten, D. G. Cationic Phenylene Ethynylene Polymers and Oligomers Exhibit Efficient Antiviral Activity. *ACS Appl. Mater. Interfaces* 2011, *3* (7), 2209–2214.

(18) Wang, Y.; Chi, E. Y.; Schanze, K. S.; Whitten, D. G. Membrane Activity of Antimicrobial Phenylene Ethynylene Based Polymers and Oligomers. *Soft Matter* 2012, *8* (33), 8547.

(19) Siedenbiedel, F.; Fuchs, A.; Moll, T.; Weide, M.; Breves, R.; Tiller, J. C. Star-Shaped Poly(Styrene)-Block-Poly(4-Vinyl-N-Methylpyridiniumiodide) for Semipermanent Antimicrobial Coatings. *Macromol. Biosci.* 2013, *13* (10), 1447–1455.

(20) Tiller, J. C.; Lee, S. B.; Lewis, K.; Klibanov, A. M. Polymer Surfaces Derivatized with Poly(Vinyl-N-Hexylpyridinium) Kill Airborne and Waterborne Bacteria. *Biotechnol. Bioeng.* 2002, *79* (4), 465–471.

(21) Irwansyah, I.; Li, Y.-Q.; Shi, W.; Qi, D.; Leow, W. R.; Tang, M. B. Y.; Li, S.; Chen, X. Gram-Positive Antimicrobial Activity of Amino Acid-Based Hydrogels. *Adv. Mater.* 2015, *27* (4), 648–654.

(22) Huang, R.; Qi, W.; Feng, L.; Su, R.; He, Z. Self-Assembling Peptide–polysaccharide Hybrid Hydrogel as a Potential Carrier for Drug Delivery. *Soft Matter* 2011, *7*, 6222.

(23) Zhou, M.; Smith, A. M.; Das, A. K.; Hodson, N. W.; Collins, R. F.; Ulijn, R. V.; Gough, J. E. Self-Assembled Peptide-Based Hydrogels as Scaffolds for Anchorage-Dependent Cells. *Biomaterials* 2009, *30* (13), 2523–2530.

(24) Ng, V. W. L.; Chan, J. M. W.; Sardon, H.; Ono, R. J.; García, J. M.; Yang, Y. Y.; Hedrick, J. L. Antimicrobial Hydrogels: A New Weapon in the Arsenal against Multidrug-Resistant Infections. *Adv. Drug Deliv. Rev.* 2014, *78*, 46–62.

(25) Gaharwar, A. K.; Avery, R. K.; Assmann, A.; Paul, A.; McKinley, G. H.; Khademhosseini, A.; Olsen, B. D. Shear-Thinning Nanocomposite Hydrogels for the Treatment of Hemorrhage. *ACS Nano* 2014, *8* (10), 9833–9842.

(26) Salick, D. A.; Kretsinger, J. K.; Pochan, D. J.; Schneider, J. P. Inherent Antibacterial Activity of a Peptide-Based β-Hairpin Hydrogel. *J. Am. Chem. Soc.* 2007, *129* (47), 14793–14799.

(27) Liu, Y.; Yang, Y.; Wang, C.; Zhao, X. Stimuli-Responsive Self-Assembling Peptides Made from Antibacterial Peptides. *Nanoscale* 2013, *5* (14), 6413.

(28) Veiga, A. S.; Sinthuvanich, C.; Gaspar, D.; Franquelim, H. G.; Castanho, MA.; Schneider, J. P. Arginine-Rich Self-Assembling Peptides as Potent Antibacterial Gels. *Biomaterials* 2012, *33* (35), 8907–8916.

(29) Salick, D. A.; Pochan, D. J.; Schneider, J. P. Design of an Injectable β-Hairpin Peptide Hydrogel That Kills Methicillin-Resistant Staphylococcus Aureus. *Adv. Mater.* 2009, *21* (41), 4120–4123.

(30) Yang, Z.; Liang, G.; Guo, Z.; Guo, Z.; Xu, B. Intracellular Hydrogelation of Small Molecules Inhibits Bacterial Growth. *Angew. Chem. Int. Ed.* 2007, *46* (43), 8216–8219.

(31) Hughes, M.; Debnath, S.; Knapp, C. W.; Ulijn, R. V. Antimicrobial Properties of Enzymatically Triggered Self-Assembling Aromatic Peptide Amphiphiles. *Biomater. Sci.* 2013, *1* (11), 1138.

(32) Das, D.; Kar, T.; Das, P. K. Gel-Nanocomposites: Materials with Promising Applications. *Soft Matter* 2012, *8* (8), 2348–2365.

(33) Ramyadevi, J.; Jeyasubramanian, K.; Marikani, A.; Rajakumar, G.; Rahuman, A. A. Synthesis and Antimicrobial Activity of Copper Nanoparticles. *Mater. Lett.* 2012, *71*, 114–116.

(34) Dastjerdi, R.; Montazer, M. A Review on the Application of Inorganic Nano-Structured Materials in the Modification of Textiles: Focus on Anti-Microbial Properties. *Coll. Surf. B Biointerfaces* 2010, *79* (1), 5–18.

(35) Ren, G.; Hu, D.; Cheng, E. W. C.; Vargas-Reus, M. A.; Reip, P.; Allaker, R. P. Characterisation of Copper Oxide Nanoparticles for Antimicrobial Applications. *Int. J. Antimicrob. Agents* 2009, *33* (6), 587–590.

(36) Schwartz, V. B.; Thétiot, F.; Ritz, S.; Pütz, S.; Choritz, L.; Lappas, A.; Förch, R.; Landfester, K.; Jonas, U. Antibacterial Surface Coatings from Zinc Oxide Nanoparticles Embedded in Poly(N-Isopropylacrylamide) Hydrogel Surface Layers. *Adv. Funct. Mater.* 2012, *22* (11), 2376–2386.

(37) Hassan, S. F.; Gupta, M. Development of High Performance Magnesium Nano-Composites Using Nano-Al2O3 as Reinforcement. *Mater. Sci. Eng. A* 2005, *392* (1–2), 163–168.

(38) Li, X.; Robinson, S. M.; Gupta, A.; Saha, K.; Jiang, Z.; Moyano, D. F.; Sahar, A.; Riley, M. A.; Rotello, V. M. Functional Gold Nanoparticles as Potent Antimicrobial Agents against Multi-Drug-Resistant Bacteria. *ACS Nano* 2014, *8* (10), 10682–10686.

(39) Zheng, K.; Setyawati, M. I.; Leong, D. T.; Xie, J. Antimicrobial Gold Nanoclusters. *ACS Nano* 2017, *11* (7), 6904–6910.

(40) Kim, J. S.; Kuk, E.; Yu, K. N.; Kim, J. H.; Park, S. J.; Lee, H. J.; Kim, S. H.; Park, Y. K.; Park, Y. H.; Hwang, C. Y.; Kim, Y. K.; Lee, Y. S.; Jeong, D. H.; Cho, M. H. Antimicrobial Effects of Silver Nanoparticles. *Nanomedicine Nanotechnology, Biol. Med.* 2007, *3* (1), 95–101.

(41) Sharma, V. K.; Yngard, R. A.; Lin, Y. Silver Nanoparticles: Green Synthesis and Their Antimicrobial Activities. *Advances in Colloid and Interface Science*. 2009, 83–96.

(42) Morones, J. R.; Elechiguerra, J. L.; Camacho, A.; Holt, K.; Kouri, J. B.; Ramírez, J. T.; Yacaman, M. J. The Bactericidal Effect of Silver Nanoparticles. *Nanotechnology* 2005, *16* (10), 2346–2353.

(43) Sondi, I.; Salopek-Sondi, B. Silver Nanoparticles as Antimicrobial Agent: A Case Study on E. Coli as a Model for Gram-Negative Bacteria. *J. Colloid Interface Sci.* 2004, *275* (1), 177–182.

(44) Shrivastava, S.; Bera, T.; Roy, A.; Singh, G.; Ramachandrarao, P.; Dash, D. Characterization of Enhanced Antibacterial Effects of Novel Silver Nanoparticles. *Nanotechnology* 2010, *18* (22), 1–9.

(45) Prabhu, S.; Poulose, E. K. Silver Nanoparticles: Mechanism of Antimicrobial Action, Synthesis, Medical Applications, and Toxicity Effects. *Int. Nano Lett.* 2012, *2* (1), 32.

(46) Feng, Q. L.; Wu, J.; Chen, G. Q.; Cui, F. Z.; Kim, T. N.; Kim, J. O. A Mechanistic Study of the Antibacterial Effect of Silver Ions on *Escherichia Coli* and *Staphylococcus Aureus. J. Biomed. Mater. Res*. 2000, 662–668.

(47) Jung, W. K.; Koo, H. C.; Kim, K. W.; Shin, S.; Kim, S. H.; Park, Y. H. Antibacterial Activity and Mechanism of Action of the Silver Ion in Staphylococcus Aureus and Escherichia Coli. *Appl. Environ. Microbiol.* 2008, *74* (7), 2171–2178.

(48) Matsumura, Y.; Yoshikata, K.; Kunisaki, S.; Tsuchido, T. Mode of Bactericidal Action of Silver Zeolite and Its Comparison with That of Silver Nitrate. *Appl. Environ. Microbiol.* 2003, *69* (7), 4278–4281.

(49) Hwang, E. T.; Lee, J. H.; Chae, Y. J.; Kim, Y. S.; Kim, B. C.; Sang, B.-I.; Gu, M. B. Analysis of the Toxic Mode of Action of Silver Nanoparticles Using Stress-Specific Bioluminescent Bacteria. *Small* 2008, *4* (6), 746–750.

(50) Schreurs, W. J. A.; Rosenberg, H. Effect of Silver Ions on Transport and Retention of Phosphate by Escherichia Coli. *J. Bacteriol.* 1982, *152* (1), 7–13.

(51) Park, H.; Yeon, J.; Kim, J. J. Y.; Lee, J.; Hahn, J.; Bock, M.; Yoon, J.; Kim, J. J. Y.; Lee, J.; Hahn, J.; Gu, M. B.; Yoon, J.; Yeon, J.; Kim, J. J. Y.; Lee, J.; Hahn, J.; Bock, M.; Yoon, J. Silver-Ion-Mediated Reactive Oxygen Species Generation Affecting Bactericidal Activity. *Water Res.* 2009, *43* (4),

1027–1032.

(52) Yamanaka, M.; Hara, K.; Kudo, J. Bactericidal Actions of a Silver Ion Solution on Escherichia Coli , Studied by Energy-Filtering Transmission Electron Microscopy and Proteomic Analysis. *Appl. Environ. Microbiol.* 2005, *71* (11), 7589–7593.

(53) Xu, H.; Qu, F.; Xu, H.; Lai, W.; Wang, Y. A.; Aguilar, Z. P.; Wei, H. Role of Reactive Oxygen Species in the Antibacterial Mechanism of Silver Nanoparticles on Escherichia Coli O157:H7. *BioMetals* 2012, *25* (1), 45–53.

(54) Arakawa, H.; Neault, J.; Tajmir-Riahi, H. Silver(I) Complexes with DNA and RNA Studied by Fourier Transform Infrared Spectroscopy and Capillary Electrophoresis. *Biophys J* 2001, *81* (3), 1580–1587.

(55) Excitation, A. F. Reactive Oxygen Species (ROS) Detection Reagents. 2006, 1–5.

(56) Rastogi, R. P.; Singh, S. P.; Häder, D. P.; Sinha, R. P. Detection of Reactive Oxygen Species (ROS) by the Oxidant-Sensing Probe 2',7'-Dichlorodihydrofluorescein Diacetate in the Cyanobacterium Anabaena Variabilis PCC 7937. *Biochem. Biophys. Res. Commun.* 2010, *397* (3), 603–607.

(57) Gomes, A.; Fernandes, E.; Lima, J. L. F. C. Fluorescence Probes Used for Detection of Reactive Oxygen Species. *J. Biochem. Biophys. Methods* 2005, *65* (2–3), 45–80.

(58) Lee, W.; Kim, K.-J.; Lee, D. G. A Novel Mechanism for the Antibacterial Effect of Silver Nanoparticles on Escherichia Coli. *Biometals* 2014, *27* (6), 1191–1201.

(59) Fichman, G.; Guterman, T.; Adler-abramovich, L.; Gazit, E. Synergetic Functional Properties of Two-Component Single Amino Acid-Based Hydrogels. *CrystEngComm* 2015, *17* (42), 8105–8112.

(60) Roy, S.; Banerjee, A. Amino Acid Based Smart Hydrogel: Formation, Characterization and Fluorescence Properties of Silver Nanoclusters within the Hydrogel Matrix. *Soft Matter* 2011, *7* (11), 5300.

(61) Dutta, S.; Shome, A.; Debnath, S.; Das, P. K. Counterion Dependent Hydrogelation of Amino Acid Based Amphiphiles: Switching from Non-Gelators to Gelators and Facile Synthesis of Silver Nanoparticles. *Soft Matter* 2009, *5* (8), 1607.

(62) Li, M.; Oakley, R. J.; Bevan, H.; Smarsly, B. M.; Mann, S.; Faul, C. F. J. Nucleotide-Based Templates for Nanoparticle Production-Exploiting Multiple Noncovalent Interactions. *Chem. Mater* 2009, *21*, 3270–3274.

(63) Loo, K.; Degtyareva, N.; Park, J.; Sengupta, B.; Reddish, M.; Rogers, C. C.; Bryant, A.; Petty, J. T. Ag + -Mediated Assembly of 5'-Guanosine Monophosphate. *J. Phys. Chem. B* 2010, *114* (12), 4320–4326.

(64) Tu, A. T.; Reinosa, J. A. The Interaction of Silver Ion with Guanosine, Guanosine Monophosphate, and Related Compounds. Determination of Possible Sites of Complexing. *Biochemistry* 1966, *5* (10), 3375–3383.

(65) Dash, J.; Patil, A. J.; Das, R. N.; Dowdall, F. L.; Mann, S. Supramolecular Hydrogels Derived from Silver Ion-Mediated Self-Assembly of 5'-Guanosine Monophosphate. *Soft Matter* 2011, *7* (18), 8120.

(66) Hinshelwood, C. C. N. *The Chemical Kinetics of the Bacterial Cell*; The Clarendon Press: Oxford, 1946.

(67) Gram Staining | BioNinja http://ib.bioninja.com.au/options/untitled/b1-microbiology-organisms/gram-staining.html (accessed Mar 12, 2018).

(68) Murray, R. G. E.; Steed, P.; Elson, H. E. The Location of the Mucopeptide in Sections of the Cell All of Escherichia Coli and Other Gram-Negative Bacteria. *Can. J. Microbiol.* 1965, *11* (3), 547–560.

(69) Shockman, G. D.; Barrett, J. F. Structure, Function, and Assembly of Cell Walls of Gram-Positive. *Ann. Rev. Microbiol* 1983, *37*, 132–134.

(70) Promega Corporation. Wizard ® Genomic DNA Purification Kit. 2010.

(71) Zheng, C.-Y.; Li, H. Chirality Delivery through Multiple and Helical H-Bonding from Chiral Coordination Complex to Its Supramolecular Architecture. *Inorg. Chem. Commun.* 2013, *34*, 30–33.

(72) Pandoli, O.; Massi, A.; Cavazzini, A.; Spada, G. P.; Cui, D. Circular Dichroism and UV-Vis Absorption Spectroscopic Monitoring of Production of Chiral Silver Nanoparticles Templated by Guanosine 5'-Monophosphate. *Analyst* 2011, *136* (18), 3713–3719.

(73) Adams, D. J.; Butler, M. F.; Frith, W. J.; Kirkland, M.; Mullen, L.; Sanderson, P. A New Method for Maintaining Homogeneity during Liquid–hydrogel Transitions Using Low Molecular Weight Hydrogelators. *Soft Matter* 2009, *5* (9), 1856.

(74) Tang, C.; Smith, A. M.; Collins, R. F.; Ulijn, R. V.; Saiani, A. Fmoc-Diphenylalanine Self-Assembly Mechanism Induces Apparent PKa Shifts. *Langmuir* 2009, *25* (16), 9447–9453.

(75) Sato-Berrú, R.; Redón, R.; Vázquez-Olmos, A.; Saniger, J. M. Silver Nanoparticles Synthesized by Direct Photoreduction of Metal Salts. Application in Surface-Enhanced Raman Spectroscopy. *J. Raman Spectrosc.* 2009, *40* (4), 376–380.

(76) Sun, Y.; Xia, Y. Gold and Silver Nanoparticles: A Class of Chromophores with Colors Tunable in the Range from 400 to 750 Nm. *Analyst* 2003, *128* (6), 686.

(77) Huang, H. H.; Ni, X. P.; Loy, G. L.; Chew, C. H.; Tan, K. L.; Loh, F. C.; Deng, J. F.; Xu, G. Q. Photochemical Formation of Silver Nanoparticles in Poly(N -Vinylpyrrolidone). *Langmuir* 1996, *12* (4), 909–912.

(78) Patil, A. J.; Kumar, R. K.; Barron, N. J.; Mann, S. Cerium Oxide Nanoparticle-Mediated Self-Assembly of Hybrid Supramolecular Hydrogels. *Chem. Commun.* 2012, *48* (64), 7934.

(79) Raeburn, J.; Adams, D. J. Multicomponent Low Molecular Weight Gelators. *Chem. Commun.* 2015, *51* (25), 5170–5180.

(80) Thornton, K.; Abul-Haija, Y. M.; Hodson, N.; Ulijn, R. V. Mechanistic Insights into Phosphatase Triggered Self-Assembly Including Enhancement of Biocatalytic Conversion Rate. *Soft Matter* 2013, *9* (39), 9430.

(81) Zuidema, J. M.; Rivet, C. J.; Gilbert, R. J.; Morrison, F. a. A Protocol for Rheological Characterization of Hydrogels for Tissue Engineering Strategies. *J. Biomed. Mater. Res. - Part B Appl. Biomater.* 2014, *102* (5), 1063–1073.

(82) Chen, G.; Hoffman, A. S. Graft Copolymers That Exhibit Temperature-Induced Phase Transitions over a Wide Range of PH. *Nature* 1995, *373* (6509), 49–52.

(83) Mahler, A.; Reches, M.; Rechter, M.; Cohen, S.; Gazit, E. Rigid, Self-Assembled Hydrogel Composed of a Modified Aromatic Dipeptide. *Adv. Mater.* 2006, *18* (11), 1365–1370.

(84) Guvendiren, M.; Lu, H. D.; Burdick, J. a. Shear-Thinning Hydrogels for Biomedical Applications. *Soft Matter* 2012, *8* (2), 260.

(85) Anker, J. N.; Hall, W. P.; Lyandres, O.; Shah, N. C.; Zhao, J.; Van Duyne, R. P. Biosensing with Plasmonic Nanosensors. *Nat. Mater.* 2008, *7* (6), 442–453.

(86) Sun, Y. Shape-Controlled Synthesis of Gold and Silver Nanoparticles. *Science.* 2002, *298* (5601), 2176–2179.

(87) Shlaes, D. M.; Bouvet, A.; Devine, C.; Shlaes, J. H.; Al-Obeid, S.; Williamson, R. Inducible, Transferable Resistance to Vancomycin in Enterococcus Faecalis A256. *Antimicrob. Agents Chemother.* 1989, *33* (2), 198–203.

(88) Shankar, N.; Baghdayan, a S.; Gilmore, M. S. Modulation of Virulence within a Pathogenicity Island in Vancomycin- Resistant Enterococcus Faecalis. *Nature* 2002, *417* (6890), 746–50.

(89) Ruiz-Garbajosa, P.; Bonten, M. J. M.; Robinson, D. A.; Top, J.; Nallapareddy, S. R.; Torres, C.; Coque, T. M.; Cant??n, R.; Baquero, F.; Murray, B. E.; Del Campo, R.; Willems, R. J. L. Multilocus Sequence Typing Scheme for Enterococcus Faecalis Reveals Hospital-Adapted Genetic Complexes in a Background of High Rates of Recombination. *J. Clin. Microbiol.* 2006, *44* (6), 2220–2228.

(90) Stoddart, M. J. Cell Viability Assays: Introduction; Humana Press, New York, 2011; 1–6.

(91) Wang, S.; Liu, X.; Liu, H.; Zhang, L.; Guo, Y.; Yu, S.; Wozniak, D. J.; Ma, L. Z. The Exopolysaccharide PsL-EDNA Interaction Enables the Formation of a Biofilm Skeleton in Pseudomonas Aeruginosa. *Environ. Microbiol. Rep.* 2015, *7* (2), 330–340.

(92) He, D.; Ikeda-Ohno, A.; Boland, D. D.; Waite, T. D. Synthesis and Characterization of Antibacterial Silver Nanoparticle-Impregnated Rice Husks and Rice Husk Ash. *Environ. Sci. Technol.* 2013, *47* (10), 5276–5284.

(93) Tilton, R. C.; Rosenberg, B. Reversal of the Silver Inhibition of Microorganisms by Agar. *Appl. Environ. Microbiol.* 1978, *35* (6), 1116–1120.

(94) Liu, S. Tracking Bacterial Growth in Liquid Media and a New Bacterial Life Model. *Sci. China Ser. C Life Sci.* 1999, *42* (6), 644–654.

(95) Kümmerli, R.; Griffin, A. S.; West, S. A.; Buckling, A.; Harrison, F. Viscous Medium Promotes Cooperation in the Pathogenic Bacterium Pseudomonas Aeruginosa. *Proc. Biol. Sci.* 2009, *276* (1672), 3531–3538.

(96) Chowdhury, S.; Basu, A.; Kundu, S. Green Synthesis of Protein Capped Silver Nanoparticles from Phytopathogenic Fungus Macrophomina Phaseolina (Tassi) Goid with Antimicrobial Properties against Multidrug-Resistant Bacteria. *Nanoscale Res. Lett.* 2014, *9* (1), 365.

(97) Hsueh, Y.-H.; Lin, K.-S.; Ke, W.-J.; Hsieh, C.-T.; Chiang, C.-L.; Tzou, D.-Y.; Liu, S.-T. The Antimicrobial Properties of Silver Nanoparticles in Bacillus Subtilis Are Mediated by Released Ag+ Ions. *PLoS One* 2015, *10* (12), e0144306.

(98) Southern, E. M. Detection of Specific Sequences among DNA Fragments Separated by Gel Electrophoresis. *J. Mol. Biol.* 1975, *98* (3), 503–517.

(99) Aaij, C.; Borst, P. The Gel Electrophoresis of DNA. *Biochim. Biophys. Acta - Nucleic Acids Protein Synth.* 1972, *269* (2), 192–200.

(100) Matés, J. M.; Sánchez-Jiménez, F. M. Role of Reactive Oxygen Species in Apoptosis: Implications for Cancer Therapy. *Int. J. Biochem. Cell Biol.* 2000, *32* (2), 157–170.

(101) Wright, A.; Bubb, W. A.; Hawkins, C. L.; Davies, M. J. Singlet Oxygen-Mediated Protein Oxidation: Evidence for the Formation of Reactive Side Chain Peroxides on Tyrosine Residues. *Photochem Photobiol* 2002, *76* (1), 35–46.

(102) Thomas, C. E.; Darley-Usmar, V. Forum : Therapeutic Applications of Reactive Oxygen and Nitrogen Species in Human Disease. *Free Radic. Biol. Med.* 2000, *28* (10), 1478–1486.

(103) Oturan, M. A. Electrochemically Generated Hydroxyl Radicals for in Situ Destruction of Organic

Pollutants. *J. Appl. Electrochem.* 2000, *30* (4), 475–482.

(104) Malencik, D. A.; Anderson, S. R. Dityrosine as a Product of Oxidative Stress and Fluorescent Probe. *Amino Acids* 2003, *25* (3–4), 233–247.

(105) Sies, H. Oxidative Stress: Oxidants and Antioxidants. *Exp. Physiol.* 1997, *82* (2), 291–295.

(106) Aranda, A.; Sequedo, L.; Tolosa, L.; Quintas, G.; Burello, E.; Castell, J. V.; Gombau, L. Dichloro-Dihydro-Fluorescein Diacetate (DCFH-DA) Assay: A Quantitative Method for Oxidative Stress Assessment of Nanoparticle-Treated Cells. *Toxicol. Vitr.* 2013, *27* (2), 954–963.

(107) Nowicka, A. M.; Kowalczyk, A.; Donten, M.; Krysinski, P.; Stojek, Z. Influence of a Magnetic Nanoparticle As a Drug Carrier on the Activity of Anticancer Drugs : Interactions of Double Stranded DNA and Doxorubicin Modified with a Carrier. *Anal. Chem.* 2009, *81* (17), 7474–7483.

(108) Marnett, L. J. Lipid Peroxidation—DNA Damage by Malondialdehyde. *Mutat. Res. Mol. Mech. Mutagen.* 1999, *424* (1), 83–95.

(109) Rosenkranz, A. R.; Schmaldienst, S.; Stuhlmeier, K. M.; Chen, W.; Knapp, W.; Zlabinger, G. J. A Microplate Assay for the Detection of Oxidative Products Using 2',7'-Dichlorofluorescin-Diacetate. *J. Immunol. Methods* 1992, *156* (1), 39–45.

(110) Hassan, H. M.; Fridovich, I. Superoxide Radical and the Oxygen Enhancement of the Toxicity of Paraquat in *Escherichia Coli*. *J. Biol. Chem.* 1978, *253* (22), 8143–8148.

(111) Aslam, S.; Darouiche, R. O. Role of Antibiofilm-Antimicrobial Agents in Controlling Device-Related Infections. *Int. J. Artif. Organs* 2011, *34* (9), 752–758.

Chapter 6
General Conclusions and Future Work

Conclusions and Future Work

This thesis presents new stimuli for the formation of single and multicomponent hybrid supramolecular hydrogels and explored the consequences of the self-assembly processes for these samples. Chapter 3 demonstrates a novel route for gelation in which nitric oxide radicals are used to dephosphorylate the amino acid derivative, Fmoc-tyrosine-phosphate, to yield supramolecular hydrogels. Further to this, the consequences of different methodologies were explored and demonstrated striking differences in the filament morphology compared with filaments produced *via* enzymatic dephosphorylation. Filaments formed in the presence of sodium nitroprusside (SNP) were thinner (*ca.* 2-4 nm diameter) and exhibited an opposing supramolecular chirality compared to gels formed through conventional means. CD and FT-IR were used to demonstrate that self-assembly in the presence of SNP (sodium nitroprusside) facilitated the formation of the kinetically trapped nanofilaments. It is envisioned that nitric oxide radicals can be readily employed in dephosphorylation of other important functional amino acid and peptide derivatives for the construction of nanocomposite hydrogels and should open new routes to altering the molecular packing of gelator molecules for the construction of supramolecular architectures with chirality.

The work presented in Chapter 4 is an example of the gelation of one gelator used to trigger the gelation of the second gelator which is used to form the construction of nucleotide-amino acid multi-component hydrogels. The second gelator is more susceptible to pH and thus it possible to selectively remove one gelator. This is an exciting avenue to modulate the gel architecture to create complex materials which may be relevant to a myriad of applications, *e.g.*, drug delivery, tissue culture scaffolds *etc.* It is also demonstrated that the kinetics of assembly dramatically affects the properties of the resulting hydrogel.

From this work it is clear that unexpected interactions between components were responsible for interesting behaviour for the systems presented in Chapters 3 and 4, *i.e.* opposing chirality in the filament structure and disruptive assembly at particular Ag:GMP molar ratios. Therefore, the *in-situ*

analysis of these interactions between components prior to gelation in necessary focusing on any alterations to structures present prior to gelation would be insightful. Such studies would ideally avoid artefacts common to many techniques such as drying processes which can affect the supramolecular structures. Where possible it would also be advantageous to study the gelation process to better understand the mechanism of assembly and any associated structural reorganisations and how these, and the assembly process more broadly, are perturbed by the presence of other components, *i.e.* SNP or other gelators.

Further characterisation of gelators prior to gelation is necessary. For instance, the presence of SNP in solution affected the filament chirality regardless of whether the nitric oxide radicals were involved in the dephosphorylation. It was demonstrated that this was a kinetically trapped structure and a more thermodynamically favoured structure could be reached through melting and cooling of the gel. This indicates that the interactions responsible for the kinetically trapped structure occur prior to and/or during the gelation process since it is possible for the expected chirality to occur in the presence of SNP after the heating and cooling cycle. Further to this, circular dichroism analysis for the work presented in Chapter 4 indicated disruption to the FY micellar organisation prior to gelation. This could arise from intermolecular interactions between GMP and FY such that the gelator molecules are not separate in solution and thus do not assemble orthogonally to one another. This could be due to possible interactions between the tyrosine and guanine residues,[1,2] such that either gelator could disrupt supramolecular assemblies that exist before gelation. Such interactions could be probed *via* two-dimensional nuclear magnetic resonance spectroscopy, in particular, 2D Nuclear Overhauser effect spectroscopy (NOESY).[3,4] NOESY uses information about the nuclear Overhauser cross relaxation between nuclear spins (the transfer of nuclear spin polarization) to determine through space, dipolar interactions. Two-dimensional plots are created, with spectra along the horizontal and vertical axis, whereby cross-peaks appearing off the diagonal of the plot indicates close localisation of protons from different molecules (Figure 6.1). [5,6] As these peaks can be related to protons of certain functional groups it can be possible to rationalise stacking arrangements for the co-gelators with the

knowledge of which functional groups are interacting with one another. Thus, it is also possible to characterise and quantify the mixing of components prior to gelation. For instance, Draper *et al.* demonstrated that two naphthalene based gelators intermixed at high pHs.[7] They demonstrated a reversal of positive to negative NOE signals, that corresponds to aggregation,[8,9] upon addition of a second component. This was supported by shifts in the aromatic protons, indicating a changed environment. Such studies summarised above could be very insightful to understand any interactions between the two gelators and therefore determine whether any mixing of the gelators occurs prior to gelation.

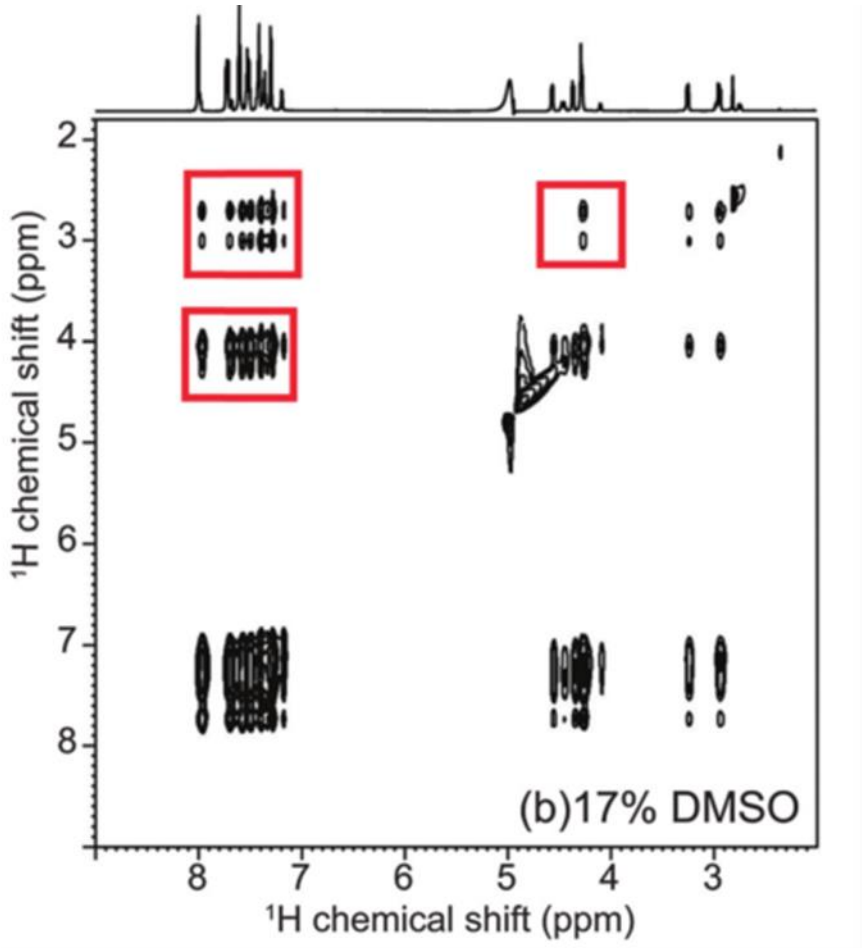

Figure 6.1 2D NOESY 1H spectra of FmocF in DMSO-d6. The off-diagonal cross peaks are highlighted with squares. Adapted from 6

As mentioned previously, FY and similar gelators have been shown to exist as micellar aggregates prior to gelation and it is currently unclear whether these structures persist during gelation, whether there

is a structural reorganisation or whether they completely disassemble and reform to form different filament structures during gelation.[10] Therefore, any interactions may affect these processes or affect how the filaments entangle.[7] Thus, it would also be informative to undertake more experiments to probe the assembly *in-situ*. For instance, using circular dichroism and rheology indicated structural reorganisation for sample E in Chapter 4.

For these experiments, small angle neutron scattering (SANS) could meet these requirements. For instance, SANS is capable of structural interrogation of hydrogels across multiple lengths scales (*ca.* 0.6-600 nm) and therefore can resolve individual nanofilaments and is a highly powerful tool for quantitative evaluation of hydrogel networks in aqueous environments.[11–15] Neutrons interact weakly with the nuclei of the sample and, therefore, will not cause radiation damage (as with synchrotron x-rays). The neutrons can penetrate the sample giving nanometre scale determination of structures within thick samples. As gelled samples exhibit relatively strong intensities, it could be possible to characterise the gelation process *in situ* without the need for modification, therefore overcoming drying artefacts.[16] Ultra-small-angle neutron scattering (USANS) can also be used in conjunction with SANS to probe the microstructure of gels and could provide information regarding the bundling of filaments and network properties. [17–19] This could be particularly relevant to understand the multicomponent systems. Preliminary SANS experiments have been carried out of on the gels presented in chapters 3 and 4 and demonstrate promising results.

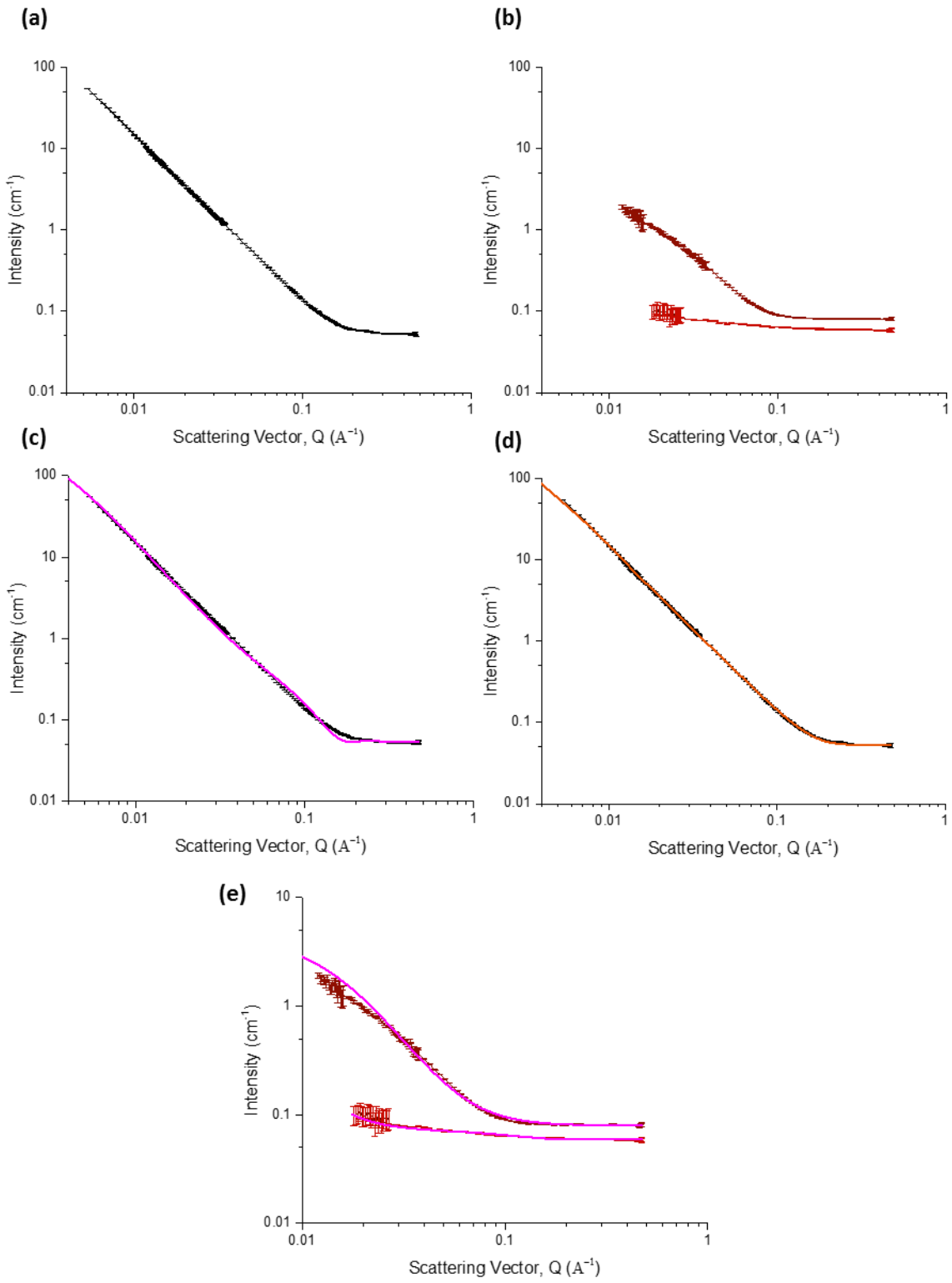

Figure 6.2 SANS profiles for single component gels. (a) FY GdL gel, (b) AgGMP gels, (c) FY sample using fractal model, (d) FY sample using flexible cylinder (elliptical), and (e) AgGMP using fractal model

The branching nature of hydrogel networks can be described as fractal objects, and be described by the fractal dimension (D_f) which quantifies the complexity of the network.[11,19–26] This parameter is only an effective fractal dimension as gels are not rigorous fractal objects,[20] but can be used to give insight into the network structure.[19,26] For instance, Lam *et al* correlated a higher D_f to crystallographic mismatches to filaments formed rapidly to create a more complex network and conversely a lower D_f to longer filaments formed more slowly.[27] All three single component gels could be fitted to a fractal model (Figure 6.2c and e). The FY gel had a D_f of 2.3 and the AgGMP gels had higher fractal dimensions of 3 and 2.7 for the 1:1 and 2:1 molar ratios, respectively. Fractal models fit less well at higher Q as they describe the junction zones of bundling filaments or branching points from crystallographic mismatches and not the filament structure of the filaments. [11] However, supramolecular gels can be modelled by various cylinder models to probe filament structure. [10,12,23,28,29] The FY sample fits very well to an elliptical flexible cylinder (Figure 6.4d), which describes the flat tape morphology observed in TEM images. AgGMP gels could also be fitted with cylinder models but need to be combined with the power-law model first (Not shown).

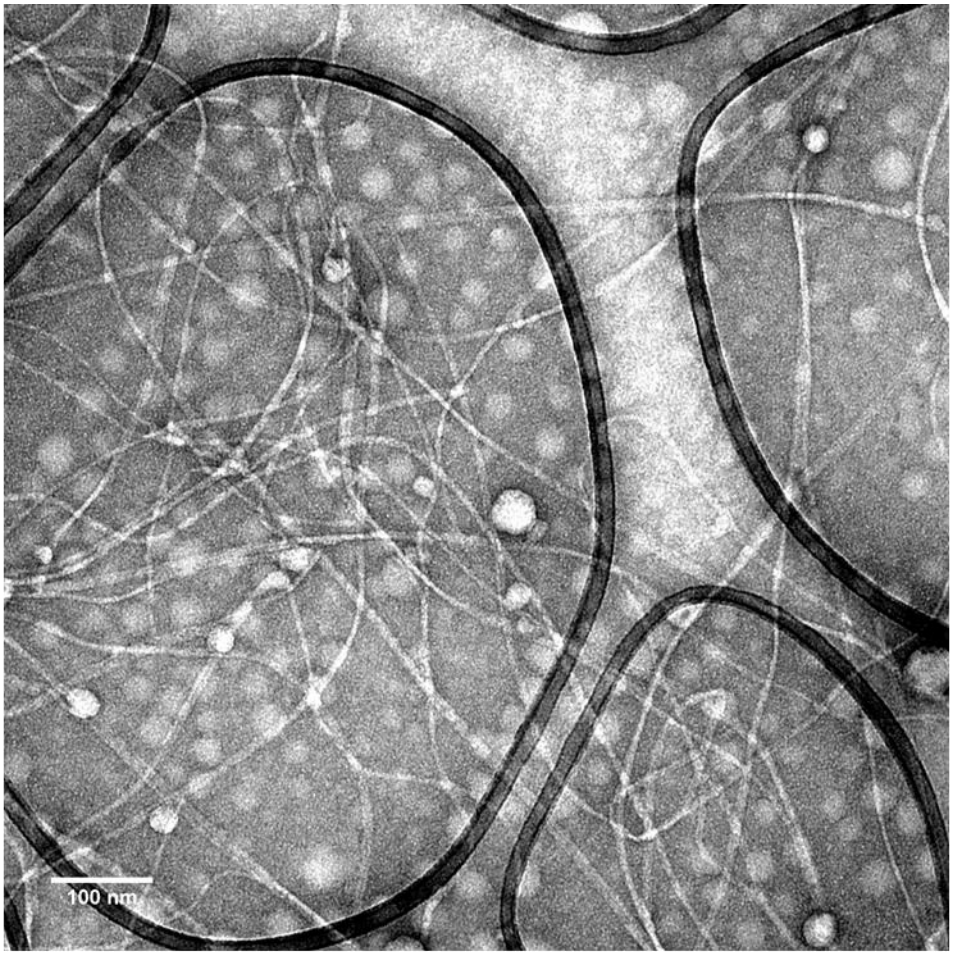

Figure 6.3 TEM images of FY filaments negatively stained with uranyl acetate and Ag-GMP gels at (b and c) 2:1 ratio and (d) 1:1 ratio. (Scale bar 100 nm).

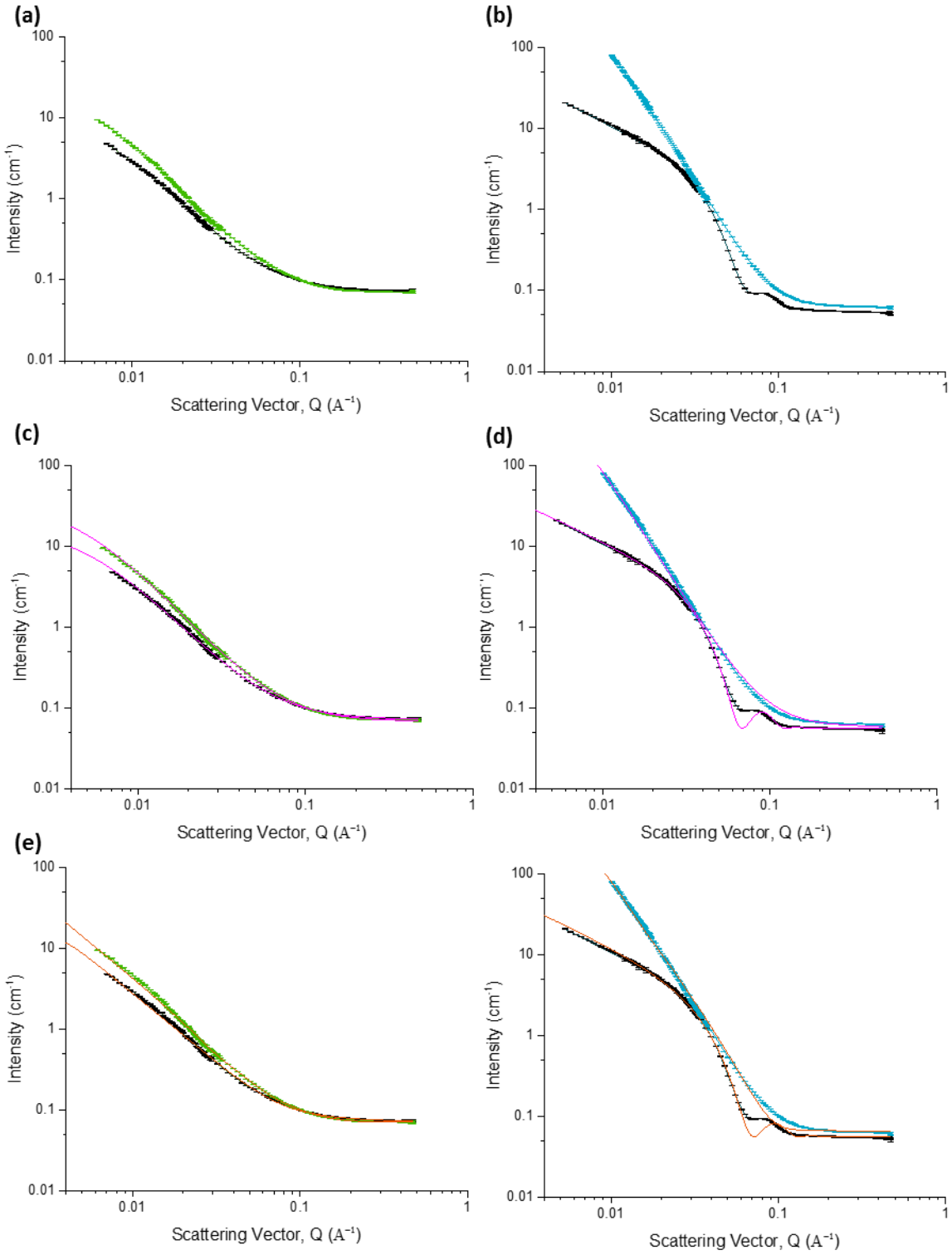

Figure 6.4 SANS profile for single component gels. (a) Multicomponent hydrogels at 1-1 AgGMP stoichiometry, (b) multicomponent hydrogels at 2-1 AgGMP stoichiometry, (c) multicomponent gels fitted using fractal models, (d) multicomponent gels fitted using fractal models, (e) multicomponent gels fitted using flexible cylinder models, and (f) multicomponent gels using fitting using cylinder models

SANS profiles were also obtained for four of the multicomponent samples (Figure 6.4). (Sample codes and colours summarised below in Table 6.1) All samples could be fitted to fractal models. Sample D

best match a core-shell fractal model. Interestingly, the SANS data for sample D (equimolar GMP and FY) was different from either of the individual gelators and other multicomponent profiles. The peak at high Q is indicative of a core-shell structure present in solution.[13,30,31] Therefore, sample D was fitted to a core-shell fractal model. Different scattering data demonstrated the formation of a new structure which has previously been interoperated as evidence for a co-assembled system.[29,32] This is supported by substantially different D_f values for sample D, compared to the individual gelators and other multicomponent samples. Samples A and B both had D_f values of 2.2 and sample E had a D_f value of 2.8, which is likely due to a denser hydrogel network due to the lower pH reached this stoichiometry. However, sample D had a much lower D_f of 1.1. This indicates severe disruption to the branching in the hydrogel network. The lower scattering intensity for sample D despite the higher gelator content also indicates disruption to the hydrogel network. [7] Both of these agree with the observations made in Chapter 4.

Sample		Label	Legend
FY			
GMP			
FY-GMP			
FY 25mM GdL			
1-1 AgGMP 25 mM			
2-1 AgGMP 25mM			
1-1 AgGMP FY	GMP 25 FY 25	A	
	GMP 25 FY 12.5	B	
	GMP 12.5 FY 25	C	
2-1 AgGMP FY	GMP 25 FY 25	D	
	GMP 25 FY 12.5	E	
	GMP 12.5 FY 25	F	

Table 6.1 Summary of gels prepared with their associated label and legend colour.

All multicomponent samples could also be fitted to the flexible elliptical cylinder model, except D which was modelled as a hollow cylinder (Figure 6.4 d and e). These different models indicate different filament structure. This could be studied further with SANS. The multicomponent system, in particular, could also be studied further by partly deuterating one of the components, which would reduce scattering intensity from this component and therefore it would be possible to see whether the resulting scattering matched that of the other component which could be used to further determine whether self-sorting or co-assembly has occurred. [33]

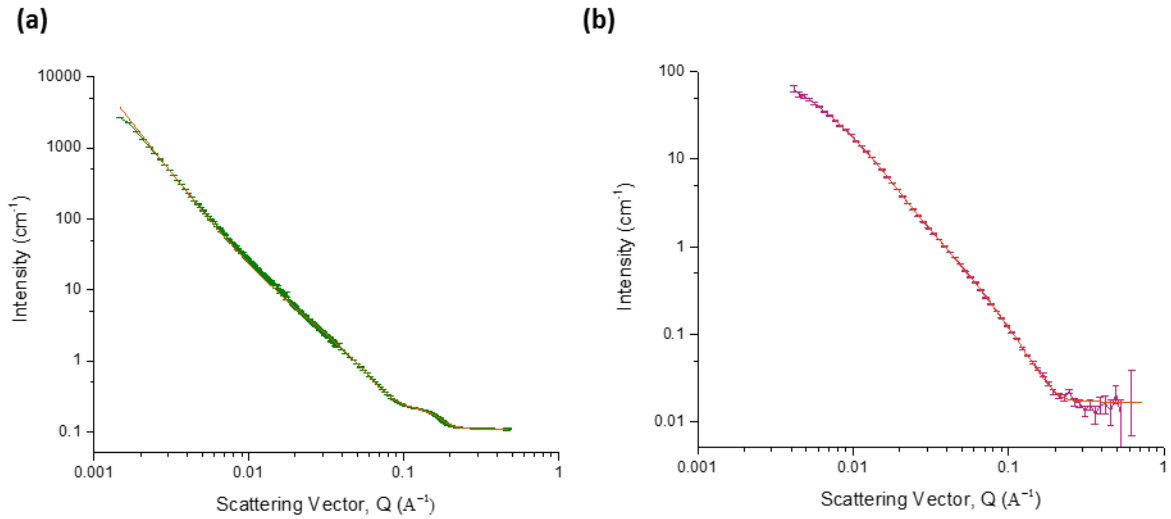

Figure 6.5 SANS profile for (a) SNP-FYP gel at 5:1 ratio fitted with a combined power law and core-shell cylinder and (b) ALP-FYP gel fitted with an flexible elliptical cylinder model

The SNP-FYP gels exhibited significantly different SANS profiles compared to the ALP-FYP gels, displaying a peak at high Q, characteristic of a core-shell structure (Figure 6.5). [13,30,31] As with the FY gel, the ALP-FYP gel was fitted using the flexible elliptical cylinder model. Whereas, the SNP-FYP gel was fitted with a core-shell cylinder, combined with a power law model to describe the low Q data. The different morphology for the SNP-FYP gels is described by the core-shell element describing the coiled tape structure discovered *via* cryo-TEM (Figure 6.6).

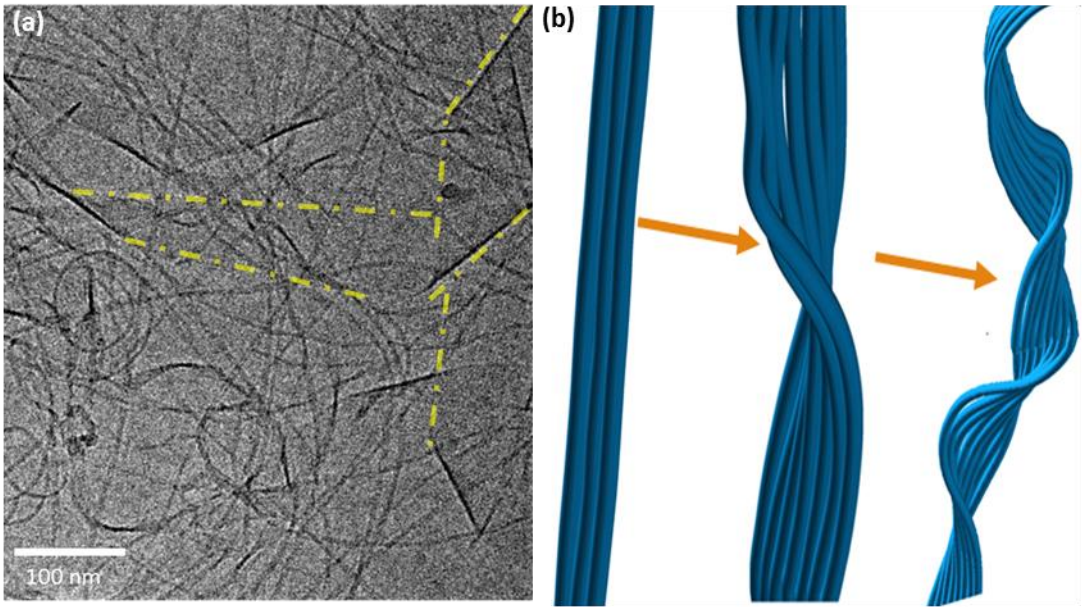

Figure 6.6 (a) cryo-TEM image of unravelled SNP-FYP nanofilaments with striations along the filament axis. (b) Coiling of a flat filament into a twisted ribbon and then into a helical ribbon.

Work by Adams group has used SANS to demonstrate the difference in structures in solution and hydrogel phases [28] and different network structures based on the preparation method.[10] It is not clear whether the structures in the solution phase are retained and reorganise or whether these structures are depleted as hydrogel filaments form.[34] SANS could conceivably be used to track gelation *in situ* for both gelator systems, which could be used to probe structural reorganisations prior, due to interactions with other components, or during gelation though considerations will need to be made about the rate of gelation against measurement times.

Finally, chapter 5 investigated the potential application of the Ag-GMP gel. As silver is integral to the assembly of GMP and decorates the filaments of the gel the antibacterial properties of this gel were characterised. It was demonstrated that the stimuli chosen, *i.e.* the stoichiometry of silver substantial influence over the rheological properties of the resulting hydrogel and its subsequent antibacterial behaviour. Through CFU counts substantial antibacterial activity was demonstrated against candidate gram-negative bacteria (*E. coli*) and gram-positive bacteria (*E. faecalis)*. Further, as would be expected, higher levels of silver corresponded to higher killing. However, the killing at the lower molar ratio can be increased by irradiating these gels Control gels formed in the absence of silver did not demonstrate anti-bacterial activity.

However, further study in combination with other materials is recommended. As discovered in Chapter 4, this second component should be one that doesn't interact with silver or guanosine monophosphate. For instance, this could be a suitable supramolecular hydrogel or even a polymeric hydrogel. This could allow for a reasonably mechanical strong material to be produced, allowing for lower silver concentrations. This would be advantageous as it may alleviate cytotoxicity issues arising from using silver, which also require investigation.

To end, the work demonstrated within this thesis has demonstrated that the stimulus and the environmental conditions affect how single and multicomponent hydrogels form and can also affect the properties of the gels relevant to the application.

References

(1) Gupta, A. P.; Taylor, W. J.; McGown, L. B.; Kempf, J. G. NMR Studies of the Chiral Selectivity of Self-Assembled Guanosine Monophosphate. *J. Phys. Chem. B* 2014, *118* (49), 14243–14256.

(2) Dong, Y.; McGown, L. B. Chiral Selectivity of Guanosine Media in Capillary Electrophoresis. *Electrophoresis* 2011, *32* (13), 1735–1741.

(3) Yu, G.; Yan, X.; Han, C.; Huang, F. Characterization of Supramolecular Gels. *Chem. Soc. Rev.* 2013, *42* (16), 6697.

(4) Wu, G.; Kwan, I. C. M. Helical Structure of Disodium 5'-Guanosine Monophosphate Self-Assembly in Neutral Solution. *J. Am. Chem. Soc.* 2009, *131* (9), 3180–3182.

(5) Rao, K. V.; Jayaramulu, K.; Maji, T. K.; George, S. J. Supramolecular Hydrogels and High-Aspect-Ratio Nanofibers through Charge-Transfer-Induced Alternate Coassembly. *Angew. Chemie* 2010, *122* (25), 4314–4318.

(6) Singh, V.; Snigdha, K.; Singh, C.; Sinha, N.; Thakur, A. K. Understanding the Self-Assembly of Fmoc–phenylalanine to Hydrogel Formation. *Soft Matter* 2015, *11* (26), 5353–5364.

(7) Draper, E. R.; Wallace, M.; Schweins, R.; Poole, R. J.; Adams, D. J. Nonlinear Effects in Multicomponent Supramolecular Hydrogels. *Langmuir* 2017, *33* (9), 2387–2395.

(8) Chen, J.-Y.; Yuan, B.; Li, Z.-Y.; Tang, B.; Gupta, A.; Bhosale, S.-V.; Li, J.-L. Synergistic Coassembly of Two Structurally Different Molecular Gelators. *Langmuir* 2016, *32* (46), 12175–12183.

(9) Hirst, A. R. R.; Miravet, J. F. F.; Escuder, B.; Noirez, L.; Castelletto, V.; Hamley, I. W. W.; Smith, D. K. K. Self-Assembly of Two-Component Gels: Stoichiometric Control and Component Selection. *Chem. - A Eur. J.* 2009, *15* (2), 372–379.

(10) Colquhoun, C.; Draper, E. R.; Schweins, R.; Marcello, M.; Vadukul, D.; Serpell, L. C.; Adams, D. J.; Yang, Z.; Ding, D.; Kong, D.; Liu, J.; Atkins, D.; Adams, D. J.; Schatz, G. C.; Stupp, S. I. Controlling the Network Type in Self-Assembled Dipeptide Hydrogels. *Soft Matter* 2017, *13* (9), 1914–1919.

(11) Weiss, R. G.; Terech, P. *Molecular Gels*; Weiss, R. G., Terech, P., Eds.; Springer Netherlands: Dordrecht, 2006.

(12) Jamieson, S. A.; Tong, K. W. K.; Hamilton, W. A.; He, L.; James, M.; Thordarson, P. Small Angle Neutron Scattering (SANS) Studies on the Structural Evolution of Pyromellitamide Self-Assembled Gels. *Langmuir* 2014, *30* (46), 13987–13993.

(13) Li, Z.; Buerkle, L. E.; Orseno, M. R.; Streletzky, K. A.; Seifert, S.; Jamieson, A. M.; Rowan, S. J. Structure and Gelation Mechanism of Tunable Guanosine-Based Supramolecular Hydrogels. *Langmuir* 2010, *26* (12), 10093–10101.

(14) Willemen, H. M.; Marcelis, A. T. M.; Sudhölter, E. J. R.; Bouwman, W. G.; Demé, B.; Terech, P. A Small-Angle Neutron Scattering Study of Cholic Acid-Based Organogel Systems. *Langmuir* 2004, *20* (6), 2075–2080.

(15) King, S. M. Small Angle Neutron Scattering. *Mod. Tech. Polym. Characterisation* 1999, 1-10

(16) Mears, L. L. E.; Draper, E. R.; Castilla, A. M.; Su, H.; Zhuola; Dietrich, B.; Nolan, M. C.; Smith, G. N.; Doutch, J.; Rogers, S.; Akhtar, R.; Cui, H.; Adams, D. J. Drying Affects the Fiber Network in Low Molecular Weight Hydrogels. *Biomacromolecules* 2017,

(17) Nolan, M. C.; Fuentes Caparrós, A. M.; Dietrich, B.; Barrow, M.; Cross, E. R.; Bleuel, M.; King, S.

M.; Adams, D. J. Optimising Low Molecular Weight Hydrogels for Automated 3D Printing. *Soft Matter* 2017, *13* (45), 8426–8432.

(18) Draper, E. R.; Adams, D. J. How Should Multicomponent Supramolecular Gels Be Characterised? *Chem. Soc. Rev.* 2018. 3395-3405

(19) Hule, R. A.; Nagarkar, R. P.; Altunbas, A.; Ramay, H. R.; Branco, M. C.; Schneider, J. P.; Pochan, D. J. Correlations between Structure, Material Properties and Bioproperties in Self-Assembled β-Hairpin Peptide Hydrogels. *Faraday Discuss.* 2008, *139* (0), 251.

(20) Lattuada, M.; Wu, H.; Hasmy, A.; Morbidelli, M. Estimation of Fractal Dimension in Colloidal Gels. *Langmuir* 2003, *19* (15), 6312–6316.

(21) Ikeda, S.; Foegeding, E. A.; Hagiwara, T. Rheological Study on the Fractal Nature of the Protein Gel Structure. *Langmuir* 1999, *15* (25), 8584–8589.

(22) Gmachowski, L. Calculation of the Fractal Dimension of Aggregates. *Colloids Surfaces A Physicochem. Eng. Asp.* 2002, *211* (2–3), 197–203.

(23) Berts, I.; Gerelli, Y.; Hilborn, J.; Rennie, A. R. Structure of Polymer and Particle Aggregates in Hydrogel Composites. *J. Polym. Sci. Part B Polym. Phys.* 2013, *51* (6), 421–429.

(24) Guilbaud, J.-B.; Saiani, A. Using Small Angle Scattering (SAS) to Structurally Characterise Peptide and Protein Self-Assembled Materials. *Chem. Soc. Rev.* 2011, *40* (3), 1200–1210.

(25) Cheng, G.; Castelletto, V.; Moulton, C. M.; Newby, G. E.; Hamley, I. W. Hydrogelation and Self-Assembly of Fmoc-Tripeptides: Unexpected Influence of Sequence on Self-Assembled Fibril Structure, and Hydrogel Modulus and Anisotropy. *Langmuir* 2010, *26* (7), 4990–4998.

(26) Chen, L.; Raeburn, J.; Sutton, S.; Spiller, D. G.; Williams, J.; Sharp, J. S.; Griffiths, P. C.; Heenan, R. K.; King, S. M.; Paul, A.; Furzeland, S.; Atkins, D.; Adams, D. J. Tuneable Mechanical Properties in Low Molecular Weight Gels. *Soft Matter* 2011, *7* (20), 9721.

(27) Lam, R.; Quaroni, L.; Pedersen, T.; Rogers, M. A. A Molecular Insight into the Nature of Crystallographic Mismatches in Self-Assembled Fibrillar Networks under Non-Isothermal Crystallization Conditions. *Soft Matter* 2010, *6* (2), 404–408.

(28) Cardoso, A. Z.; Mears, L. L. E.; Cattoz, B. N.; Griffiths, P. C.; Schweins, R.; Adams, D. J. Linking Micellar Structures to Hydrogelation for Salt-Triggered Dipeptide Gelators. *Soft Matter* 2016, *12* (15), 3612–3621.

(29) Colquhoun, C.; Draper, E. R.; Eden, E. G. B.; Cattoz, B. N.; Morris, K. L.; Chen, L.; McDonald, T. O.; Terry, A. E.; Griffiths, P. C.; Serpell, L. C.; Adams, D. J. The Effect of Self-Sorting and Co-Assembly on the Mechanical Properties of Low Molecular Weight Hydrogels. *Nanoscale* 2014, *6* (22), 13719–13725.

(30) Buerkle, L. E.; Li, Z.; Jamieson, A. M.; Rowan, S. J. Tailoring the Properties of Guanosine-Based Supramolecular Hydrogels. *Langmuir* 2009, *25* (15), 8833–8840.

(31) Morris, K. L.; Chen, L.; Raeburn, J.; Sellick, O. R.; Cotanda, P.; Paul, A.; Griffiths, P. C.; King, S. M.; O'Reilly, R. K.; Serpell, L. C.; Adams, D. J.; O'Reilly, R. K.; Serpell, L. C.; Adams, D. J. Chemically Programmed Self-Sorting of Gelator Networks. *Nat. Commun.* 2013, *4*, 1480.

(32) Horgan, C. C.; Rodriguez, A. L.; Li, R.; Bruggeman, K. F.; Stupka, N.; Raynes, J. K.; Day, L.; White, J. W.; Williams, R. J.; Nisbet, D. R. Characterisation of Minimalist Co-Assembled Fluorenylmethyloxycarbonyl Self-Assembling Peptide Systems for Presentation of Multiple Bioactive Peptides. *Acta Biomater.* 2016, *38*, 11–22.

(33) Woodward, J.; Mattingly, S. M.; Danson, M.; Hough, D.; Ward, N.; Adams, M. In Vitro Hydrogen Production by Glucose Dehydrogenase and Hydrogenase. *Nat. Biotechnol.* 1996, *14* (7), 872–874.

(34) Draper, E. R.; Adams, D. J. Low-Molecular-Weight Gels: The State of the Art. *Chem* 2017, *3* (3), 390–410.